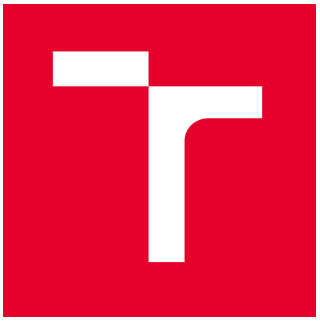

BRNO UNIVERSITY OF TECHNOLOGY

VYSOKÉ UČENÍ TECHNICKÉ V BRNĚ

FACULTY OF MECHANICAL ENGINEERING

FAKULTA STROJNÍHO INŽENÝRSTVÍ

INSTITUTE OF MACHINE AND INDUSTRIAL DESIGN

ÚSTAV KONSTRUOVÁNÍ

TRIBOLOGICAL PROCESSES OF AN ADDITIVELY MANUFACTURED SMALL JOINT IMPLANT UNDER SIMULATED CONDITIONS

TRIBOLOGICKÉ PROCESY ADITIVNĚ VYROBENÉHO IMPLANTÁTU MALÉHO KLOUBU V SIMULOVANÝCH PODMÍNKÁCH

DOCTORAL THESIS

DIZERTAČNÍ PRÁCE

AUTHOR — **Ing. Lukáš Odehnal**

AUTOR PRÁCE

SUPERVISOR — **prof. Ing. Martin Vrbka, Ph.D.**

ŠKOLITEL

BRNO 2026

STATEMENT

I hereby declare that I have written the PhD thesis, "Tribological Processes of an Additively Manufactured Small Joint Implant under Simulated Conditions," on my own, under the guidance of my supervisor, prof. Ing. Martin Vrbka, Ph.D., and using the sources listed in the references.

Brno, …….. ……..……..

Lukáš Odehnal

BIBLIOGRAPHICAL REFERENCE

ODEHNAL, Lukáš. *Tribological Processes of an Additively Manufactured Small Joint Implant under Simulated Conditions*. Doctoral Thesis. Martin VRBKA (supervisor). Brno: Brno University of Technology, Faculty of Mechanical Engineering, 2026.

ACKNOWLEDGEMENT

I would like to express my sincere gratitude to my supervisor, prof. Ing. Martin Vrbka, Ph.D., for his professional guidance, valuable advice, and continuous support throughout my doctoral studies. I also thank the supervisor, specialist Ing. Matúš Ranuša, Ph.D., for professional consultations, insightful comments, and in-depth discussions that expanded my perspective on the studied topic and contributed to improving the overall quality of the research.

My sincere thanks go to the members of the Biotribology Research Group for the inspiring working environment, collaboration, knowledge sharing, and their commitment to assist with experiments, discussions, and everyday research challenges. I would also like to thank my colleagues from the office for fostering an atmosphere that was occasionally less conducive to focused work, but important for relaxation and mental balance. Without such moments of distraction and shared humour, completing the doctoral studies would have been considerably more difficult.

Last but not least, I would like to express my greatest gratitude to my family for their constant support, patience, and understanding throughout my studies. Without their support and trust, this work would not have been possible.

ABSTRACT

Joint replacement surgery is a common procedure that intends to restore patients´ mobility and improve their quality of life. However, the durability of these implants is constrained by various factors, including friction, wear, lubrication failure, and material degradation at the articulating surfaces. These challenges are especially important in small joints, where lubricant supply is restricted, sliding velocities are low, and contact operates primarily in boundary or mixed lubrication. Despite Ti6Al4V's well-established status as a biomaterial with excellent biocompatibility and strong potential for additive manufacturing, its tribological behaviour under these conditions remains insufficiently understood. The present dissertation aims to address this knowledge gap by investigating the tribological performance of Ti6Al4V in small joint implant conditions, with particular emphasis on additively manufactured surfaces and their interaction with synovial fluid.

The dissertation is based on four interconnected studies. The research began with a comparison of conventionally manufactured Ti6Al4V and CoCr30Mo6 under model small joint conditions. This was followed by an examination of the effects of surface texturing and electrochemical polishing on lubrication formation. Subsequently, the additively manufactured Ti6Al4V with controlled surface structures produced during printing was evaluated. Furthermore, long-term wear experiments involving microstructural analysis were conducted. The methodology comprised a combination of friction measurements, colourimetric interferometry, fluorescence microscopy, and surface analysis.

The findings indicated that conventionally manufactured Ti6Al4V is not optimally suited for direct articulation under the tested conditions. While the material was capable of forming a lubricant film, its surface characteristics prevented effective separation of the surfaces, leading to increased wear. Nevertheless, applied surface texturing improved the tribological response of Ti6Al4V by promoting its lubrication behaviour. Among the additively manufactured designs, the grid-structured surface provided the best balance of lubricant retention, lubrication film formation, lubrication recovery, and wear resistance.

The dissertation demonstrates that the tribological performance of Ti6Al4V is dependent on the manufacturing route, surface morphology, and near-surface structural state. The findings demonstrate that additive manufacturing can transform Ti6Al4V into a functionally optimised surface with more stable lubrication and improved wear behaviour. This work provides mechanistic insight into synovial lubrication and supports the preclinical development of additively manufactured small joint implants.

KEYWORDS

Ti6Al4V Alloy; Additive Manufacturing; Small Joint Implant Tribology; Synovial Fluid Lubrication; Surface Texturing

ABSTRAKT

Kloubní náhrady představují zavedené řešení pro obnovu mobility pacientů a zlepšení kvality jejich života. Jejich dlouhodobá funkčnost je však stále limitována řadou faktorů, zejména třením, opotřebením, poruchami mazání a degradací materiálu na artikulačních površích. Tyto problémy jsou obzvlášť významné u implantátů malých kloubů, kde je přísun maziva omezený, kluzné rychlosti nízké a kontakt probíhá převážně v režimu mezného nebo smíšeného mazání. Přestože je slitina Ti6Al4V etablovaným biomateriálem s výbornou biokompatibilitou a významným potenciálem pro aditivní výrobu, její tribologické chování v těchto podmínkách dosud nebylo dostatečně objasněno. Předkládaná disertační práce se proto zaměřuje na studium tribologického chování slitiny Ti6Al4V v kontaktech implantátů malých kloubů, se zvláštním důrazem na povrchy připravené aditivní výrobou a jejich interakci se synoviální tekutinou.

Disertační práce vychází ze čtyř vzájemně propojených studií. Výzkum byl zahájen porovnáním konvenčně vyráběných materiálů Ti6Al4V a CoCr30Mo6 v modelových podmínkách malých kloubů. Následně byl hodnocen vliv texturování povrchu a elektrochemického leštění na tvorbu mazacího filmu. V další části byla zkoumána slitina Ti6Al4V připravená aditivní výrobou s řízenými povrchovými strukturami vznikajícími přímo během tisku. Součástí práce byly rovněž dlouhodobé experimenty opotřebení doplněné o mikrostrukturní analýzu. Experimentální metodika zahrnovala měření tření, kolorimetrickou interferometrii, fluorescenční mikroskopii a analýzu povrchu.

Výsledky ukázaly, že konvenčně vyráběná slitina Ti6Al4V není za testovaných podmínek optimálně vhodná pro přímou artikulaci. Přestože byla schopna vytvořit mazací film, charakter jejího povrchu neumožnil dostatečné oddělení kontaktních ploch, což vedlo ke zvýšenému opotřebení. Tribologická odezva Ti6Al4V se však významně zlepšila po úpravě povrchu texturováním, které podpořilo příznivější mazací režim. Z hodnocených povrchů připravených aditivní výrobou vykázala nejlepší kombinaci retence maziva, tvorby mazacího filmu, obnovy mazání a odolnosti proti opotřebení mřížková struktura.

Disertační práce prokazuje, že tribologická výkonnost slitiny Ti6Al4V je zásadně ovlivněna způsobem výroby, morfologií povrchu a stavem podpovrchové struktury. Získané poznatky ukazují, že aditivní výroba může transformovat Ti6Al4V na funkčně optimalizovaný povrch s vyšší stabilitou mazání a lepší odolností vůči opotřebení. Práce tak přináší hlubší mechanistické porozumění synoviálnímu mazání a současně poskytuje podklad pro preklinický vývoj implantátů malých kloubů vyráběných aditivní technologií.

KLÍČOVÁ SLOVA

Slitina Ti6Al4V; Aditivní výroba; Tribologie implantátů malých kloubů; Mazání synoviální kapalinou; Povrchové texturování

CONTENT

1

INTRODUCTION

The development of artificial joint replacement surgery represents a major milestone in modern medicine, with major consequences for patients' quality of life worldwide. However, with the increasing number of implantations and the extended lifespan of the population, there is a growing need to better understand the long-term performance of these implants within the human body.

A thorough examination of data from multiple sources consistently indicates an escalating trend in the volume of joint replacement procedures. Recent estimates indicate that more than 2 million joint replacement procedures are performed worldwide annually [1]. Demand is anticipated to increase substantially over the coming decades, driven by two key factors. Firstly, the population is ageing, and secondly, levels of physical activity are rising. Projections indicate that the number of hip and knee replacements may increase by almost 40% by 2060 if current demographic trends persist [1]. This trend is clearly evident in the data from the 22nd Annual Report (see Fig. 1-1), which was obtained by the National Joint Registry [2]. The registry is responsible for collecting data from hospitals across England, Wales, Northern Ireland, the Isle of Man, and Guernsey. The data differs from the trend solely in 2020 and 2021, which were nevertheless years significantly affected by the global pandemic of the novel Coronavirus (SARS-CoV-2).

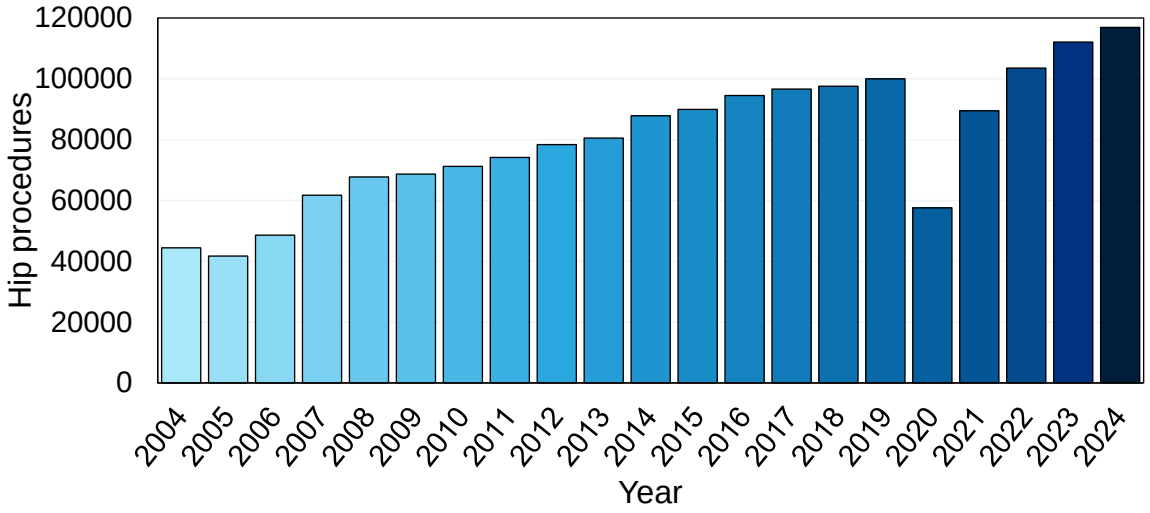

Fig. 1-1 Number of primary operations performed for the hip joint according to the National Joint Registry (Based on data from [2]).

From the patient's perspective, joint replacement has been shown to markedly improve quality of life by restoring mobility, reducing chronic pain, and enabling the return to independent living or employment [3]. The aforementioned benefits result in reduced indirect costs, including long-term disability support, lost productivity, and social care expenses [4]. Evidence has demonstrated that patients who regain mobility often experience improved mental health, greater social participation, and enhanced general well-being. Collectively, these factors help to reduce societal dependence and higher quality-adjusted life years (QALYs) [5].

However, the extensive utilisation of joint replacements also results in considerable direct healthcare expenditures. Surgical procedures, implant materials, hospitalisation, and postoperative rehabilitation all represent considerable financial burdens for healthcare providers [6]. Despite the significant initial financial investment, a substantial body of research has demonstrated that total joint arthroplasty is a cost-effective intervention over time [7]. The intervention has been demonstrated to reduce the requirement for chronic pain management, pharmacotherapy, and care for secondary conditions associated with immobility, including cardiovascular and metabolic complications. Furthermore, reductions in hospital readmissions and caregiver dependency have been shown to yield additional financial savings for the healthcare system [8,9].

At the social level, joint replacements have been demonstrated to support economic productivity via enabling older adults and individuals with disabilities to remain active in the workforce or community [10]. The aforementioned factors have been demonstrated to engender positive macroeconomic effects, including a reduction in the dependency ratio and alleviation of the fiscal strain associated with an ageing population. Investments in implant development, biomaterials, and surgical innovation also stimulate research and industrial growth, strengthening the link between medical technology and economic advancement [11].

As the socioeconomic relevance of joint replacement continues to grow, ensuring its long-term functional stability becomes not only a medical but also a financial necessity. Despite the remarkable clinical success of joint replacement surgery, numerous challenges remain that prevent these systems from achieving truly lifelong performance. The service life and reliability of artificial joints are determined mainly by the intricate interplay among mechanical, chemical, and biological factors that act at the articulating surfaces. Moreover, as younger, more physically active patients increasingly use modern implants, the procedural demands placed on them are increasing significantly [12,13]. The original intent of the technology, which was primarily designed to restore mobility in elderly individuals with low activity levels, has now evolved to necessitate resistance to extended cyclic loading, elevated contact stresses, and increasingly complicated motion cycles. This shift poses additional challenges to the design and selection of materials, which must not only maintain superior mechanical strength and wear resistance but also secure long-term biocompatibility and corrosion stability in a chemically active physiological environment.

To address these issues, it is essential to engage in continuous research and innovation. Substantial progress within materials science, manufacturing technologies, and surface engineering has already led to considerable improvements in implant design and performance. The introduction of highly cross-linked polymers, ceramic composites, and advanced titanium alloys has enhanced both wear resistance and biocompatibility. Concurrently, contemporary additive manufacturing techniques enable the fabrication of more complex geometries and customised designs that were previously unattainable.

Nevertheless, despite these advances, the tribological and corrosion behaviour of implant materials under physiological conditions is an essential factor limiting their long-term reliability. The presence of wear particles and corrosion products has been shown to initiate biological reactions, inducing inflammation, osteolysis, and subsequent implant loosening. These phenomena have been shown to adversely affect implant service life and clinical outcomes.

Consequently, a thorough investigation of the tribological properties of implant materials, encompassing both wear and tribocorrosion mechanisms, is imperative for advancing the next generation of artificial joints. Such studies not only deepen our understanding of the fundamental processes at the implant/tissue interface but also provide a basis for optimising surface treatments, lubrication regimes, and material pairings to guarantee long-term stability, safety, and economic efficiency in clinical applications.

Fig. 1-2 From clinical and socioeconomic context to tribological mechanisms: factors shaping artificial joint performance.

2

STATE OF THE ART

The concept of artificial joint replacement has a long and fascinating history that reflects the progress of both materials science and medical technology. The earliest documented attempts to restore mobility in damaged joints date back to the late 19th century, when Themistocles Glück [14] implanted ivory prostheses to replace hip joints. Despite being limited by the absence of suitable biomaterials and aseptic surgical techniques, these revolutionary experiments established the basis for the concept that mechanical components could potentially substitute for biological articulation. The development of modern arthroplasty was significantly advanced by the pioneering work of Sir John Charnley in the early 1960s, who introduced the concept of low-friction total hip replacement [15]. The design, incorporating a metallic femoral head that articulates with an ultra-high-molecular-weight polyethylene (UHMWPE) cup fixed with acrylic bone cement, established the basis for contemporary joint replacement technology and was widely adopted during the subsequent decade [16].

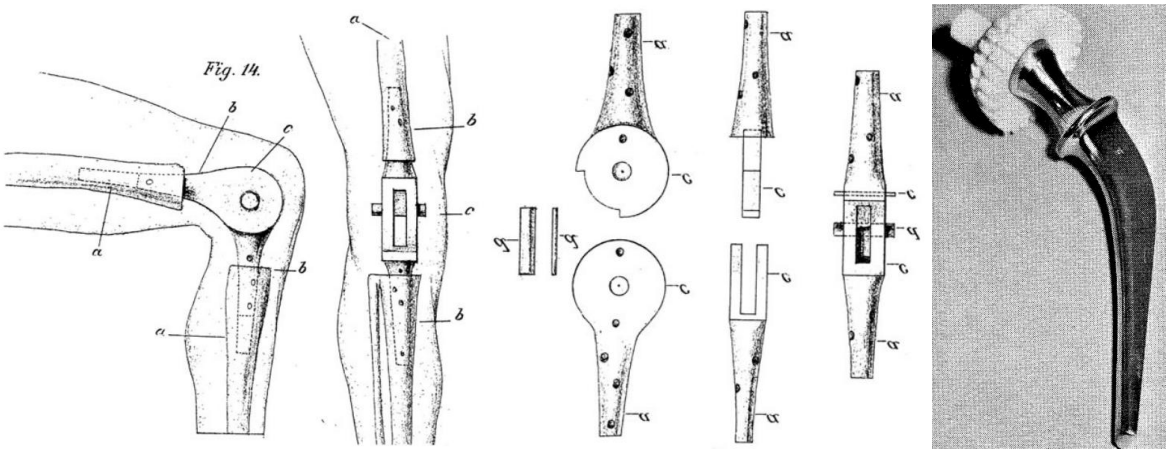

Fig. 2-1 Illustrations of joint replacement suggested by Glück (left) [14]; Charnley´s low-friction arthroplasty (right) [15].

Following Charnley's innovation, the field of joint replacement technology has undergone rapid evolution. Progress in surgical methodologies, implant geometry, and biomaterials [17] has markedly increased the longevity and performance of artificial joints. Initially, the concept was applied exclusively to hip and knee replacements. However, it has since been expanded to include other joints, such as the shoulder, elbow, ankle, and even smaller hand and foot articulations. The worldwide success of arthroplasty procedures has resulted in a continuous increase in implantations [2], driven by two factors. Firstly, the ageing population, and secondly, younger, more active patients seeking long-term mobility and pain relief. Total joint replacement is regarded as one of the most successful surgical procedures in medicine, with studies proving its effectiveness in restoring function and quality of life for millions of individuals each year.

Over several decades, research has progressively focused on understanding the complex interactions among mechanical loading, material wear, corrosion, and biological responses.

The development of new metallic alloys, ceramics, and polymeric materials is driven by the objective of enhancing biocompatibility and reducing wear complications, such as particle-induced osteolysis. Concurrently, surface engineering, coating technologies and advanced manufacturing techniques, including additive manufacturing, have engendered new possibilities for optimising implant design and customising surface properties to the physiological environment.

To present a comprehensive overview of current knowledge, the following sections (see Fig. 2-2) address the essential factors that influence the performance, reliability, and long-term success of artificial joint replacements.

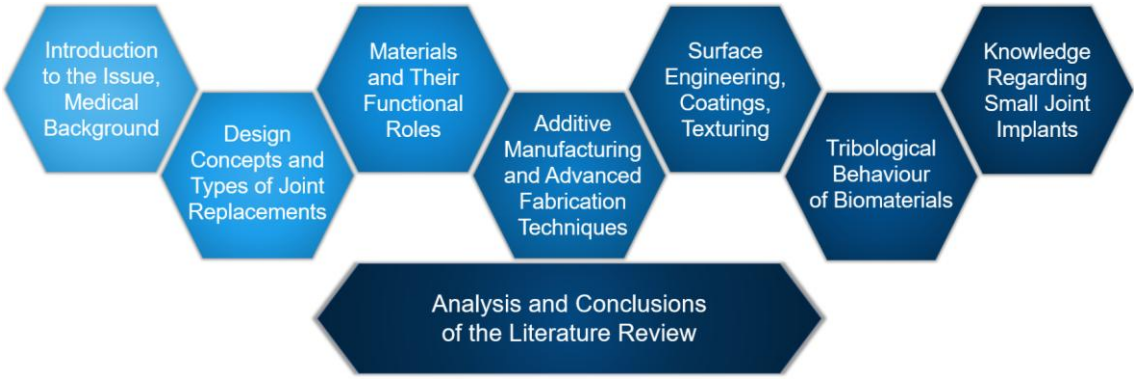

Fig. 2-2 Structure and thematic framework of the literature review.

As described in Section 2.1, the medical background and contextual framework are introduced, which are necessary for understanding the clinical and functional reasons for joint replacement. Section 2.2 discusses the fundamental design principles and categorises the main types of joint replacements currently in use, while Section 2.3 examines the materials employed in artificial joints and their specific functional roles within the articulating system. Section 2.4 explores advances in additive manufacturing and other contemporary fabrication techniques that facilitate greater customisation, enhanced mechanical integrity, and patient-specific optimisation of implant structures. The subsequent Section 2.5 examines surface engineering methodologies, including coatings and texturing strategies, designed to enhance both mechanical performance and biocompatibility. Section 2.6 provides an analysis of the tribological behaviour of biomaterials under physiological conditions, with particular attention to the complex interplay among friction, wear, and lubrication mechanisms. Section 2.7 provides a comprehensive survey of current knowledge regarding small joint implants. Despite their growing clinical relevance, these implants have received less extensive study compared to large joint replacements. Finally, Section 2.8 presents an analysis and synthesis of the reviewed literature, drawing key conclusions and identifying knowledge gaps that guide further research directions.

2.1 Introduction to the Issue, Medical Background

The human body is composed of numerous joints, which enable the performance of activities of daily living. Human joints are complex biomechanical structures that facilitate the transmission of loads, enable movement, and reduce friction between articulating surfaces. The structural integrity and lubrication mechanisms of these joints are important for maintaining pain-free mobility throughout life.

The human joints are susceptible to the development of the most common disease, known as osteoarthritis (OA), which is a degenerative joint disease that develops due to a number of possible causes, but is mainly associated with ageing, long-term mechanical loading, and genetic predispositions that lead to progressive alterations in the structure and composition of articular cartilage and subchondral bone [18]. Over time, the balance between cartilage synthesis and degradation is disrupted, leading to gradual cartilage thinning, increased joint friction, and the formation of osteophytes [19]. The disease most frequently affects weight-bearing joints, such as the knee (gonarthrosis) and hip (coxarthrosis), but it can also occur in the small joints of the hand and foot, the elbow, the spine, and, less commonly, the shoulder or ankle. A schematic overview of joints affected by osteoarthritis is depicted in Fig. 2-3.

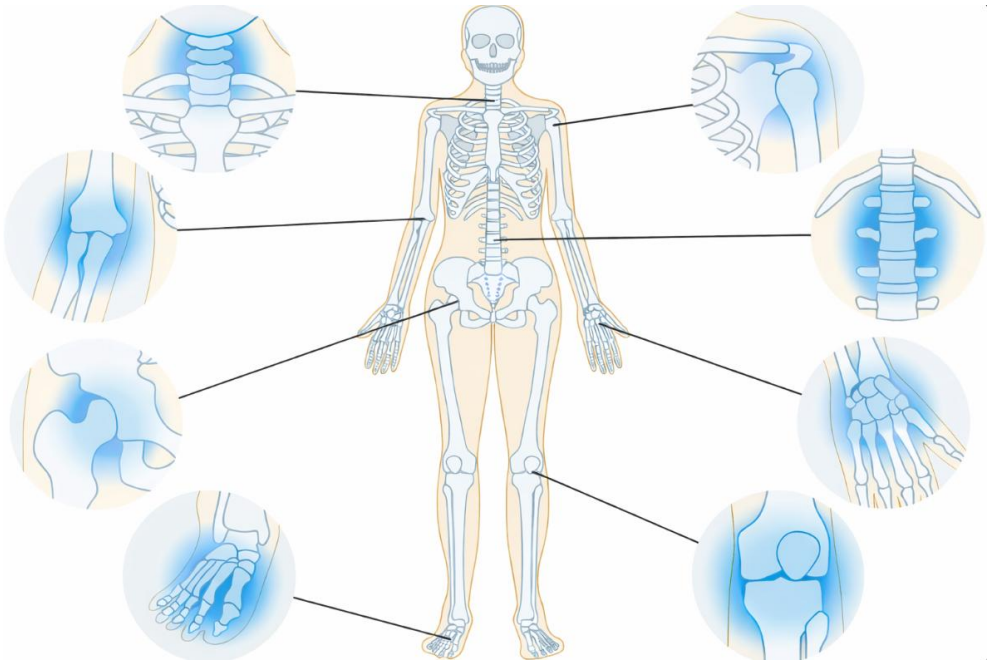

Fig. 2-3 Typical osteoarthritis locations in the human body (modified from [20]).

The progression of osteoarthritis is typically classified into five grades based on the Kellgren-Lawrence classification [21]. In the medical field, grade 0 indicates a healthy joint, free of signs of osteoarthritis. The presence of minimal cartilage wear, accompanied by minor osteophyte formation and an absence of joint space narrowing, is indicative of Grade 1. The presence of mild cartilage degradation, early subchondral

sclerosis, and joint space narrowing is indicative of Grade 2. In the case of Grade 3, there is evidence of moderate to severe cartilage loss, evident narrowing of the joint space, and more pronounced osteophytes. These symptoms are often accompanied by pain and stiffness. The fourth grade, the most advanced stage, is characterised by considerable cartilage destruction, bone remodelling, the presence of large osteophytes, and pronounced loss of joint function. In such cases, the need for surgical intervention, specifically joint replacement, is often identified. Furthermore, joints are also affected by other diseases, some of which are specific to certain joints, such as post-traumatic arthritis, avascular necrosis (AVN), rheumatoid arthritis (RA), and gout.

Osteoarthritis and other degenerative joint diseases are among the foremost causes of disability on a global scale. According to epidemiological data from the World Health Organisation (WHO) [22], osteoarthritis, a prevalent form of arthritis, affects more than 500 million people worldwide, with the hip and knee joints being the most commonly affected, driven by population ageing, obesity, and increased life expectancy. Although conservative interventions, including physiotherapy, pharmacotherapy for pain management, and intra-articular injections, have been shown to relieve symptoms in early stages of the condition, they frequently fail to restore function in advanced cases. Consequently, joint replacement surgery is regarded as the definitive solution for restoring mobility and alleviating pain. The evolution of joint replacement surgery has shifted the paradigm in the management of end-stage joint diseases, enabling the restoration of mobility and independence for millions of patients. The joints most frequently replaced are the hip, knee, and shoulder, followed by the ankle, elbow, and the smaller joints of the hand and foot.

2.2 Design Concepts and Types of Joint Replacements

The design of artificial joint replacements has advanced considerably over the past decades, driven by the growing demand for durable, functional implants that restore mobility and reduce pain in patients with joint diseases or trauma [23]. The success of a joint replacement depends on the ability to reproduce the natural kinematics of the replaced joint, withstand physiological loading conditions, and maintain long-term stability within the biological environment. Therefore, implant design combines principles of biomechanics, materials science, and surface engineering to achieve a balance between mechanical strength, wear resistance, and biocompatibility.

In general, joint replacements can be classified according to their design concept and mechanical constraint, with a focus on describing this in the context of a knee replacement [17]. Constrained designs restrict motion to ensure maximum joint stability and are typically used in cases of severe bone loss or ligament deficiency [24]. Semi-constrained systems allow partial freedom of movement while sustaining stability through the geometry of the components or supporting soft tissues [25]. Unconstrained

designs [26] provide the highest degree of mobility, closely resembling the kinematics of the natural joint and relying primarily on surrounding ligaments and muscles for stabilisation. The selection of the most appropriate design is contingent on patient-related factors, including, but not limited to, bone quality, age, and activity level.

Joint replacements also differ by the extent of reconstruction. Total joint replacements involve the substitution of both articulating components, thereby providing an entirely new bearing surface and load transfer mechanism. Conversely, partial or hemiarthroplasties involve the replacement of only one side of the articulating pair and are typically indicated when the opposite surface is intact. Surface replacements are considered a more conservative approach, as they preserve the majority of the patient's bone stock by resurfacing only the damaged articular surface. It is necessary to recognise these differentiations when assessing implant longevity, load distribution, and joint function preservation.

The geometrical configuration and component morphology of joint replacements are customised to replicate the anatomical and functional characteristics of the natural joint. For instance, spherical or hemispherical components are utilised in hip implants to replicate the ball-and-socket motion. Concurrently, more sophisticated geometries are necessitated for knee or shoulder joints, owing to their combined rolling and sliding kinematics. Modern design approaches use computational modelling and biomechanical simulations to optimise joint congruency, contact stress distribution, and the overall range of motion.

The following types of joint replacements may be encountered: metal-on-polymer (MoP), ceramic-on-ceramic (CoC), metal-on-metal (MoM), ceramic-on-polymer (CoP), ceramic-on-metal (CoM), and polymer-on-polymer (PoP). However, in contemporary practice, only three of these combinations are predominantly utilised: MoP, CoC, and CoP.

2.3 Materials and Their Functional Roles

The selection of materials for joint implants primarily depends on the implant design, which can be categorised into various configurations, including MoP, CoC, MoM, CoP, CoM, and PoP. According to this classification, implant materials can be broadly categorised into three main groups: metallic, polymeric, and ceramic. The metallic components of joint replacements are most commonly manufactured from cobalt-chromium, titanium, or stainless-steel alloys [27,28]. Among polymeric materials, UHMWPE remains the standard choice [29], although highly cross-linked polyethylene (HXLPE) [30] and polyether-ether-ketone (PEEK) [31] have gained increasing attention in recent years. In ceramics, alumina (Al_2O_3) and zirconia (ZrO_2) are the most widely used materials [32].

Each material group has a distinct functional role within the implant system. Metallic alloys form the structural core of most implants, providing mechanical strength, fatigue resistance, and load-bearing capability. Polymers such as UHMWPE act as articulating counterfaces, offering low friction and high wear resistance under lubricated conditions.

Ceramics, with their chemical inertness and extreme hardness, are primarily used in articulating pairs or coatings, where minimal wear and superior biocompatibility are required. In addition, fixation materials such as bone cements or bioactive coatings contribute to mechanical stability and promote osseointegration at the bone/implant interface.

Among metallic materials, cobalt-chromium alloys remain extensively used due to their excellent wear and corrosion resistance. However, titanium and its alloys have acquired prominence owing to their lower elastic modulus and superior biocompatibility. The Ti6Al4V alloy, with a modulus of approximately 110 GPa, exhibits the closest mechanical compatibility with cortical bone among metallic biomaterials. Nevertheless, the remaining modulus mismatch can still induce stress shielding [33], which may lead to bone resorption (osteolysis) and subsequent implant loosening due to insufficient bone-implant integration. The mechanism of stress shielding occurrence is depicted in Fig. 2-4. In the native bone (point 1), a load *F1* causes a displacement *ΔX1*. After adding a metal implant, both materials must deform equally. Because the implant has a higher elastic modulus, its displacement under the same load is smaller (*ΔX2*, point 2). The bone is therefore forced to match this reduced displacement (*point 3*), which lowers the load it actually carries to *F2*. According to Wolff's law, this decreased loading leads to bone resorption and may eventually cause implant loosening. Moreover, the presence of vanadium and aluminium in Ti6Al4V has raised concerns related to potential toxicity [33] and long-term biological safety.

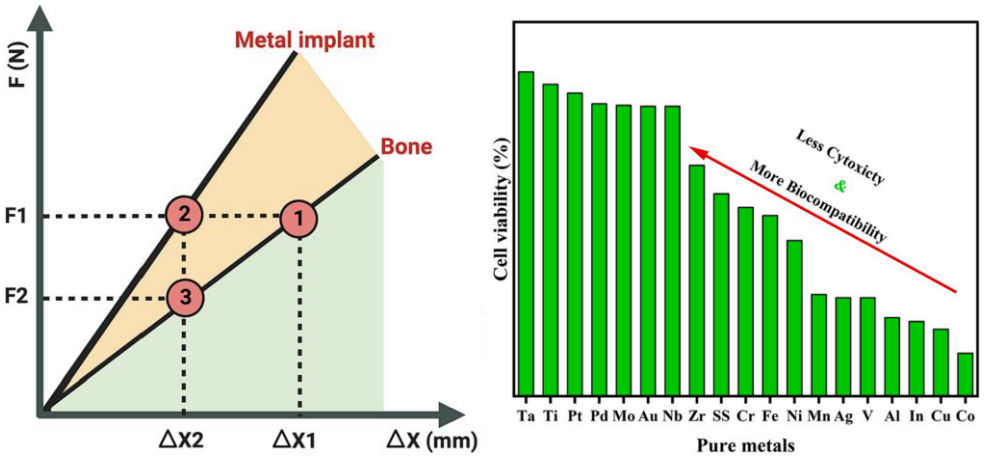

Fig. 2-4 The stress shielding effect (left), and the cell viability of pure metals (right) [33].

To address these issues, alternative titanium alloys [34–38], such as Ti–Nb–Zr–Ta–Si, Ti–15Zr–4Nb–4Ta, Ti–Nb–Zr–Ta–Si–Fe, Ti–24Nb–4Zr–8Sn, and Ti–Nb–Ga are being explored to improve osseointegration while reducing stress shielding and adverse biological effects. Nevertheless, when the wear values for β-Ti-Nb alloys are compared with those of Ti6Al4V, rather large differences can be observed (see Fig. 2-5), which Alberta et al. [34] assigned to differences in their microhardness, also, for these particulat materials,

it is clearly visible that Ti6Al4V ELI wear scars are somewhat separate grooves, while for other materials the wear scars are quite homogenous.

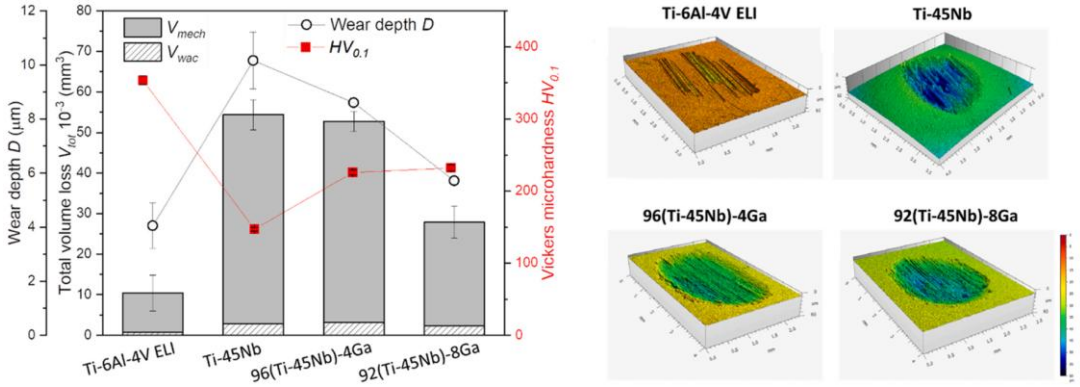

Fig. 2-5 Total volume loss (left), and wear scars (right) of different Ti-based alloys [34].

Beyond chemical composition, the microstructure of metallic alloys plays a decisive role in their mechanical and biological performance [39,40]. Control of the α/β-phase ratio, grain size, and crystallographic texture can tailor yield strength, fatigue behaviour, and corrosion resistance [41]. Surface oxide layers, especially the stable TiO_2 film on titanium alloys, provide natural passivation and enhance biocompatibility by supporting protein adsorption and cell adhesion [42]. Similarly, in ceramics, phase transformation toughening in zirconia or grain refinement in alumina can markedly improve fracture resistance and longevity [43,44]. For polymers, the degree of crosslinking and oxidation resistance determines the balance between wear durability and mechanical integrity, as demonstrated by the development of HXLPE [45].

Metallic biomaterials are also prone to corrosion and tribocorrosion in the physiological environment, where mechanical loading and electrochemical reactions interact [46,47]. The release of metal ions such as Co^{2+}, Cr^{3+}, or Ni^{2+} can cause inflammatory responses and contribute to periprosthetic osteolysis [48]. Therefore, corrosion-resistant alloy design and surface refinements, such as anodisation, nitriding, or coating with bioinert or bioactive films, are progressively employed to reduce these effects [49].

Porous, lattice-structured Ti6Al4V produced by Selective Laser Melting allows tailoring of stiffness for bone integration. Controlled porosity significantly affects mechanical behaviour and enhances *in vivo* osseointegration, as demonstrated in a rat femoral implantation study lasting up to 16 weeks [50]. Nevertheless, systematic animal studies verify that additively manufactured implants require surface treatments (acid etching, anodization, hydroxyapatite, UV activation, TiO_2 nanotubes, polydopamine, etc.) to improve osseointegration and avoid detachment of partially fused particles [51].

Recent advances in additive manufacturing have further broadened the possibilities for adjusting material microstructure and porosity. Titanium implants with controlled lattice architectures can closely mimic the stiffness of cancellous bone, improving load transfer

and enhancing osseointegration. At the same time, surface engineering and coating technologies, discussed in Section 2.5, provide additional opportunities to optimise frictional, chemical, and biological properties of the implant surface.

2.4 Additive Manufacturing and Advanced Fabrication Techniques

Additive manufacturing (AM) has appeared as a new method of production through multiple industries, offering new approaches to the production of individual components. This trend is also making its way into the domain of orthopaedic implants, where it offers multiple advantages, the most important of which are the ability to create patient-specific implants, simplification of construction [52], and reduced production costs. The most common additive manufacturing methods used in joint implants [53] are Selective Laser Melting (SLM), Selective Laser Sintering (SLS), Laser Direct Metal Deposition (LDMD), and Selective Electron Beam Melting (SEBM).

Additive manufacturing techniques differ in their energy sources, process atmospheres, and achievable precision. For instance, SLM and SEBM both enable the fabrication of dense metallic components. However, under different process conditions, SLM operates in an inert gas atmosphere with a laser source, while SEBM employs an electron beam under vacuum [54]. The choice of process directly influences the resulting microstructure, porosity, and residual stress levels in the component [55]. LDMD, in contrast, allows localised material addition or repair of existing parts, opening the possibility of multimaterial or functionally graded implants [56]. Each method, therefore, provides distinctive benefits but also poses challenges related to surface roughness, dimensional accuracy, and microstructural anisotropy.

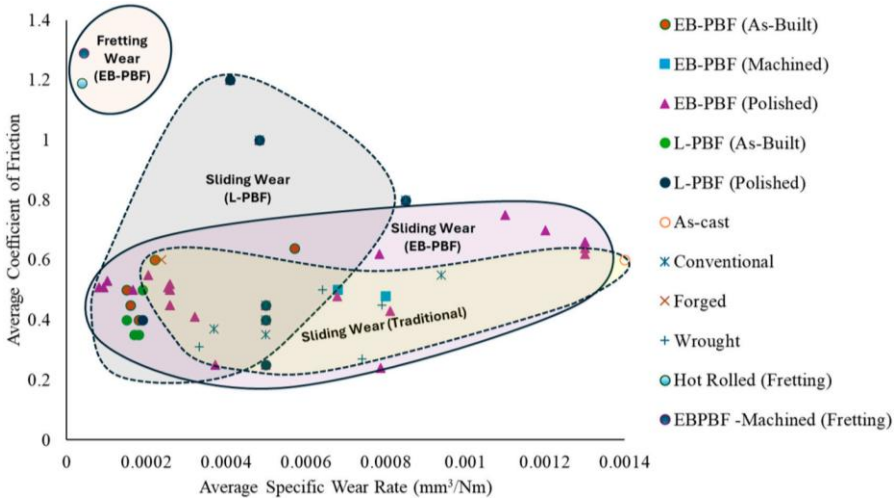

Fig. 2-6 Average CoF vs specific wear rate of EB-PBF, CM and L-PBF Ti6Al4V [56].

All of these methods present the creation of implants with optimised shapes, including lightweight, porous, or lattice designs. These parameters play a key role in the manufacturing process, aiming to achieve optimal mechanical properties and enhance biological response during osseointegration (bone ingrowth). When we move beyond the scope of this use, we will encounter the possibilities for the entire implant or the frictional surfaces. In these cases, 3D printing enables the creation of custom-made implants for specific patients or complex shapes that would not be possible with conventional methods. Moreover, if it were possible to overcome the worse tribological behaviour as opposed to conventional surfaces, we could simplify the design of the entire implant, for example, by reducing the number of parts used.

The microstructure of additively manufactured metals is typically characterised by rapid solidification and directional grain growth. In Ti6Al4V, additive manufacturing often yields fine acicular martensitic α′ phase, which increases hardness but may also reduce ductility [57]. Compared with wrought Ti6Al4V, which typically shows a lamellar α+β structure [58,59], AM variants often possess finer microstructural features, columnar prior-β grains, and higher defect density [59,60].

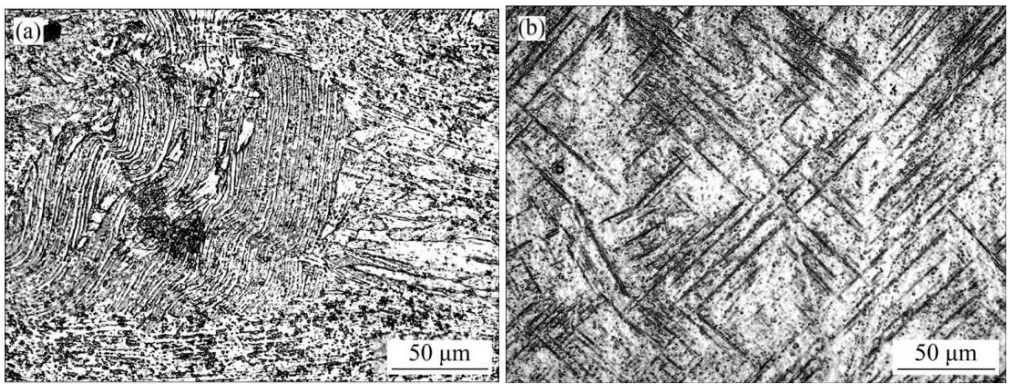

Fig. 2-7 Structural homogeneity of a) wrought and b) LPBF Ti6Al4V specimens [58].

Increasing laser power or slowing scan speed improves densification and hardness, but may also produce “depressions” and “highlands” due to melt-pool overlap [61]. Processing parameters such as line energy density, hatch spacing, and scan orientation strongly determine porosity, roughness, grain morphology, and mechanical anisotropy [62,63]. At the same time, localised remelting between layers can introduce heterogeneity and internal defects, such as lack-of-fusion zones or gas pores [56]. These microstructural features have a direct impact on the mechanical, corrosion, and tribological behaviour of printed alloys [64]. To improve mechanical integrity and surface quality, several postprocessing techniques are employed. Hot Isostatic Pressing (HIP) effectively reduces porosity and homogenises the microstructure, improving fatigue strength and corrosion resistance [64]. Thermal annealing transforms the metastable α′ phase into a stable α + β structure, optimising hardness and wear resistance [54]. Moreover, surface finishing operations, such as polishing, microblasting, or electrochemical polishing, are critical

for achieving the required tribological performance [56]. In recent studies, additional surface modification techniques, such as plasma nitriding, anodic oxidation, and diamond-like carbon (DLC) coatings, have been used to further enhance the wear and corrosion resistance of 3D printed Ti6Al4V alloys [65].

Bartolomeu et al. [66] and Goyal et al. [67] reported that the materials manufactured this way showed reduced wear compared to conventionally prepared samples. Fischer et al. [68] stated that, compared to conventionally manufactured Ti6Al4V, SLM-produced Ti6Al4V exhibits distinct electrochemical behaviour owing to its specific oxide layer and microstructure, which affect its corrosion resistance and protein adsorption. Similarly, Patel et al. [69] found that the CoCr30Mo6 alloy is more prone to degradation under combined mechanical and oxidative conditions, whereas Ti6Al4V shows greater durability, making it a more suitable material for load-bearing orthopaedic implants. Mechanically, AM Ti6Al4V often achieves higher hardness (20–40%), higher yield strength, and a unique combination of strength and ductility. LPBF Ti6Al4V showed ~32% higher hardness but slightly lower ductility than the wrought alloy [58]. Other studies revealed that AM martensitic microstructures can even fail at ~40% elongation, far above the ~6% typical of quenched wrought martensitic Ti6Al4V [59]. Build orientation significantly affects tensile properties and fracture modes [60,70]. Heat treatments (ageing, annealing, stress-relief) convert α′ martensite to α+β, precipitate Ti_3Al clusters, or reduce residual stresses, each altering friction, ductility, and corrosion response [71].

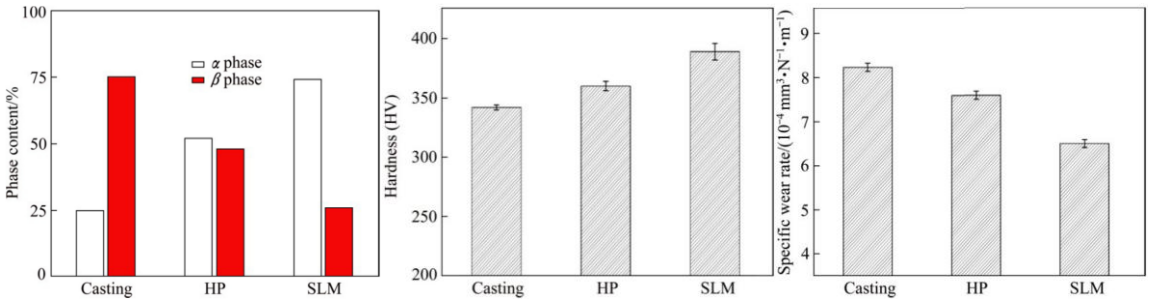

Fig. 2-8 Percentual contents of α and β phases (left), Vickers hardness (middle), Specific wear rate (right) for different methods of Ti6Al4V production [66].

Even with these advances, difficulties persist in obtaining consistent surface finish, reproducible mechanical behaviour, and predictable tribological response. Future research is expected to focus on *in situ* process monitoring, optimisation of printing parameters for surface integrity, and the development of hybrid additive–subtractive systems. These approaches could enable patient-specific implant geometries and functional surface architectures with customised frictional and corrosion properties suitable for long-term biomedical applications.

2.5 Surface Engineering, Coatings, and Texturing

Titanium alloys, most notably Ti6Al4V, are among the most widely utilised metallic biomaterials, owing to their superior strength-to-weight ratio, excellent corrosion resistance, and proven biocompatibility. However, under physiological conditions, their tribological performance is often inadequate, necessitating surface modification to improve frictional and wear behaviour [72]. In the context of contemporary implant design, surface engineering of metallic biomaterials, most notably titanium alloys, has consequently become imperative. In this case, the bulk material provides the mechanical strength and biocompatibility essential for load-carrying applications. Conversely, the surface exerts a key influence on the fundamental interactions with the biological environment, including friction, wear, corrosion, and protein adsorption [73].

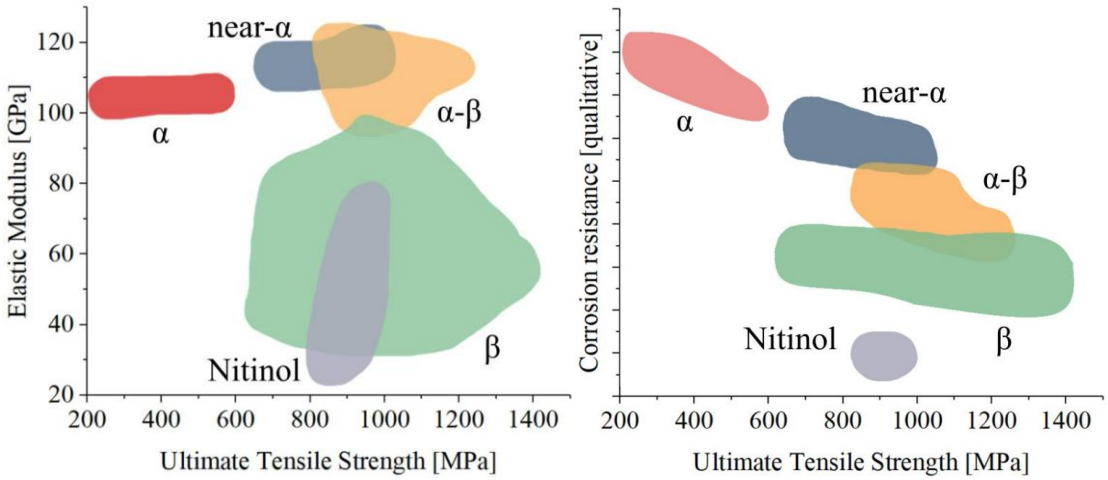

Fig. 2-9 Relationship between ultimate strength and elastic modulus (left) and between ultimate tensile strength and qualitative corrosion resistance (right) for titanium alloys commonly used in the biomedical field [73].

The primary strategies for surface modification encompass physical and chemical vapour deposition (PVD/CVD), ion implantation, thermal oxidation, and anodic oxidation, which are commonly enhanced by pre-treatments such as plasma nitriding or sand-blasting to improve adhesion and microstructure [74]. These methods aim to enhance hardness, reduce friction, and mitigate mechanical and electrochemical degradation while maintaining biocompatibility. Among the most widely studied surface refinements for titanium alloys are nitride-based coatings such as titanium nitride (TiN), which have been shown to markedly enhance wear resistance and reduce metallic ion release when applied to Ti6Al4V substrates. Recent research demonstrated that TiN coatings improved wear performance in a bovine serum environment and significantly reduced ion leaching from the underlying alloy [75]. Earlier studies also confirmed that TiN-coated implants exhibited favourable biocompatibility and low friction coefficients under lubricated conditions; however, challenges such as delamination, internal stress accumulation,

and increased UHMWPE counterface wear have been reported, underscoring the importance of coating quality, adhesion control, and process standardisation [76]. In addition to the utilisation of deposited coatings, substrate pre-treatments and surface chemistry modifications have been identified as pivotal factors in determining the ultimate tribological and biological performance of titanium alloys. Plasma nitriding, for instance, produces a bilayer structure composed of TiN and Ti2N phases with an underlying α-Ti(N) diffusion zone, resulting in enhanced hardness, improved fatigue resistance, and superior corrosion protection under physiological conditions [77]. More advanced techniques, such as plasma ion implantation, have been shown to refine the near-surface nanostructure, further increase wettability, and promote beneficial protein adsorption, all without affecting biocompatibility [78]. Furthermore, laser-based surface modification has emerged as an effective and controllable approach for improving the surface properties of titanium. Processes such as laser texturing, laser hardening, and laser nitriding can precisely tailor surface topographies, refine grain structures, and induce beneficial compressive residual stresses. These microstructural changes have been shown to enhance the substrate's resistance to fatigue and wear, thereby promoting enhanced coating adhesion and overall tribological stability under simulated body-fluid conditions [79].

Diamond-like carbon coatings have attracted notable attention as multifunctional surface treatments for titanium alloys in biomedical applications. Their unique amorphous structure, composed of both sp^2- and sp^3-hybridised carbon bonds, provides a combination of high hardness, low friction, chemical inertness, and biocompatibility. Typical hardness values range from 15 to 25 GPa, while the coefficient of friction can reach as low as 0.05 under lubricated conditions [80]. The smooth, chemically stable surface of DLC limits tribochemical reactions and inhibits corrosion-assisted wear of metallic substrates, which is notably favourable for load-bearing implants operating under mixed lubrication conditions. Recent studies have demonstrated that DLC coatings on Ti6Al4V can markedly reduce both friction and wear when tested in physiological lubricants such as simulated synovial fluid or artificial saliva. Madej et al. [81] reported that plasma-assisted chemical vapour deposition (PACVD) DLC films on Ti6Al4V exhibited a substantial improvement in tribocorrosion resistance, with a lower corrosion current density and a higher open-circuit potential compared to the uncoated alloy. Similarly, Jędrzejczak et al. [82] found that Si-doped DLC coatings maintained low friction and wear rates in protein-rich environments, confirming their chemical and mechanical stability under simulated body-fluid conditions. These findings correspond with those of Li et al. [83], who showed that DLC coatings effectively suppress metallic ion release and mitigate surface oxidation during tribological contact. Despite their excellent performance, DLC coatings face lasting challenges in biomedical use. High internal stresses, typically generated during energetic deposition techniques or magnetron sputtering, can induce microcracking or delamination, particularly on metallic substrates with differing thermal expansion coefficients. Poor adhesion between DLC and Ti6Al4V has been widely recognised as a major limitation [80].

To address this, interlayers are often introduced to create a graded interface and improve adhesion strength, as demonstrated by Joska et al. [84], who achieved significantly improved coating durability using Ti and Cr buffer layers. Furthermore, recent advances have focused on doped and composite DLC films, such as Ti-DLC, Si-DLC, and Ag-DLC, which enhance adhesion, reduce residual stresses, and bring additional functionalities, such as antibacterial activity or improved hemocompatibility [85].

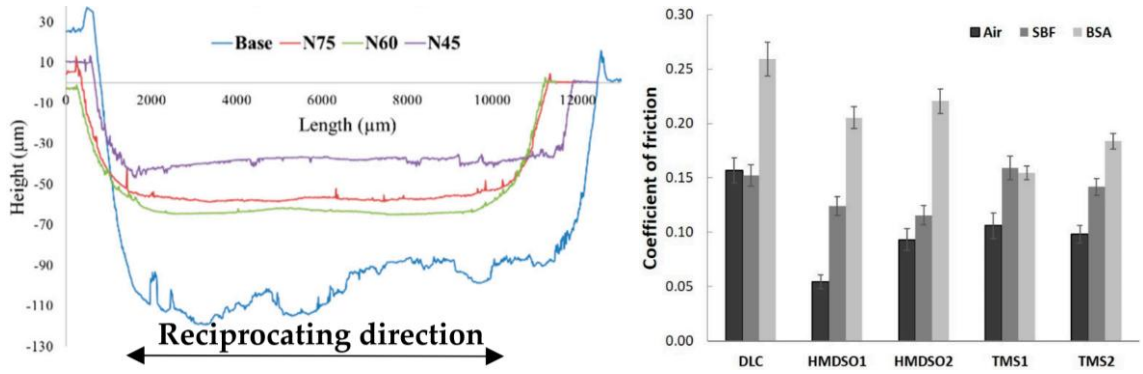

Fig. 2-10 Longitudinal wear profile of titanium nitrided at different speeds(left) [79], CoF of silicon-incorporated DLC (right) [82].

Beyond coatings, surface treatments that modify surface chemistry and microstructure are just as important. Among these, surface texturing has been established as a highly effective approach to improve the functional performance of titanium alloys used in biomedical implants. By introducing well-defined micro- and nano-scale features, surface texturing can directly influence friction, wear, lubrication, and biological interactions occurring at the interface between implant and surrounding tissues. Unlike coatings, which alter surface chemistry, texturing modifies the topography itself, thereby controlling how the surface interacts with both lubricants and biological fluids during articulation. Experimental research on Ti6Al4V has demonstrated that micro-textured surfaces, especially those containing dimples or grooves, can act as micro-reservoirs for lubricants under mixed or boundary lubrication regimes, markedly reducing contact pressure and friction. Lin et al. [86] showed that micro-dimp patterns on Ti6Al4V surfaces facilitated lubricant entrainment and reduced wear by up to 30% compared with polished samples under simulated joint conditions. Similar findings were reported by Woźniak et al. [87], who found that laser-textured Ti6Al4V ELI alloys exhibited lower friction coefficients and improved wear resistance in reciprocating motion tests under physiological lubrication.

Laser-based technologies have become especially suitable for producing precise and reproducible textures on complex implant geometries. Femtosecond and picosecond laser texturing enable the creation of periodic micro- and nano-structures, often referred to as laser-induced periodic surface structures (LIPSS), that can improve both tribological and biological performance. Schweitzer et al. [88] demonstrated that LIPSS formed on Ti6Al4V and Ti6Al7Nb alloys enhanced osteoblastic activity and surface wettability while maintaining mechanical stability. Choudhury et al. [89] showed that micro-dimple

textures significantly increase lubricant film thickness and accelerate hydrodynamic film formation in artificial hip joints, and that square-dimple patterns produce faster, thicker films than triangular arrays and result in fewer surface scratches under serum lubrication. Mechanically fabricated micro-dimples on Ti6Al4V surfaces improve wettability and reduce friction under synovial-like lubrication [90]. Texture densities of 10–40% maximise hydrodynamic pressure and film thickness in hard-on-soft bearings according to soft-EHL modelling [91]. Micro-textures act as lubricant reservoirs and debris traps, reducing polyethylene wear and delaying transition to boundary lubrication.

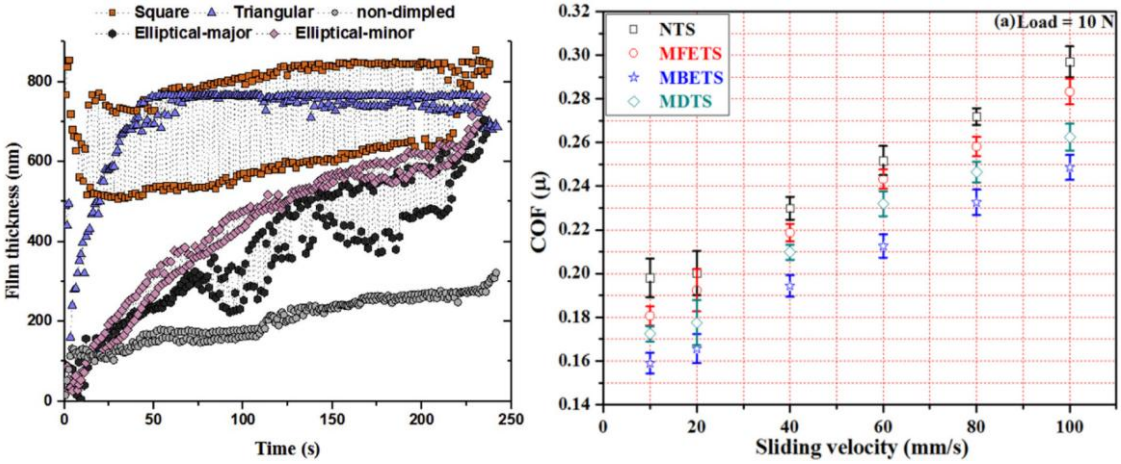

Fig. 2-11 Lubricant film thickness for different texture shapes (left) [89], CoF for different types of surfaces (NTS – non-textured, MFETS – micro flat-end textured, MBETS – micro ball-end textured, MDTS – micro-drill textured) (right) [90].

Laser polishing reduces roughness by 80–90%, eliminates surface pores, and improves both wear and corrosion resistance [92,93]. Micro-arc oxidation produces a ceramic TiO_2 layer that doubles hardness and greatly improves fretting resistance [94]. Laser-deposited Nb and Ti-13Nb coatings enhance hardness, passivation, and SBF corrosion resistance, outperforming the base alloy [95]. Additional modifications, plasma nitriding, CrN/CrNiN coatings, and laser shock peening, further refine surface integrity and anisotropy. Overall, the complete data set reinforces that processing path, microstructure control, surface engineering, and environment collectively dictate the mechanical, tribological, corrosive, and biological performance of Ti6Al4V. When properly processed and surface-treated, AM Ti6Al4V meets or exceeds the performance of wrought alloys in nearly all relevant categories [93,94].

Despite these advances, fabricating multiscale textures on complex implant geometries remains challenging, particularly in terms of process repeatability, residual stress control, and long-term mechanical stability. Future developments are therefore expected to focus on hybrid strategies that combine laser-generated textures with protective coatings. For example, applying DLC or TiN coatings to laser-textured Ti6Al4V substrates can enhance lubricant retention, delay coating failure, and reduce overall wear rates [96].

2.6 Tribological Behaviour of Biomaterials

The tribological behaviour of biomaterials [97] plays a key role in determining the long-term performance and reliability of load-bearing implants. Friction, wear, and lubrication mechanisms at the articulating interfaces directly influence implant stability, the generation of wear debris, and the biological response of surrounding tissues. Understanding these processes requires not only a mechanical description of contact interactions, along with an appreciation of the complex biochemical environment in which they occur. Factors such as surface topography, hardness, microstructure, and the presence of body fluids or synovial components strongly affect the formation and stability of lubricating films. Therefore, tribological evaluation of biomaterials provides essential knowledge of how material combinations, surface modifications, and environmental conditions contribute to the overall functional longevity.

Under dry friction, AM Ti6Al4V shows adhesive–abrasive–oxidative wear, with wear rates strongly governed by hardness and microstructure [94,98]. Studies against Al_2O_3, WC-Co, and cemented carbide consistently show that AM alloys form protective oxide tribolayers at higher loads or temperatures, reducing both wear and friction [59,94]. Diffusion wear and tungsten-oxide self-lubrication were observed in Ti6Al4V vs carbide contacts at elevated temperature.

Lubrication mechanisms in biological applications differ significantly from those in conventional engineering. For the joint implants, we encounter a highly complex problem, as the joints in the human body are lubricated by synovial fluid (SF), a complex non-Newtonian fluid containing numerous biomolecules, such as albumin, γ-globulin, phospholipids, hyaluronic acid, and lubricin, which may affect its behaviour under certain conditions. Researchers who are trying to describe the behaviour of joint implant frictional surfaces have historically used different types of lubricants to mimic the behaviour of real synovial fluid, as working with the real one is not simple due to the limited amount available for extraction from patients. Numerous studies began with phosphate-buffered saline (PBS), some used bovine calf serum (BCS), which also shows non-Newtonian behaviour [99], and the most reliable option is to prepare a synthetic model synovial fluid (M-SF) based on the composition [100] of the real SF. Based on the conditions under which the joint implants can operate, we can encounter several lubrication mechanisms. In the context of rapid articulation, the predominant lubrication mechanisms [101] are hydrodynamic (HD) and elastohydrodynamic (EHL). In addition to these two, under certain conditions, especially with high load or slow motion, the predominant lubrication mechanism is boundary lubrication.

Bovine serum, commonly used as a synovial fluid analogue, exhibits shear-thinning behaviour and a strong, thermally dependent viscosity similar to that of human SF [102]. Under high pressures, serum forms speed-independent thin films of roughly 40–50 nm due

to multilayer protein adsorption [103]. Even under static load, residual boundary films of 9-19 nm persist, protecting low-motion phases. Accurate tribological testing, therefore, requires physiological temperature, shear rates, and clinically relevant lubricant chemistry [102]. The choice of lubricant diluent (PBS vs deionised water) significantly influences protein degradation and can alter polyethylene wear rates by more than a factor of two [104].

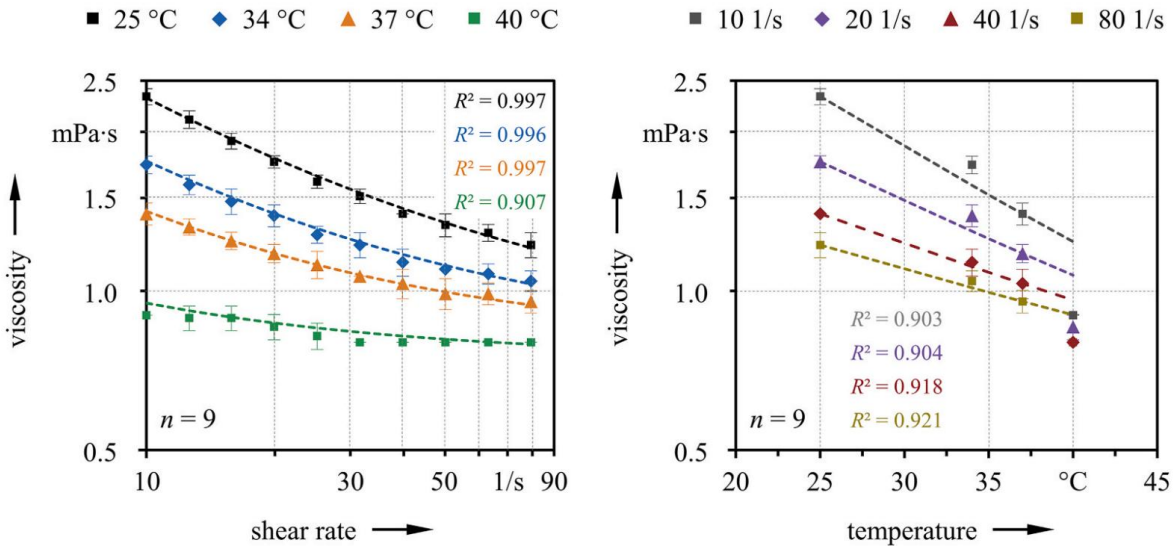

Fig. 2-12 BSA viscosity vs shear rate (left) and viscosity vs temperature (right) [102].

A fundamental discovery in this area was the research conducted by Myant, Cann and their group [105–108], who showed the necessity of conducting the experiments connected to joint implants with lubricants as close as possible to the real SF, as they proposed and described a novel lubrication mechanism typical for these particular problems, called Protein Aggregation Lubrication (PAL). This mechanism is typical for lubricants containing biomolecules, especially proteins, as it is based on the formation of a protein-rich, high-viscosity phase of aggregated molecules at the inlet of the contact area. The PAL was also later analytically modelled [109], based on classical EHL lubrication theory, supplemented by a protein-concentration-dependent constitutive equation for fluid viscosity.

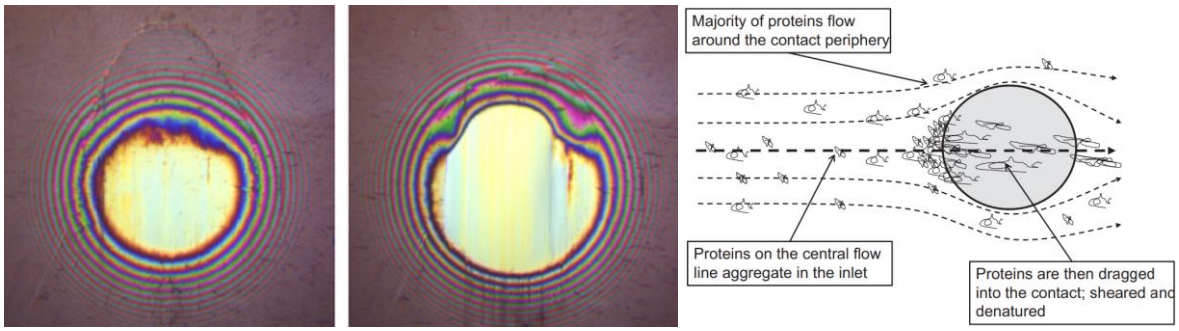

Fig. 2-13 Optical interference images at a relative speed of 10 and 50 mm/s with visible protein-rich inlet region (left); Sketch of contact flow lines (right) [108].

Natural joint lubricant (synovial fluid) comprises proteins (e.g., albumin, γ-globulin), glycoproteins (e.g., lubricin), phospholipids, and high molecular-weight hyaluronic acid, which are known to adsorb onto implant surfaces, forming thin boundary layers that strongly influence friction and wear in synovial environments [110]. The structure and effectiveness of these films depend on the relative concentrations of albumin and γ-globulin, which can either stabilise or destabilise boundary lubrication. These molecular layers reduce direct asperity contact and friction, enabling boundary or mixed lubrication regimes depending on load, sliding velocity, fluid viscosity, and contact kinematics. The effectiveness of such boundary films depends on the ability to form, maintain, and regenerate under motion. However, mechanical shearing or denaturation of lubricant components may degrade the film, reducing its stability and increasing wear rates. It is therefore essential for *in vitro* tests to replicate realistic synovial fluid composition and rheological behaviour to obtain physiologically relevant tribological results. Therefore, it is important to understand each SF constituent's behaviour well in order to describe the behaviour of the whole SF, as demonstrated by Nečas et al. [111]. In the following study by Nečas et al. [112], the direct behaviour was incorporated into the individual constituents. It was found that γ-globulin and hyaluronic acid (HA) form a thin yet highly stable and uniform boundary layer, whereas the subsequent increase in film thickness is mainly due to albumin, which forms alternating layers. Phospholipids may further modify these interactions, reducing wear only under protein-rich conditions but increasing it under protein-poor conditions [110]. During sliding, these proteins can denature into β-sheet-rich, gel-like films that intermittently contact the surface and act as a viscous, load-bearing phase, substantially reducing wear [110]. In polymeric bearings such as UHMWPE, proteins can also increase friction and wear by shifting the mechanism from abrasive to adhesive [113].

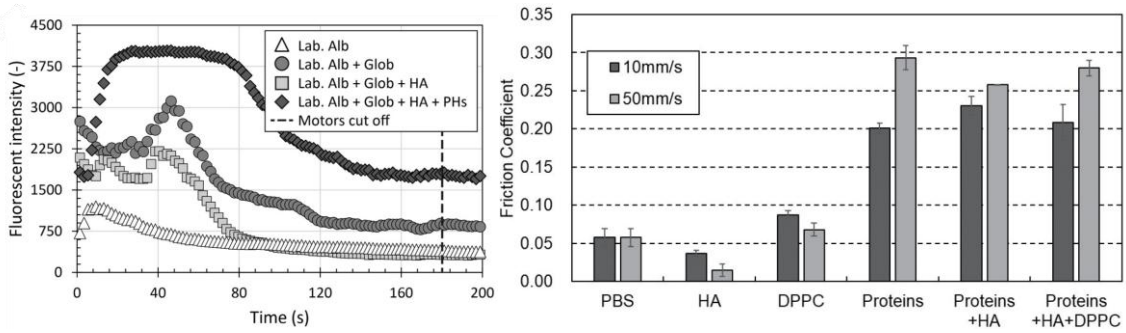

Fig. 2-14 Development of fluorescence intensity (with marked albumin) for lubricants with the addition of SF components (left) [112], Average values of CoF for lubricants containing different components of SF(right) [113].

Friction and wear in biomaterials originate from complex mechanical interactions at the interface between contacting surfaces. Under repeated cyclic loading and micro-motions typical of joint replacements, multiple wear mechanisms may act simultaneously, including adhesive, abrasive, fatigue, and tribochemical wear [114]. Adhesive wear emerges from localised bonding and subsequent tearing or removal

of asperities [115], whereas abrasive wear is driven by hard particles or counterface asperities ploughing or cutting the surface. Fatigue wear results from repeated stress cycles, causing subsurface cracks and delamination or spallation of material layers [116]. The balance between these mechanisms depends on the mechanical properties of the contacting materials, such as hardness, elastic modulus, yield strength, or viscoelastic behaviour in polymers, which govern their resistance to plastic deformation and material removal. For metallic biomaterials, higher ductility or adhesion may increase the tendency for material transfer or ploughing; in contrast, ceramics tend to behave in a brittle manner and may fracture under contact stresses.

In addition to these classical mechanisms, tribochemical wear, driven by reactions between the material and its environment, is particularly relevant in physiological conditions. The synergistic interaction between mechanical wear and electrochemical corrosion, known as tribocorrosion [47], may result in the release of metallic ions and the formation of surface oxides, thereby influencing both wear rate and biological response. Surface treatments such as anodisation, nitriding, and deposition of bioinert or bioactive coatings have been shown to reduce tribocorrosive degradation by stabilising surface chemistry and minimising ion release.

In biological and oxidising environments, AM Ti6Al4V exhibits high corrosion resistance due to a stable TiO_2 film. However, passive currents are sometimes slightly higher than those of wrought alloys due to martensitic stress [58]. In seawater, Ti6Al4V outperforms stainless steel 316L in resisting combined wear–corrosion and shows lower wear loss, despite TiO_2's lower wear resistance compared to Cr_2O_3 [117]. Tribocorrosion in seawater accelerates corrosion currents by three orders of magnitude relative to static exposure and increases wear rates. Similar tribocorrosion synergies appear in PBS, SBF, and albumin-containing media, where LPBF Ti6Al4V (as-built, stress-relieved, annealed) consistently exhibits ~30–40% lower total volume loss than conventional alloys under OCP and potentiostatic conditions [118]. Annealing especially improves oxide stability in corrosive media.

Modern tribological studies increasingly employ *in situ* techniques such as atomic force microscopy (AFM) nanotribometry, Raman spectroscopy, and fluorescence imaging to visualise film formation and protein adsorption at the micro-scale. These methods, combined with numerical simulations of contact mechanics and lubrication, enable correlation of film thickness, viscosity distribution, and shear stress with frictional behaviour under physiological conditions. Furthermore, bioinspired lubrication strategies [119] that replicate natural cartilage lubrication (e.g., phospholipid–hyaluronan complexes or polymer brushes) are being developed to engineer surfaces with superior boundary film stability and self-healing properties.

2.7 Knowledge regarding small joint implants

In the context of small joint implants, particularly those of the first metatarsophalangeal (1.MTP) joint, the extant knowledge in this field remains comparatively limited across the literature. A wide range of implant designs have been utilised historically [120], including silicone double-stemmed flexible hinges, metallic hemiarthroplasties, and MoP total replacements. The most prevalent configuration of this implant, the MoP total replacement, which also serves as the focal point of the present research, closely resembles the design principles of the hip joint implant, as both systems represent ball-and-socket articulations. However, the main differences lie in the significantly smaller size, lower overall contact pressures, and reduced contact area of the 1.MTP joint, which together create a distinct biomechanical and tribological environment.

The first metatarsophalangeal joint plays a key role in ensuring optimal gait mechanics, weight distribution, and push-off during walking. Degenerative diseases such as hallux rigidus, trauma, or rheumatoid arthritis can considerably impair its function, leading to pain, stiffness, and restricted mobility [121]. In cases where conservative treatment has failed, arthroplasty of the 1.MTP joint can be considered as a surgical intervention to restore motion and alleviate pain [122,123]. Compared with larger joints, such as the hip or knee, implants for smaller joints are subjected to significantly lower loads. However, they are exposed to higher localised stresses and more complex, multidirectional motions. This makes the biomechanical and tribological optimisation of such implants challenging.

The earliest 1.MTP joint implants were silicone spacers, first introduced in the 1960s. These were primarily designed to act as flexible hinges that maintain joint space and reduce pain, rather than fully reproduce physiological kinematics [124]. Although silicone implants initially showed success, long-term follow-up studies have reported high rates of implant fracture, deformation, and synovial membrane inflammation due to silicone debris [125]. Subsequent generations of designs incorporated metallic components, including stainless steel, cobalt chromium-molybdenum alloys, and titanium alloys. These components are often used with UHMWPE bearings, therefore enhancing wear resistance and overall mechanical stability. Recent approaches have also explored the use of pyrolytic carbon and ceramic materials, which more closely approximate the elastic modulus and tribological characteristics of natural cartilage. The aim of this is to achieve smoother articulation and improved load transfer [126].

From a biomechanical and tribological perspective, the 1.MTP joint exhibits complex motion that combines dorsiflexion, plantarflexion, and minor rotational components. The contact area is relatively small, and the lubrication regime is believed to be predominantly boundary or mixed, given the limited synovial fluid volume and low sliding speed during normal gait. For instance, the passive dorsiflexion range and sagittal-plane kinematics of the 1st MTP have been examined in relation to gait patterns

[127,128]. These conditions leave the joint particularly susceptible to micro-motion, third-body wear, and localised surface damage. Titanium alloys, most notably Ti6Al4V, have attracted notable attention; however, they exhibit comparatively lower wear resistance under sliding conditions. A recent study found that conventional Ti6Al4V did not form a sufficient lubrication film in small joint conditions and suffered surface damage. The tribological performance of surfaces can be enhanced and the risk of fretting and corrosion reduced through surface modifications such as texturing, anodising, and the application of hard coatings (TiN, DLC) [129]. UHMWPE remains the most common bearing material, though oxidative degradation and fatigue wear can occur under repeated micro-movements, leading to particle release and potential osteolytic reactions. A study of the tribological behaviour of UHMWPE in contact with Ti6Al4V has indicated the potential for wear in this combination [130].

The clinical outcomes of 1.MTP arthroplasties exhibit considerable variability, contingent on implant design, fixation method, and patient-specific factors. While silicone implants remain an option for patients with low demand, metal-polymer and pyrocarbon systems have been shown to exhibit superior mechanical integrity and greater physiological mobility. Nevertheless, complications such as loosening, subsidence, malalignment, and wear-induced osteolysis continue to limit long-term success rates. Recent studies have emphasised the importance of understanding the interplay between mechanical wear, corrosion, and lubrication breakdown at the articulating surfaces, particularly in the context of mixed tribocorrosion mechanisms that may accelerate material degradation [131].

2.8 Analysis and Conclusions of the Literature Review

The reviewed literature provides a comprehensive, multidimensional overview of the current state of knowledge regarding joint replacement technology, the tribological behaviour of biomaterials, the additive manufacturing of metallic implants, and the specific biomechanical and lubrication challenges associated with small joint arthroplasty. Historically, joint replacement has evolved from early concepts introduced in the late 19th century employing rudimentary materials such as ivory [14], through the technological breakthrough of Charnley's low-friction arthroplasty in the 1960s [15,16], to the modern era characterised by advanced biomaterials, computationally optimised designs, and improved long-term outcomes [17]. Although these advancements have been made, the literature consistently emphasises that the functional success of any joint replacement remains tightly bound to the relationship between mechanical loading, wear, corrosion, lubrication mechanisms, and the biological response of the surrounding tissues.

A significant outcome of the review is the recognition that joint replacements must be evaluated not only in terms of their geometry and load-transfer capability, but also in light of the tribological demands of the articulating surfaces. Various implant configurations: metal-on-polymer (MoP), ceramic-on-ceramic (CoC), metal-on-metal

(MoM), ceramic-on-polymer (CoP), and others have been employed throughout the evolution of arthroplasty [23–26]. Nevertheless, the literature shows that only a limited number of these bearing combinations are used clinically today, primarily MoP, CoC, and CoP, due to their favourable balance of friction, stability, and biocompatibility. Successful implant design relies on replication of natural joint kinematics, adequate constraint, and minimisation of contact stresses, with patient-specific factors such as age, bone quality, and activity level playing important roles [17,24–26].

The material selection for modern implants remains centred around three major groups: metallic alloys, polymeric materials, and ceramics [27–32]. Titanium alloys, most notably Ti6Al4V, are widely used due to their favourable mechanical properties, biocompatibility, and relatively low elastic modulus, which is closer to that of bone than that of other metals. Nonetheless, the literature highlights significant limitations, including stress-shielding effects [33], concerns regarding aluminium and vanadium toxicity [33], and susceptibility to tribocorrosion under physiological conditions [46–48]. These findings motivate the investigation of alternative titanium alloy compositions [34–38], microstructural optimisation [39–41], and surface modification strategies [49].

Additive manufacturing (AM), especially methods such as selective laser melting (SLM), selective electron beam melting (SEBM), and laser direct metal deposition (LDMD), has significantly expanded the design possibilities for orthopaedic implants, providing complex geometries, lattice structures, and patient-specific solutions [21,52–56]. However, AM Ti6Al4V exhibits a unique martensitic α′ microstructure [57], anisotropic grain morphology [59–63], higher defect concentration [62–63], and characteristic surface roughness due to melt-pool overlaps and partially fused particles [61]. These microstructural and surface features influence mechanical properties, corrosion behaviour, protein adsorption, and tribological response [54,59–64,68,69]. Although postprocessing techniques such as hot isostatic pressing (HIP), annealing, polishing, microblasting, or electrochemical polishing can improve densification, ductility, and surface integrity [54,56,64], the literature consistently notes that as-built AM surfaces often display inferior tribological performance without additional modification [56,65].

Among the numerous surface engineering strategies investigated, nitride-based coatings (e.g., TiN) have shown significant improvements in wear resistance and reduced ion release in lubricants containing proteins [72–76]. Plasma nitriding, plasma ion implantation, and anodic oxidation generate hardened diffusion layers, promote beneficial residual stresses, and improve corrosion resistance [74,77,78]. Diamond-like carbon (DLC) coatings exhibit excellent hardness, low friction coefficients (down to ~0.05 under lubrication), chemical inertness, and favourable biocompatibility [80–83]. The literature also documents challenges associated with DLC, including internal residual stresses and adhesion issues, which may require the introduction of interlayers such as Ti or Cr to improve coating durability [84,85].

Beyond coatings, surface texturing has been established as a key strategy to improve lubrication and wear resistance. Micro- and nano-scale textures, including dimples, grooves, and laser-induced periodic surface structures (LIPSS), can act as lubricant reservoirs, reduce contact pressures, and enhance hydrodynamic and mixed lubrication in joint-like conditions [86–91]. Studies show that laser polishing can reduce surface roughness by up to 90% and improve corrosion and wear resistance [92,93]. At the same time, micro-arc oxidation produces a TiO_2 layer that significantly improves fretting resistance [94]. Additional laser-deposited Nb or Ti-Nb coatings demonstrate improved passivation and tribocorrosion resistance [95]. Taken together, the literature confirms that the combination of AM processing, microstructure control, and suitable surface modification can improve the overall mechanical, corrosion, and tribological performance of Ti6Al4V, possibly exceeding that of conventionally manufactured alloys [93,94].

A key theme of the review is the complexity of lubrication in artificial joints. Synovial fluid (SF) is a non-Newtonian, protein-rich medium composed of albumin, γ-globulin, lubricin, hyaluronic acid, and phospholipids [99–111]. Its behaviour differs fundamentally from that of engineering lubricants, with the formation of ultrathin boundary layers and protein-based films dominating friction and wear. A significant contribution of recent research is the Protein Aggregation Lubrication (PAL) mechanism proposed by Myant, Cann, and colleagues [102–106], which demonstrates that protein aggregation at the inlet of the contact zone can generate a highly viscous, load-bearing film not predicted by classical hydrodynamic lubrication theory. Research additionally shows that γ-globulin and hyaluronic acid form stable, uniform boundary layers, while albumin contributes to film thickness via multilayer adsorption [107–109]. Depending on biochemical conditions, phospholipids may either enhance or diminish lubrication [109]. However, under low motion or high load, boundary lubrication dominates, and proteins may denature into β-sheet-rich gel-like films that provide local load support but may also increase wear in polymeric materials such as UHMWPE [110].

Finally, the review underscores distinctive challenges associated with small joint implants, particularly those of the first metatarsophalangeal joint. Compared to larger joints, 1. MTP implants undergo lower absolute loads but higher localised stresses, small contact areas, limited lubricant volume, and complex movement combining dorsiflexion, plantarflexion, and rotational components [121–128]. The lubrication regime is therefore predominantly boundary or mixed, and Ti6Al4V surfaces may fail to form sufficiently stable lubricating films under these conditions, leading to surface degradation and increased friction. Wear mechanisms such as adhesive wear, third-body abrasion, fretting, and tribocorrosion are particularly relevant. The literature further indicates that UHMWPE, despite being the most common bearing material, is susceptible to oxidative and fatigue wear, which can generate wear particles and trigger osteolytic reactions [129–130]. Complications such as loosening, subsidence, and wear-induced osteolysis remain significant issues in the clinical performance of small joint implants [131].

To summarise, the literature identifies a clear research gap concerning the behaviour of additively manufactured Ti6Al4V surfaces in the tribological environment of small joints. While numerous studies address AM microstructures, surface engineering techniques, and lubrication mechanisms, very few investigate how the inherent surface morphology and the subsurface microstructure formed by AM influence protein adsorption, lubrication stability, friction, and wear in boundary-dominated conditions typical of the 1.MTP joint. This gap provides a strong justification for continued experimental research to determine whether AM micro- and nanoscale features can serve as beneficial surface textures and how additional surface treatments may enhance tribological performance under physiologically relevant conditions.

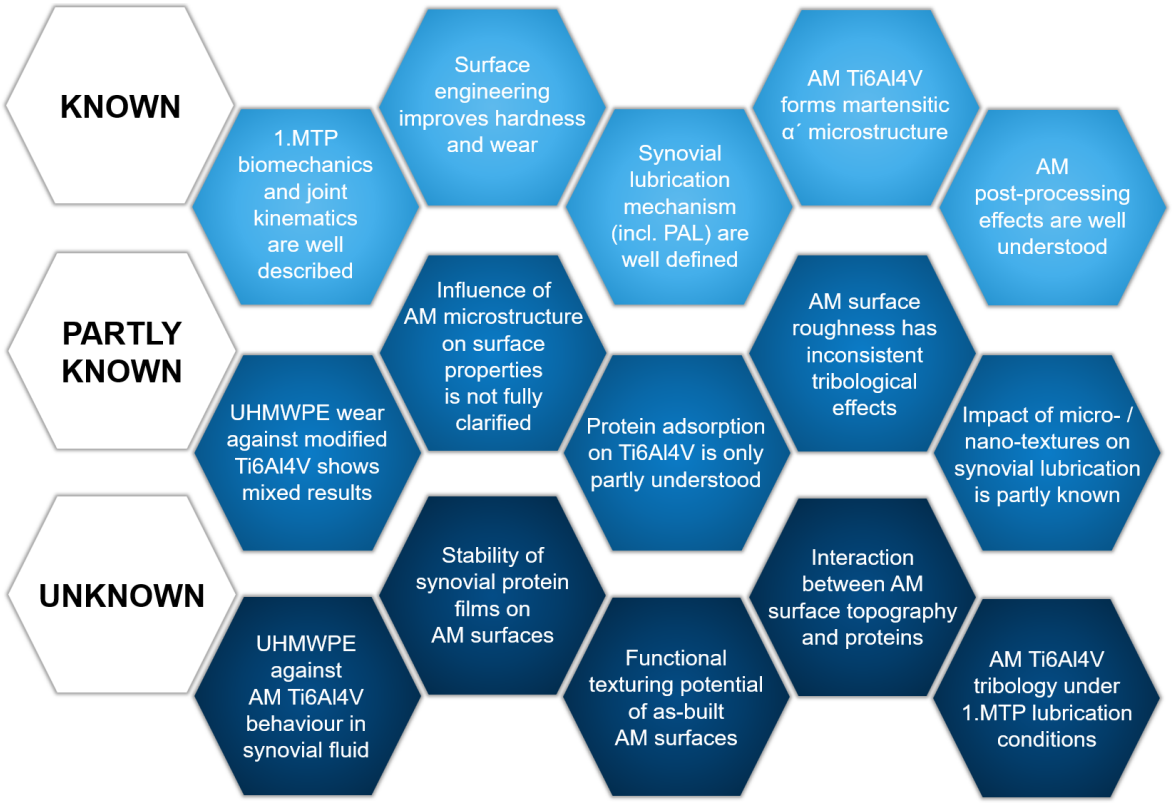

Fig. 2-15 Graphical overview of the current state of knowledge.

2.9 Identified Knowledge Gaps

Based on the comprehensive literature review and its subsequent analysis, several critical knowledge gaps have been identified regarding the tribological behaviour of small joint implants manufactured by additive technologies. These gaps highlight areas where existing research is insufficient and where further investigation is necessary, particularly for understanding the performance of Ti6Al4V in the first metatarsophalangeal (1.MTP) joint under physiologically relevant conditions.

1. **A limited number of studies on the tribological behaviour of AM Ti6Al4V under small joint conditions.** Most existing tribological research focuses on large joints (hip, knee) or simplified laboratory configurations, not on small joints such as the 1.MTP, which operate predominantly in boundary lubrication regimes [23, 101, 121–128]. No systematic studies examine how additively manufactured (AM) surface features and microstructures influence lubrication film formation, protein adsorption, friction, or wear in the low velocity, low lubricant volume conditions typical of small joints.
2. **Insufficient understanding of how inherent AM micro- and sub-surface structures interact with synovial fluid.** Additive manufacturing produces distinct features, including martensitic α′ phases, columnar β-grain orientation, residual stresses, pores, and melt-pool overlaps [57–63]. It remains unknown how these features influence the behaviour of synovial fluid constituents: albumin, γ-globulin, hyaluronic acid, phospholipids [107–109] and whether they support or hinder the Protein Aggregation Lubrication (PAL) mechanism [102–106].
3. **Lack of knowledge regarding the "functional texturing" potential of as-built AM surfaces.** Artificial textures (dimples, grooves, LIPSS) have been shown to enhance lubrication and reduce wear [86–91]. However, it is unclear whether as-built AM surface features, partially fused particles, melt-pool boundaries, and inherent roughness can:
    - act as functional micro-textures,
    - serve as lubricant reservoirs,
    - stabilise protein adsorption,
    - or improve boundary lubrication performance.
4. **Lack of data on UHMWPE – AM Ti6Al4V interactions in synovial environments relevant to small joints.** UHMWPE is the standard bearing material for small joint arthroplasty, but it is susceptible to oxidative and fatigue wear [129,130]. There is no systematic comparison of:
    - conventional vs AM Ti6Al4V surfaces,
    - surface-treated vs untreated AM surfaces,
    - performance in real or model synovial fluids, specifically under boundary dominated conditions typical for small joints.

3

AIM OF THE THESIS

The dissertation aims to describe the tribological behaviour of additively manufactured Ti6Al4V alloy for use in joint implants, focusing on its comparison with the conventionally used CoCr30Mo6 alloy, particularly regarding lubrication film formation and wear durability. To achieve the primary goal of this thesis, the solution of the following sub-goals is necessary:

- Design of experiments and approaches for their evaluation.
- Implementation of the optical observing methods, such as fluorescent microscopy and colourimetric interferometry, for this particular contact pair.
- Development of the methodology for evaluating the results for samples with controlled surface structure by optical methods.
- Development and design of the experimental device (long-term wear simulator).
- Description of tribological processes, such as friction, lubrication and wear.
- Data analysis.
- Results discussion and summarising publications.

3.1 Layout of the Dissertation

To achieve the previously mentioned aims, the dissertation presents comprehensive research across four consecutive articles, each building on the knowledge gained in the previous one, from conventionally manufactured samples through laser texturing to the creation of whole samples using additive manufacturing with controlled surface structure. A schematic representation of this process is presented in Fig. 3-1, while a detailed overview and description of each publication are in Chapter 5, Results and Discussion of Hypotheses.

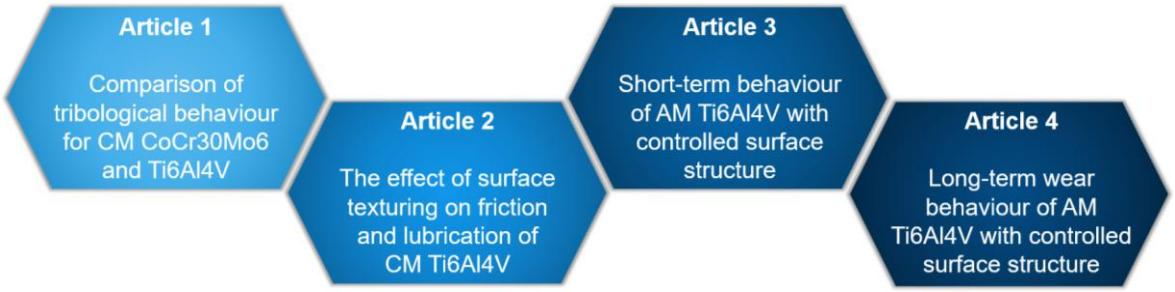

Fig. 3-1 The layout of the dissertation from the perspective of the presented articles and the topics they cover.

The dissertation addresses three main scientific questions, which are answered in the first three articles (Articles 1, 3, and 4) published individually. The fourth publication (Article 2), a second author article, introduced textures and their performance, which helped understand their effects and design the final structure created on the final sample using 3D printing.

3.2 Scientific Questions and Hypotheses

3.2.1 Scientific question 1 (Article 1)

How do conventionally manufactured CoCr30Mo6 and Ti6Al4V differ in tribological behaviour under simulated small joint implant conditions?

Rationale

The comparison between conventionally manufactured CoCr30Mo6 and Ti6Al4V alloys is fundamental for understanding the mechanisms that depend on material and govern friction, wear, and lubrication in orthopaedic implants. Although both alloys are widely used in load-bearing joint replacements, their intrinsic mechanical, chemical, and tribological properties differ significantly, resulting in distinct surface interactions under simulated physiological conditions.

Cobalt-chromium alloys are characterised by high hardness, superior wear resistance, and chemical stability, primarily due to the formation of a stable Cr_2O_3 passive film [27,46]. These features enable CoCr30Mo6 to resist plastic deformation and micro-adhesion during articulation, thus favouring lower friction and reduced material loss under mixed or boundary lubrication regimes [97,114]. In contrast, Ti6Al4V offers a lower elastic modulus and outstanding biocompatibility, which make it suitable for osseointegration and stress distribution [33,41]. However, its relatively low hardness and strong chemical reactivity lead to a higher susceptibility to adhesive and tribochemical wear when exposed to protein-rich lubricants [47,83]. The passive TiO_2 layer, although biocompatible and self-healing, can be mechanically disrupted under cyclic loading, exposing the underlying alloy and accelerating tribocorrosion [46,47].

The differences between these alloys are further emphasised when considering their interaction with synovial fluid constituents. Biological lubricants, composed of proteins such as albumin, γ-globulin, and lubricin, form boundary films that mediate friction and wear [101,105]. The ability of a metallic surface to adsorb and retain these proteins depends strongly on its surface energy, charge, and oxide chemistry [42,111,112]. CoCr30Mo6, with its chemically stable surface, tends to promote the formation of compact, adherent protein layers that sustain mixed lubrication and prevent direct asperity contact [105–108]. In contrast, Ti6Al4V exhibits variable adsorption behaviour due to the dynamic nature of the TiO_2 film and its interaction with biomolecules, often resulting in thinner or discontinuous boundary layers [112]. As a result, titanium alloys typically demonstrate higher friction coefficients and greater wear rates than cobalt-chromium alloys under comparable physiological test conditions [69,97,114].

Previous tribocorrosion studies have reported that CoCr-based alloys maintain a more stable electrochemical potential and exhibit lower current density fluctuations during sliding

in simulated body fluids, indicating a better ability to preserve passive films [69,75,81]. Conversely, Ti6Al4V tends to show stronger tribochemical reactivity and a higher tendency toward surface material transfer under identical conditions [47,116]. The combined mechanical and electrochemical degradation of titanium alloys can thus amplify wear particle generation, which may contribute to biological reactions and inflammatory responses *in vivo* [48].

While extensive data exist for large joint replacements such as hip and knee prostheses, the tribological behaviour in small joint configurations remains comparatively underexplored [120–125]. The reduced contact area, lower normal load, and different kinematic conditions in these joints alter the lubrication regime, often shifting toward boundary-dominated conditions where protein film stability and surface hardness play critical roles [101,109]. Understanding these mechanisms is therefore crucial for optimising material selection for small joint implants, where the interplay of scale, lubrication, and material surface chemistry becomes more pronounced.

Hypothesis

The conventionally manufactured CoCr30Mo6 alloy is expected to exhibit lower friction and wear than Ti6Al4V under simulated small joint conditions. This behaviour is hypothesised to result primarily from its higher hardness, greater chemical stability, and better ability to maintain stable lubrication conditions under physiological loading.

3.2.2 Scientific question 2 (Article 3)

How does a controlled surface structure affect the tribological behaviour of additively manufactured Ti6Al4V compared with the as-built surface under simulated joint conditions?

Rationale

Additive manufacturing (AM) of metallic biomaterials, particularly Ti6Al4V, has enabled the fabrication of complex geometries for patient-specific implants; however, the process inherently introduces surface irregularities, partially melted particles, and anisotropic microstructures that influence the tribological performance of the final component [52,53,55,56]. The as-built surface of AM Ti6Al4V typically exhibits higher roughness and porosity than conventionally manufactured counterparts, leading to increased asperity contact, elevated friction, and accelerated wear under sliding conditions [56,64]. In biomedical applications, such surface features can also act as initiation sites for tribocorrosion and fatigue, limiting the long-term functional stability of the implant [57,69].

Recent advances in surface engineering have focused on controlled texturing of AM Ti6Al4V surfaces to manipulate their tribological response [86,87]. Controlled surface structures, such as periodic micro-grooves, dimples, or laser-induced periodic

surface structures (LIPSS), can modify contact mechanics and hydrodynamic behaviour by reducing the real contact area and facilitating lubricant entrainment [87,88,96]. Such modifications not only enhance wear resistance but also stabilise the running-in period, which is crucial for achieving steady-state friction in articulating pairs [56,96].

From a tribological standpoint, micro-textures act as micro-reservoirs that retain lubricants and debris, thereby improving lubrication and mitigating abrasive and adhesive wear [87,97]. Under boundary or mixed lubrication conditions, as typically encountered in biotribological environments, these structures can promote the adsorption and retention of proteins and synovial fluid constituents, facilitating the formation of boundary films [100,101,105–109,111,112]. The local variation in pressure and shear stress induced by micro-patterns also influences the development of tribochemical reaction layers, which further contribute to surface protection [47,83].

Moreover, additive manufacturing provides a unique opportunity to design the surface structure directly during fabrication, allowing for integration of texture geometry into the digital model prior to printing. This integration enables tailoring of the surface function without the need for extensive post-processing [52,55]. However, while several studies report beneficial effects of micro-textures on tribological performance in model tests, the interplay between texture geometry, surface chemistry, and lubrication behaviour in additively manufactured Ti6Al4V under realistic joint conditions remains insufficiently explored [67,68,87].

Hypothesis

It is hypothesised that a controlled surface structure on additively manufactured Ti6Al4V will reduce friction and wear and improve running-in stability compared with the as-built surface under comparable loading and kinematic conditions. This improvement is expected to result from reduced real contact area and more stable lubrication conditions promoted by the surface structure.

3.2.3 Scientific question 3 (Article 4)

How does additively manufactured Ti6Al4V with a targeted grid surface structure affect the long-term wear performance compared to the conventional CoCr30Mo6 alloy?

Rationale

The comparison between conventionally manufactured CoCr30Mo6 and 3D printed Ti6Al4V with a targeted grid-type surface structure provides an important step toward understanding the balance between material properties and engineered topography in long-term tribological performance. While CoCr30Mo6 remains the benchmark alloy for orthopaedic bearings due to its high hardness, excellent corrosion resistance, and long clinical track record [27,46,114], Ti6Al4V has gained increasing interest for additive

manufacturing (AM) because of its biocompatibility, low density, and design flexibility [33,52,53]. However, the as-built AM surface typically exhibits partially fused particles, high roughness, and residual porosity that accelerate wear and tribocorrosion under articulation [56,64,68].

The introduction of targeted surface structures, such as periodic grids, dimples, or cross-groove patterns, onto AM Ti6Al4V aims to counteract these deficiencies by modifying local contact mechanics and lubrication conditions [86,87]. Such micro-lattice textures can serve as reservoirs for lubricants or protein aggregates, reduce asperity contact, and stabilise the transition from running-in to steady-state sliding [87,96]. These effects are particularly valuable in mixed and boundary lubrication regimes, which dominate the behaviour of small joint implants where the fluid film thickness is comparable to surface roughness [101,109].

Compared with CoCr30Mo6, Ti6Al4V generally displays lower hardness and higher susceptibility to tribochemical wear, especially under long-term articulation in proteinaceous media [46,47,83]. However, micro-texturing and grid-like structuring have been shown to substantially mitigate these effects by promoting tribofilm formation and retention and limiting surface adhesion. The grid geometry can further influence lubricant entrainment and stress distribution, promoting the establishment of quasi-hydrodynamic pockets that delay direct metal-metal contact.

Over extended sliding cycles, the synergy between micro-texture geometry and the Ti6Al4V passive TiO_2 film becomes critical. Stable passive layers combined with well-designed textural reservoirs can preserve lubrication and limit oxide disruption, thereby improving wear resistance and friction stability [47,57,69]. Nonetheless, due to inherent differences in hardness, elastic modulus, and corrosion potential between Ti6Al4V and CoCr30Mo6, the tribological performance of the structured Ti alloy may only partially match that of cobalt-based materials, unless the texture design is optimised for both load support and lubricant retention [46,56,96].

Hypothesis

It is hypothesised that additively manufactured Ti6Al4V with a targeted grid surface structure will exhibit stable running-in and good wear resistance, but will not surpass conventionally manufactured CoCr30Mo6 in terms of friction and wear performance under comparable loading and kinematic conditions.

4

MATERIALS AND METHODS

4.1 Experimental equipment

To achieve the main goals of this work, which aimed to comprehensively describe the tribological behaviour of the studied contact pair, several complementary experimental techniques were utilised. Each device was chosen to address a particular aspect of the problem, from simulating mechanical loading and relative motion to precisely characterising surface topography and film formation. Together, these instruments formed an integrated system for evaluating the mechanisms occurring at the sliding interface relevant to artificial joint applications. The initial phases of the research were primarily conducted on the universal tribometer using a pin-on-plate configuration (see Fig. 4-1). This device enabled simultaneous measurement of the coefficient of friction and direct optical observation of the contact area, allowing correlation of the frictional response with the development of the lubricant film and the behaviour of the model synovial fluid constituents within the contact region.

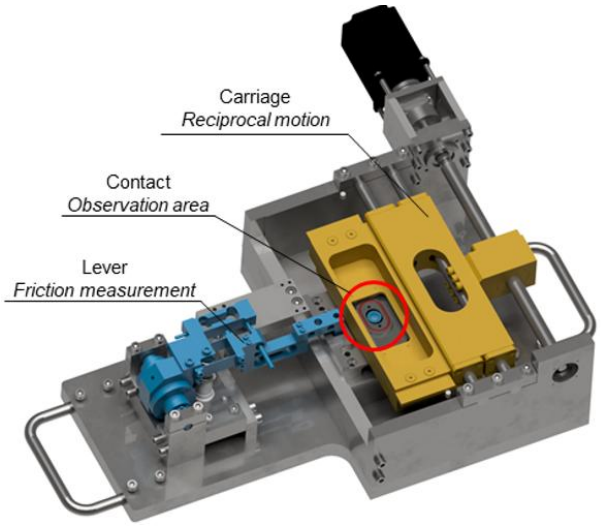

Fig. 4-1 Tribometer with pin-on-plate configuration.

In the case of colourimetric interferometry (see Fig. 4-2a), the measuring system consisted of a microscope, a light source, a high speed camera, and a coated transparent plate. The glass plate was coated with a semi-reflective chromium layer and an anti-reflective layer to enhance the contrast of the interference fringes. The film thickness evaluation was based on calibration curves obtained from a lightly loaded static contact, followed by recording interferograms during the fully loaded reciprocating motion and correlating the captured colour information with the calibration data. This arrangement was used especially in Articles 1 and 2, where the main goal was to evaluate the development of the lubrication film thickness under simplified but well-controlled conditions. In addition to interferometric observations, the same experimental platform was adapted for fluorescent microscopy (see Fig. 4-2b), which enabled direct visualisation of selected constituents

of the model synovial fluid within the contact area and their behaviour during reciprocating motion. These observations were mainly used in Articles 3 and 4.

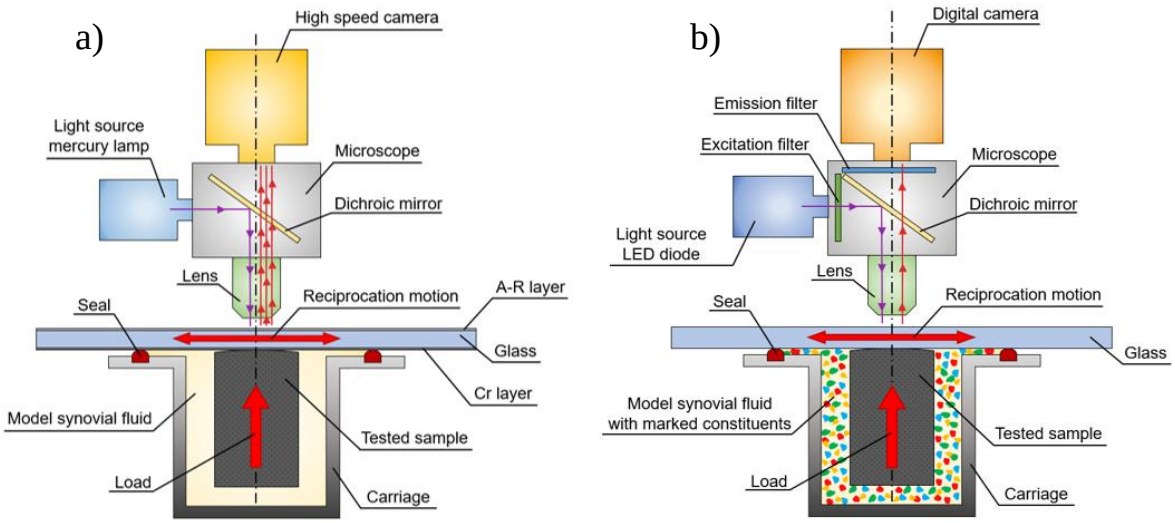

Fig. 4-2 a) Scheme of colourimetric interferometry, b) Scheme of fluorescent microscopy.

In later phases of the research, a new long-term wear simulator was developed (see Fig. 4-3). The simulator is equipped with two independent test stations, enabling direct comparison of parallel experiments and identifying possible differences between measurements.

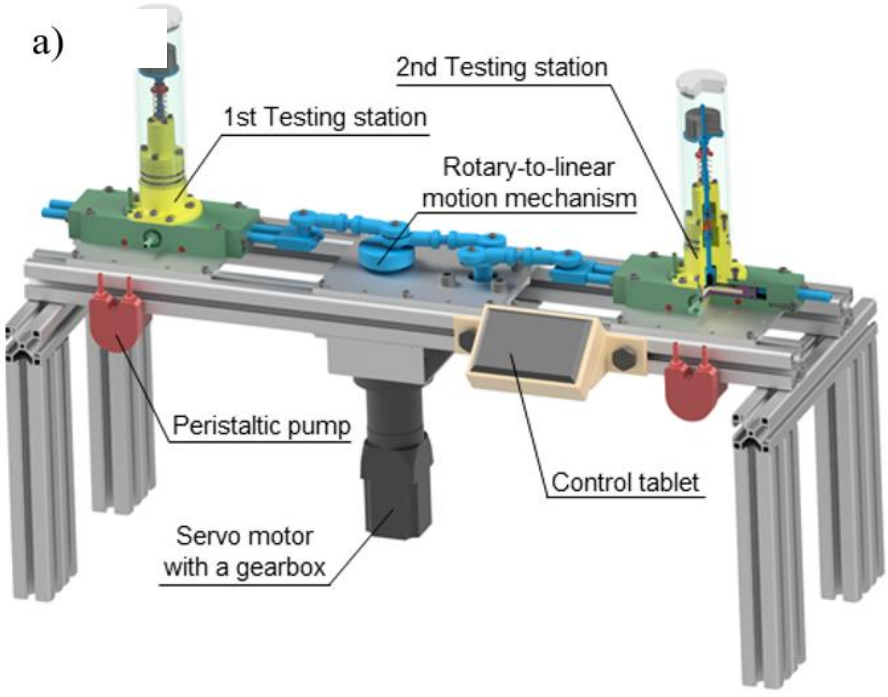

Fig. 4-3 Long-term wear simulator.

The simulator operates via a servo motor connected to a gearbox, while the mechanical design converts the rotary motion into linear reciprocation with a sinusoidal velocity profile. A spring mechanism balances the inherent weight of the loading arm; an additional normal

load is applied using calibrated masses; and a force transducer continuously monitors the applied load. Each station also incorporates a peristaltic pump system, which fills the chamber before testing, maintains lubricant supply during operation, and collects lubricant containing wear debris after the test for subsequent analytical evaluation. The testing station of the simulator is depicted in Fig. 4-4. This apparatus served as the basis for the long-term experiments presented in Article 4.

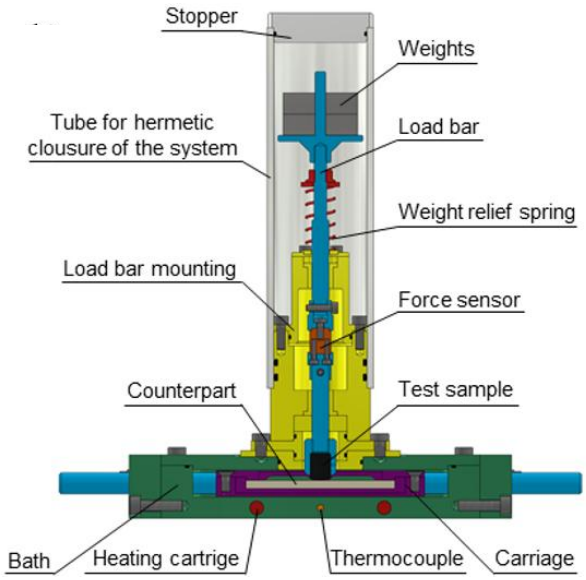

Fig. 4-4 Detail of the testing station.

For further analysis following the experiments, several additional devices were used to characterise the surface topography, microstructure, and chemistry of the tested samples. Initial surface characterisation was always performed using an optical profilometer (Bruker Contour GT-X8). In the final phase of the research, where long-term wear tests were conducted, a Tescan LYRA 3 XMH FEG/, equipped with Energy Dispersive X-ray Spectroscopy (EDS) detectors from Oxford Instruments, a DualBeam scanning electron microscope FEI Helios NanoLab 660 for FIB lamella preparation, and a JEOL JEM-2100F transmission electron microscope were used to characterise the worn surfaces and subsurface regions of the tested pins. These analyses enabled complementing the macroscopic tribological results with morphological, chemical, and microstructural observations.

4.2 Contact Pair and Lubricant

The entire research was conducted in a simplified pin-on-plate configuration, which allowed a more precise description of the complex tribological behaviour of the studied contact pair under lubrication by a fluid containing physiological components. The target contact pair of additively manufactured Ti6Al4V alloy with a controlled surface structure against UHMWPE was used only in the final phase of this research. In earlier phases, the UHMWPE plate had to be replaced with transparent counterparts to enable optical observation of the contact area using colourimetric interferometry and fluorescent

microscopy. This simplified configuration was intentionally selected because it allowed individual lubrication and wear-related phenomena to be studied directly, even though it did not fully reproduce the geometry and conformity of a real implant contact.

The metallic parts were always prepared in a way that ensured comparability between the individual stages of the research. Conventionally manufactured CoCr30Mo6 (ASTM F75) and Ti6Al4V (ISO 5832-3) samples were produced by cold drawing, cut from bars, and machined. In Article 1, these conventionally prepared materials served as a reference for the basic comparison of tribological behaviour. In Article 2, the Ti6Al4V and CoCr30Mo6 pins were further modified by surface texturing. The textures were designed as circular dimples arranged in a triangular pattern, because this geometry is suitable for picosecond laser manufacturing and remains insensitive to changes in the direction of motion. A coverage density of 15% was selected, the dimple radius was 15 µm, the centre-to-centre distance was 74 µm, and the texture depth was varied from 0.4 to 6 µm to change the texture's aspect ratio. The textures were created using picosecond laser micromachining and were subsequently treated by the DLyte electrochemical polishing method to reduce the rims formed during laser processing.

The additively manufactured Ti6Al4V samples were produced using Laser Powder Bed Fusion technology with Ti6Al4V Grade 23 powder meeting ASTM F3001 requirements. The 3D printer used was an SLM 280HL from Nikon SLM Solutions AG. The samples were fabricated in an argon atmosphere with a low oxygen level, with a layer thickness of 30 µm, a laser power of 100 W, and a scan speed of 450 mm/s. In Article 3, three surface variants were studied: a homogeneous surface, a grid structure, and a line structure. The structured variants were created by increasing the hatch distance to 179 µm and by using a meander printing strategy with a rotation of either 0° or 90° between layers. In Article 4, only the grid structure was selected for further experiments, because it had shown the most favourable behaviour in the preceding short-term optical studies. In both cases, the structured region was created only in the top part of the sample, while the remaining volume stayed homogeneous. After production, all pins were polished to the required curvature radius and surface roughness.

For optical experiments, transparent PMMA or B270 glass plates were used. PMMA was selected for fluorescence microscopy because it enabled direct observation of lubricant constituents in the contact area. Glass was used for colourimetric interferometry and was coated with chromium and an anti-reflective layer to improve interferometric contrast. In the final phase of the research, the real counterpart material, UHMWPE, was used in long-term wear experiments. At the same time, PMMA was retained for mid-term fluorescence observations because direct optical access to the contact area was required. This progression from transparent, simplified counterparts to the real material combination reflects the overall logic of the dissertation, in which the first studies focused on mechanism description and the final study on long-term behaviour under more realistic conditions.

In Tab. 4-1, the material configurations used for each article in this thesis are summarised.

Tab. 4-1 Contact pair configurations throughout the dissertation thesis.

Article	Material combination
1	CM Ti6Al4V / Glass
	CM CoCr30Mo6 / Glass
2	CM Ti6Al4V with laser textures / Glass
	CM CoCr30Mo6 with laser textures / Glass
3	AM Ti6Al4V with homogeneous surface / Glass
	AM Ti6Al4V with grid structure / Glass
	AM Ti6Al4V with line surface / Glass
4	AM Ti6Al4V with grid structure/ UHMWPE
	AM Ti6Al4V with grid structure / PMMA
	CM CoCr30Mo6 / UHMWPE
	CM CoCr30Mo6 / PMMA

The lubricant used in all experiments was a synthetically prepared model synovial fluid (M-SF) that closely matches the composition of synovial fluid found in human joints after arthroplasty [132]. The final base composition was as follows: albumin (26.3 mg/ml), γ-globulin (8.2 mg/ml), hyaluronic acid (0.82 mg/ml), and phospholipids (0.35 mg/ml), all diluted in phosphate-buffered saline. In addition to this base M-SF, which was used for the experiments using colourimetric interferometry, it was necessary to adjust it for the experiments using fluorescence microscopy, where the main constituents (albumin, γ-globulin, and hyaluronic acid) were fluorescently labelled. The dyes for each component are as follows: rhodamine-B-isothiocyanate (RBITC) for albumin, and fluorescein-5-isothiocyanate (FITC) for γ-globulin and hyaluronic acid. Moreover, in the long-term wear experiments, a high level of bacterial growth was observed in the solution, manifested as blackening and odour. To suppress bacterial growth, a 1% solution of L-Glutamine-Penicillin-Streptomycin was added to the M-SF.

4.3 Experimental Design

Throughout the dissertation, several complementary experiments and methods were used to provide a comprehensive overview of the examined problem. The experimental design can be divided into two main groups. The first group corresponds to Articles 1–3, in which the real implant contact pair had to be partially simplified to enable direct optical observation of the contact region. The second group corresponds to Article 4, where the material configuration already more closely matched the real metal-on-polyethene concept and where the main emphasis was on long-term wear and durability. In this way, the dissertation progresses from mechanistic short-term studies toward a more realistic

long-term validation of the selected material concept. During the dissertation, several parameters were obtained at different stages of the research, while all obtained parameters are summarised in the following bullet points:

- Friction (tribometer)
- Lubrication film thickness (colourimetric interferometry)
- Area covered by the M-SF constituents (fluorescence microscopy)
- M-SF constituents fluorescence intensity (fluorescence microscopy)
- Wear – Volume loss (optical profilometer)
- Surface topography – roughness (optical profilometer)
- Microstructural and chemical analysis (SEM, EDS, STEM)

The kinematic and loading conditions used throughout the work were derived from available knowledge of the first metatarsophalangeal joint and from standards for larger joint replacements. The experimental cycle was designed as a 1-second cycle. Based on the reported movement of the 1. MTP joint, the path in which the real joint remains in contact was recalculated to be approximately 12 mm. However, in the experiments, the stroke was increased to 20 mm in order to provide a sufficiently long region with constant speed and stable loading, unaffected by the dead ends of the reciprocating motion. The analysis of the joint kinematics showed that the relative speed is low during most of the cycle, while higher values occur only during part of the movement. Therefore, the main experimental speeds of 20 mm/s and 40 mm/s were selected for the short- and medium-term studies. The kinematic and loading conditions used in the experiments in this study are summarised in Tab. 4-2.

Tab. 4-2 Summarised kinematic and loading conditions used in each article.

Article	Material combination	Pin radius	Load	Contact pressure	Relative speed	stroke
1	CM Ti6Al4V / Glass	15 mm	0.73 N	105.5 MPa	20 mm/s	20 mm
	CM CoCr30Mo6 / Glass		0.5 N		40 mm/s	
2	CM Ti6Al4V / Glass	100 mm	0.5 N	26.3 MPa*	20 mm/s	20 mm
	CM CoCr30Mo6 / Glass			29.6 MPa*		
3	AM Ti6Al4V / Glass	100 mm	1 N	35.1 MPa*	20 mm/s	20 mm
4	AM Ti6Al4V / UHMWPE	100 mm	2 N	7.6 MPa*	40 mm/s	20 mm
	AM Ti6Al4V / PMMA			3.4 MPa*		
	CM CoCr30Mo6 / UHMWPE			7.7 MPa		
	CM CoCr30Mo6 / PMMA			3.4 MPa		

*Values of the contact pressure were calculated for a homogeneous surface without textures/structures.

In Article 1, the aim was to compare conventionally manufactured CoCr30Mo6 and Ti6Al4V under short-term conditions using colourimetric interferometry. The applied loads were recalculated using Hertzian contact theory to achieve comparable contact pressure between the two materials despite their different elastic properties. In Article 3, the experiments were designed to compare additively manufactured Ti6Al4V with homogeneous, grid, and line surface structures. These experiments consisted of 60 cycles, with unloading after every 20 cycles to simulate joint relief. The line structures were oriented parallel to the direction of motion, while the grid structures were aligned consistently to ensure meaningful comparison. The loading force was kept uniform for all variants, and the midpoint of the one-way motion was selected as the most suitable location for evaluating film thickness and fluorescence behaviour because this region was not affected by dead-end artefacts.

Article 2 focused on the effects of laser-produced microtextures on lubrication and friction. In this case, the experiments were also derived from 1st MTP joint kinematics, but the main variable was the texture geometry rather than the bulk material alone. The experiments were carried out under fully flooded conditions, and the texturing design was chosen to reveal how texture depth and subsequent electrochemical smoothing influence the formation of the lubrication film. This article, therefore, represents a separate methodological branch of the dissertation, because it introduced an intentionally manufactured deterministic surface modification, unlike the built-in structures created directly during additive manufacturing in Articles 3 and 4.

Article 4 represented the final and most complex phase of the dissertation. The long-term wear tests were performed at a stroke of 20 mm, relative speed of 40 mm/s, and load of 2 N, corresponding to a contact pressure of approximately 3.5 MPa. The tests were carried out at 100,000, 200,000, and 300,000 cycles. In parallel, mid-term fluorescence microscopy experiments were performed for 1000 cycles, which was the maximum duration possible before critical wear of the PMMA counterpart made further optical evaluation unreliable. The same study also included a post-test evaluation of volume loss, wear rate, surface topography, and detailed SEM/EDS/FIB/STEM analysis of the worn pins, enabling a relationship between tribological behaviour and microstructural and chemical changes beneath the worn surface.

4.4 Experimental data collection and evaluation

Throughout this work, the collected data were evaluated according to the main objective of each experimental stage. The coefficient of friction was continuously recorded and subsequently processed, excluding the dead-end regions of the cycle. In colourimetric interferometry, film thickness was obtained from interferograms using calibration curves and custom evaluation software. In fluorescence microscopy, two complementary approaches were used: evaluation of the area covered by the M-SF constituents

and evaluation of the fluorescence intensity inside the contact area. In Article 3, the fluorescence analysis focused on albumin, whereas in Article 4, the same principle was extended to albumin, γ-globulin, and hyaluronic acid. For structured samples, regions corresponding to surface structures were excluded from fluorescence evaluation using a calibration image to prevent quantification of M-SF constituents retained within the structures themselves. The fluorescence images in the final study were processed using Andor Solis software and subsequently evaluated in MATLAB.

The number of repetitions was selected based on the type and duration of the experiment. Measurements of lubrication film thickness, friction, and fluorescence-based behaviour of M-SF constituents were generally repeated three times for each configuration to verify repeatability and reduce the influence of random fluctuations typical of biotribological systems. Long-term wear tests were more time-consuming and experimentally demanding and were therefore repeated at two independent stations of the wear simulator, which still enabled direct comparison and a reliable assessment of the dominant wear mechanisms. This strategy provided a compromise between practical feasibility and sufficient robustness of the obtained results.

Methodologically, it is also important to note that the chosen experimental design deliberately combines simplification and gradual validation. The pin-on-plate geometry, the use of glass and PMMA transparent counterparts, and the use of optical observation methods do not fully reproduce the conformity and pressure distribution of a real implant. On the other hand, these simplifications enabled direct observation of mechanisms that would otherwise stay hidden, such as film formation, retention of synovial fluid constituents, and the influence of surface structures on local lubrication behaviour. The final long-term experiments on the Ti6Al4V/UHMWPE and CoCr30Mo6/UHMWPE pairs were therefore conceived as a complementary validation step, linking the mechanistic observations from the earlier articles with more realistic wear behaviour.

5

RESULTS AND DISCUSSION OF HYPOTHESES

This chapter traces the systematic progression of the research, which is comprehensively documented through four peer-reviewed scientific papers introduced at the beginning of the chapter and included in the Attachments. Conducted chronologically, each study built upon the conceptual and experimental foundations established by the preceding studies, enabling a gradual refinement of methodologies, hypotheses, and interpretations. This iterative approach not only strengthened the overall unity of the research but also provided valuable insights into the complex mechanisms governing the studied contact pair, ultimately intending to improve its tribological performance and advance artificial joint technology.

5.1 Article overview

2023

Tribological Behaviour of Ti6Al4V Alloy: An Application in Small Joint Implants [134]

Lukáš Odehnal, *Matúš Ranuša, Martin Vrbka, Ivan Křupka, Martin Hartl*

Author's contribution	58%
Journal Impact Factor	2.9
JIF/AIS Quartile	Q2/Q2
Citations: WoS/Scopus (03/2026)	10/10

2025

Effect of Surface Texturing on Friction and Lubrication of Ti6Al4V Biomaterials for Joint Implants [135]

Matúš Ranuša, ***Lukáš Odehnal****, Ondřej Kučera, David Nečas, Martin Hartl, Ivan Křupka, Martin Vrbka*

Author's contribution	20%
Journal Impact Factor	3.3*
JIF/AIS Quartile	Q2/Q2*
Citations: WoS/Scopus (03/2026)	8/9

2025

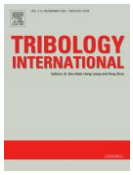

Tribological Behaviour of Additively Manufactured Ti6Al4V with Controlled Surface Structure: An Application in Small Joint Implants [136]

Lukáš Odehnal*, Matúš Ranuša, Martin Malý, Ivan Křupka, Daniel Koutný, Martin Hartl, Martin Vrbka*

Author's contribution	55%
Journal Impact Factor	6.9*
JIF/AIS Quartile	Q1/Q1*
Citations: WoS/Scopus (03/2026)	7/7

2025

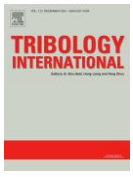

Additively manufactured Ti6Al4V with controlled surface Structure as a Potential Material for Joint Implants: Long-Term Wear Performance and Durability [137]

Lukáš Odehnal*, Matúš Ranuša, Pavel Čípek, Martin Malý, Veronika Mazánová, Antonín Dlouhý, Daniel Koutný, Martin Hartl, Martin Vrbka*

Author's contribution	55%
Journal Impact Factor	6.9*
JIF/AIS Quartile	Q1/Q1*
Citations: WoS/Scopus (03/2026)	1/1

*The metrics listed are for the year 2024, as they have not yet been published for 2025

5.2 Summary of the Main Findings

The present research was motivated by a fundamental contradiction associated with the Ti6Al4V alloy in orthopaedic applications. On the one hand, Ti6Al4V offers a combination of excellent biocompatibility, corrosion resistance, and a modulus of elasticity that is considerably closer to that of cortical bone than that of conventional CoCr-based alloys, making it highly attractive for implant fixation and patient-specific, additively manufactured implant designs. On the other hand, its use as a frictional material remains limited by its insufficient tribological performance in boundary and mixed lubrication regimes typical of joint arthroplasty. The four studies included in this thesis, therefore, followed a logical progression. The first aimed to identify the governing limitation of conventionally manufactured Ti6Al4V, the second to determine whether this limitation could be mitigated by targeted surface texturing and finishing, the third to investigate whether additive manufacturing could integrate beneficial surface structures directly into the material, and the fourth to verify whether the resulting advantages remain relevant under extended long-term wear experiments.

The initial study [134] established the baseline behaviour of conventionally manufactured Ti6Al4V alloy under simulated small joint conditions. The experimental system used a pin-on-plate configuration with a transparent glass plate, facilitating simultaneous friction measurement and *in situ* observation of the contact zone via colourimetric interferometry. The experimental tests were conducted in a model synovial fluid containing albumin, γ-globulin, hyaluronic acid, and phospholipids. This ensured that the principal constituents and rheological behaviour of natural synovial fluid were replicated. Although Ti6Al4V produced a thicker lubricant film than CoCr30Mo6 at low speed, the achieved film thickness remained insufficient relative to its roughness. At 20 mm/s and at the 30th cycle, the film thickness at the evaluated point was about 15 nm for CoCr30Mo6 and about 55 nm for Ti6Al4V, but the 95% separation thresholds were approximately 35 nm for CoCr30Mo6 and 110 nm for Ti6Al4V. As a result, Ti6Al4V did not achieve stable separation of the contact pair. At 40 mm/s, full or near-full separation was observed only for CoCr30Mo6, whereas Ti6Al4V again failed to maintain a sufficiently thick film. This insufficient separation was directly reflected in wear. For CoCr30Mo6 at 40 mm/s, no visible wear was observed on any of the pins, whereas Ti6Al4V at the same speed developed pronounced grooves with central depths of 583, 437, and 984 nm for the three pins. Even at 20 mm/s, Ti6Al4V showed deeper and less regular wear scars than CoCr30Mo6, showing a transition toward three-body abrasion. At the same time, the friction coefficients of both alloys were comparable and stabilised around 0.4, indicating that, in this system, friction alone was not a sufficient indicator of damage severity. The key conclusion of the baseline study was therefore not that Ti6Al4V is chemically unsuitable,

but that its conventionally prepared surface does not provide the topography required for stable lubrication conditions.

The second phase [135] of the work demonstrated that this limitation can be mitigated by targeted surface engineering. For polished CoCr30Mo6, the reference film thickness was 39 ± 11 nm, and a shallow 0.4 µm texture increased it to 50 ± 12 nm. In contrast, Ti6Al4V responded much more strongly to texturing: for shallow textures of 0.4 and 1 µm after electrochemical finishing, the measured lubricating film thickness reached 310–320 nm, whereas the untextured reference after finishing remained around 60 nm. This shows that the main benefit of texturing was not a marginal shift but a pronounced increase in film thickness, moving the system from partial to effective separation. The same study also clarified that higher friction after texturing did not necessarily indicate worse tribological behaviour. The polished CoCr30Mo6 reference exhibited a CoF of 0.50 ± 0.02. The polished Ti6Al4V reference was markedly lower, 0.32 ± 0.01, but texturing increased the CoF by 28–118%, with the 6 µm texture reaching 0.71 ± 0.02. After DLyte finishing, the Ti6Al4V reference increased from 0.32 to 0.47, while most textured samples changed only slightly. In this case, the increase in friction corresponded to stronger protein accumulation and shear within the contact, not to a deterioration in lubrication quality. Importantly, electrochemical finishing reduced rim height by 53–80%, which was essential because untreated rims promoted local collisions with the glass and increased the risk of abrasive damage.

The third phase [136] of the research moved from post-processed conventional material to additively manufactured Ti6Al4V with built-in surface structures. Among the tested variants, the grid-structured surface produced the most promising behaviour. Its friction stabilised at approximately 0.43, which was essentially the same as the homogeneous surface, whereas the line-structured surface stabilised at a higher value of about 0.48. More importantly, only the grid structure showed recovery of the lubrication film after unloading. This was accompanied by a temporary reduction in CoF from about 0.43 to about 0.38 at the start of the second phase, which supports the interpretation that the structured surface improved short-term reformation of the lubrication film. Fluorescence microscopy further showed that the grid structure retained a higher and more stable amount of albumin in the contact zone than the homogeneous or line-structured surfaces. After 60 cycles, virtually no wear was observed on the grid-structured surface, whereas the homogeneous surface already showed visible grooves and material pile-up.

The final phase of the work [137] verified whether these short-term advantages were relevant under extended wear conditions. In long-term tests performed at 100,000, 200,000, and 300,000 cycles, corresponding to 4, 8, and 12 km, the UHMWPE wear rate against additively manufactured Ti6Al4V remained nearly constant at 1.1033, 1.1148, and 1.0475 × 10^{-6} mm^3/Nm, respectively. For CoCr30Mo6, the corresponding wear rates were higher at every stage: 2.6374, 1.6769, and 1.2562 × 10^{-6} mm^3/Nm. Thus, the additively manufactured Ti6Al4V surface not only reduced total UHMWPE volume loss but also

suppressed the pronounced running-in wear observed for CoCr30Mo6 in the first 100,000 cycles. The metallic pins showed the same trend: CoCr30Mo6 developed larger, deeper wear areas, whereas Ti6Al4V exhibited only shallow, localised grooves. Fluorescence microscopy in the long-term study also explained why the additively manufactured surface performed better, and for Ti6Al4V, a relatively stable regime of constituent retention persisted for approximately 400–500 cycles, whereas CoCr30Mo6 flushed the model synovial fluid components out of the contact much more rapidly. The Ti6Al4V structures repeatedly accumulated albumin, γ-globulin, and hyaluronic acid and then released them back into the contact area, effectively functioning as local lubricant reservoirs. In parallel, the coefficient of friction for Ti6Al4V increased only during the initial ~400 cycles, then stabilised, whereas the CoCr30Mo6 friction continued to increase throughout the experiment. These observations show that the advantage of the structured Ti6Al4V surface was not only lower wear, but also more stable lubricant support over time. Post-test microstructural analysis supported this interpretation. In Ti6Al4V, STEM/EDS revealed an approximately 35 nm thick amorphous surface oxide and a subsurface nanograin layer with an average width of about 200 nm. This tribologically transformed zone near the surface, together with the structured topography covered by oxide, likely contributed to the more stable wear response of the additively manufactured alloy. Unlike CoCr30Mo6, which showed more severe scratching and higher initial wear, the Ti6Al4V surface combined structural retention of lubricant with a mechanically and chemically stabilised near-surface layer.

Taken together, the four studies show a clear progression in mechanism and performance. Conventionally manufactured Ti6Al4V failed primarily because the formed film thickness was insufficient relative to surface roughness, leading to asperity contact and groove formation. Surface texturing and electrochemical finishing increased film thickness from roughly tens of nanometres to more than 300 nm in the best Ti6Al4V configurations, demonstrating that the main limitation was surface design rather than the alloy itself. Additive manufacturing then extended this concept via integrating functional structures directly into the surface, enabling not only the trapping of proteins but also the regeneration of the lubrication film after unloading and the reduction of wear over long sliding distances. Overall, the work shows that Ti6Al4V can be transformed from a biocompatible but tribologically limited alloy into a functionally optimised articulating material when its surface topography and condition beneath the surface are deliberately designed to support lubrication.

5.2.1 Comparative Summary of the Key Results

The Tab. 5-1 summarises the key quantitative results obtained in this thesis and presents them in a comparative form. Cells marked with a dash indicate that the given parameter was not directly measured or observed in the respective article.

Tab. 5-1 Summary of the key Results.

Article	Material combination	Coefficient of friction	Lubrication film thickness
1	CM CoCr30Mo6 / Glass	Stabilised at ~0.4, a decrease occurred after rehydration, lasting only one cycle.	~20 nm (20 mm/s); ~55 nm (40 mm/s). Separation threshold from roughness: 99% ≈ 45 nm. Only the 40 mm/s condition achieved separation.
	CM Ti6Al4V / Glass	Stabilised at ~0.4; slight transient decrease after rehydration at 40 mm/s.	~75 nm (20 mm/s); ~65 nm (40 mm/s). Separation threshold: 99% ≈ 160 nm; full separation was not achieved.
2	CM CoCr30Mo6 / Glass (textured)	0.5 (REF); 0.33 (0.4 µm); 0.52 (1 µm); 0.59 (2 µm); 0.55 (4 µm); 0.47 (6 µm)	0.4 µm: 50 ± 12 nm; 1 µm: local rise to ~200 nm, later >200 nm. Deeper textures could not be reliably evaluated because rims scratched the glass.
	CM CoCr30Mo6 / Glass (textured + DLyte)	0.55 (REF); 0.4 (0.4 µm); 0.4 (1 µm); 0.34 (2 µm); 0.57 (4 µm); 0.29 (6 µm)	Not reliably evaluable after DLyte.
	CM Ti6Al4V / Glass (textured)	0.32 (REF); 0.41 (0.4 µm); 0.5 (1 µm); 0.49 (2 µm); 0.53 (4 µm); 0.71 (6 µm)	Textured surfaces: shallow textures (0.4–1 µm) gave ~310–320 nm; deeper textures still showed >230 nm, but rim contact remained an issue.
	CM Ti6Al4V / Glass (textured + DLyte)	0.47 (REF); 0.49 (0.4 µm); 0.6 (1 µm); 0.5 (2 µm); 0.56 (4 µm); 0.62 (6 µm)	All textures showed film thickness >180 nm; the best values for 0.4–4 µm were 280–321 nm; at 6 µm, the film thickness decreased to ~180 nm.
3	AM Ti6Al4V / Glass (homogeneous surface)	Stabilised at ~0.43.	The film was disrupted during the experiment; no durable recovery after unloading.
	AM Ti6Al4V / Glass (grid structure)	Stabilised at ~0.43; after unloading, CoF temporarily decreased to ~0.38.	The film was disrupted, but after the first unloading, there was a temporary restoration and momentary re-separation of the pair.
	AM Ti6Al4V / Glass (line structure)	Stabilised at ~0.48.	Lower film thickness than homogeneous/grid; no meaningful post-unloading recovery.
4	CM CoCr30Mo6 / UHMWPE	—	—
	CM CoCr30Mo6 / PMMA	CoF increased continuously throughout the entire experiment, reaching 0.45.	—
	AM Ti6Al4V / UHMWPE (grid structure)	—	—
	AM Ti6Al4V / PMMA (grid structure)	CoF stabilised shortly after the beginning of the experiment at ~0.38.	—

Tab. 5-1 Summary of the key Results (continuation).

Article	Material combination	M-SF constituents behaviour	Wear / Surface damage
1	CM CoCr30Mo6 / Glass	PAL inlet aggregation occurred only randomly / under specific conditions.	At 20 mm/s, regular oval wear scars formed; at 40 mm/s, wear was not visible.
	CM Ti6Al4V / Glass	Overall, higher protein presence in contact, but non-visible PAL behaviour.	Deeper separated grooves (depth of 583, 437, and 984 nm) and three-body abrasion.
2	CM CoCr30Mo6 / Glass (textured)	—	Deeper textures caused scratches and damage to the Cr layer on the glass.
	CM CoCr30Mo6 / Glass (textured + DLyte)	—	Severe surface damage; post-DLyte colourimetric interferometry results were not evaluated.
	CM Ti6Al4V / Glass (textured)	—	Non-visible signs for 0.4 µm texture, other textures (their rims) caused scratches.
	CM Ti6Al4V / Glass (textured + DLyte)	—	Non-visible signs of wear as textures + DLyte, caused a full separation of surfaces.
3	AM Ti6Al4V / Glass (homogeneous surface)	The behaviour of albumin was unstable; protein clusters passed through the contact and did not remain there.	Wear was improved compared with CM Ti6Al4V, but was the most visible among the AM samples.
	AM Ti6Al4V / Glass (grid structure)	Highest albumin retention; protein amount increased above the original value and remained stable through a cycle.	No wear area was found; released particles were observed moving in dimples, indicating trapping ability.
	AM Ti6Al4V / Glass (line structure)	The albumin amount remained below the original value, the worst behaviour among AM structures.	Slight central deformation only, but tribologically worse than the grid structure.
4	CM CoCr30Mo6 / UHMWPE	—	UHMWPE volume loss was higher than against AM Ti6Al4V; CoCr30Mo6 showed significant initial wear.
	CM CoCr30Mo6 / PMMA	A substantial portion of M-SF constituents was rapidly flushed out from the contact area.	—
	AM Ti6Al4V / UHMWPE (grid structure)	—	Lower UHMWPE volume loss and more consistent wear than CoCr30Mo6. Only a few shallow grooves (Ti6Al4V).
	AM Ti6Al4V / PMMA (grid structure)	The stable region for about 500 cycles, with better retention of M-SF constituents than CoCr30Mo6.	—

5.3 Verification and Discussion of Hypotheses

Following the formulation of the scientific questions and hypotheses in Chapter 3.2, their verification is presented below based on the experimental results obtained in the individual studies. The evaluation is not limited to a simple confirmed/unconfirmed statement, but instead reflects the actual degree to which the measured tribological behaviour supported the original expectations.

5.3.1 Hypotheses 1

The conventionally manufactured CoCr30Mo6 alloy is expected to exhibit lower friction and wear than Ti6Al4V under simulated small joint conditions. This behaviour is hypothesised to result primarily from its higher hardness, greater chemical stability, and better ability to preserve stable lubrication conditions under physiological loading.

Although the conventional CoCr30Mo6 alloy showed clearly better wear performance and more effective contact separation than Ti6Al4V under the tested small joint conditions, the expected reduction in friction was not confirmed. In all configurations, the coefficient of friction stabilised at approximately 0.4 after the initial running-in phase. In contrast, the wear results supported the hypothesis. At 20 mm/s, CoCr30Mo6 showed shallower wear scars, with central depths of 81–92 nm, whereas Ti6Al4V reached 127–203 nm in two of the three pins. At 40 mm/s, the difference became much more pronounced: all CoCr30Mo6 pins showed non-visible signs of wear, while Ti6Al4V exhibited pronounced wear scars with central depths of 437–984 nm. Similarly, only the CoCr30Mo6 configuration at 40 mm/s generated a lubrication film sufficient to separate the contact pair, while Ti6Al4V, despite producing a numerically thicker film, failed to overcome its higher surface roughness.

Therefore, the hypothesis is only **partially verified**, as the expected frictional performance was not observed. However, it was supported for wear resistance and effective lubrication, particularly at 40 mm/s, where CoCr30Mo6 achieved contact separation and prevented measurable wear.

5.3.2 Hypotheses 2

It is hypothesised that a controlled surface structure on additively manufactured Ti6Al4V will reduce friction and wear and improve running-in stability compared with the as-built surface under comparable loading and kinematic conditions. This improvement is expected to result from reduced real contact area and more stable lubrication conditions promoted by the surface structure.

Grid structure – verified. Although the grid-structured additively manufactured Ti6Al4V did not show a sustained reduction in friction compared with the homogeneous surface, it exhibited the most favourable overall tribological behaviour under the tested conditions (1 N, 20 mm stroke, 20 mm/s, 60 cycles). The coefficient of friction stabilised at approximately 0.43, i.e., a value comparable to that of the homogeneous surface. However, after the first unloading phase, it temporarily decreased from about 0.43 to 0.38, an effect not observed for the other surfaces. More importantly, the grid structure was the only surface that restored the lubrication film after unloading, indicating improved lubrication stability. Fluorescence microscopy results also supported this. In addition, virtually no wear area was found on the grid structured sample after the experiment. Therefore, even though the part of the hypothesis related to friction was only partially supported, the grid structure clearly improved wear resistance and lubrication behaviour relative to the as-built surface.

Line structure – falsified. The line-structured additively manufactured Ti6Al4V did not confirm the proposed hypothesis when compared with the homogeneous surface. Its coefficient of friction stabilised at approximately 0.48, which was the highest of all tested surfaces and clearly above the value of about 0.43 measured for the homogeneous and grid-structured samples. The results related to lubrication were also unfavourable: the line structure showed a notable reduction in lubrication film thickness, no restoration of the film after unloading, and poor protein retention. In the static fluorescence analysis, albumin coverage after the three phases reached only about 648, 744, and 1041 px, which was markedly lower than for the grid structure (2860, 3114, 2652). Moreover, during the representative analysis, the albumin value for the line structure remained below its initial value throughout the cycle, indicating unstable lubrication conditions. Although the wear damage was less pronounced than on the homogeneous sample, with only slight deformation in the middle of the contact area, this partial improvement is insufficient for verification, as the structure failed to reduce friction and did not improve lubrication stability.

5.3.3 Hypotheses 3

It is hypothesised that additively manufactured Ti6Al4V with a targeted grid surface structure will exhibit stable running-in and good wear resistance, but will not surpass conventionally manufactured CoCr30Mo6 in terms of friction and wear performance under comparable loading and kinematic conditions.

This hypothesis was **falsified**. Although the additively manufactured Ti6Al4V alloy with a targeted grid surface structure exhibited stable running-in and good wear resistance, the prediction that it would not surpass conventionally manufactured CoCr30Mo6 in friction and wear performance was not confirmed. Under the applied conditions (20 mm stroke, 40 mm/s, 2 N), the UHMWPE wear rate against Ti6Al4V remained nearly constant

at 1.1033, 1.1148, and 1.0475 × 10^{-6} mm^3/Nm after 100,000, 200,000, and 300,000 cycles, respectively, whereas the corresponding values for CoCr30Mo6 were consistently higher: 2.6374, 1.6769, and 1.2562 × 10^{-6} mm^3/Nm. This corresponds to approximately 58%, 34%, and 17% lower wear rates for the Ti6Al4V configuration. In addition, the total volumetric loss of UHMWPE was lower for Ti6Al4V, and after 300,000 cycles, the Ti6Al4V pins showed only shallow, localised grooves, while CoCr30Mo6 exhibited visibly deeper, larger wear areas. The results regarding friction also favoured Ti6Al4V: its coefficient of friction increased during the first approximately 400 cycles and then stabilised at about 0.35–0.38, whereas CoCr30Mo6 showed a continuous increase throughout the experiment, reaching approximately 0.45–0.50 by the end of the test. Fluorescence microscopy further showed more stable lubricant retention for Ti6Al4V, with a relatively stable region lasting about 400–500 cycles. Therefore, while the first part of the hypothesis was supported, the overall hypothesis must be considered falsified, because the structured additively manufactured Ti6Al4V not only approached but, within this study, outperformed conventional CoCr30Mo6 in both wear and friction stability.

6

CONCLUSIONS

6.1 General Conclusions

This dissertation systematically investigated the tribological behaviour of the Ti6Al4V alloy under simulated conditions for small joint arthroplasty, with emphasis on the role of surface design in contact lubricated by synovial fluid. The work progressed from conventionally manufactured Ti6Al4V, through surface texturing and electrochemical finishing, to additively manufactured Ti6Al4V with integrated functional surface structures. Taken together, the results show that the tribological limitations of Ti6Al4V are not determined by the bulk alloy alone, but mainly by the ability of its surface to support the formation, retention, and regeneration of a protein-rich lubricating film. Conventionally manufactured Ti6Al4V remained tribologically limited, whereas deliberately engineered AM surfaces showed substantially improved lubrication support and long-term wear behaviour.

- Conventionally manufactured Ti6Al4V is not suitable as an untreated articulating surface for small joint implants. Its main limitation is insufficient functional separation of the contact, not simple chemical incompatibility with synovial fluid.
- The tribological behaviour of Ti6Al4V is governed primarily by surface condition. The same alloy can perform poorly or favourably depending on whether the surface supports protein aggregation and stable film formation.
- Surface texturing combined with electrochemical finishing significantly enhances the lubrication performance. In the best Ti6Al4V configurations, film thickness increased from about 60 nm on the reference surface to 280–321 nm on shallow textured and finished surfaces, clearly exceeding the scale of the surface irregularities.
- The benefit of texturing is not universal, but dependent on geometry. Shallow textures were the most effective, whereas deeper or less regular features could locally reduce film thickness or increase interactions with edges. Proper control of texture depth, spacing, and surface finishing is therefore essential.
- Additive manufacturing enables a qualitatively new approach to surface design. The functional structure can be integrated directly during fabrication, rather than added only as a post-processing step. In this work, the grid structure acted as a lubricant reservoir, promoted albumin retention, and enabled film regeneration after unloading.
- The long-term superiority of AM Ti6Al4V was demonstrated by both lower wear and more stable wear evolution. Unlike CoCr30Mo6, which showed pronounced running-in wear, Ti6Al4V maintained an almost constant UHMWPE wear rate throughout the long-term test.
- A stabilised near-surface structure supported the improved performance of AM Ti6Al4V. After testing, the material exhibited a nanograin subsurface layer of about 200 nm and an oxide layer of about 35 nm, both of which likely contributed to the stable wear response.

- The main scientific contribution of the dissertation is the demonstration that Ti6Al4V can be transformed from a biocompatible but tribologically limited alloy into a functionally optimised articulating material when its surface is deliberately engineered to support lubrication. This finding is relevant not only for small joint implants but also for the broader design of future additively manufactured orthopaedic surfaces.
- Further optimisation is still required before direct clinical application. The remaining localised grooves and imperfections related to edges indicate that future work should focus on more precise control of structural geometry, AM parameters, and, possibly, hybrid surface treatments.

In summary, this dissertation shows that tribological performance in small joint implant materials cannot be explained solely by bulk material selection. Instead, it is determined by the interaction between topography, near-surface structure, oxide chemistry, and synovial fluid constituents. Within this framework, additively manufactured Ti6Al4V with a targeted functional surface architecture represents a promising route towards implant surfaces with improved wear resistance, more stable lubrication, and enhanced long-term functional durability.

6.2 Answers to the scientific questions

6.2.1 Scientific Question 1

How do conventionally manufactured CoCr30Mo6 and Ti6Al4V differ in tribological behaviour under simulated small joint implant conditions?

Answer: Conventionally manufactured CoCr30Mo6 showed better functional tribological performance than conventionally manufactured Ti6Al4V. The decisive difference was not a markedly lower friction coefficient, but the ability of CoCr30Mo6 to achieve effective contact separation and to suppress wear under the tested conditions.

Evidence: Article 1 showed that Ti6Al4V could form a relatively thick lubricant film, but this film remained insufficient given its higher roughness. By contrast, CoCr30Mo6 was the only tested configuration to form a film thick enough to separate the contact pair at 40 mm/s, and it was also the only configuration without visible wear. At the same time, the friction values of both alloys were comparable (see Article 1: Fig. 3–5, and Fig. 7).

Key quantitative results: CoCr30Mo6 had a lower initial roughness ($Ra = 0.01 \pm 0.005$ µm) than Ti6Al4V ($Ra = 0.04 \pm 0.01$ µm). The 95% probability of separated contact was 30–35 nm for CoCr30Mo6 and 100–113 nm for Ti6Al4V. At 40 mm/s, Ti6Al4V developed grooves with depths of 583 nm**,** 437 nm, and 984 nm, whereas CoCr30Mo6 showed non-visible signs of wear in the corresponding configuration.

6.2.2 Scientific Question 2

How does a controlled surface structure affect the tribological behaviour of additively manufactured Ti6Al4V compared with the as-built surface under simulated joint conditions?

Answer: A controlled surface structure improved the tribological behaviour of additively manufactured Ti6Al4V, but the effect was strongly geometry-dependent. Among the tested structures, the grid pattern showed the most favourable behaviour.

Evidence: Article 3 showed that the grid structure retained the highest amount of albumin in the contact area, was the only structure that enabled lubrication film restoration after unloading, and exhibited the least wear after the experiment. In contrast, the line structure showed the lowest protein retention and the highest steady-state friction (see Article 3: Fig. 5–8, and Fig. 10).

Key quantitative results: The coefficient of friction stabilised at approximately 0.43 for the homogeneous and grid-structured surfaces, while the line structure stabilised at approximately 0.48**.** After unloading, the grid structure showed a temporary reduction in friction from approximately 0.43 to 0.38. The short-term tests lasted 60 cycles, and after this period, the grid structure showed virtually no wear, whereas the homogeneous sample exhibited visible grooves and material pile-up.

6.2.3 Scientific Question 3

How does additively manufactured Ti6Al4V with a targeted grid surface structure affect the long-term wear performance compared to the conventional CoCr30Mo6 alloy?

Answer: Over the long term, the additively manufactured Ti6Al4V alloy with the targeted grid structure outperformed conventional CoCr30Mo6 in wear performance and in retaining synovial fluid constituents within the contact area.

Evidence: Article 4 demonstrated lower UHMWPE wear against Ti6Al4V at all tested distances, a more stable wear-rate evolution, higher retention of model synovial-fluid constituents during fluorescence microscopy, and less severe damage on the Ti6Al4V pins after 300,000 cycles. Microstructural analysis further showed a nanograin near-surface layer and a stable oxide layer on Ti6Al4V, both of which likely contributed to this behaviour (see Article 4: Fig. 2, and Fig. 5–10).

Key quantitative results: The UHMWPE wear rates against Ti6Al4V were 1.1033×10^{-6}, 1.1148×10^{-6}, and 1.0475×10^{-6} mm^3/Nm after 100,000, 200,000, and 300,000 cycles, respectively, while for CoCr30Mo6 the corresponding values were 2.6374×10^{-6}, 1.6769×10^{-6}, and 1.2562×10^{-6} mm^3/Nm. During fluorescence microscopy, Ti6Al4V showed a relatively stable region of constituent retention for approximately

400–500 cycles. The Ti6Al4V surface also exhibited a nanograin layer approximately 200 nm thick and an oxide layer approximately 35 nm thick.

6.3 Future Work

The findings of this dissertation identify several research directions that can improve the understanding and tribological performance of additively manufactured small joint implants. The present work provides a systematic experimental evaluation of AM Ti6Al4V under tribological conditions representative of small joint arthroplasty. However, several aspects require further investigation before making broader preclinical conclusions.

A key strategy for future research is a more detailed analysis of the relationship between additive manufacturing parameters, the resulting surface and subsurface microstructure, and the long-term tribological response under physiologically relevant lubrication conditions. In particular, the effects of build orientation, volumetric energy density, layer strategy, and post-processing routes, such as heat treatment or hot isostatic pressing, should be investigated on surface morphology, protein adsorption, boundary film formation, and tribocorrosion resistance.

Further work should also focus on optimising the geometry and reproducibility of the beneficial AM surface structures identified in this dissertation. The present results show that not all surface morphologies provide the same tribological benefit, and that structured surfaces with favourable lubricant-retention capability may significantly improve lubrication and reduce wear. Future studies should therefore examine how geometric parameters, such as feature spacing, depth, edge definition, and manufacturing accuracy, affect lubrication stability, local stress concentrations, and long-term wear evolution.

Another important step is to extend the current experimental framework towards more complex loading and motion conditions. These should better approximate the *in vivo* function of small joints. Incorporating multidirectional motion, variable load amplitudes, transient contact conditions, and interrupted boundary-lubrication regimes would provide a more realistic description of the mechanisms responsible for wear initiation, film breakdown, and surface adaptation during gait-related cycles.

It would also be valuable to investigate the interaction of AM Ti6Al4V with a broader range of bearing materials relevant to orthopaedic applications, including advanced UHMWPE grades, PEEK-based polymers, and ceramic counterfaces. In addition, combining the inherent surface morphology created by additive manufacturing with controlled post-processing strategies, such as laser texturing, anodic oxidation, or thin protective coatings, may represent a promising route for further improving tribological performance while preserving structural integrity.

An equally important future direction is the connection between tribological findings and biological response. For meaningful preclinical assessment, future studies should

include systematic evaluation of wear debris generation, metallic ion release, and their possible biological consequences. Such work should ideally be complemented by *in vitro* cell-based testing and, where appropriate, by preclinical animal studies in order to assess both the safety and the functional relevance of the proposed surface concepts.

Although the experimental framework of this dissertation was primarily designed for small joint arthroplasty, the identified relationships between AM surface morphology, lubrication film formation, protein adsorption, and wear mechanisms are grounded in general tribological principles. For this reason, the methodological approach and some of the observed mechanisms may also be relevant to other orthopaedic applications, provided that differences in contact geometry, kinematics, loading regime, and lubrication environment are appropriately accounted for.

6.4 Clinical and Medical Applicability

The findings of this dissertation are relevant primarily to the preclinical design and optimisation of small joint implants, particularly for demanding applications such as the first metatarsophalangeal joint. Small joint arthroplasty operates under tribologically challenging conditions, including limited lubricant volume, relatively low sliding velocities, and predominantly boundary or mixed lubrication regimes. Under such conditions, implant performance is strongly influenced by surface integrity, the stability of the lubrication film, and the resistance of the articulating materials to wear.

The present results show that the tribological response of Ti6Al4V cannot be considered solely as a basic material property, but must be understood in relation to the manufacturing route and the resulting surface morphology. While conventionally manufactured Ti6Al4V showed limited suitability under the tested conditions, additively manufactured surfaces with an appropriate structural morphology exhibited more favourable lubrication behaviour and, in selected configurations, improved long-term wear performance. This suggests that AM surface morphology may function not only as a consequence of the manufacturing process, but also as a functionally relevant tribological feature.

From a preclinical design perspective, the ability of AM Ti6Al4V surfaces to support boundary film formation and lubricant retention is particularly important. These effects may contribute to more stable lubrication conditions and reduced direct surface interaction during articulation. In practical terms, such behaviour could help limit damage to the metallic component and reduce wear of the polymeric counterface, which is especially relevant in small joint systems where even moderate material degradation may compromise implant function.

The results also support the wider concept that additive manufacturing may offer advantages beyond geometric customisation alone. In addition to enabling patient-specific implant design and more flexible control of contact geometry, AM may provide a route

towards customising surface morphology in a tribologically meaningful way. This combination of shape and functional optimisation is of considerable interest for the future development of orthopaedic implants operating in biologically demanding environments.

At the same time, the present findings should be interpreted with appropriate caution. The experimental models used in this dissertation were designed to reveal tribological mechanisms under controlled laboratory conditions and do not directly simulate the full clinical situation. Therefore, the results should not be interpreted as direct evidence of clinical superiority or reduced revision risk. Rather, they provide mechanistically relevant knowledge of how additively manufactured Ti6Al4V surfaces may be designed and further developed for small joint applications.

Overall, this dissertation supports the view that additive manufacturing has significant potential in orthopaedic implant development, not only from a structural and geometric standpoint, but also as a tool for influencing tribological performance. The presented findings may therefore assist implant designers, manufacturers, and clinical researchers in developing next generation small joint replacements with improved preclinical tribological characteristics and stronger justification for subsequent translational research.

7

LIST OF OUTPUTS

7.1 Published Articles Included in the Dissertation

- **Odehnal L**, Ranuša M, Vrbka M, Křupka I, Hartl M. Tribological Behaviour of Ti6Al4V Alloy: An Application in Small Joint Implants. Tribol Lett 2023;71:125. (https://doi.org/10.1007/s11249-023-01795-4)

- Ranuša M, **Odehnal L**, Kučera O, Nečas D, Hartl M, Křupka I, Vrbka M. Effect of Surface Texturing on Friction and Lubrication of Ti6Al4V Biomaterials for Joint Implants. Tribol Lett 2025;73:15. (https://doi.org/10.1007/s11249-024-01950-5)

- **Odehnal L**, Ranuša M, Malý M, Křupka I, Koutný D, Hartl M, Vrbka M. Tribological behaviour of additively manufactured Ti6Al4V with controlled surface structure: An application in small joint implants. Tribol Int 2025;211:110832. (https://doi.org/10.1016/j.triboint.2025.110832)

- **Odehnal L**, Ranuša M, Čípek P, Malý M, Mazánová V, Dlouhý A, Koutný D, Hartl M, Vrbka M. Additively manufactured Ti6Al4V with controlled surface structure as a Potential Material for Joint Implants: Long-Term Wear Performance and Durability. Tribol Int 2026;216:111599. (https://doi.org/10.1016/j.triboint.2025.111599)

7.2 Published Articles Not Included in the Dissertation

- **Odehnal L**, Ranuša M, Wimmer MA, Vrbka M, Křupka I. Development of lubrication film and influence on friction in a total knee replacement during a gait cycle. Tribol Int 2023;178:108073. (https://doi.org/10.1016/j.triboint.2022.108073)

- Rebenda D, **Odehnal L**, Uhrová S, Nečas D, Vrbka M. On the Friction and Lubrication of 3D Printed Ti6Al4V Hip Joint Replacement. Tribol Lett 2025;73:68. (https://doi.org/10.1007/s11249-025-02002-2)

7.3 Conference Contributions

- **Odehnal L**, Ranuša M, Malý M, Vrbka M, Hartl M. Additive Manufacturing as a Potential Method to Produce Friction Surfaces of Joint Implants: The Tribological Behaviour of Ti6Al4V.
  ECOTRIB23, 2023, Bari, Italy.

- **Odehnal L**, Ranuša M, Malý M, Vrbka M. Additively Manufactured Ti6Al4V with Controlled Surface Structure as a Potential Material for Small Joint Implants.
  ICTMP2024, 2024, Alcoy, Spain.

- **Odehnal L**, Ranuša M, Malý M, Vrbka M, Hartl M. Additive Manufacturing as a Potential Method to Produce Friction Surfaces of Joint Implants: The Tribological Behaviour of Ti6Al4V.
  49th Leeds-Lyon Symposium on Tribology, 2024, Lyon, France.

- **Odehnal L**, Ranuša M, Vrbka M, Křupka I, Hartl M. AM Ti6Al4V with Controlled Surface Structure: Long-Term Wear Performance and Durability.
  ECOTRIB25, 2025, Zurich, Switzerland.

- **Odehnal L**, Ranuša M, Malý M, Vrbka M, Hartl M. Tribocorrosion Study of AM Ti6Al4V with Surface Structure and UHMWPE Interfaces Under Synovial Fluid Degradation: Insights from a Scientific Mobility at EPFL.
  Conference MEBioSys 2025, Brno, Czech Republic.

7.4 Functional Prototypes

- Čípek P, Ranuša M, **Odehnal L**, Vrbka M. Simulator for Examination of Wear in Small Joint Implants. (Functional Prototype)
  (https://intranet.ustavkonstruovani.cz/file-download/get-project-pdf/486)

7.5 Scientific Mobilities

- École Polytechnique fédérale de Lausanne (EPFL), Switzerland, June – August 2025. Tribocorrosion Study of AM Ti6Al4V with Surface Structure and UHMWPE Interfaces Under Synovial Fluid Degradation.

7.6 Research projects funding this work

- *"Friction and lubrication of small joint implants produced by 3D metal printing additive technology"*, funded as project No. 22-02154S by Czech Science Foundation.

- *"Mechanical Engineering of Biological and Bio-inspired Systems"*, funded as project No. CZ.02.01.01/00/22_008/0004634 by Programme Johannes Amos Comenius, call Excellent Research, administered by the Ministry of Education, Sports and Youth.

- *"3D printed individualised segmental joint implant: optimisation of fixation to bone and biotribology of articular surface"*, funded as project No. NW25-08-00044 by the Ministry of Health of the Czech Republic in cooperation with the Czech Health Research Council.

8

APPENDICES AND SUPPORTING INFORMATION

8.1 References

[1] Matharu G, Culliford D, Blom A, Judge A. Projections for primary hip and knee replacement surgery up to the year 2060: an analysis based on data from The National Joint Registry for England, Wales, Northern Ireland and the Isle of Man. The Annals of The Royal College of Surgeons of England 2022;104:443–8. https://doi.org/10.1308/rcsann.2021.0206.

[2] 22nd Annual Report by the National Joint Registry n.d. https://reports.njrcentre.org.uk/downloads (accessed October 8, 2025).

[3] Geilen JEJW, Hermans SMM, Droeghaag R, Schotanus MGM, van Haaren EH, van Hemert WLW. A systematic review comparing the cost-effectiveness of the direct anterior, posterior, and straight lateral approach in total hip arthroplasty. EFORT Open Rev 2023;8:443–50. https://doi.org/10.1530/EOR-22-0108.

[4] Fordham R, Skinner J, Wang X, Nolan J. The economic benefit of hip replacement: a 5-year follow-up of costs and outcomes in the Exeter Primary Outcomes Study. BMJ Open 2012;2:e000752. https://doi.org/10.1136/bmjopen-2011-000752.

[5] Konopka JF, Lee Y, Su EP, McLawhorn AS. Quality-Adjusted Life Years After Hip and Knee Arthroplasty. JBJS Open Access 2018;3:e0007. https://doi.org/10.2106/JBJS.OA.18.00007.

[6] Daigle ME, Weinstein AM, Katz JN, Losina E. The cost-effectiveness of total joint arthroplasty: A systematic review of published literature. Best Pract Res Clin Rheumatol 2012;26:649–58. https://doi.org/10.1016/j.berh.2012.07.013.

[7] Lan RH, Yu J, Samuel LT, Pappas MA, Brooks PJ, Kamath AF. How Are We Measuring Cost-Effectiveness in Total Joint Arthroplasty Studies? Systematic Review of the Literature. J Arthroplasty 2020;35:3364–74. https://doi.org/10.1016/j.arth.2020.06.046.

[8] Kurtz SM, Lau EC, Ong KL, Adler EM, Kolisek FR, Manley MT. Has Health Care Reform Legislation Reduced the Economic Burden of Hospital Readmissions Following Primary Total Joint Arthroplasty? J Arthroplasty 2017;32:3274–85. https://doi.org/10.1016/j.arth.2017.05.059.

[9] Phillips JLH, Rondon AJ, Vannello C, Fillingham YA, Austin MS, Courtney PM. How Much Does a Readmission Cost the Bundle Following Primary Hip and Knee Arthroplasty? J Arthroplasty 2019;34:819–23. https://doi.org/10.1016/j.arth.2019.01.029.

[10] Koenig L, Zhang Q, Austin MS, Demiralp B, Fehring TK, Feng C, et al. Estimating the Societal Benefits of THA After Accounting for Work Status and Productivity: A Markov Model Approach. Clin Orthop Relat Res 2016;474:2645–54. https://doi.org/10.1007/s11999-016-5084-9.

[11] Thacharodi A, Singh P, Meenatchi R, Tawfeeq Ahmed ZH, Kumar RRS, V N, et al. Revolutionizing healthcare and medicine: The impact of modern technologies for a healthier future—A comprehensive review. Health Care Science 2024;3:329–49. https://doi.org/10.1002/hcs2.115.

[12] Affatato S, Spinelli M, Zavalloni M, Mazzega-Fabbro C, Viceconti M. Tribology and total hip joint replacement: Current concepts in mechanical simulation. Med Eng Phys 2008;30:1305–17. https://doi.org/10.1016/j.medengphy.2008.07.006.

[13] Mei XY, Gong YJ, Safir O, Gross A, Kuzyk P. Long-term outcomes of total hip arthroplasty in patients younger than 55 years: a systematic review of the contemporary literature. Canadian Journal of Surgery 2019;62:249–58. https://doi.org/10.1503/cjs.013118.

[14] Brand RA, Mont MA, Manring MM. Biographical Sketch: Themistocles Gluck (1853-1942). Clin Orthop Relat Res 2011;469:1525–7. https://doi.org/10.1007/s11999-011-1836-8.

[15] CHARNLEY J. ARTHROPLASTY OF THE HIP A New Operation. The Lancet 1961;277:1129–32. https://doi.org/10.1016/S0140-6736(61)92063-3.

[16] Hernández-Vaquero D, Suárez-Vazquez A, Fernandez-Lombardia J. Charnley low-friction arthroplasty of the hip. Five to 25 years survivorship in a general hospital. BMC Musculoskelet Disord 2008;9:69. https://doi.org/10.1186/1471-2474-9-69.

[17] Savin L, Pinteala T, Mihai DN, Mihailescu D, Miu SS, Sirbu MT, et al. Updates on Biomaterials Used in Total Hip Arthroplasty (THA). Polymers (Basel) 2023;15:3278. https://doi.org/10.3390/polym15153278.

[18] Tong L, Yu H, Huang X, Shen J, Xiao G, Chen L, et al. Current understanding of osteoarthritis pathogenesis and relevant new approaches. Bone Res 2022;10:60. https://doi.org/10.1038/s41413-022-00226-9.

[19] Chen D, Shen J, Zhao W, Wang T, Han L, Hamilton JL, et al. Osteoarthritis: toward a comprehensive understanding of pathological mechanism. Bone Res 2017;5:16044. https://doi.org/10.1038/boneres.2016.44.

[20] Universitäts Spital Zürich n.d. https://www.usz.ch/en/disease/osteoarthritis/ (accessed October 14, 2025).

[21] Kohn MD, Sassoon AA, Fernando ND. Classifications in Brief: Kellgren-Lawrence Classification of Osteoarthritis. Clin Orthop Relat Res 2016;474:1886–93. https://doi.org/10.1007/s11999-016-4732-4.

[22] World Health Organisation n.d. https://www.who.int/ (accessed October 8, 2025).

[23] Poliakov A, Pakhaliuk V, Popov VL. Current Trends in Improving of Artificial Joints Design and Technologies for Their Arthroplasty. Front Mech Eng 2020;6. https://doi.org/10.3389/fmech.2020.00004.

[24] Pasquier G, Ehlinger M, Mainard D. The role of rotating hinge implants in revision total knee arthroplasty. EFORT Open Rev 2019;4:269–78. https://doi.org/10.1302/2058-5241.4.180070.

[25] Vasso M, Beaufils P, Schiavone Panni A. Constraint choice in revision knee arthroplasty. Int Orthop 2013;37:1279–84. https://doi.org/10.1007/s00264-013-1929-y.

[26] Nolte P-C, Schlentrich K, Raisch P, Jung MK, Grützner PA, Bischel O. Survival and Clinical Outcomes after Unconstrained Total Knee Arthroplasty for Tibial Plateau Fractures–A Retrospective Study with Minimum 4-Year Follow-Up. J Clin Med 2023;12:7303. https://doi.org/10.3390/jcm12237303.

[27] S. AD, P. SPA, Naveen J, Khan T, Khahro SH. Advancement in biomedical implant materials—a mini review. Front Bioeng Biotechnol 2024;12. https://doi.org/10.3389/fbioe.2024.1400918.

[28] Bandyopadhyay A, Mitra I, Goodman SB, Kumar M, Bose S. Improving biocompatibility for next generation of metallic implants. Prog Mater Sci 2023;133:101053. https://doi.org/10.1016/j.pmatsci.2022.101053.

[29] Hasegawa M, Tone S, Naito Y, Sudo A. Ultra-High-Molecular-Weight Polyethylene in Hip and Knee Arthroplasties. Materials 2023;16:2140. https://doi.org/10.3390/ma16062140.

[30] Prentice HA, Chan PH, Fasig BH, Kelly MP, Hinman AD, Kurtz SM, et al. Highly Crosslinked Polyethylene Is Associated With a Lower Revision Risk Out to 20-Year Follow-Up Versus Conventional Polyethylene in Total Knee Arthroplasty. J Arthroplasty 2025. https://doi.org/10.1016/j.arth.2025.07.005.

[31] Dallal S, Eslami B, Tiari S. Recent Advances in PEEK for Biomedical Applications: A Comprehensive Review of Material Properties, Processing, and Additive Manufacturing. Polymers (Basel) 2025;17:1968. https://doi.org/10.3390/polym17141968.

[32] Li Z. Advancements of biomaterial in hip replacement technology incorporating ceramic materials. J Orthop 2025;62:27–35. https://doi.org/10.1016/j.jor.2024.09.021.

[33] Abd-Elaziem W, Darwish MA, Hamada A, Daoush WM. Titanium-Based alloys and composites for orthopedic implants Applications: A comprehensive review. Mater Des 2024;241:112850. https://doi.org/10.1016/j.matdes.2024.112850.

[34] Alberta LA, Vishnu J, Douest Y, Perrin K, Trunfio-Sfarghiu A-M, Courtois N, et al. Tribocorrosion behavior of β-type Ti-Nb-Ga alloys in a physiological solution. Tribol Int 2023;181:108325. https://doi.org/10.1016/j.triboint.2023.108325.

[35] Injeti VSY, Nune KC, Reyes E, Yue G, Li SJ, Misra RDK. A comparative study on the tribological behavior of Ti-6Al-4V and Ti-24Nb-4Zr-8Sn alloys in simulated body fluid. Materials Technology 2019;34:270–84. https://doi.org/10.1080/10667857.2018.1550138.

[36] Kopova I, Stráský J, Harcuba P, Landa M, Janeček M, Bačákova L. Newly developed Ti–Nb–Zr–Ta–Si–Fe biomedical beta titanium alloys with increased strength and enhanced biocompatibility. Materials Science and Engineering: C 2016;60:230–8. https://doi.org/10.1016/j.msec.2015.11.043.

[37] Okazaki Y. A New Ti–15Zr–4Nb–4Ta alloy for medical applications. Curr Opin Solid State Mater Sci 2001;5:45–53. https://doi.org/10.1016/S1359-0286(00)00025-5.

[38] Sun Y, Liu Q, Yu Z, Ren L, Zhao X, Wang J. Study on Osseointegration Capability of β-Type Ti–Nb–Zr–Ta–Si Alloy for Orthopedic Implants. Materials 2024;17:472. https://doi.org/10.3390/ma17020472.

[39] Kolli RP, Devaraj A. A Review of Metastable Beta Titanium Alloys. Metals (Basel) 2018;8:506. https://doi.org/10.3390/met8070506.

[40] Du S, Song Y, He Y, Wei C, Chen R, Guo S, et al. Evolution of Microstructure and Mechanical Properties of Ti-6Al-4V Alloy under Heat Treatment and Multi-Axial Forging. Materials 2024;17:1060. https://doi.org/10.3390/ma17051060.

[41] Nath P, Marandi L, Sen I. Processing-microstructure-property correlation in thermo-mechanically processed Ti-6Al-4V alloys: A comparative study between conventional and novel approaches. J Alloys Compd 2022;927:167039. https://doi.org/10.1016/j.jallcom.2022.167039.

[42] Ellingsen JE. A study on the mechanism of protein adsorption to TiO2. Biomaterials 1991;12:593–6. https://doi.org/10.1016/0142-9612(91)90057-H.

[43] Wang W, Chen J, Sun X, Sun G, Liang Y, Bi J. Influence of Additives on Microstructure and Mechanical Properties of Alumina Ceramics. Materials 2022;15:2956. https://doi.org/10.3390/ma15082956.

[44] Bai R, Sun Q, He Y, Peng L, Zhang Y, Zhang L, et al. Ceramic Toughening Strategies for Biomedical Applications. Front Bioeng Biotechnol 2022;10. https://doi.org/10.3389/fbioe.2022.840372.

[45] Langlois J, Hamadouche M. Recent update on crosslinked polyethylene in total hip arthroplasty. SICOT J 2020;6:13. https://doi.org/10.1051/sicotj/2020013.

[46] Eliaz N. Corrosion of Metallic Biomaterials: A Review. Materials 2019;12:407. https://doi.org/10.3390/ma12030407.

[47] Takadoum J. Review on Corrosion, Tribocorrosion and Osseointegration of Titanium Alloys as Biomaterials. Corrosion and Materials Degradation 2023;4:644–58. https://doi.org/10.3390/cmd4040033.

[48] Zais IE, Sammali S, Pavan M, Chisari E, Krueger CA. The Local Toxicity of Cobalt Chrome implants: A Systematic Review of Preclinical Studies 2022. https://doi.org/10.21203/rs.3.rs-1240755/v1.

[49] Asri RIM, Harun WSW, Samykano M, Lah NAC, Ghani SAC, Tarlochan F, et al. Corrosion and surface modification on biocompatible metals: A review. Materials Science and Engineering: C 2017;77:1261–74. https://doi.org/10.1016/j.msec.2017.04.102.

[50] Bandyopadhyay A, Espana F, Balla VK, Bose S, Ohgami Y, Davies NM. Influence of porosity on mechanical properties and in vivo response of Ti6Al4V implants. Acta Biomater 2010;6:1640–8. https://doi.org/10.1016/j.actbio.2009.11.011.

[51] Calazans Neto JV, Reis AC dos, Valente ML da C. Osseointegration in additive-manufactured titanium implants: A systematic review of animal studies on the need for surface treatment. Heliyon 2023;9:e17105. https://doi.org/10.1016/j.heliyon.2023.e17105.

[52] Das A, Rajkumar P. Metal 3D printing of biometals for prostheses and implants: a review. Exploration of BioMat-X 2025;2. https://doi.org/10.37349/ebmx.2025.101338.

[53] Ni J, Ling H, Zhang S, Wang Z, Peng Z, Benyshek C, et al. Three-dimensional printing of metals for biomedical applications. Mater Today Bio 2019;3:100024. https://doi.org/10.1016/j.mtbio.2019.100024.

[54] Estupinán-López F, Orquiz-Muela C, Gaona-Tiburcio C, Cabral-Miramontes J, Bautista-Margulis RG, Nieves-Mendoza D, et al. Oxidation Kinetics of Ti-6Al-4V Alloys by Conventional and Electron Beam Additive Manufacturing. Materials 2023;16:1187. https://doi.org/10.3390/ma16031187.

[55] Kathiresan M, Karthikeyan M, Immanuel RJ. A short review on SLM-processed Ti6Al4V composites. Proceedings of the Institution of Mechanical Engineers, Part E: Journal of Process Mechanical Engineering 2024;238:3054–69. https://doi.org/10.1177/09544089231169380.

[56] Bin Abdullah MS, Ramulu M. The Tribological Behavior of Electron Beam Powder Bed Fused Ti-6Al-4V: A Review. Metals (Basel) 2025;15:1170. https://doi.org/10.3390/met15111170.

[57] Shahsavari M, Imani A, Schaller RF, Asselin E. Corrosion evaluation of Ti–6Al–4V manufactured by electron beam melting in Ringer's physiological solution: an in vitro study of the passive film. J Appl Electrochem 2022;52:1003–19. https://doi.org/10.1007/s10800-022-01683-0.

[58] LEKATOU AG, EFREMENKO BV, HAOUI V, EFREMENKO VG, EMMANOUILIDOU S, ZURNADZHY VI, et al. Microstructure, electrochemical, wear and corrosive wear performance of laser-based powder bed fusion and wrought biomedical Ti−6Al−4V alloys. Transactions of Nonferrous Metals Society of China 2025;35:2612–31. https://doi.org/10.1016/S1003-6326(25)66836-1.

[59] Ricci S, Iannitti G. Mechanical Behavior of Additive Manufacturing (AM) and Wrought Ti6Al4V with a Martensitic Microstructure. Metals (Basel) 2024;14:1028. https://doi.org/10.3390/met14091028.

[60] Eskandari H, Lashgari HR, Zangeneh Sh, Kong C, Ye L, Eizadjou M, et al. Microstructural characterization and mechanical properties of SLM-printed Ti–6Al–4V alloy: Effect of build orientation. J Mater Res 2022;37:2645–60. https://doi.org/10.1557/s43578-021-00468-z.

[61] Shi X, Lu P, Ye X, Ren S, Wang Y, Xie Z, et al. Study of mechanical and tribological properties of Ti–6Al–4V alloy fabricated by powder bed fusion laser beam. Powder Metallurgy 2023;66:116–28. https://doi.org/10.1080/00325899.2022.2116405.

[62] Song B, Dong S, Zhang B, Liao H, Coddet C. Effects of processing parameters on microstructure and mechanical property of selective laser melted Ti6Al4V. Mater Des 2012;35:120–5. https://doi.org/10.1016/j.matdes.2011.09.051.

[63] Goyal V, Verma G. Tribological Behavior of Direct Metal Laser Sintering–Manufactured Ti6Al4V Alloy in Different Biofluids for Orthopedic Implants. J Tribol 2024;146. https://doi.org/10.1115/1.4064506.

[64] Karasoglu M, Öteyaka MÖ, Yasa E, Tan E, Kuşhan MC. Effect of Heat Treatment and Hot Isostatic Pressing on the Corrosion Behavior of Ti $_6$ Al $_4$ V Parts Produced by Electron Beam Melting Additive Manufacturing Technology. ACS Omega 2024;9:29904–16. https://doi.org/10.1021/acsomega.4c04218.

[65] Kathiresan M, Karthikeyan M, Immanuel RJ. A short review on SLM-processed Ti6Al4V composites. Proceedings of the Institution of Mechanical Engineers, Part E: Journal of Process Mechanical Engineering 2024;238:3054–69. https://doi.org/10.1177/09544089231169380.

[66] BARTOLOMEU F, BUCIUMEANU M, PINTO E, ALVES N, SILVA FS, CARVALHO O, et al. Wear behavior of Ti6Al4V biomedical alloys processed by selective laser melting, hot pressing and conventional casting. Transactions of Nonferrous Metals Society of China 2017;27:829–38. https://doi.org/10.1016/S1003-6326(17)60060-8.

[67] Goyal V, Verma G. Tribological Behavior of Direct Metal Laser Sintering–Manufactured Ti6Al4V Alloy in Different Biofluids for Orthopedic Implants. J Tribol 2024;146. https://doi.org/10.1115/1.4064506.

[68] Fischer D, Cheng K, Neto MQ, Hall D, Bijukumar D, Espinoza Orías AA, et al. Corrosion Behavior of Selective Laser Melting (SLM) Manufactured Ti6Al4V Alloy in Saline and BCS Solution. J Bio Tribocorros 2022;8:63. https://doi.org/10.1007/s40735-022-00657-1.

[69] Patel M V., Cudjoe E, Ryu JJ. Sliding Contact Fatigue Damage of Metallic Implants in a Simulated Body Fluid Environment. Lubricants 2024;12:437. https://doi.org/10.3390/lubricants12120437.

[70] Liang X, Du P, Li S, Zhang C. Tribological properties of additive manufactured Ti6Al4V against cemented carbide under dry sliding conditions. Tribol Int 2022;167:107358. https://doi.org/10.1016/j.triboint.2021.107358.

[71] Yao L, He Y, Wang Z, Peng B, Li G, Liu Y. Effect of Heat Treatment on the Wear Properties of Selective Laser Melted Ti–6Al–4V Alloy Under Different Loads. Acta Metallurgica Sinica (English Letters) 2022;35:517–25. https://doi.org/10.1007/s40195-021-01280-8.

[72] Geetha M, Singh AK, Asokamani R, Gogia AK. Ti based biomaterials, the ultimate choice for orthopaedic implants – A review. Prog Mater Sci 2009;54:397–425. https://doi.org/10.1016/j.pmatsci.2008.06.004.

[73] Marin E, Lanzutti A. Biomedical Applications of Titanium Alloys: A Comprehensive Review. Materials 2023;17:114. https://doi.org/10.3390/ma17010114.

[74] Xu J, Zhang J, Shi Y, Tang J, Huang D, Yan M, et al. Surface Modification of Biomedical Ti and Ti Alloys: A Review on Current Advances. Materials 2022;15:1749. https://doi.org/10.3390/ma15051749.

[75] AbuAlia M, Fullam S, Cinotti F, Manninen N, Wimmer MA. Titanium Nitride Coatings on CoCrMo and Ti6Al4V Alloys: Effects on Wear and Ion Release. Lubricants 2024;12:96. https://doi.org/10.3390/lubricants12030096.

[76] van Hove RP, Sierevelt IN, van Royen BJ, Nolte PA. Titanium-Nitride Coating of Orthopaedic Implants: A Review of the Literature. Biomed Res Int 2015;2015:1–9. https://doi.org/10.1155/2015/485975.

[77] Sitek R, Kamiński J, Adamczyk-Cieślak B, Molak R, Spychalski M, Cowell B, et al. Effect of Plasma Nitriding on Structure and Properties of Titanium Grade 2 Produced by Direct Metal Laser Sintering. Metallography, Microstructure, and Analysis 2022;11:852–63. https://doi.org/10.1007/s13632-022-00903-5.

[78] Senna PM, Mourão CF, Dodo CG, Rutkowski JL, Cury AADB. Nitriding Titanium by Plasma Ion Implantation: Surface Properties and Initial Osteoblast Cell Response. Braz Dent J 2024;35. https://doi.org/10.1590/0103-6440202406111.

[79] Kamat AM, Copley SM, Segall AE, Todd JA. Laser-Sustained Plasma (LSP) Nitriding of Titanium: A Review. Coatings 2019;9:283. https://doi.org/10.3390/coatings9050283.

[80] Malisz K, Świeczko-Żurek B, Sionkowska A. Preparation and Characterization of Diamond-like Carbon Coatings for Biomedical Applications—A Review. Materials 2023;16:3420. https://doi.org/10.3390/ma16093420.

[81] Madej M, Piotrowska K, Vicen M, Zatkaliková V. Wear and Corrosion Behavior of Diamond-like Carbon Coatings in Artificial Saliva. Coatings 2025;15:305. https://doi.org/10.3390/coatings15030305.

[82] Jedrzejczak A, Szymanski W, Kolodziejczyk L, Sobczyk-Guzenda A, Kaczorowski W, Grabarczyk J, et al. Tribological Characteristics of a-C:H:Si and a-C:H:SiOx Coatings Tested in Simulated Body Fluid and Protein Environment. Materials 2022;15:2082. https://doi.org/10.3390/ma15062082.

[83] Li Y, Zhou Z, He Y. Tribocorrosion and Surface Protection Technology of Titanium Alloys: A Review. Materials 2023;17:65. https://doi.org/10.3390/ma17010065.

[84] Joska L, Fojt J, Mestek O, Cvrcek L, Brezina V. The effect of a DLC coating adhesion layer on the corrosion behavior of titanium and the Ti6Al4V alloy for dental implants. Surf Coat Technol 2012;206:4899–906. https://doi.org/10.1016/j.surfcoat.2012.05.089.

[85] Wei C, Wu B-C, Hung M-S. Effects of Ti6Al4V Substrate Roughness on the Surface Morphology, Mechanical Properties, and Cell Proliferation of Diamond-like Carbon Films. Coatings 2025;15:1086. https://doi.org/10.3390/coatings15091086.

[86] Lin N, Li D, Zou J, Xie R, Wang Z, Tang B. Surface Texture-Based Surface Treatments on Ti6Al4V Titanium Alloys for Tribological and Biological Applications: A Mini Review. Materials 2018;11:487. https://doi.org/10.3390/ma11040487.

[87] Woźniak A, Bialas O, Adamiak M, Hadzima B, Szewczenko J. The influence of laser texturing on the tribological behavior of titanium alloy Ti6Al4V in medical applications. Archives of Civil and Mechanical Engineering 2024;24:146. https://doi.org/10.1007/s43452-024-00960-3.

[88] Schweitzer L, Schoon J, Bläß N, Huesker K, Neufend J V., Siemens N, et al. Ultraviolet laser induced periodic surface structures positively influence osteogenic activity on titanium alloys. Front Bioeng Biotechnol 2024;12. https://doi.org/10.3389/fbioe.2024.1462232.

[89] Choudhury D, Rebenda D, Sasaki S, Hekrle P, Vrbka M, Zou M. Enhanced lubricant film formation through micro-dimpled hard-on-hard artificial hip joint: An in-situ observation of dimple shape effects. J Mech Behav Biomed Mater 2018;81:120–9. https://doi.org/10.1016/j.jmbbm.2018.02.014.

[90] Pratap T, Patra K. Mechanical micro-texturing of Ti-6Al-4V surfaces for improved wettability and bio-tribological performances. Surf Coat Technol 2018;349:71–81. https://doi.org/10.1016/j.surfcoat.2018.05.056.

[91] Allen Q, Raeymaekers B. Maximizing the Lubricant Film Thickness Between a Rigid Microtextured and a Smooth Deformable Surface in Relative Motion, Using a Soft Elasto-Hydrodynamic Lubrication Model. J Tribol 2020;142. https://doi.org/10.1115/1.4046291.

[92] Obeidi MA, Mussatto A, Dogu MN, Sreenilayam SP, McCarthy E, Ahad IU, et al. Laser surface polishing of Ti-6Al-4V parts manufactured by laser powder bed fusion. Surf Coat Technol 2022;434:128179. https://doi.org/10.1016/j.surfcoat.2022.128179.

[93] Li J, Wu H, Liu H, Zuo D. Surface and property characterization of selective laser-melted Ti-6Al-4V alloy after laser polishing. The International Journal of Advanced Manufacturing Technology 2023;128:703–14. https://doi.org/10.1007/s00170-023-11880-6.

[94] LIN X, ZHU M, ZHENG J, LUO J, MO J. Fretting wear of micro-arc oxidation coating prepared on Ti6Al4V alloy. Transactions of Nonferrous Metals Society of China 2010;20:537–46. https://doi.org/10.1016/S1003-6326(09)60175-8.

[95] BALOYI NM, POPOOLA API, PITYANA SL. Microstructure, hardness and corrosion properties of laser processed Ti6Al4V-based composites. Transactions of Nonferrous Metals Society of China 2015;25:2912–23. https://doi.org/10.1016/S1003-6326(15)63917-6.

[96] Muniyappan A, Muthuvel PA, Sanmugam A, Wadaan MA, Baabbad A, Muthuchamy N, et al. Enhanced Tribological Performance of Laser-Textured TiN-Coated Ti6Al4V Alloy Surfaces: A Comparative Study with Untextured Surfaces. Processes 2025;13:204. https://doi.org/10.3390/pr13010204.

[97] E SF, Shi L, Guo ZG, Liu WM. The recent progress of tribological biomaterials. Biosurf Biotribol 2015;1:81–97. https://doi.org/10.1016/j.bsbt.2015.06.002.

[98] Ahmed T, Rack HJ. Phase transformations during cooling in α+β titanium alloys. Materials Science and Engineering: A 1998;243:206–11. https://doi.org/10.1016/S0921-5093(97)00802-2.

[99] Mavraki A, Cann PM. Lubricating film thickness measurements with bovine serum. Tribol Int 2011;44:550–6. https://doi.org/10.1016/j.triboint.2010.07.008.

[100] Galandáková A, Ulrichová J, Langová K, Hanáková A, Vrbka M, Hartl M, et al. Characteristics of synovial fluid required for optimization of lubrication fluid for biotribological experiments. J Biomed Mater Res B Appl Biomater 2017;105:1422–31. https://doi.org/10.1002/jbm.b.33663.

[101] Marian M, Shah R, Gashi B, Zhang S, Bhavnani K, Wartzack S, et al. Exploring the lubrication mechanisms of synovial fluids for joint longevity – A perspective. Colloids Surf B Biointerfaces 2021;206:111926. https://doi.org/10.1016/j.colsurfb.2021.111926.

[102] Rothammer B, Marian M, Rummel F, Schroeder S, Uhler M, Kretzer JP, et al. Rheological behavior of an artificial synovial fluid – influence of temperature, shear rate and pressure. J Mech Behav Biomed Mater 2021;115:104278. https://doi.org/10.1016/j.jmbbm.2020.104278.

[103] Mavraki A, Cann PM. Lubricating film thickness measurements with bovine serum. Tribol Int 2011;44:550–6. https://doi.org/10.1016/j.triboint.2010.07.008.

[104] Brandt J-M, Charron KD, Zhao L, MacDonald SJ, Medley JB. Lubricant Biochemistry Affects Polyethylene Wear in Knee Simulator Testing. Biotribology 2021;27:100185. https://doi.org/10.1016/j.biotri.2021.100185.

[105] Myant C, Underwood R, Fan J, Cann PM. Lubrication of metal-on-metal hip joints: The effect of protein content and load on film formation and wear. J Mech Behav Biomed Mater 2012;6:30–40. https://doi.org/10.1016/j.jmbbm.2011.09.008.

[106] Myant C, Cann P. In contact observation of model synovial fluid lubricating mechanisms. Tribol Int, vol. 63, Elsevier Ltd; 2013, p. 97–104. https://doi.org/10.1016/j.triboint.2012.04.029.

[107] Myant CW, Cann P. The effect of transient conditions on synovial fluid protein aggregation lubrication. J Mech Behav Biomed Mater 2014;34:349–57. https://doi.org/10.1016/j.jmbbm.2014.02.005.

[108] Myant C, Cann P. On the matter of synovial fluid lubrication: Implications for Metal-on-Metal hip tribology. J Mech Behav Biomed Mater 2014;34:338–48. https://doi.org/10.1016/j.jmbbm.2013.12.016.

[109] Nissim L, Butt H, Gao L, Myant C, Hewson R. Role of protein concentration on transient film thickness in synovial fluid lubricated joints. Biotribology 2021;28:100191. https://doi.org/10.1016/j.biotri.2021.100191.

[110] Stevenson H, Cann PM. Protein Content of Model Synovial Fluid and CoCrMo Wear. Biotribology 2021;26:100172. https://doi.org/10.1016/j.biotri.2021.100172.

[111] Nečas D, Vrbka M, Rebenda D, Gallo J, Galandáková A, Wolfová L, et al. In situ observation of lubricant film formation in THR considering real conformity: The effect of model synovial fluid composition. Tribol Int 2018;117:206–16. https://doi.org/10.1016/j.triboint.2017.09.001.

[112] Nečas D, Vrbka M, Galandáková A, Křupka I, Hartl M. On the observation of lubrication mechanisms within hip joint replacements. Part I: Hard-on-soft bearing pairs. J Mech Behav Biomed Mater 2019;89:237–48. https://doi.org/10.1016/j.jmbbm.2018.09.022.

[113] Shinmori H, Kubota M, Morita T, Yamaguchi T, Sawae Y. Effects of Synovial Fluid Constituents on Friction between UHMWPE and CoCrMo. Tribology Online 2020;15:283–92. https://doi.org/10.2474/trol.15.283.

[114] Hussein M, Mohammed A, Al-Aqeeli N. Wear Characteristics of Metallic Biomaterials: A Review. Materials 2015;8:2749–68. https://doi.org/10.3390/ma8052749.

[115] Zakerin N, Morshed-Behbahani K, Bishop DP, Nasiri A. Review of Tribological and Wear Behavior of Alloys Fabricated via Directed Energy Deposition Additive Manufacturing. Journal of Manufacturing and Materials Processing 2025;9:194. https://doi.org/10.3390/jmmp9060194.

[116] Shi W, Dong H, Bell T. Tribological behaviour and microscopic wear mechanisms of UHMWPE sliding against thermal oxidation-treated Ti6Al4V. Materials Science and Engineering: A 2000;291:27–36. https://doi.org/10.1016/S0921-5093(00)00972-2.

[117] CHEN J, ZHANG Q, LI Q, FU S, WANG J. Corrosion and tribocorrosion behaviors of AISI 316 stainless steel and Ti6Al4V alloys in artificial seawater. Transactions of Nonferrous Metals Society of China 2014;24:1022–31. https://doi.org/10.1016/S1003-6326(14)63157-5.

[118] Feyzi M, Baghi AD, Fallahnezhad K, Nafisi S, Ghomashchi R, Hashemi R. Bio-tribocorrosive performance of additively manufactured Ti-6Al-4 V alloy via laser powder bed fusion (L-PBF). Progress in Additive Manufacturing 2025;10:5043–56. https://doi.org/10.1007/s40964-024-00886-5.

[119] Shao J, Lan G, Song H, Dong X, Li M. Recent Advances in Biomimetic Related Lubrication. Lubricants 2024;12:377. https://doi.org/10.3390/lubricants12110377.

[120] Esway J-E, Conti SF. Joint Replacement in the Hallux Metatarsophalangeal Joint. Foot Ankle Clin 2005;10:97–115. https://doi.org/10.1016/j.fcl.2004.09.002.

[121] França G, Nunes J, Pinho P, Freitas D, Andrade R, Espregueira-Mendes J, et al. Is arthrodesis still the best treatment option for first metatarsophalangeal joint arthritis?—a systematic review of arthrodesis and arthroplasty outcomes. Ann Jt 2021;6:5–5. https://doi.org/10.21037/aoj-20-88.

[122] Erkocak OF, Senaran H, Altan E, Aydin BK, Acar MA. Short-Term Functional Outcomes of First Metatarsophalangeal Total Joint Replacement for Hallux Rigidus. Foot Ankle Int 2013;34:1569–79. https://doi.org/10.1177/1071100713496770.

[123] Daniilidis K, Martinelli N, Marinozzi A, Denaro V, Gosheger G, Pejman Z, et al. Recreational sport activity after total replacement of the first metatarsophalangeal joint: a prospective study. Int Orthop 2010;34:973–9. https://doi.org/10.1007/s00264-009-0935-6.

[124] Clough TM, Ring J. Silastic first metatarsophalangeal joint arthroplasty for the treatment of end-stage hallux rigidus. Bone Joint J 2020;102-B:220–6. https://doi.org/10.1302/0301-620X.102B2.BJJ-2019-0518.R2.

[125] Gupta S, Masud S. Long term results of the Toefit-Plus replacement for first metatarsophalangeal joint arthritis. The Foot 2017;31:67–71. https://doi.org/10.1016/j.foot.2017.04.006.

[126] Fieschi S, Redaelli C, Fazzini A. Short-Term Outcomes of First Metatarsophalangeal Arthroplasty Using the Silktoe Double-Stemmed Silicone Implant. Diagnostics 2025;15:1349. https://doi.org/10.3390/diagnostics15111349.

[127] Allan JJ, McClelland JA, Munteanu SE, Buldt AK, Landorf KB, Roddy E, et al. First metatarsophalangeal joint range of motion is associated with lower limb kinematics in individuals with first metatarsophalangeal joint osteoarthritis. J Foot Ankle Res 2020;13. https://doi.org/10.1186/s13047-020-00404-0.

[128] Embaby OM, Elalfy MM. First metatarsophalangeal joint: Embryology, anatomy and biomechanics. World J Orthop 2025;16. https://doi.org/10.5312/wjo.v16.i4.102506.

[129] Kaur S, Ghadirinejad K, H. Oskouei R. An Overview on the Tribological Performance of Titanium Alloys with Surface Modifications for Biomedical Applications. Lubricants 2019;7:65. https://doi.org/10.3390/lubricants7080065.

[130] Visco A, Grasso A, Scolaro C, Belhamdi H, Sili A. Tribological Behavior of UHMWPE (Disc) against Ti6Al4V (Pin) under Different Lubrication Conditions. Macromol Symp 2022;404. https://doi.org/10.1002/masy.202100294.

[131] Barros CD dos R, Rocha JC, Bastos IN, Ponciano Gomes JA da C. Tribocorrosion of Ti6Al4V and NiCr Implant Alloys: Effect of Galvanic Interaction. J Bio Tribocorros 2020;6:117. https://doi.org/10.1007/s40735-020-00415-1.

[132] Galandáková A, Ulrichová J, Langová K, Hanáková A, Vrbka M, Hartl M, et al. Characteristics of synovial fluid required for optimization of lubrication fluid for biotribological experiments. J Biomed Mater Res B Appl Biomater 2017;105:1422–31. https://doi.org/10.1002/jbm.b.33663.

[133] Durrant M, Durrant L, McElroy T. Establishing a common instantaneous center of rotation for the metatarso-phalangeal and metatarso-sesamoid joints: A theoretical geometric model based on specific morphometrics. J Orthop Surg Res 2019;14. https://doi.org/10.1186/s13018-019-1110-4.

[134] Odehnal L, Ranuša M, Vrbka M, Křupka I, Hartl M. Tribological Behaviour of Ti6Al4V Alloy: An Application in Small Joint Implants. Tribol Lett 2023;71:125. https://doi.org/10.1007/s11249-023-01795-4.

[135] Ranuša M, Odehnal L, Kučera O, Nečas D, Hartl M, Křupka I, et al. Effect of Surface Texturing on Friction and Lubrication of Ti6Al4V Biomaterials for Joint Implants. Tribol Lett 2025;73:15. https://doi.org/10.1007/s11249-024-01950-5.

[136] Odehnal L, Ranuša M, Malý M, Křupka I, Koutný D, Hartl M, et al. Tribological behaviour of additively manufactured Ti6Al4V with controlled surface structure: An application in small joint implants. Tribol Int 2025;211:110832. https://doi.org/10.1016/j.triboint.2025.110832.

[137] Odehnal L, Ranuša M, Čípek P, Malý M, Mazánová V, Dlouhý A, et al. Additively manufactured Ti6Al4V with controlled surface structure as a potential material for joint implants: Long-term wear performance and durability. Tribol Int 2026;216:111599. https://doi.org/10.1016/j.triboint.2025.111599.

8.2 List of Figures

8.3 List of Tables

8.4 List of Symbols and Abbreviations

1.MTP	first metatarsophalangeal joint
AFM	atomic force microscopy
AM	additive manufacturing
AVN	avascular necrosis
BCS	bovine calf serum
CM	conventional manufacturing
CoC	ceramic-on-ceramic
CoM	ceramic-on-metal
CoP	ceramic-on-polymer
CVD	chemical vapour deposition
DLC	diamond-like carbon
EHL	elastohydrodynamic lubrication mechanism
EDS	energy dispersive X-ray Spectroscopy
FITC	fluorescein-5-isothiocyanate
HA	hyaluronic acid
HD	hydrodynamic lubrication mechanism
HXLPE	highly cross-linked polyethylene

LDMD	laser Direct Metal Deposition
LIPSS	laser-induced periodic surface structures
L-PBF	laser powder bed fusion
M-SF	model synovial fluid
MoM	metal-on-metal
MoP	metal-on-polymer
OA	osteoarthritis
PACVD	plasma-assisted chemical vapour deposition
PAL	protein aggregation lubrication
PBS	phosphate-buffered saline
PEEK	poly-ether-ketone
PoP	polymer-on-polymer
PVD	physical vapour deposition
QALYs	quality-adjusted life years
RA	rheumatoid arthritis
RBITC	rhodamine-B-isothiocyanate
SF	synovial fluid
SEBM	selective electron beam melting
SLM	selective laser melting
SLS	selective laser sintering
UHMWPE	ultra-high-molecular-weight polyethylene
WHO	World Health Organisation

8.5 Declaration of Generative AI and AI-assisted Technologies in the Writing Process

During the preparation of this thesis, the author utilised Grammarly and ChatGPT to enhance language quality and improve readability. After using these tools, the author reviewed and edited the content as needed, taking full responsibility for the thesis.

9

ATTACHMENTS: PUBLISHED ARTICLES

Tribology Letters (2023) 71:125
https://doi.org/10.1007/s11249-023-01795-4

ORIGINAL PAPER

Tribological Behaviour of Ti6Al4V Alloy: An Application in Small Joint Implants

Lukáš Odehnal[1] · Matúš Ranuša[1] · Martin Vrbka[1] · Ivan Křupka[1] · Martin Hartl[1]

Received: 15 June 2023 / Accepted: 4 October 2023 / Published online: 8 November 2023

Abstract

The presented study deals with the analysis of the tribological behaviour of the Ti6Al4V alloy manufactured conventionally. The study aimed to verify whether the titanium alloy is suitable for use as a contact material in small joint implants, as additive manufacturing of this alloy can in the future provide certain benefits, such as individualization and simplification of the implant construction, or controlled porosity. The tested pair consisted of a pin and a glass plate lubricated with model synovial fluid. The contact area was observed with colorimetric interferometry. Alongside film thickness, friction, and wear scars were measured. From the designed experimental conditions, the titanium alloy was not able to create a sufficiently thick lubrication film to overcome its surface roughness and damage to contact surfaces occurred. Friction was comparable for all the tested configurations. The application of conventionally manufactured titanium alloy as a contact surface in small joint implants seems to not be suitable since its performance fell short when compared to conventional cobaltous alloy. Nevertheless, there are various alternative methods available, such as unconventional manufacturing, polishing, surface texturing, and coating.

✉ Lukáš Odehnal
Lukas.Odehnal@vut.cz

[1] Department of Tribology, Faculty of Mechanical Engineering, Brno University of Technology, Technická 2896/2, 616 69 Brno, Czech Republic

Graphical Abstract

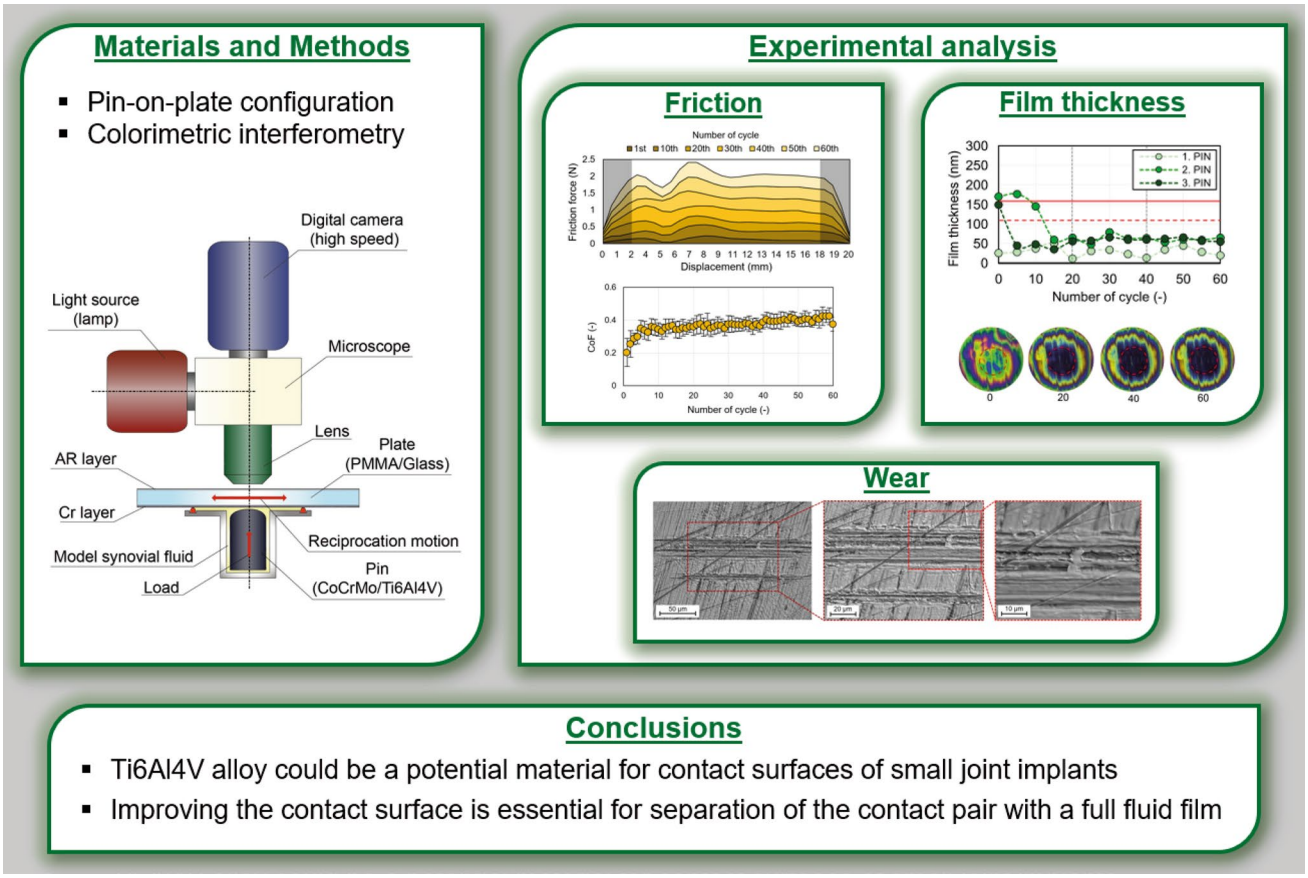

Keywords First MTP joint replacement · Biocompatible materials · Pin-on-plate configuration · Lubrication film thickness

1 Introduction

Interventions, especially the replacements of human joints, have become a necessity for today's population. The number of all joint replacements applied to the human body is rising every year. In the human body, there are various kinds of joints, and their full functionality is necessary for everyday life, for example, small joints, such as the big toe's first metatarsophalangeal joint (first MTP joint). This joint is responsible for a person's stability and is the most stressed joint in the foot during normal movement activities. Based on the study by Korim et al. [1] which reviewed the conducted arthrodesis, hallux valgus and hallux rigidus are the most frequent diseases affecting the first MTP joint, accounting for 36.6% and 34% of the cases, respectively. Recently, mainly hallux valgus has been discussed, as many middle-aged women suffer from this deformity because it is closely associated with wearing tight shoes or high heels. There are two main approaches to treating these deformities. The first, which is mainly invasive, is arthrodesis (fusion). This is a definitive and irreversible operation in which the affected joint is immobilized by fusing the bones together. The second option is joint arthroplasty. With this method, the joint motion can be preserved and this intervention does not affect the gait pattern [2]. Based on the statistics from Germany [3], between 2008 and 2017, only a few of the first MTP joint arthroplasties were made compared to arthrodesis, although it may have certain benefits. On the other hand, the first MTP joint replacements are not as reliable as arthrodesis these days. One of the most common types of total arthroplasty for the first MTP joint is ToeFit-Plus® [2]. Titchener et al. [4] reported a revision rate of 24% at an average of 33 months post-operatively for this implant, while the majority of revisions were caused by frank loosening or progressive lucency, mainly on the phalangeal side.

The first MTP joint replacements evolved in shape or used materials in the past [5]. During these days, the most common type is a metal-on-polyethylene total MTP replacement. These replacements consist of two stems from titanium alloy with porous structures, a CoCrMo metatarsal head, and

UHMWPE phalangeal plateau. Lately, additive manufacturing (AM) has become more frequent in all production areas, and this method is also suitable for joint replacements as the AM might bring benefits in the production of personalized metal-on-metal (MoM) small joint implants [6]. The most common method for producing artificial joints is selective laser melting (SLM) [7]. In such manufacturing, Ti6Al4V is more suitable than common CoCrMo alloy which is the most common contact surface in joint replacements these days [8]. The titanium alloy has excellent biocompatibility, good corrosion resistance, and high strength ratio [9]. Moreover, this alloy fabricated with a porous structure has comparable mechanical properties to a natural bone and can improve ingrowth of the stems and increases bone-implant stability [10]. To ensure the applicability of Ti alloy, the material must be subjected to detailed testing and compared with conventional Co alloy based on their performances.

To bring the experimental conditions close to reality, boundary conditions, such as kinematics and load, have to be defined. The kinematics of the first MTP joint was described by Durrant et al. [11]. The model provided knowledge about the joint movements and described their variance between the individual subjects. The loading of the joint, or the contact pressure, was examined by Flavin et al. [12] and Al-Munajjed et al. [13]. The main feature ensuring the proper behaviour of the replacement in the human body is the ability to form a sufficiently thick lubrication film that can separate interacting parts of the replacement in order to reduce the generation of wear particles.

The formation and thickness of the lubrication film can be influenced by various parameters. Myant et al. [14] demonstrated the impact of contact pressure, where its increase resulted in a decrease of lubrication film thickness. Kinematics, respectively the relative speed and slide-to-roll ratio (SRR) was described by Nečas et al. [15], who showed that the relative speed works differently for various SRR, i.e., the increase in relative speed for SRR 0 led to an increase in film thickness; on the other hand, for SRR 1.5, it led to a decrease in film thickness. Another factor potentially influencing the behaviour may be connected to contact surfaces, as human joints are tested with synovial fluid (SF) consisting of proteins with the ability to adsorb on the contact surfaces and its presence can affect the overall behaviour [16] of the system. The ability to form a stable and sufficiently thick lubrication film is usually connected to the number of proteins in the contact area. Nečas et al. [17] presented that the behaviour of lubrication film thickness is dependent on the composition of SF and tried to connect the behaviour of individual constituents, such as albumin and γ-globulin, to the lubrication film thickness. It was found that the trends of albumin and lubrication film thickness were comparable, while the γ-globulin development was observed only on a small scale [15]. Therefore, it appears that the main role of forming the lubrication film lies in albumin, while its presence and maintenance in the contact area might be affected by other constituents [18, 19]. The study made by Ranuša et al. [20] showed differences in the behaviour of samples with differences in surface topography. The tested Ti alloy had significantly worse surface roughness compared to Co alloy, resulting in the presence of a larger amount of proteins in the contact area. The well-formed and stable lubrication film is closely connected to other observed parameters, such as friction and wear, while these two parameters are closely related to good functionality and the lifetime of the replacement.

In the case of load, the increase of normal force leads to a decrease in friction [21, 22]. On the other hand, while lower friction occurs in higher load conditions, findings by Gao et al. [23] showed that the higher load contact is more likely to produce a higher rate of wear particles; therefore, lower friction does not always mean a lower wear rate. The studies dealing with the lubricant concentration [24–26] similarly showed that friction increases with an increasing number of proteins in the lubricant. When comparing the Co and Ti alloys according to the coefficient of friction (CoF), the values are not so different [27] On the other hand, when comparing the generation of wear particles, the titanium alloy is worse, while the released particles were approximately twice as high as for CoCrMo [28]. These findings could mean that the titanium alloy is incompatible with the use in the joint implants for contact surfaces, as the excessive number of released particles is undesirable for the patient's health [29]. Nevertheless, the benefits coming with additive manufacturing and simplifying the implant shape construction predetermine that the use of this alloy could find its application.

Based on the performed research and the knowledge gained in the past in this area of interest, further and complementary research seems more than needed since a better understanding of the given phenomena can lead to an increase in the lifespan and functionality of the implant, which are currently a big problem, as the revision operations rate is still too high for this joint [4]. To obtain such research that can reveal the behaviour in the contact area, the problem has to be examined at its roots. The main question posed in this publication was *"What are the main differences in the tribological behaviour of conventionally manufactured CoCrMo and Ti6Al4V alloys in the simulated small joint implant (first MTP joint)?"* and the sub-question: *"Is the Ti6Al4V alloy suitable for further investigation as a potential material for human joints?"* To answer these questions, the research is supplemented with the development of lubrication film thickness, an analysis of friction, and an analysis of contact pair roughness, or its wear scars. Combining these observed aspects should provide the necessary insight into the issue and show whether it makes sense to conduct further research on Ti6Al4V alloys as possibilities for contact

surfaces in small human joints, where additive manufacturing might find its application.

2 Materials and Methods

2.1 Experimental Apparatus

The experiments were performed on the universal tribometer [20, 30], providing reciprocal movement in a pin-on-plate configuration with a stable sample (pin) and a moving plate (glass). The experimental apparatus is shown in Fig. 1. The tribometer construction enables the use of optical methods to observe the contact area and measurement of the friction simultaneously. As the main goal of the study was to describe the lubrication mechanism, colorimetric interferometry [31] was used to observe the contact area to obtain information on the film thickness and its development.

2.2 Contact Pair and Lubricant

The contact pair consisted of a pin made from alloys used in implantology: CoCrMo (ASTM-F75) or Ti6Al4V (ISO 5832-3). The implant manufacturer [32] produced the test pins using a certified process involving cold drawing, followed by machining to a 15 mm radius, and polishing to a roughness of $Ra = 0.01 \pm 0.005$ µm for CoCrMo, and $Ra = 0.04 \pm 0.01$ µm for Ti6Al4V as the conventional machining for joint implants allowed for the used materials. The finishing process followed the certified method, which showed that it was not possible to bring the surface roughness of Ti6Al4V alloy closer to the one obtained for CoCrMo alloy. The second articulating part was a plate made from B270 glass, as one transparent part was necessary for observations using colorimetric interferometry. To enhance the observation conditions, the plate was on the contact surface coated with the Chromium layer (reflectivity of 25%). The other side of the plate was covered with an antireflective layer. The use of counterpart made from glass shows that the observed simulated joint more likely corresponds to the metal-on-metal joint implant type, as the material characteristics are closer to each other than for the metal-on-polymer type. The material characteristics of contact bodies are shown in Table 1.

The presented study used the model SF as the testing lubricant. The model SF was synthetically prepared based on the samples extracted from patients with arthroplasty [33]. The final composition of the model SF was made by diluting the required number of constituents in phosphate-buffered saline (PBS). The concentration of diluted components, respecting the properties of SF for patients after arthroplasty, is as follows: albumin (26.3 mg/ml), γ-globulin (8.2 mg/ml), hyaluronic acid (0.82 mg/ml), and phospholipids (0.35 mg/ml).

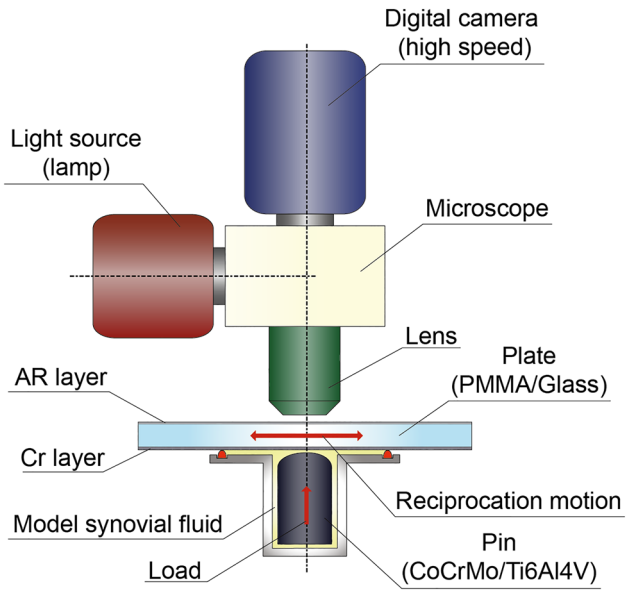

Fig. 1 Scheme of the experimental apparatus

2.3 Loading and Kinematic Conditions of Experiments

As there is no available ISO standard for testing of small joint implants, especially the first MTP joint investigated in this study, the loading and kinematic conditions had to be determined based on the analytic models or ISO standards used for testing of total knee replacement (TKR) [34] or total hip replacements (THR) [35]. Durrant et al. [11] presented a model where the initial metatarsal declination angle is 15°, and the terminal declination angle is approximately 80°; these angles can vary for different subjects. Using a

Table 1 Material characteristics, loading, and the resulting contact area based on the Hertz theory

Material	Young's modulus	Poisson's ratio	Applied load	Contact pressure	Calculated contact area
CoCrMo	241 GPa	0.29	0.5 N	105.5 MPa	0.095 mm
Ti6Al4V	114 GPa	0.34	0.73 N	105.5 MPa	0.115 mm
Glass B270	71 GPa	0.22			

typical radius of total replacements for this joint, the contact path was calculated for ~ 12 mm. Nevertheless, the 20 mm stroke was used in the experiments due to dead ends occurring in the testing cycle as the measuring of friction and observing the contact area requires a sufficiently long stroke with stable normal load and speed stabilization. The tested speeds were chosen according to the speeds that may appear in the 1. MTP joint during the gait cycle based on the sagittal plane kinematics presented by Allan et al. [36]. Based on the development of the declination angle, the recalculation of peripheral speed was made. Considering that the duration of the cycle is one second [34, 35] and the typical radius of rotation for the 1. MTP joint is about 13 mm [37, 38]; the recalculation showed that for the most of the cycle, the speed is very low (approx. 1–6 mm/s). The considerable speeds occur between 40 and 65% of the cycle, varying from 7 to 65 mm/s. Two speeds, 20 mm/s and 40 mm/s, were selected from this range for the experiments. The expected contact pressure is in the 1. MTP joint highly influenced by high conformity of the implant´s parts, where both curvature radiuses are 10 mm. This results in contact pressure at about 7–8 MPa [12]. When transformed to the experimental conditions (pin-on-plate), this contact pressure (~ 7.9 MPa) is obtained for the material combination of CoCrMo and UHMWPE by applying 0.5 N. In order to maintain the recalculated contact force of 0.5 N on the material combination used in experiments (CoCrMo on Glass), the resulting contact pressure was 105.5 MPa. To compare the behaviour of two tested materials (CoCrMo and Ti6Al4V), the contact pressure was unified in this study. The resulting contact forces applied on two tested configurations after recalculation based on the contact Hertz theory are as follows: 0.5 N (CoCrMo/Glass) and 0.73 (Ti6Al4V/Glass). The load was monitored and controlled during the experiments to ensure no more than ± 5% deviation from the desired value.

2.4 Experimental Setup and Evaluation of the Results

The experiments were designed to observe the behaviour of lubrication film thickness in short terms. The experiment was divided into three parts. After each part, the contact pair was unloaded to depict the relief of the joint. Each partial experiment consisted of 20 cycles, which gives the number of 60 cycles for the whole experiment, composed of two unloading stages. Each configuration was tested on three different contact pairs to achieve sufficient repeatability. The presented results were evaluated from the observation of contact in only one direction (marked as "Evaluated area" in Fig. 2A). This area is also cropped off the first and last 2 mm of the deflection; as in these parts (dead ends) of the cycle, the relative speed was not constant and it was not marked as relevant to the results. Continuous development of both

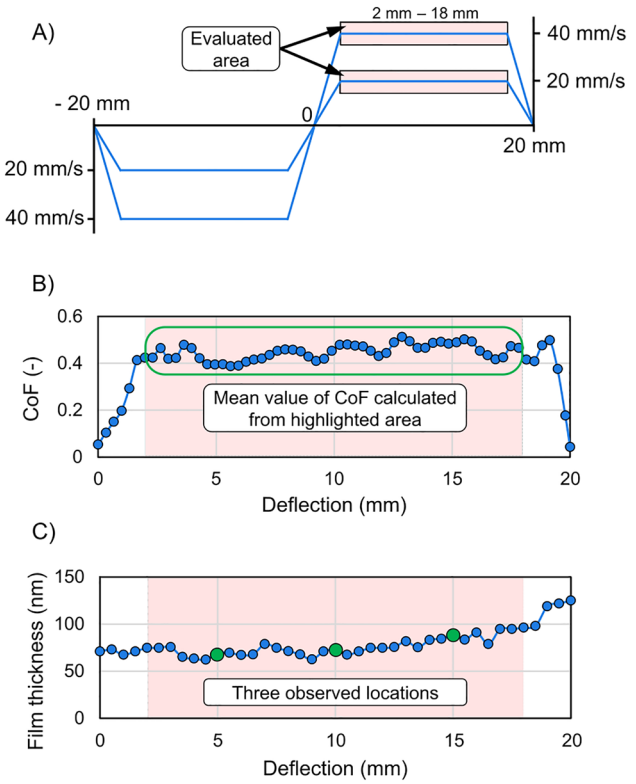

Fig. 2 Scheme for the evaluation of the results: **A** relative speeds with a marked area of evaluation; **B** evaluation of CoF; **C** evaluation of lubrication film thickness

CoF and lubrication film thickness was recorded during the experiment (see Fig. 2B, C). For CoF, the whole marked area – green oval (see Fig. 2B) is represented in the results by the average value for each cycle. While observing the lubrication film thickness and its development over time, it was found out that the thickness was dependent on the observed point of the cycle. In light of this finding, three points were selected and observed to describe possible inconsistencies during the cycle. These points are marked green in Fig. 2C.

3 Results

3.1 Analysis of Surface Roughness Before the Experiment

A roughness analysis of the samples was carried out to define the boundaries of lubrication film thickness, i.e., a separation of the contact surfaces with a certain probability. A sufficiently close zone adjacent to the contact area was selected for this observation. The zone was based on the expected size of the calculated contact area, which was doubled in cases where the contact area did not appear on the expected canopy. The surface roughness distribution

(its irregularities) of both examined alloys was Gaussian. Two borders were determined, the first representing a 95% probability of separation of contact pairs and the second a 99% probability. The values were established based on the measurements (see Table 2) to 35 nm (CoCrMo) and 110 nm (Ti6Al4V) for a probability of 95%, or to 45 nm (CoCrMo), and 160 nm (Ti6Al4V) for a probability of 99%. These borders are represented in the results graphs as red dashed, or solid lines.

3.2 Lubrication Film Thickness

For the lubrication film thickness, the experiments with an entrainment speed of 20 mm/s (see Fig. 3) showed similar results in case of reaching a sufficiently thick film layer for both of the materials, and the separation of contact pairs did not occur (except for the first few cycles for 2. PIN made from Ti alloy). The measured thickness was generally higher for the Ti alloy (e.g. point at 10 mm deflection at 30th cycle: ~ 15 nm for CoCrMo and ~ 55 nm for Ti6Al4V). Nevertheless, due to its worse surface roughness, it was not sufficiently high as the thickness did not reach either of the shown boundaries (red dashed or solid line).

On the other hand, the experiments with an entrainment speed of 40 mm/s showed different results for each material (see Fig. 4). While using the CoCrMo alloy, the contact pairs were separated for almost the whole experiment (except for the first few cycles for 1. PIN). On the contrary, while the Ti6Al4V alloy was used, the film thickness showed quite similar behaviour as at a lower speed and it did not reach sufficient values to separate the contact pair completely (except for the first few cycles for 2. and 3. PIN).

3.3 Wear Scars after Experiments

The findings regarding the lubrication film thickness of tested samples correspond with the roughness measurements (wear scar analysis) after experiments, where a combination of CoCrMo and glass at 40 mm/s showed no signs of wear.

Table 2 Probability of full film lubrication based on contact pair roughness

Material	Sample	95% Probability of separated contact pairs	99% Probability of separated contact pairs
CoCrMo	PIN 1	30 nm	41 nm
	PIN 2	35 nm	47 nm
	PIN 3	34 nm	48 nm
Ti6Al4V	PIN 1	102 nm	166 nm
	PIN 2	113 nm	182 nm
	PIN 3	100 nm	128 nm

Overall, the wear scars on the tested samples differ for each material and relative speed applied (see Fig. 5 and Table 3).

The CoCrMo samples are most likely to create a regular oval wear area oriented with a longer axis in the direction of the movement (Fig. 5A). On the other hand, the Ti6Al4V pins did not create such an oval wear area, but these samples were characterized by the formation of separated grooves that were considerably deeper and also longer in the direction of the movement (Fig. 5B). Table 3 shows the characteristics of the wear scars for all tested samples. Significant differences were observed for Ti alloy pins at 20 mm/s where 1. PIN showed similar wear scars as Co pins (oval area) and 2. PIN had no scars at all.

The typical wear scars for each material are illustrated more precisely in Fig. 6. The wear mechanism of Ti6Al4V and CoCrMo alloys differs, as observed in the images. The images of Ti6Al4V show a non-uniform wear pattern accompanied by the creation of deeper separate grooves, while the wear area of the CoCrMo sample is characterized by the creation of regular oval wear areas without irregularities. The images depict the abrasion for both materials, but the release of Ti6Al4V wear particles caused the three-body abrasion.

3.4 Coefficient of Friction

Figure 7 shows the evolution of CoF for all tested configurations. The yellow dots, representing the average value of CoF for three samples are in the graphs supplemented with standard deviation (SD). All configurations showed a similar behaviour, with CoF settled down at values around 0.4 after an initial increase. The rehydration stages after 20 or 40 cycles (marked with vertical black dashed lines) did not significantly affect the behaviour of CoF at the tested speeds of 20 mm/s. On the other hand, when the relative speed of 40 mm/s was applied, a slight decrease of CoF can be seen after the rehydration stages for Ti6Al4V and a much greater decrease for CoCrMo. Nevertheless, the decrease lasted only one cycle and then the friction returned to the expected value. The values of CoF for CoCrMo at 40 mm/s (the only configuration that reached the selected boundaries for separated contact pairs) were the most inconsistent with the highest SD (see Fig. 7D).

The development of friction was supplemented with stacked graphs of friction force evolution throughout the experiments for each configuration (see Fig. 8).

The friction force values were evaluated using the methodology outlined in Fig. 2A as averages of three repeated experiments. Grey stripes indicate the beginning and end of each cycle, representing parts of the cycle, where the relative speed was unstable. Each material displayed a unique stacked pattern of the evolution due to the application of different loading forces. The development in each cycle

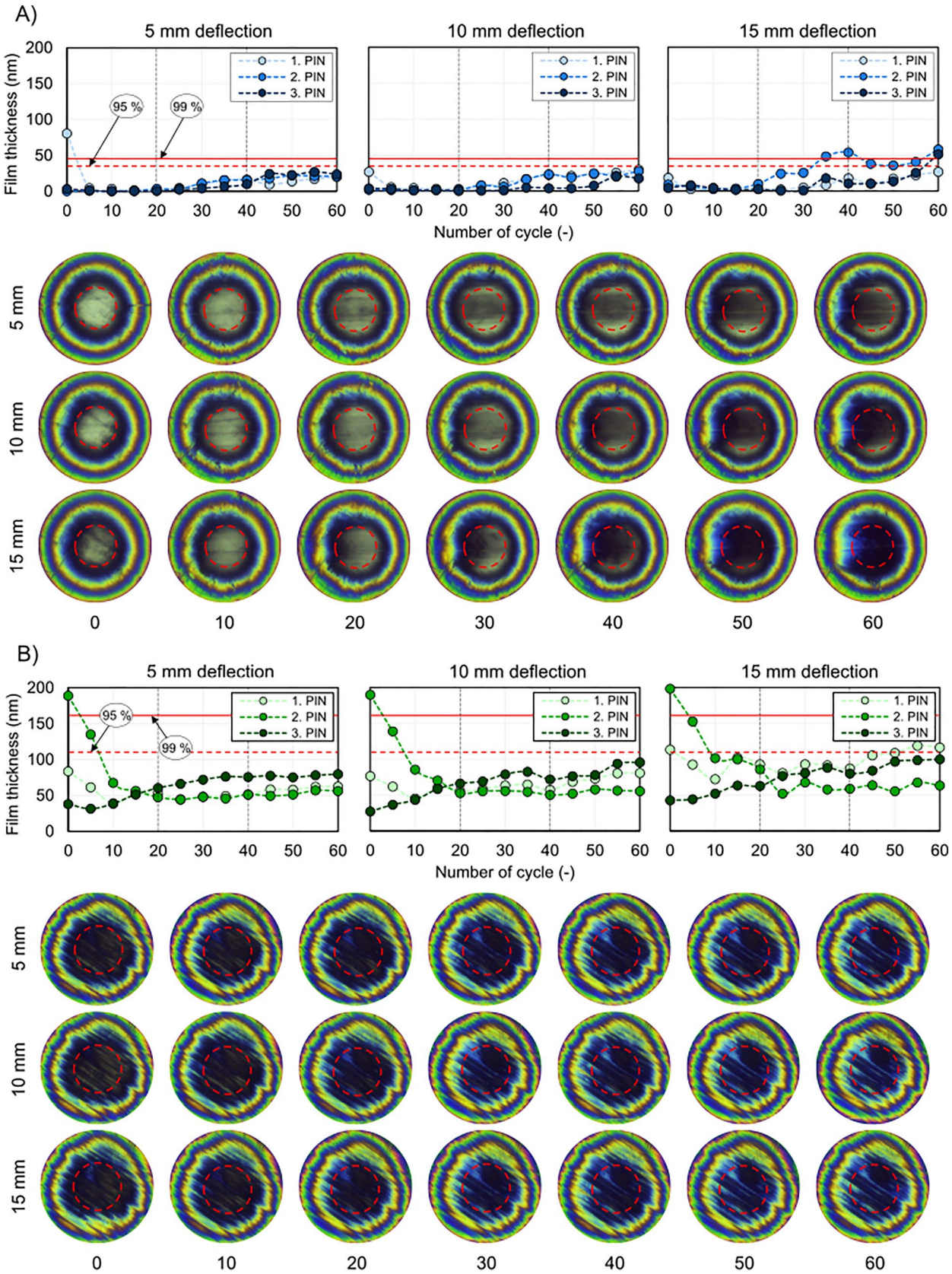

Fig. 3 Development of film thickness at 20 mm/s for **A** CoCrMo and **B** Ti6Al4V. Interferograms with marked contact areas correspond to 3. PIN for each configuration (the inlet zone is on the left side)

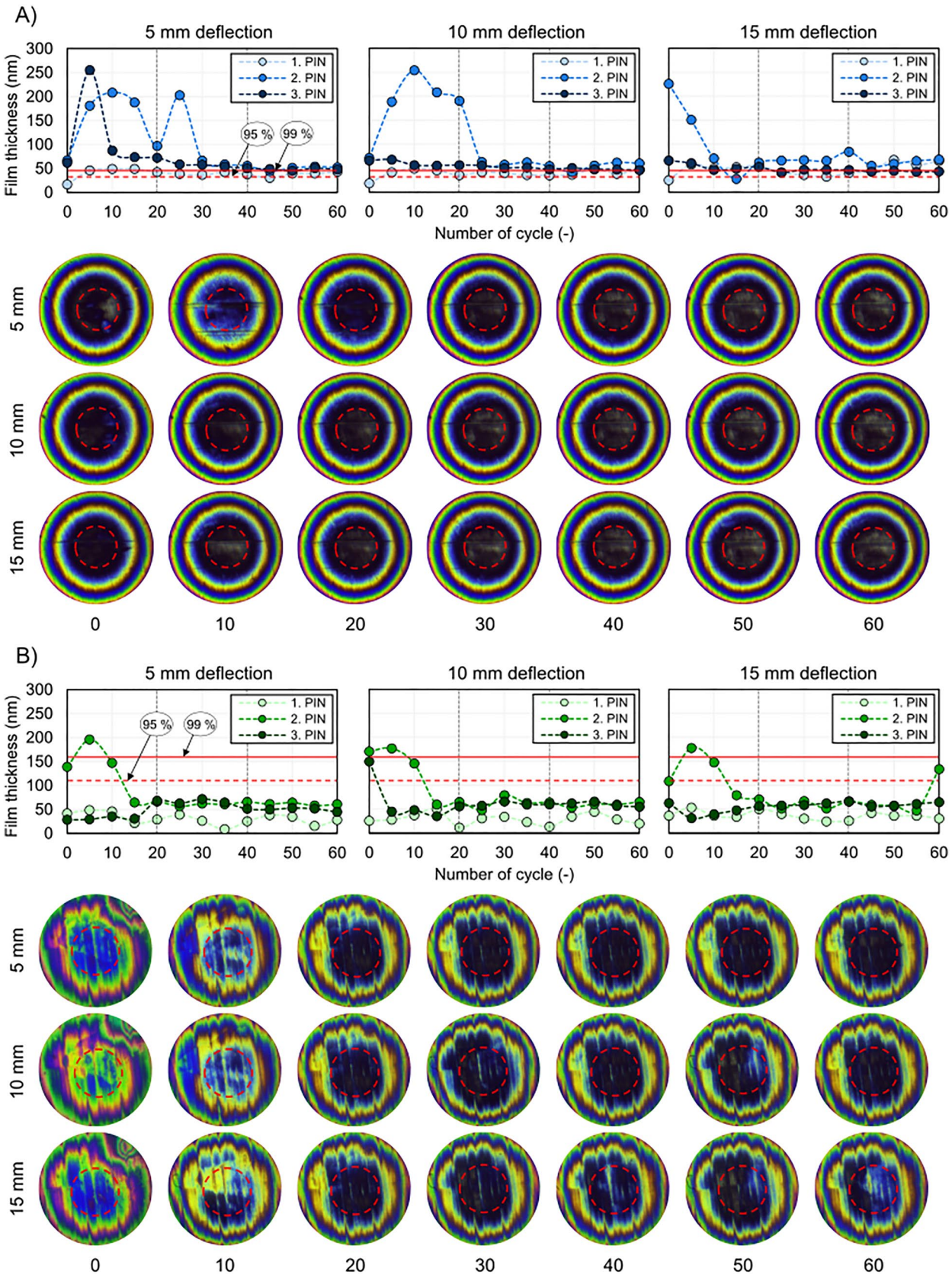

Fig. 4 Development of film thickness at 40 mm/s for **A** CoCrMo and **B** Ti6Al4V. Interferograms with marked contact areas correspond to 3. PIN (CoCrMo) and 2.PIN (Ti6Al4V) (the inlet zone is on the left side)

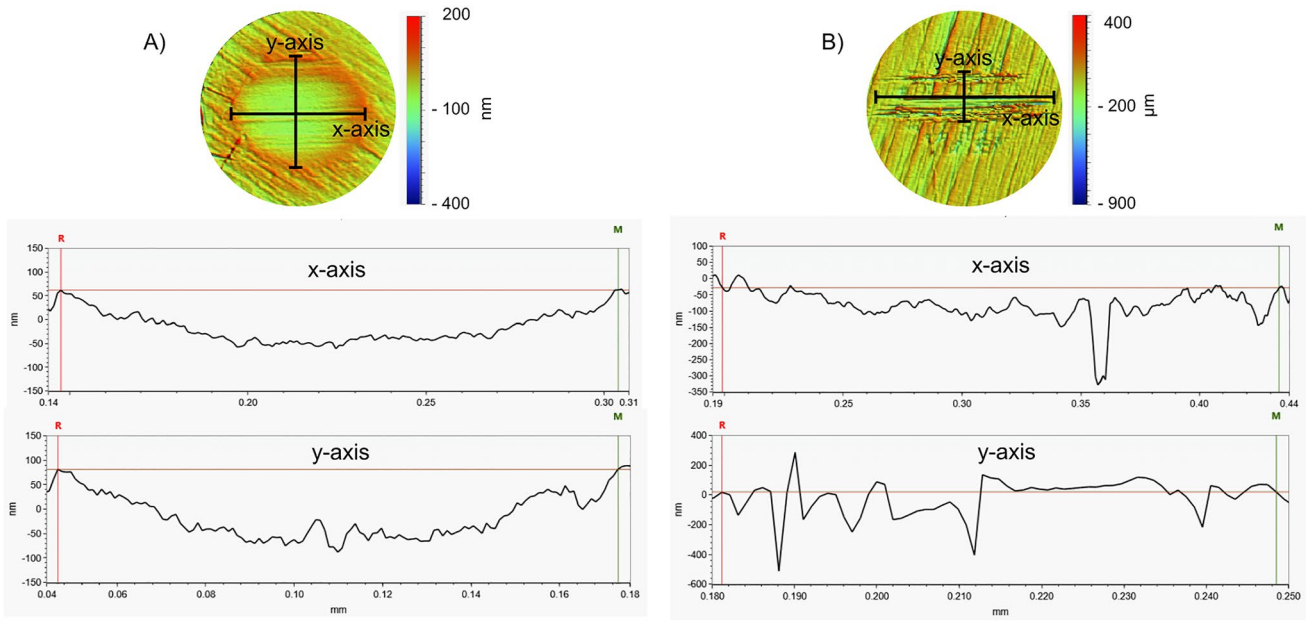

Fig. 5 Wear scars on **A** CoCrMo samples, and **B** Ti6Al4V samples. Graphs represent the profile cuts of PIN 1 of each material with marked borders (red and green lines), corresponding to surface pictures of wear areas

Table 3 Wear scars on tested samples

Tested conditions	Sample	x-axis width	y-axis width	Central depth	Tested conditions	Sample	x-axis width	y-axis width	Central depth
CoCrMo Glass 20 mm/s	PIN 1	157 µm	124 µm	86 nm	Ti6Al4V Glass 20 mm/s	PIN 1*	168 µm	123 µm	127 nm
	PIN 2	139 µm	120 µm	92 nm		PIN 2	Non-visible signs of wear		
	PIN 3	126 µm	86 µm	81 nm		PIN 3	139 µm	87 µm	203 nm
CoCrMo Glass 40 mm/s	PIN 1	Non-visible signs of wear			Ti6Al4V Glass 40 mm/s	PIN 1	255 µm	154 µm	583 nm
	PIN 2	Non-visible signs of wear				PIN 2	196 µm	65 µm	437 nm
	PIN 3	Non-visible signs of wear				PIN 3	298 µm	131 µm	984 nm

*The wear scar of the Pin was similar to the ones in CoCrMo/Glass configuration

remained quite stable during the entire experiment after the initial rise due to the increase in relative speed for all configurations except for the Ti6Al4V at 40 mm/s, where an additional lower peak occurred at around 5 mm, and the upper peak at around 7 mm of displacement.

4 Discussion General Discussion

The presented study focused on comparing and describing the tribological behaviour in the contact area of two materials suitable for human joint implants, a conventional CoCrMo alloy, and a 3D printing-friendly Ti6Al4V alloy. The experiments were designed to provide a general overview of these two conventionally manufactured materials. Three tribological parameters were measured or observed: lubrication film thickness, friction coefficient, and wear scars on the tested pins. The kinematics and load used in the experiments on the reciprocal tribometer with pin-on-plate configuration [30] were designed based on the literature [11–13] or ISO standards [34, 35], while the deflection in one direction was set at 20 mm. To obtain a frequency of 0.5 Hz and 1 Hz, the applied entrainment speed was 20 mm/s and 40 mm/s, respectively. The load was set to 0.5 N for CoCrMo alloy and 0.73 N for Ti6Al4V, as it was recalculated using the Hertz contact theory based on similar contact pressures.

The experiments showed that it is difficult to create a sufficiently thick lubrication film layer under the experimental conditions designed, as the height of the lubricant did not reach values sufficient to overcome the average roughness of the contact pair (see Figs. 3 and 4). This is accompanied by the formation of wear scars that are undesirable in human joints (see Fig. 5 and Table 3), as

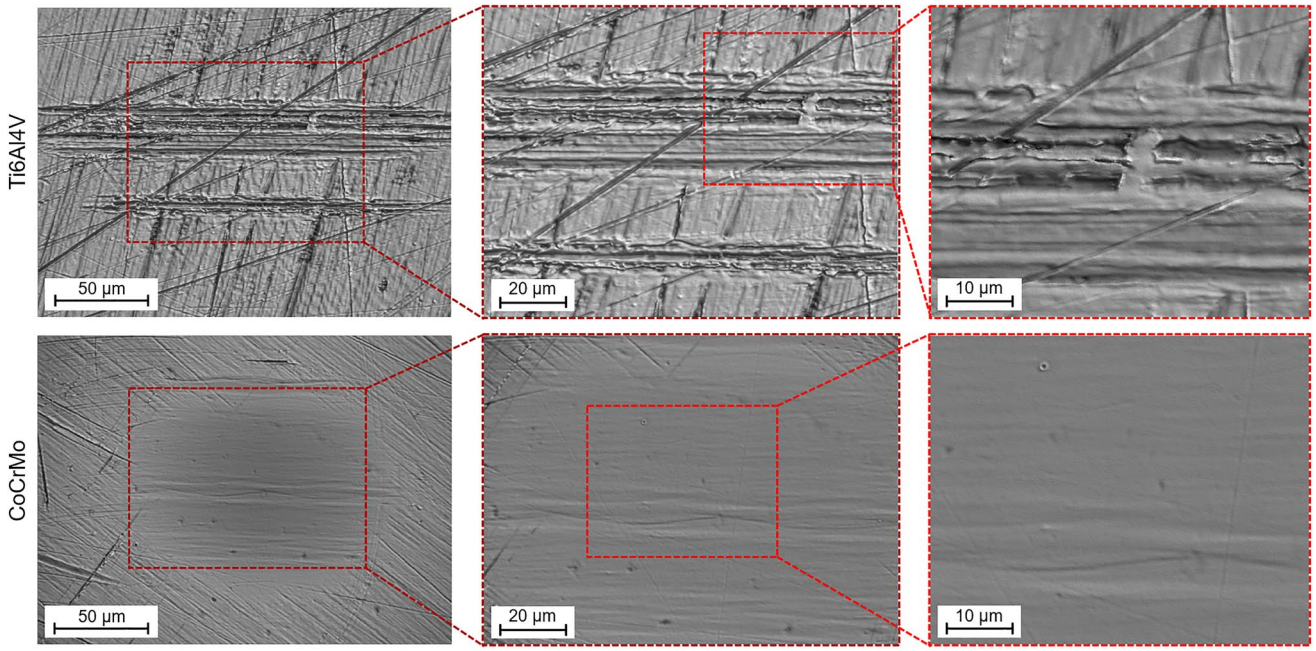

Fig. 6 Comparison of wear scars for Ti6Al4V and CoCrMo alloy at 20 mm/s

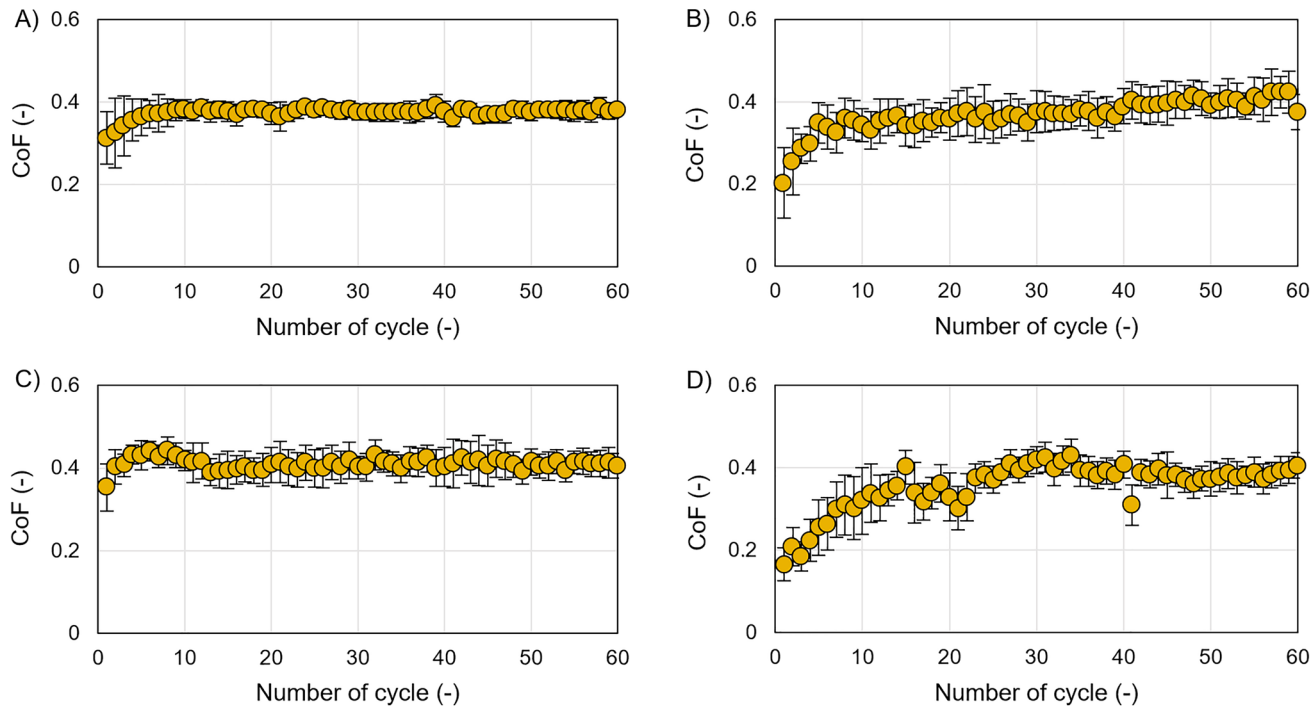

Fig. 7 Development of CoF for Ti6Al4V **A** 20 mm/s, **B** 40 mm/s and CoCrMo **C** 20 mm/s, **D** 40 mm/s

they are associated with the release of wear particles into the human body. The only difference was observed for the CoCrMo alloy at 40 mm/s, where the lubrication film thickness reached the limit of 95% probability of contact separation and also reached the 99% probability in some cycles. The formation of a sufficiently thick film layer is accompanied by non-visible signs of wear on these pins (see Table 3). Throughout all experiments, the lubrication film thickness in the observed points did not change much over time. The film thickness tended to stabilize at

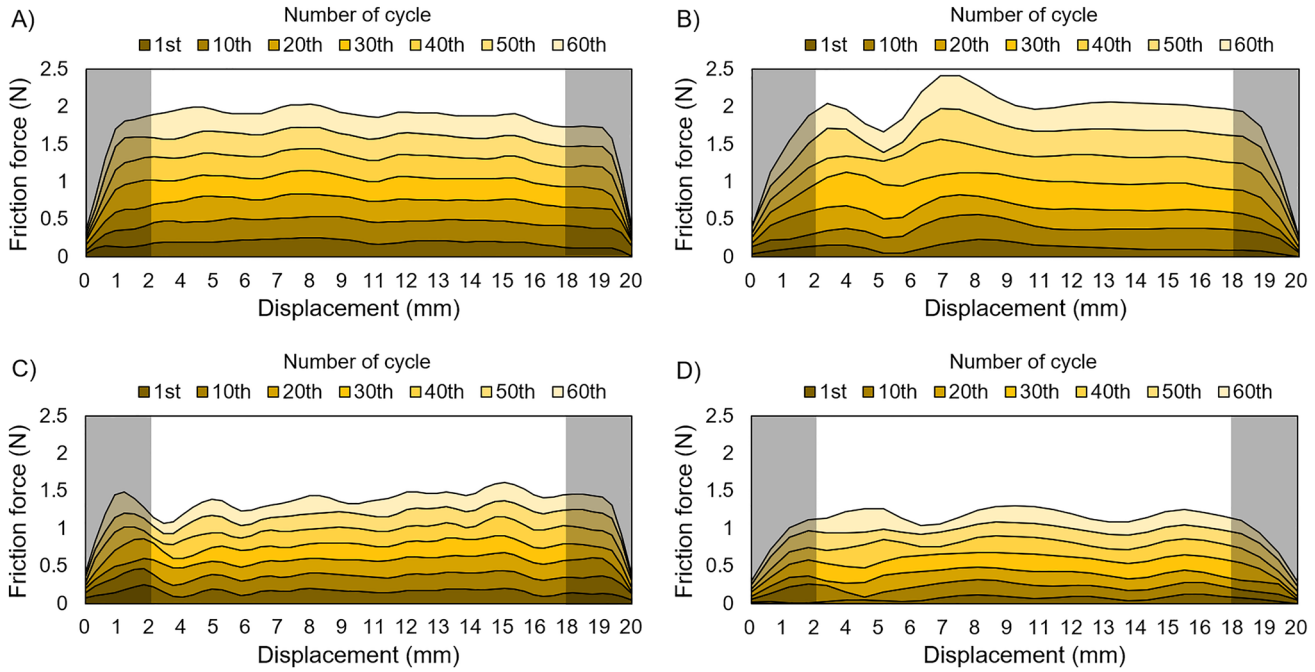

Fig. 8 Friction force development for Ti6Al4V **A** 20 mm/s, **B** 40 mm/s and CoCrMo, **C** 20 mm/s, **D** 40 mm/s

different values depending on the configuration: ~ 20 nm (CoCrMo), ~ 75 nm (Ti6Al4V) at 20 mm/s; and ~ 55 nm (CoCrMo), ~ 65 (Ti6Al4V) at 40 mm/s. As shown in the previous average values of film thicknesses, the Ti alloy reached overall higher values. These findings are related to the study of Ranuša et al. [20], where, in the experiments with Ti alloy, there were more adhered proteins in the contact area compared to the experiments with Co alloy. Therefore, we believe that a higher number of proteins in the contact area leads to an increase in lubrication film thickness. This statement is also supported by the study of Nečas et al. [15], where the development trends of film thickness measured by colorimetric interferometry were similar to the trends obtained by observing individual constituents in SF by fluorescent microscopy.

The behaviour of lubrication film formation with synovial fluid described by Myant et al. [39] showed the formation of aggregated proteins in the inlet zone. In the experiments performed in this study, the changes in the inlet zone, such as the formation of proteins, only occurred under specific conditions which appeared randomly. For example, the second pin from CoCrMo at 40 mm/s (see Fig. 5), where the film thickness increased significantly in the initial cycles until stabilizing at a similar value to other samples. After 10–30 cycles (depending on the observed point), the inlet zone disappeared (see Fig. 9), and the observed contact area behaved in the same way as in the other configurations. The reason, why the inlet zone appeared, was apparently due to the denser occurrence of proteins, which, however, were moved away over time and the aforementioned stabilization occurred.

Although Protein Aggregation Lubrication (PAL) characteristics occurred, it was only under specific conditions (mentioned above) or at the beginning and end of the cycles, where the relative speed was very low and these values were not considered in the evaluation. Based on the observations, a higher number of proteins is needed to create characteristic PAL conditions. Nevertheless, the used model SF was prepared on the basis of the extracted samples from patients after arthroplasty [33], so the composition of the model SF should correspond to the real state of the human joints. Also, artificial starvation of the contact due to a lack of lubricant should not occur, as the contact pair was completely flooded. At the same time, the good flooding was checked during the experiments, and, if necessary, lubricant was added to prevent its occurrence. As can be seen from the pictures, while a visible inlet zone occurs, the film thickness is much higher (see Figs. 2, 4. PIN from CoCrMo). In order to improve the lubrication mechanism, an effort should be made to keep as many proteins as possible in the contact zone and its surroundings, which will lead to an increase in the overall thickness of the lubrication film.

Nissim et al. [40] created a computational model for PAL, which is typical for SF-lubricated contacts with. For the evaluation of the computational model, the results from Myant et al. [41] were used. The model showed quite a good compliance between experimental and simulation data. Furthermore, the model described the differences between PAL

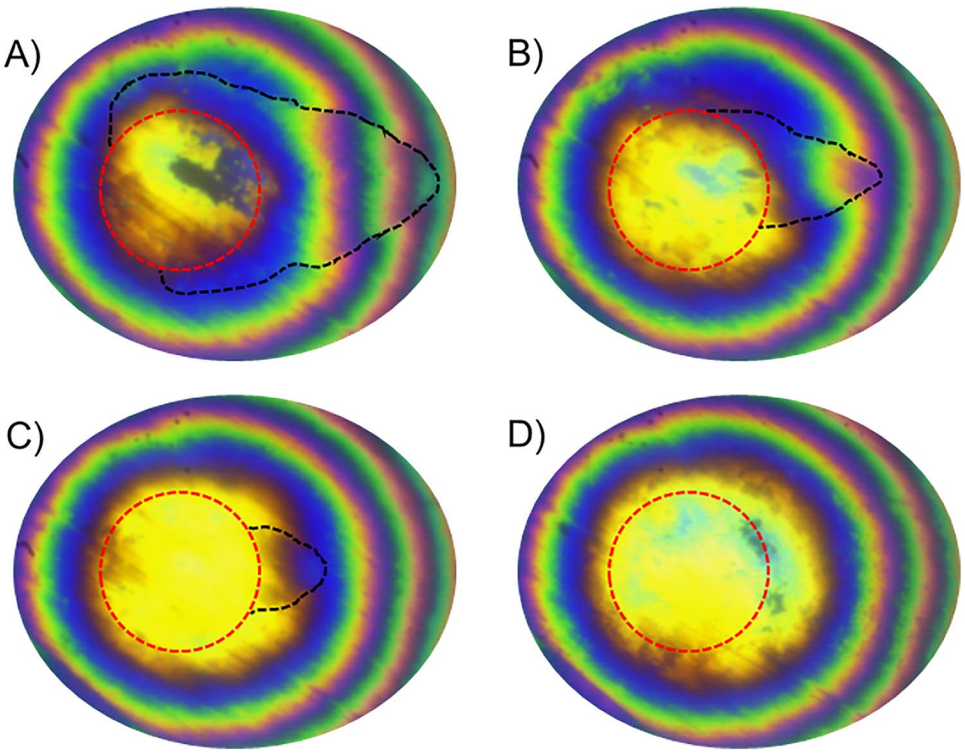

Fig. 9 Creation of inlet zone (on the right side) with protein aggregation (marked with black dashed lines) for CoCrMo at 40 mm/s: **A** 5th cycle, **B** 15th cycle, **C** 25th cycle, **D** 30th cycle

and EHL regimes and showed that the presented model for PAL is more in coincidence with experimental data. For the presented study, the obtained data do not fully correspond with the described model. The experimental results, such as the height of the lubrication film thickness did not reach such values as the model presents, but it also did not behave as a classic EHL regime. As both this study and the described simulation worked with the same contact pairs (CoCrMo on glass), it is possible to compare these results. For a steady lubrication film thickness, the values are as follows: 20 nm (EHL model), 140 nm (PAL model), and 40 nm (experiments in this study) for relative speed of 20 mm/s, and 30 nm (EHL model), 190 nm (PAL model), and 55 nm (experiments in this study) for relative speed of 40 mm/s. The main differences occur in the formation of aggregated proteins in the inlet zone, as the results in this study showed that the inlet zone was formed only in a few conditions, where the lubrication film thickness was much higher and could be comparable with the PAL model. As the conformity of the contact pair could play a major role in the ability to form stable inlet zones, this problem could have occurred due to the divergence in the radius of the tested or simulated pins. While a pin radius of 15 mm was used in this study, the PAL model used a radius of 19 mm. Moreover, the commonly used first MTP joint replacements have an even higher conformity (as the structure is comparable to THR–ball-in-socket), so it may be necessary to bring the experimental setup closer to reality to achieve more accurate results for this problem.

When trying to put together the knowledge of all the parameters measured or observed in this study, certain correlations can be found. The main findings were made for the CoCrMo configuration at 40 mm/s, which showed that it is possible to generate a sufficiently thick lubrication film to separate contact pairs, as this configuration did not show any wear scars on the tested pins. This fact is accompanied by the development of friction (see Fig. 7). This configuration showed the most unstable curve (see SD in Fig. 6), as well as the lowest values of friction compared to the other configurations. Moreover, the unloading phases at the 20 and 40 cycles showed a significant momentary decrease in CoF. On the other hand, the other configurations did not show such behaviour, and it can be said that these material combinations did not show good enough results at defined speeds. In order to obtain a good behaviour of the Ti alloy, certain adjustments of the contact surface have to be made.

In all the tested configurations, the CoF stabilized at the value of 0.4 (see Fig. 7). The only observable evolution occurred at the beginning of the experiments, where the CoF increased with sequent cycles. As well as materials, the change of relative speed did not visibly influence the CoF. This finding confirms that the contact pressure mainly affects the CoF by increasing the load for identical contact pairs [21, 22, 42] when the contact is under full-slip conditions, so that the slide-to-roll ratio does not enter this problem as a variable parameter. Although the force has changed slightly in the results presented due to different

material properties (0.5 N and 0.73 N), the contact pressure has remained the same.

4.1 Data Repeatability

The data repeatability in tribological problems using model synovial fluid as a lubricant could be more difficult to obtain due to its complex composition. To avoid this problem, the SF model used was prepared at one time, so the concentration of each constituent should be similar. Also, the tested samples could differ in their geometry or surface roughness. Each configuration was tested on three different contact pairs in order to obtain a sufficiently large set of results to provide sufficient repeatability. As shown in Figs. 3 and 4, the overall development of film thickness was similar for the different samples. Nevertheless, some differences can be found. For example, the lubrication film thickness is highly affected at the beginning of the experiment, or after each unloaded phase. Figures 3 and 4 show that proteins at different concentrations can enter the contact area after the application of load, which leads to a significant increase in lubrication film thickness (e.g. Pin 2 in CoCrMo at 40 mm/s). Although this increase occurs, the lubrication film thickness stabilizes after a few cycles at a value similar to other tested samples.

4.2 Limitations of the Study

The first MTP joint is very complex, and it is not easy to precisely describe its movement during the gait. Also, no ISO standard can be used to define the movement and later to compare different designs of experiments. In this study, the task was solved in a simplified configuration (pin-on-plate) in order to easily characterize the occurring phenomena. The kinematics and load were chosen based on the literature or tribometer capabilities. However, these input conditions do not fully correspond to reality as the conformity of the real pair was not considered. Another adjustment from the real joint was that the conventional contact pair was changed, as one component had to be transparent to enable the use of colorimetric interferometry. The glass plate was used as the transparent part. This glass plate has quite different material properties to those conventionally used in joint replacements. This change may have affected the ability of protein to be absorbed onto the contact pairs, as this phenomenon was identified as one of the main tribological problems with synovial fluid. While the glass was highly hydrophilic, the alloys were almost at the boundary between hydrophobic and hydrophilic behaviour. The values of the angle of wettability (AoW) are summarized in Table 4. Another difference arises in the dimensions of the contact area. The estimated contact areas for the configuration with glass are 0.095 mm for CoCrMo, respectively, 0.115 mm for Ti6Al4V. These values represent approximately 30% of the contact area obtained in typical joint materials (CoCrMo and UHMWPE). However, if we consider the glass to represent a hard contact (as mentioned earlier), it would be better to compare the contact area with a metal-on-metal total joint replacement, where the contact areas will be practically comparable (0.112 mm for Ti6Al4V/Ti6Al4V and 0.115 mm for Ti6Al4V/Glass).

Table 4 The angles of wettability for each material

Material	Angle of wettability	SD
CoCrMo	75.43°	1.65°
Ti6Al4V	78.21°	2.27°
Glass B270	29.08°	3.12°

5 Conclusions

The complex friction, lubrication film formation, and wear scar analyses were obtained using a pin-on-plate configuration on a universal tribometer with colorimetric interferometry as the optical observation method. The experiments compared two human joint implant materials, conventional CoCrMo and Ti6Al4V that might find its use in the future for certain benefits (e.g. simplifying the joint geometry, and comparable material properties to bone) at two different relative speeds. The main conclusions, summed up in bullet points, are:

- Overall, the Ti alloys produced a thicker lubrication film than the Co alloys. Nevertheless, the thickness was not sufficient due to its inferior surface quality.
- The only tested configuration that created a lubrication film layer thick enough to separate the contact pair was the combination of CoCrMo with glass at a relative speed of 40 mm/s, where the signs of wear also did not occur.
- The described PAL, while using the SF model, was found only in specific conditions or at low speeds at the dead ends of the cycle. While protein aggregation occurred in the inlet zone, a thicker lubrication film was formed.
- The wear mechanism differs for CoCrMo and Ti6Al4V. The Co alloy is more likely to create the regular oval wear area. On the other hand, the Ti alloy creates bounded grooves that are significantly deeper.
- The values of friction were comparable for both tested alloys.

To sum up the results and answer the scientific questions mentioned in the introduction to this work. Certain differences were found in the lubrication mechanisms of tested alloys. The experiments with Ti6Al4V showed that this alloy can create a thicker lubrication film than a Co alloy. Nevertheless, it is necessary to mention the surface quality, or its

roughness. It was not possible to bring the quality of the surfaces close enough to each other by using conventional polishing methods due to the different material characteristics. This problem was observed with the Ti alloy where even a thicker film was not sufficient enough because the thickness of the lubricant did not overcome the average surface roughness, so that the contact pairs were not separated. To avoid this problem, it is necessary to improve the surface quality of Ti alloy. Two possible ways of achieving this are using non-conventional machining/polishing or applying surface coatings which in the past have shown a positive influence on the contact pair behaviour in various branches of tribology. The coating could also benefit the wear mechanism by decreasing the number of wear particles or reducing the depth of the grooves observed in this study. Another way of improving the tested tribological system could be surface texturing, which might bring the desired outcome, as it has been shown in the past that the textures can increase the film thickness.

Based on the findings of this study, it seems that the Ti6Al4V alloy may be suitable as a material for small joint implants. Nevertheless, it is not possible to use unmodified surfaces as the results of this tribological system are insufficient compared to the conventional CoCrMo alloy in terms of achieving a sufficiently thick lubrication film to separate the contact pair and thus prevent the undesirable wear of joint implants. Future studies should focus on describing the lubrication mechanism for additively manufactured Ti6Al4V with the aim of improving its behaviour by surface texturing and coating.

Acknowledgements This research was carried out under a project funded by Czech Science Foundation, grant number 22-02154S.

Author Contributions LO, MR, and MV conceived the idea. LO and MR designed the experiments. LO performed the experiments and analysed the data. LO and MR wrote the original draft of the manuscript. MV administrated the project, secured the funding, and supervised the study. IK and MH supervised the study.

Funding Open access publishing supported by the National Technical Library in Prague.

Data Availability Data will be made available on request.

Declarations

Conflict of interest The authors declare that they have no known competing financial interests or personal relationships that could have appeared to influence the work reported in this paper. The authors declare that they have no known competing financial interests or personal relationships that could have appeared to influence the work reported in this paper.

References

1. Korim, M.T., Allen, P.E.: Effect of pathology on union of first metatarsophalangeal joint arthrodesis. Foot. Ankle. Int. **36**, 51–54 (2015). https://doi.org/10.1177/1071100714549046
2. França, G., Nunes, J., Pinho, P., Freitas, D., Andrade, R., Espregueira-Mendes, J., et al.: Is arthrodesis still the best treatment option for first metatarsophalangeal joint arthritis?—a systematic review of arthrodesis and arthroplasty outcomes. Ann. Jt. **6**, 5–5 (2021). https://doi.org/10.21037/aoj-20-88
3. Milstrey, A., Domnick, C., Garcia, P., Raschke, M.J., Evers, J., Ochman, S.: Trends in arthrodeses and total joint replacements in foot and ankle surgery in Germany during the past decade—back to the fusion? Foot. Ankle. Surg. **27**, 301–304 (2021). https://doi.org/10.1016/j.fas.2020.05.008
4. Titchener, A.G., Duncan, N.S., Rajan, R.A.: Outcome following first metatarsophalangeal joint replacement using TOEFIT-PLUS™: a mid term alert. Foot. Ankle. Surg. **21**, 119–124 (2015). https://doi.org/10.1016/j.fas.2014.10.005
5. Esway, J.E., Conti, S.F.: Joint replacement in the hallux metatarsophalangeal joint. Foot. Ankle. Clin. **10**, 97–115 (2005). https://doi.org/10.1016/j.fcl.2004.09.002
6. Narra, S.P., Mittwede, P.N., DeVincent, W.S., Urish, K.L.: Additive manufacturing in total joint arthroplasty. Orthop. Clin. North Am. **50**, 13–20 (2019). https://doi.org/10.1016/j.ocl.2018.08.009
7. Ni, J., Ling, H., Zhang, S., Wang, Z., Peng, Z., Benyshek, C., et al.: Three-dimensional printing of metals for biomedical applications. Mater. Today Bio. **3**, 100024 (2019). https://doi.org/10.1016/j.mtbio.2019.100024
8. Dreyer, M.J., Taylor, W.R., Wasmer, K., Imwinkelried, T., Heuberger, R., Weisse, B., et al.: Anomalous wear behavior of UHMWPE during sliding against CoCrMo under varying cross-shear and contact pressure. Tribol. Lett. **70**, 119 (2022). https://doi.org/10.1007/s11249-022-01660-w
9. Niinomi, M.: Mechanical biocompatibilities of titanium alloys for biomedical applications. J. Mech. Behav. Biomed. Mater. **1**, 30–42 (2008). https://doi.org/10.1016/j.jmbbm.2007.07.001
10. Ran, Q., Yang, W., Hu, Y., Shen, X., Yu, Y., Xiang, Y., et al.: Osteogenesis of 3D printed porous Ti6Al4V implants with different pore sizes. J. Mech. Behav. Biomed. Mater. **84**, 1–11 (2018). https://doi.org/10.1016/j.jmbbm.2018.04.010
11. Durrant, M., Durrant, L., McElroy, T.: Establishing a common instantaneous center of rotation for the metatarso-phalangeal and metatarso-sesamoid joints: a theoretical geometric model based on specific morphometrics. J. Orthop. Surg. Res. **14**, 107 (2019). https://doi.org/10.1186/s13018-019-1110-4
12. Flavin, R., Halpin, T., O'Sullivan, R., FitzPatrick, D., Ivankovic, A., Stephens, M.M.: A finite-element analysis study of the metatarsophalangeal joint of the hallux rigidus. J. Bone Joint Surg. Br. **90-B**, 1334–1340 (2008). https://doi.org/10.1302/0301-620X.90B10.20506
13. Al-Munajjed, A.A., Bischoff, J.E., Dharia, M.A., Telfer, S., Woodburn, J., Carbes, S.: Metatarsal loading during

gait—a musculoskeletal analysis. J. Biomech. Eng. **138**, 1–6 (2016). https://doi.org/10.1115/1.4032413
14. Myant, C., Underwood, R., Fan, J., Cann, P.M.: Lubrication of metal-on-metal hip joints: the effect of protein content and load on film formation and wear. J. Mech. Behav. Biomed. Mater. **6**, 30–40 (2012). https://doi.org/10.1016/j.jmbbm.2011.09.008
15. Nečas, D., Vrbka, M., Urban, F., Křupka, I., Hartl, M.: The effect of lubricant constituents on lubrication mechanisms in hip joint replacements. J. Mech. Behav. Biomed. Mater. **55**, 295–307 (2016). https://doi.org/10.1016/j.jmbbm.2015.11.006
16. Furmann, D., Nečas, D., Rebenda, D., Čípek, P., Vrbka, M., Křupka, I., et al.: The effect of synovial fluid composition, speed and load on frictional behaviour of articular cartilage. Materials (Basel) (2020). https://doi.org/10.3390/ma13061334
17. Nečas, D., Vrbka, M., Gallo, J., Křupka, I., Hartl, M.: On the observation of lubrication mechanisms within hip joint replacements. Part II: hard-on-hard bearing pairs. J. Mech. Behav. Biomed. Mater. **89**, 249–59 (2019). https://doi.org/10.1016/j.jmbbm.2018.09.026
18. Čípek, P., Vrbka, M., Rebenda, D., Nečas, D., Křupka, I.: Biotribology of synovial cartilage: role of albumin in adsorbed film formation. Eng. Sci. Technol. an Int. J. **34**, 101090 (2022). https://doi.org/10.1016/j.jestch.2021.101090
19. Nečas, D., Vrbka, M., Marian, M., Rothammer, B., Tremmel, S., Wartzack, S., et al.: Towards the understanding of lubrication mechanisms in total knee replacements – part I: experimental investigations. Tribol. Int. **156**, 106874 (2021). https://doi.org/10.1016/j.triboint.2021.106874
20. Ranuša, M., Čípek, P., Vrbka, M., Paloušek, D., Křupka, I., Hartl, M.: Tribological behaviour of 3D printed materials for small joint implants: a pilot study. J. Mech. Behav. Biomed. Mater. **132**, 105274 (2022). https://doi.org/10.1016/j.jmbbm.2022.105274
21. Nuño, N., Amabili, M., Groppetti, R., Rossi, A.: Static coefficient of friction between Ti-6Al-4V and PMMA for cemented hip and knee implants. J. Biomed. Mater. Res. **59**, 191–200 (2002). https://doi.org/10.1002/jbm.1233
22. Saikko, V.: Effect of contact pressure on wear and friction of ultra-high molecular weight polyethylene in multidirectional sliding. Proc. Inst. Mech. Eng. Part H J. Eng. Med. **220**, 723–731 (2006). https://doi.org/10.1243/09544119JEIM146
23. Gao, L., Hua, Z., Hewson, R., Andersen, M.S., Jin, Z.: Elasto-hydrodynamic lubrication and wear modelling of the knee joint replacements with surface topography. Biosurf. Biotribol. **4**, 18–23 (2018). https://doi.org/10.1049/bsbt.2017.0003
24. Flannery, M., Jones, E., Birkinshaw, C.: Analysis of wear and friction of total knee replacements part II: Friction and lubrication as a function of wear. Wear **265**, 1009–1016 (2008). https://doi.org/10.1016/j.wear.2008.02.023
25. Barceinas-Sanchez, J.D.O., Alvarez-Vera, M., Montoya-Santiyanes, L.A., Dominguez-Lopez, I., Garcia-Garcia, A.L.: The coefficient of friction of UHMWPE along an entire walking cycle using a ball-on-disc tribometer under arthrokinematics and loading conditions prescribed by ISO 14243–3:2014. J. Mech. Behav. Biomed. Mater. **65**, 274–280 (2017). https://doi.org/10.1016/j.jmbbm.2016.08.032
26. Shinmori, H., Kubota, M., Morita, T., Yamaguchi, T., Sawae, Y.: Effects of synovial fluid constituents on friction between UHMWPE and CoCrMo. Tribol ONLINE **15**, 283–292 (2020). https://doi.org/10.2474/trol.15.283
27. Guezmil, M., Bensalah, W., Mezlini, S.: Tribological behavior of UHMWPE against TiAl6V4 and CoCr28Mo alloys under dry and lubricated conditions. J. Mech. Behav. Biomed. Mater. **63**, 375–385 (2016). https://doi.org/10.1016/j.jmbbm.2016.07.002
28. Grosse, S., Haugland, H.K., Lilleng, P., Ellison, P., Hallan, G., Høl, P.J.: Wear particles and ions from cemented and uncemented titanium-based hip prostheses—a histological and chemical analysis of retrieval material. J. Biomed. Mater. Res. Part B Appl. Biomater. **103**, 709–717 (2015). https://doi.org/10.1002/jbm.b.33243
29. Connors, J.P., Stelzer, J.W., Garvin, P.M., Wellington, I.J., Solovyova, O.: The role of the innate immune system in wear debris-induced inflammatory peri-implant osteolysis in total joint arthroplasty. Bioengineering **9**, 764 (2022). https://doi.org/10.3390/bioengineering9120764
30. Čípek, P., Rebenda, D., Nečas, D., Vrbka, M., Křupka, I., Hartl, M.: Visualization of lubrication film in model of synovial joint. Tribol. Ind. **41**, 387–93 (2019). https://doi.org/10.24874/ti.2019.41.03.08
31. Hartl, M., Krupka, I., Poliscuk, R., Liska, M., Molimard, J., Querry, M., et al.: Thin film colorimetric interferometry. Tribol. Trans. **44**, 270–276 (2001). https://doi.org/10.1080/10402000108982458
32. ProSpon n.d. https://www.prospon.cz/.
33. Galandáková, A., Ulrichová, J., Langová, K., Hanáková, A., Vrbka, M., Hartl, M., et al.: Characteristics of synovial fluid required for optimization of lubrication fluid for biotribological experiments. J. Biomed. Mater. Res. Part B Appl. Biomater. **105**, 1422–1431 (2017). https://doi.org/10.1002/jbm.b.33663
34. ISO 14243-3. Implants for surgery — wear of total knee-joint prostheses: part 3: loading and displacement parameters for wear-testing machines with displacement control and corresponding environmental conditions for test. 2nd ed. Switzerland: (2014).
35. ISO 14242-1:2014/AMD 1:2018, Implants for surgery - wear of total hip-joint protheses - part 1: loading and displacement parameters for wear-testing machines and corresponding enviromental conditions for test (2018).
36. Allan, J.J., McClelland, J.A., Munteanu, S.E., Buldt, A.K., Landorf, K.B., Roddy, E., et al.: First metatarsophalangeal joint range of motion is associated with lower limb kinematics in individuals with first metatarsophalangeal joint osteoarthritis. J. Foot. Ankle Res. **13**, 33 (2020). https://doi.org/10.1186/s13047-020-00404-0
37. Joyce, T.J.: Examination of failed ex vivo metal-on-metal metatarsophalangeal prosthesis and comparison with theoretically determined lubrication regimes. Wear **263**, 1050–1054 (2007). https://doi.org/10.1016/j.wear.2006.11.045
38. Stokes, I.A., Hutton, W.C., Stott, J.R.: Forces acting on the metatarsals during normal walking. J. Anat. **129**, 579–590 (1979)
39. Myant, C., Cann, P.: On the matter of synovial fluid lubrication: implications for metal-on-metal hip tribology. J. Mech. Behav. Biomed. Mater. **34**, 338–348 (2014). https://doi.org/10.1016/j.jmbbm.2013.12.016
40. Nissim, L., Butt, H., Gao, L., Myant, C., Hewson, R.: Role of protein concentration on transient film thickness in synovial fluid lubricated joints. Biotribology **28**, 100191 (2021). https://doi.org/10.1016/j.biotri.2021.100191
41. Myant, C.W., Cann, P.: The effect of transient conditions on synovial fluid protein aggregation lubrication. J. Mech. Behav. Biomed. Mater. **34**, 349–357 (2014). https://doi.org/10.1016/j.jmbbm.2014.02.005
42. Ranuša, M., Wimmer, M.A., Fullam, S., Vrbka, M., Křupka, I.: Analysis of friction in total knee prosthesis during a standard gait cycle. Lubricants **9**, 36 (2021). https://doi.org/10.3390/lubricants9040036

Tribology Letters (2025) 73:15
https://doi.org/10.1007/s11249-024-01950-5

ORIGINAL PAPER

Effect of Surface Texturing on Friction and Lubrication of Ti6Al4V Biomaterials for Joint Implants

Matúš Ranuša[1] · Lukáš Odehnal[1] · Ondřej Kučera[1] · David Nečas[1] · Martin Hartl[1] · Ivan Křupka[1] · Martin Vrbka[1]

Received: 6 August 2024 / Accepted: 4 December 2024 / Published online: 19 December 2024

Abstract

The number of endoprosthetic implants for both large and small joints is increasing at a steady rate, thereby creating a growing demand for durable products that closely replicate the functionality of human joints. Notwithstanding the aforementioned advancements, challenges pertaining to implant fixation and tribological surfaces persist. The advent of progressive technologies, such as three-dimensional printing, offers a promising avenue for addressing these challenges in implant design and surface engineering. The Ti6Al4V and CoCrMo alloys, renowned for their biocompatibility and osseointegration properties, represent promising printable materials, although they are susceptible to wear on articulating surfaces. In order to mitigate the effects of abrasion, it is essential to implement surface treatments to facilitate the formation of a robust lubricating film. This research investigates the potential of texturing and electrochemical polishing to enhance protein aggregation in the contact area. The study employs a reciprocating simulator and colorimetric interferometry to observe the contact area and measure the coefficient of friction (CoF) of modified surfaces. The findings demonstrate that textured surfaces and the combination of electrochemical polishing result in an increase in the thickness of the protein lubrication film, which may potentially reduce wear. These outcomes suggest the potential for the utilization of Ti6Al4V alloy implants with fewer elements manufactured by additive technology.

✉ Matúš Ranuša
Matus.Ranusa@vut.cz

[1] Biotribology Research Group, Faculty of Mechanical Engineering, Brno University of Technology, Technická 2896/2, 616 69 Brno, Czech Republic

Graphical Abstract

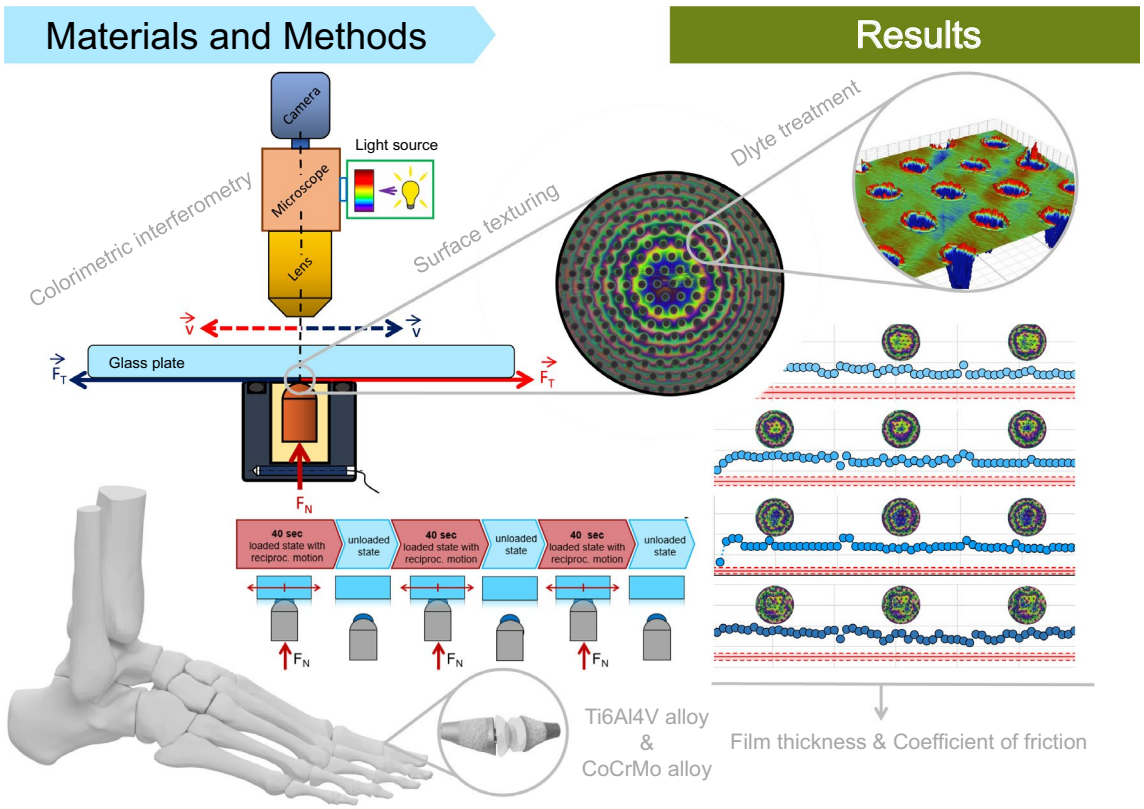

Keywords Ti6Al4V · Micro-texture · Implant · Optical interferometry · Friction · Film thickness

1 Introduction

Joint arthroplasty is a common surgery with an increasing incidence. The materials used in arthroplasty have a high standard, with a good biocompatibility, and osseointegration ability. The topic of joint wear remains a significant area of research, with the development of new materials leading to a reduction in the amount of loose material. [1]. Additive Manufacturing (AM) have advanced this field by customizing the implants for better comfort and a longer service life [2]. Nevertheless, the advent of additive technologies has also introduced a number of new challenges. One such challenge is the identification of the optimal manufacturing parameters for the production of structures suitable for osseointegration or the improvement of the tribological properties of articulating surfaces [3].

The longevity of implants is affected by the tribological behavior of the articulating surfaces, and interaction with the counterbody surface. A number of studies in this field demonstrate the interplay between individual surface materials and the complexity of the molecular components of the synovial fluid, which change with patient age [4]. The basic materials that combine the advantages of biocompatibility and resistance, while allowing the use of 3D printing by selective laser melting (SLM), are represented by the CoCrMo and Ti6Al4V alloys [5].

The possibility of 3D printing of both materials offers the advantages of customization and osteointegration, but brings new challenges at the same time. One of the challenges is the behavior of the printed articulating surface compared to conventional production. One of the differences is the tensile strength. The SLM-produced CoCrMo alloys exhibit a higher ultimate tensile strength and hardness compared to those made via investment casting. For instance, the SLM samples can achieve yield strengths around 1.4 GPa, but at the same time, they tend to have a higher wear rate compared to the cast samples, which exhibit lower wear rates due to their denser microstructure [6, 7]. However, in both cases, the wear resistance is relatively high, and both production technologies exhibit sufficient mechanical properties and corrosion resistance [8]. Furthermore, the formation of a passive oxide film on the metal surface in the human body also contributes to a better wear resistance of the CoCrMo implants [9]. This oxide layer is mainly composed of cobalt,

chromium, and molybdenum oxides. Among these, Cr_2O_3 inhibits both the anodic and cathodic reactions. It acts as a physical barrier, limiting the transport of cations and anions to the metal surface, and serves as an electronic barrier for electrons [10, 11]. In the case of the Ti6Al4V alloys, the conventional methods produce coarser grains, which can hinder dislocation movement, leading to a lower strength compared to the 3D-printed surfaces. The 3D-printed Ti6Al4V alloys can achieve strengths up to 1492.89 MPa, although with a reduced elongation (5.76%) due to microstructural defects [12]. Ti6Al4V is frequently used in oncological implants due to its mechanical properties, which are similar to those of a human bone. This minimizes the stress shielding and promotes the osseointegration [13]. However, the alloy is susceptible to a high abrasion on the articulating surfaces. This issue can be potentially resolved by various surface modifications, such as a coating or micro-texturing. Both coating and micro-texturing can enhance the mechanical properties and the durability of the implants. However, the coating techniques may suffer from an instability of the coating layer. It is, therefore, a challenging task to determine the most appropriate manufacturing technique for surface treatment and, at the same time, to design the optimal texture geometry or multi-level texture with respect to the kinematics of the selected joint. Micro-texturing has the potential to modify the behavior of the lubrication layer, thereby enhancing the sustainability of the performance, while allowing the use of different materials [14, 15]. Modified materials frequently exhibit not only enhanced durability but also the presence of highly cross-linked polyethylenes, which are often doped with a range of substances, including the E vitamin. This doping process augments the material's frictional resistance while simultaneously stabilizing the free radicals within the structural matrix. This dual effect results in a notable enhancement in the material's resistance to the oxidation and delamination at the surface [16, 17].

The texturing of surfaces has been demonstrated to exert a beneficial influence on the tribological properties, resulting in an augmented hydrodynamic pressure and diminished surface wear. However, the efficacy of this approach remains a topic of contention, particularly in the context of non-conformal contacts [18]. In contrast, for the conformal contacts, it results in the separation of the contact surfaces by a thicker layer of protein-containing lubricant, which alters the lubrication regime and reduces the wear. Simultaneously, the textures serve as lubricant reservoirs, facilitating the desired separation of the articulating surfaces [19, 20]. Additionally, the textures can capture and remove wear particles from the contact area. Aseptic wear particles are produced as a result of the abrasive wear of the materials, primarily in the boundary and mixed lubrication regimes. Carefully chosen textures can efficiently remove the particles from the contact area or retain them within the texture, thereby enabling the articulating surfaces to maintain a smooth surface topography for longer periods in vivo [21, 22].

Several studies have investigated the effect of the micro-texturing on the coefficient of friction [23–25]. Some of these studies suggest an increase in friction, which is mainly caused by the behavior of the protein components of the synovial fluid as it passes through the contact. This behavior is due to the shear stress of the aggregated proteins adhering to the surface (γ-globulin) or to the further layering of the albumin with already a lower shear. Nevertheless, it is important to supplement the given conclusions with kinematic conditions, which have a significant influence on the behavior of the lubricating layer and the design of the texture [26–28].

The potential applications of micro-texturing extend to a range of implants, with the possibility of it becoming a standard treatment for all articulating surfaces in the future. However, the current focus is mainly on small joint replacements, where the number of surgeries is steadily increasing year on year [29]. Developments in this field often provide solutions that do not reflect current trends in endoprosthetics and replace them with proven procedures that are often at the expense of patient comfort. A clear example is the metatarsophalangeal joint, which is often affected by hallux valgus and hallux rigidus. In such cases, two treatment options are simultaneously offered to the patient. One is arthrodesis, which results in the loss of joint functionality. The other option is a mobile replacement of the affected joint. Despite a number of disadvantages, arthrodesis is the most common solution due to its simplicity and reliability. This is because it does not contain interlocking moving parts [30]. These statistics also indicate the necessity for further development in the field of functional MTP replacements in order to make them the surgeons' preferred solution due to their reliability.

Micro-texturing is largely dependent on the load and the rate of movement of the interacting surfaces. As for loading, the contact conformity, contact pressure and material are important. Micro-texturing on hard materials such as the CoCrMo or Ti6Al4V is especially promising for the small joint implants, where the articulating surfaces are less exposed to contact pressure and ranges of motion. A study by Shereff et al. [31] described the kinematics of the metatarsophalangeal joint for patients with a joint disability. The average total range of motion in the sagittal plane was 111°, with approximately 76° of dorsal flexion and 34° of plantar flexion. The implant attempts to maintain a full range of motion, which has a significant impact on a person's stability and proper foot function. Zhang et al. [32] conducted a numerical study on the pressure distribution. They found that increase in the contact pressure for patients affected by the hallux valgus disease, which also led to a higher risk of the joint damage. The pressure for the normal joint is 1.53 MPa and affected joint 2.21 MPa. In the case of the Morgan et al. research [33], the contact pressures were

higher. In the case of the cadaver tests, the values were in excess of 30 MPa, with numerical simulations showing values as low as 10 MPa in the 200–230 MPa load range. The values were significantly higher for joint implants, depending on the material used. The pressure on the implant was recalculated in relation to the geometry of the pair, based on the predictions from the healthy joint [25, 34].

The CoCrMo alloy shows a good abrasion resistance. However, since its mechanical properties differ significantly from those of a human bone, it is susceptible to tribocorrosion and aseptic loosening. Wang et al. [35] compared the CoCrMo alloys with the Ti alloys, specifically in terms of the tribocorrosion. The study concluded that the Ti alloy was better alternative to the CoCrMo alloy, due to its lower wear and potential for the health hazardous ions, such as Co(III) and Cr(VI). The Ti6Al4V exhibits a high wear rate [36, 37], which can be resolved by surface modifications or modifications that create a lubricating film to separate the joint surfaces.

1.1 Production and Impact of the Micro-textures

Micro-textures are frequently used in the arthroplasty of large joints as they offer a better surface wear resistance and lubrication compared to the smooth surfaces [36, 38–40]. For small replacements, the texturing has an even greater potential due to lower contact pressures.

The most used texture shape is a circular or rounded dimple oriented in the slip direction. Conversely, alternative texture shapes have been identified that demonstrate the potential to reduce the coefficient of friction (CoF) even further. However, the question of the efficiency of the production of these shapes and their applicability in the context of more complex kinematics and in combination with different materials remains unanswered [41].

The basic texture parameter is the ratio of depth (h_p) to diameter (d_p), which is critical to the wear performance. Correct adjustment of this ratio (ε) can result in a reduction in the CoF of up to 30% due to locally varying hydrodynamic pressures [42]. In general, small depth textures (around 1 µm) can increase the CoF and wear at low loads due to insufficient hydrodynamic pressure generation. However, this statement does not apply to the use of a protein lubricating film due to the formation of protein clusters during the contact passage, and therefore, an increase in the CoF does not necessarily imply worse results in terms of the long-term wear. In the synovial joint environment, deeper textures (1–15 µm) appear optimal as they both increase the hydrodynamic pressure and act as lubricant reservoirs [43]. Despite the positive effect of the texture on the lubricity, a negative effect is possible as well, especially if the load exceeds optimum thresholds and the lubrication limit is reached [44]. Another critical parameter is the combination of the ε ratio with the texture, surface coverage density (S_p), and shape, which determine the effectiveness in the different lubrication regimes during the implant cycle [45, 46].

It is expected that the friction reduction will be more pronounced for shallow dimples (3–10 µm) having smaller diameters (100–200 µm) [47]. The effect of surface textures on friction will be further driven mainly by the parameters of the textures. Depending on the aspect ratio ε, the textures will either provide an enhanced hydrodynamic effect ($\varepsilon < 0.1$) or serve as a lubricant reservoir ($\varepsilon > 0.1$). Several studies suggest that an optimal ratio value is 0.1 or lower, depending on the material used [48]. However, the conclusions regarding the coverage density are not clear. Some studies proved that tribological properties can improve with an increasing texture density, while others showed the opposite trend, with improvement occurring with a decreasing density [49]. Qiu et al. [50] conducted experiments on the conformal contact system under the boundary lubrication conditions. They investigated three texture densities of 26%, 41%, and 58% at an ε ratio of 0.1. The results showed that the lowest friction coefficient was achieved at 58%. Li et al. [51] investigated the effect of three different densities of hemispherical pits (5%, 13%, and 35%) at the ε ratio of 0.01. They found that the lowest friction coefficient was achieved with a density of 13%. Similarly, Raeymaekers et al. [52] found that densities of approximately 15% and ε ratios in the range of 0.1 to 0.3 produced the best results. Zhang et al. [53] proposed a patelloid texture produced by a pulsed laser ablation. Pin-on-plate tests demonstrated a long-term decrease in the coefficient of friction, resulting in a reduction of the wear rate in the hydrodynamic lubrication regime.

The lubrication properties are influenced not only by the density of the micro-texture coverage but also by the arrangement of the texture. The textures are arranged according to the direction of movement, with longitudinal, transverse, or oblique orientation. The textures are arranged mainly in a square, triangular (hexagonal), or a random pattern. Choudhury et al. [54] investigated the distribution of the micro-textures in square, circular, and triangular arrays on the hip replacements. They concluded that the square arrangement provided the best tribological properties. According to Braun et al. [55], the use of the circular textures of a suitable size in a triangular arrangement can lead to a reduction in the friction of up to 80%. Schneider et al. [48] concluded that a pitting aspect ratio of 10% results in a reduction in friction of 0.1. A triangular pattern is superior to a square arrangement, provided that the texture design is of high quality.

The texturing technology has a major influence on the overall function of the texture. Among micro-machining tilling method [56], laser machining is the most common technique. However, it has a drawback: it forms sharp corners that act as stress concentrators. This leads to two-body

abrasive wear, where the sharp rims cause micro-scratches on the counter-surface, increasing the coefficient of friction. To mitigate this issue, efforts are made to round the rims and reduce their negative impact. This text discusses different methods of the surface modification or rough surface preparation in titanium implants. The methods are based on the mechanical, thermal, chemical, electrochemical, and laser techniques. It should be noted that these methods do not only remove the rims caused by the laser machining but also modify the overall surface [57, 58]. Over the past decade, the patented DLyte technology has garnered a significant attention. Unlike the conventional technologies, the DLyte only smooths the peaks of the roughness, not the valleys, through a selective surface smoothing. The DLyte operates on the principle of an ion transport by free solids, which is a combination of an electrical flow and a particle movement through an electrolytic medium [59–61].

1.2 Aim of the Study

Additive methods together with the micro-texturing and the DLyte technology have the potential to introduce a customized, on-order manufacturing of the implants. However, it is crucial to investigate closer the behavior of the specific alloys that are suitable for additive production, such as the CoCrMo and Ti6Al4V alloys, in joint implant simulations.

This study investigates the behavior of synovial fluid in the contact region of textured specimens made of Ti6Al4V alloy using colorimetric interferometry and friction coefficient. Colorimetric interferometry was proven to bring an essential insight into assessing lubrication mechanisms in hip replacements before [62]. Subsequently, the results are compared with those of a conventional CoCrMo alloy. In addition, attention is paid to the DLyte method, which has the potential to modify the final surface in terms of local irregularities.

2 Materials and Methods

2.1 Apparatus

The analysis of the lubrication film formation and the friction was conducted using a reciprocating motion simulator with a pin-on-plate configuration. This allowed for simultaneous observation of the contact and in situ friction measurements. Figure 1 displays the design of the device, which was modified from the one used by Čípek et al. for cartilage analysis [63, 64]. The device was equipped with a

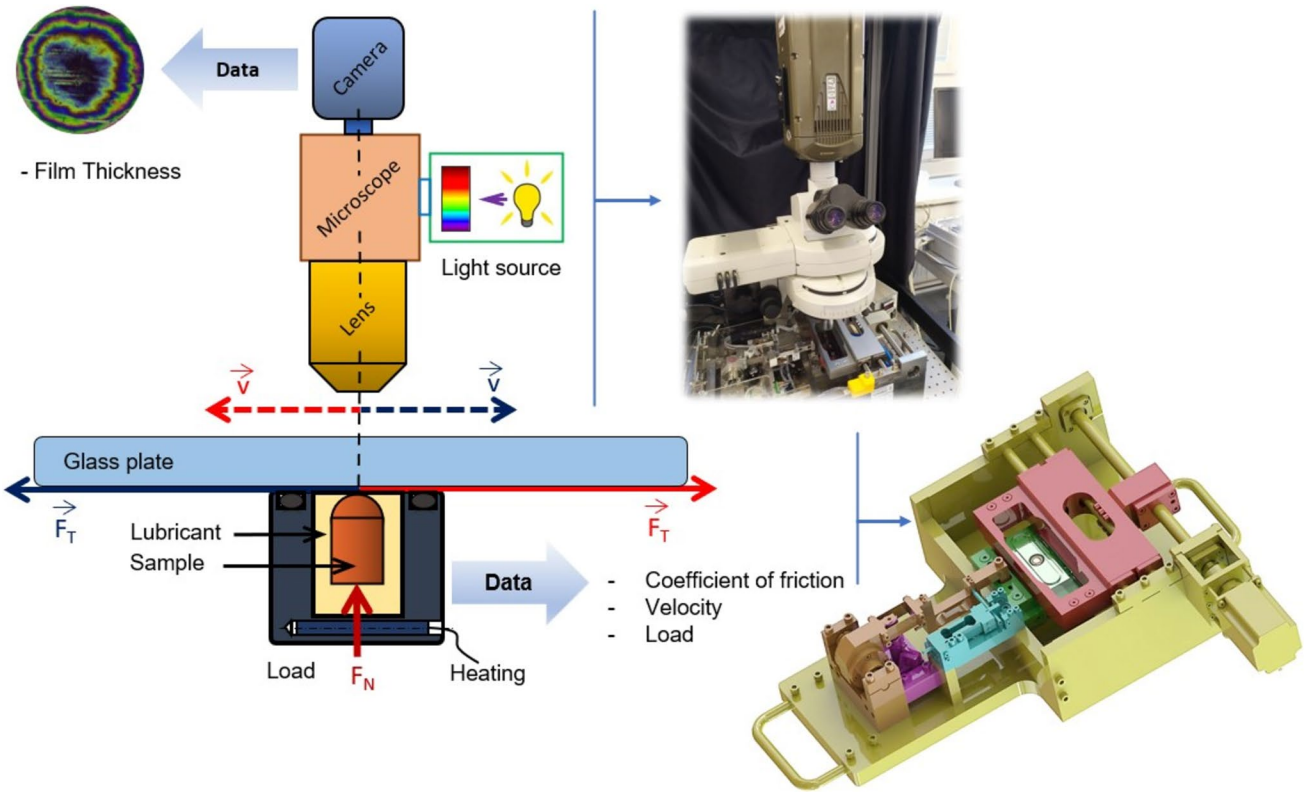

Fig. 1 Schematic of the measuring apparatus in a pin-on-plate configuration

colorimetric interferometry apparatus to observe the thickness of the lubricant film. The simulator bath was heated to a temperature of 37 °C to simulate the human body environment. A glass plate was mounted on a movable carriage, which performed a reciprocating motion, while the specimen remained stationary. The formation of the lubrication film was observed using an optical imaging system that included a microscope, a halogen light source, a CMOS digital high-speed camera (Phantom v710), and a PC. When the metal pin and the glass plate came into a contact and were illuminated, the color Newton rings were observed. Hartl et al. used a thin film colorimetric interferometry to evaluate the film thickness [65]. In our study, the contact surface of the glass plate was coated with a semi-reflective chromium layer to increase the contrast of the interference fringes. The film thickness evaluation was based on three steps:

(1) The calibration curves were obtained from an interferogram of a lightly loaded static contact, which was then matched with the measured contact profile. This provided information about the relationship between the color and the film thickness.
(2) Interferograms of a fully loaded contact during the translation of the carriage were captured using a high-speed camera (Phantom V710, Vision Research, USA).
(3) The thickness at any arbitrary location of the contact could be determined by matching the captured interferograms with the calibration curves.

2.2 Samples

A sample of an optical glass BK270 with dimensions of 155 × 44 × 4 mm was used as a plate. One side of the glass was coated with a semi-reflective chromium layer and the other with an anti-reflective layer. The experimental pins were made of two main materials used in the implantology: the medical grade cast CoCrMo alloy (ASTM-F75) and the Ti6Al4V alloy (ISO 5832-3).

The CoCrMo pin was manufactured from a cold-drawn bar, cut and turned under the same cutting conditions as the conventional joint replacement implants. The radius of the head of the pin was R_{100} and the diameter of the pin was 9.7 mm. The ball surface was further polished to the required minimum roughness R_q of 0.012 ± 0.005 µm. The Ti6Al4V pin was manufactured from a 10-mm-diameter cold-drawn bar and then machined and polished to achieve the same geometry and surface finish as the CoCrMo pin.

The surface geometry of the samples was evaluated before the experiments. An optical profilometer based on phase-shifting interferometry (Bruker, Contour GT-X8) was used to analyze the surface roughness (R_q) in the contact area with dimensions of 1 × 1.2 mm covering a theoretically calculated circular contact area with radii of 0.06 mm.

The distribution of the micro-textures was chosen to be triangular, with the basic element of this lattice being an equilateral triangle of side length 42.7 µm. The shape of the micro-texture itself was circular, while the bottom of the texture was flat as far as possible (Fig. 2). This texture shape

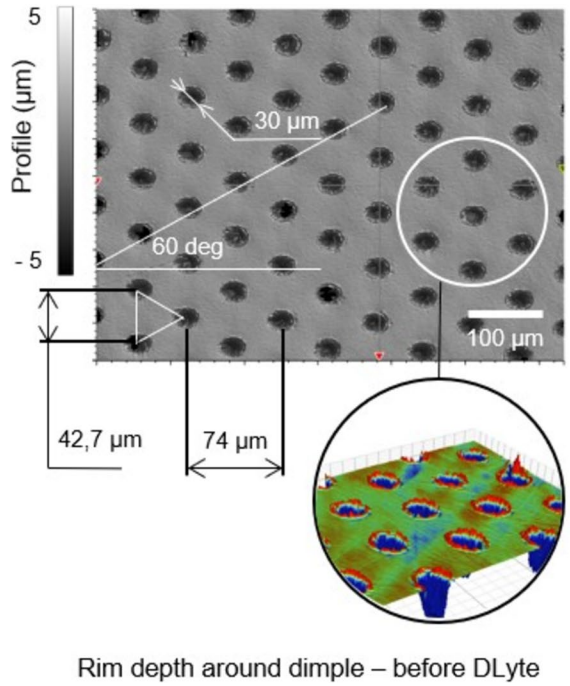

Texture depth -hp (µm)	ε - ratio	Diameter (µm)	Distance of centres (µm)	Area coverage (%)
0.4	0.013			
1	0.033			
2	0.067	30	74	15
4	0.133			
6	0.2			

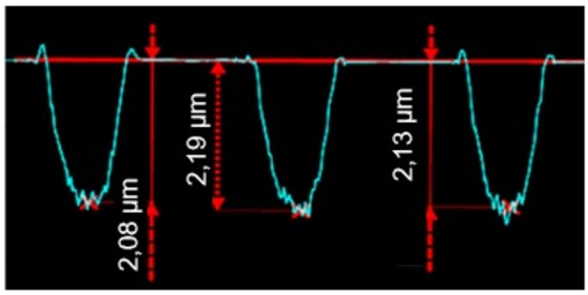

Fig. 2 Distribution and geometry of the textures on the surface of the samples

was chosen because it is easy to fabricate with a picosecond laser while maintaining the geometric repeatability at each pit. The circular shape also gives us the advantage of the consistency of the film behavior even with changes in the direction of the motion, which is expected due to its use in an articulating implant. A schematic of the arrangement and shape of the texture is shown in Fig. 2. Based on the results of the literature search, the most effective coverage density S_p of 15% was chosen in terms of the lubricant film formation, considering the number of textures in contact with the materials at full load. The condition was the participation of at least 5 textures in the contact area, which is ensured in the given configuration. The chosen variable parameter is the ratio ε. In order to vary the value in the range of 0.01–0.2, which is given in the literature as the most effective value for the given coverage, the only variable parameter left is the texture depth d_p. For this reason, 5 texture parameters were chosen (d_p 0.4–6 µm). The distance between the centers of the dimples was 74 µm, and the radii of the dimples were 15 µm.

The textures were created using a laser micromachining with a picosecond laser [Perla 100 (Hilase)] to minimize the thermal impact on the surface. The laser operated at a wavelength of 1030 nm, a pulse length of 1 ps, a repetition rate of 60 kHz, and a maximum pulse energy of 1 mJ. The laser beam was guided through a harmonic frequency attenuator and an optical combiner. The laser beam was guided through a system of mirrors to an Intelliscan 14 (Scanlab) scanning head, which was placed on a sliding z-axis stage. The textures were fabricated at an average power of 72 mW, moving the laser beam along a spiral trajectory at speeds up to 400 mm/s. Ten samples were created for each material, with each texture (0.4–6 depths). The DLyte method was used to remove the sharp rims that were produced during the process on the texture. The CoCrMo pins were polished using CoCr DLyte MIX MSA-S H FOR S100 electrolyte, while Ti DLyte MIX MSA PLUS-S electrolyte was used for polishing titanium samples.

2.3 Lubricant

The model solution comprised bovine serum albumin (BSA, Sigma Aldrich A7030, Darmstadt, Germany), bovine serum y-globulin (BSG, Sigma Aldrich G5009, Darmstadt, Germany), hyaluronic acid with a molecular weight of 1000 kDa (HA), and phospholipids. The constituents were added to a phosphate-buffered saline (PBS). Concentrations corresponded to the composition of the synovial fluid of patients after a total joint arthroplasty (albumin 26.3 mg/ml, y-globulin 8.2 mg/ml, Phospholipids 0.35 mg/ml, Hyaluronic acid 0.82 mg/ml) [66]. The lubricants were thawed prior to the testing and stored in a refrigerator to ensure a complete protein dissolution in the PBS. Each experiment used a total volume of 14 ml of lubricant and was conducted under fully flooded conditions to avoid contact starvation.

2.4 Experimental Design

The kinematic conditions of the experiment were derived from the kinematics of the first metatarsophalangeal (MTP) joint. According to Durrant et al.'s study [67], the MTP joint undergoes a 65° rotation. The angular values of the initial and the final declination differ according to the physiology, gait type, and joint damage of each person. However, an angle of 65° represents the mean value for an average person [39, 40]. For the MTP joint implants, a head and a socket with a radius of R_{100} were used. The arc path length was calculated as the product of the radius and angle in radians, resulting in an approximate length of 11.3 mm. However, due to the tribometer conditions, the length was increased to 20 mm. Each cycle involved a back-and-forth motion, resulting in a total cycle length of 40 mm. The frequency of the movement was 0.5 Hz, resulting in a speed of 20 mm/s for a 40 mm path. The kinematic conditions of the experiment are summarized in Table 1. The load of 0.5 N was applied to both micro-textures. For the CoCrMo compared to glass, the contact area diameter was 180 µm and the contact pressure was 29.6 MPa. For the Ti6Al4V compared to glass, the contact area diameter was 191 µm and the contact pressure was 26.3 MPa. The contact area diameter and pressure were calculated using the contact Hertz theory.

The overall design of the experiment was devised with the objective of observing phenomena in the contact region, to gain some fundamental insights and comparisons. In this context, several simplifications were made to the in vitro conditions in comparison to the real in vivo conditions in the MTP joint. The primary limitation is the non-conformal surface and the associated increase in contact pressure to a higher range of values that occur at the joints. Concurrently, the alteration in contact pressure results in the replacement of the articulating pair with a transparent glass with a lower Young's modulus than the Ti6Al4V alloy. These differences can affect the thickness of the lubricating film, which can ultimately have a negative effect on the overall wear. Therefore, these limitations must be considered in any wear evaluation and long-term wear tests [68, 69].

For each texture, including the reference without texture (six samples), a single measurement was conducted, comprising three consecutive cycles. A schematic of the experiment is presented in Fig. 3.

2.5 Data Processing

The tribological behavior of the lubricant and the implant materials was evaluated based on two main parameters: the coefficient of friction (CoF) and the film thickness.

Table 1 Experimental conditions (A) sample characteristics, (B) kinematic conditions

(A)

Samples	Material	Semi-finished product	Young's modulus (GPa)	Poisson's ratios	Contact pressure pin on plate (MPa)
Pin (radii 100 mm)	Ti6Al4V alloy	Bar	114	0.34	26.3
	CoCrMo alloy	Bar	230	0.28	29.6
Plate	Borosilicate glass	B270	62	0.22	–
		Albumin	γ-Globulin	Phospholipids	Hyaluronic acid
		26.3	8.2	0.35	0.82

(B)

Load (N)	Velocity (mm/s)	Stroke (mm)	Total distance (mm)	Number of cycles	Duration (s)	Temperature (°C)
0.5	20	20	2400	60	120	37

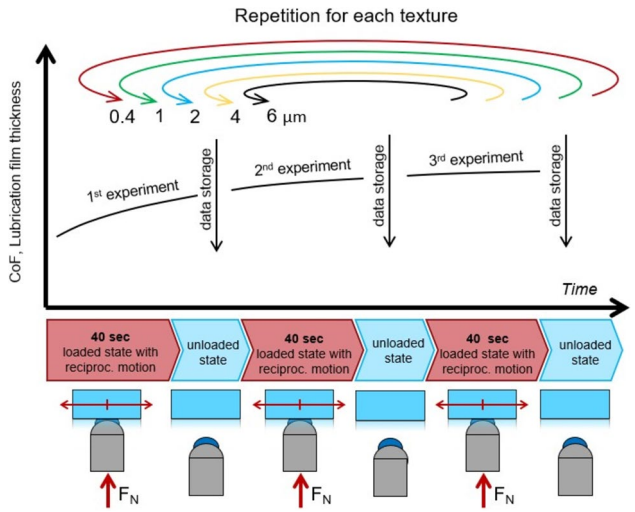

Fig. 3 Experimental set-up

The coefficient of friction was measured in three consecutive cycles, which were then combined into a single graph. The discontinuity of the measurements into individual cycles was necessary due to the memory capacity of the high-speed camera. The sampling frequency was 50 Hz, resulting in the friction coefficient values obtained for time periods of 0.02 s. Filtering and data processing were conducted using MATLAB software. The data were filtered based on a 5% deviation from the mean velocity to remove the outliers and the data from the motion change sections where the null velocity was reached. The film thickness was quantified using the colorimetric interferometry. The fundamental principle of this method is the optical recording of the contact area, captured at a rate of 100 frames/s. The frames were extracted from the scanned data at regular intervals. The glass part of the simulator was moved at a constant speed along the pin. This resulted in 20 frames for evaluation at 20 cycles. The interferograms were evaluated using a custom software [65]. In each of the 20 frames, three reference locations in the contact area were selected, and the average thickness of the lubricating film was determined. The final value for one cycle was calculated as an arithmetic mean of these three values. For each measurement, a total of 20 average thicknesses were obtained, resulting in 60 values in three cycles for each material pair tested.

3 Results and Discussion

The results presented concern the micro-textured surface and its influence on the coefficient of friction, with the objective of describing the lubrication regime using the observed film thickness in the contact area. The main contribution is the use of Ti6Al4V alloy, which has the potential for future use in the fabrication of individualized implants using additive manufacturing. The research is mainly concerned with the description of the tribological processes in the contact region, with the objective of preparing the basis for further necessary surface treatments improving wear resistance. The CoCrMo alloy was employed as a reference, enabling results comparison. The articulating surface was then augmented with a range of micro-textures, which were subsequently modified by electrochemical machining. This allowed for the investigation of the impact of these modifications on the lubrication processes in the contact area. The rationale behind modifying the surface in this manner is to identify optimal conditions for the formation of a film capable of separating the articulating surfaces, thereby reducing the quantity of loose abrasive particles.

3.1 Surface Topography

In the initial stage of the study, the articulating surfaces of the samples were evaluated without texture, and subsequently, after texture production and electrochemical treatment with DLyte. The initial surface was polished to achieve a roughness value below 10 nm (without texture), which meets the ISO 7206-2 standard for articulating surfaces of metallic implants [70]. The surface itself was also evaluated in terms of its overall geometry, with respect to the possible influence on the contact area and, thus the contact pressure to be induced [71]. Overall, a deviation of up to 10% of the required nominal radius R_{100} was accepted. This deviation was based on the accuracy of the measurements themselves and the manufacturing capabilities. It was also considered that the specimens were manufactured using the same method as commonly used implants, which guaranteed the same manufacturing deviations and surface quality achieved in endoprosthetics. However, an issue arose in the evaluation of the overall surface waviness, where irregularities were more frequent, which influenced the shape of the contact area. Based on these conditions, the specimens that demonstrated the most favorable results in the analysis of the contact area were selected. The samples were then textured with five different texture depths of the same distribution and diameter using a picosecond laser. Laser surface texturing process has a thermal ablation process, due to these high temperatures are encountered around the dimple and cause microstructural changes, residual thermal stresses, rim formation in the laser-irradiated zone and substrate [72]. As the depth of the texture increased, the rim of dimples relative to the reference surface also increased. This was caused by the greater material removal and material melting at the rim of the texture. Some larger rims (270–380 nm) around the dimples (2–6 µm) were observed for the Ti6Al4V alloy (Fig. 4C, D). For the CoCrMo, the rims were significantly lower, the maximum rim heights were up to 270 nm. To eliminate these inequalities, the electrochemical method DLyte has proven and led to a relative decrease in the rims for both materials. However, despite the removal of the rims, this method proved to be unsuitable for the CoCrMo alloy. Even a short exposure with the DLyte method (0.4 s) resulted in the removal of rims, at the same time it led to damage to the rest of the surface, severely damaging the observed area and making further evaluation of the results impossible. This phenomenon can be observed in the plot of total roughness (Fig. 4A, B), where notable discrepancies were observed in the CoCrMo alloy. Several studies found that Co–Cr–Mo alloys have a dendritic surface structure with a 1 to 4 nm thick oxide layer, providing a corrosion barrier in the human body. Corrosion barrier can affect processes during electrochemical machining, which prevents us from creating an ideal geometry with a uniform contact surface. For this reason, the results from colorimetric interferometry

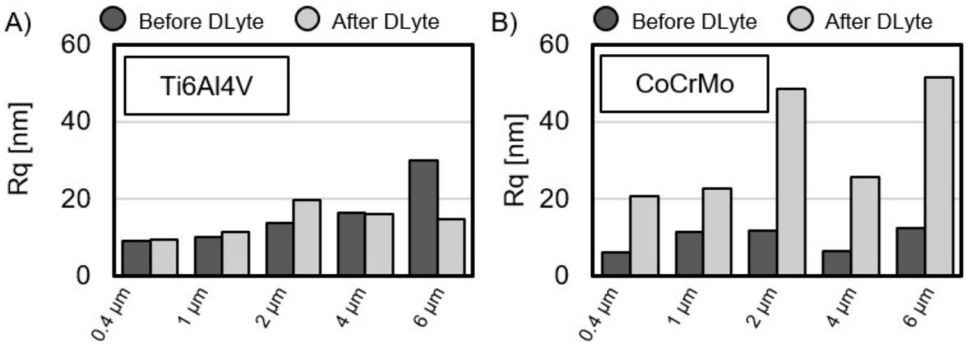

C)

Texture depth (µm)	Rim height (nm) – before DLyte							Average (nm)	SD (nm)
	No. 1	No. 2	No. 3	No. 4	No. 5	No. 6	No. 7		
0.4 µm	73	84	55.1	69.8	35.5	150.8	61.3	75.6	33.8
1 µm	155.2	308.5	305.7	156	143.7	224.5	181.6	210.7	65.7
2 µm	349.2	275.9	286.7	303.1	254.2	294.4	132.5	270.9	62.6
4 µm	288	420.7	329.8	409.5	368.6	340.5	505.4	380.4	66.5
6 µm	275.6	190.6	301.1	285.1	214.3	302	470.6	291.3	83.4

D)

Texture depth (µm)	Rim height (nm) – after DLyte							Average (nm)	SD (nm)
	No. 1	No. 2	No. 3	No. 4	No. 5	No. 6	No. 7		
0.4 µm	81	187.7	138.2	105	61.3	13.9	165.2	107.5	56.5
1 µm	127.9	174.9	104.1	88.9	46.9	113.7	39	99.3	43.5
2 µm	49.8	65.9	148	58.4	61.4	101.9	85.9	81.6	31.7
4 µm	179.2	75.8	59.5	75.2	102	112.9	94.9	99.9	36.5
6 µm	72.4	28.7	62.7	43.7	47	73	83.1	58.7	18

Fig. 4 Average surface roughness with masked texture: **A** Ti6Al4V, **B** CoCrMo, rim height of textures for Ti6Al4V: **C** before DLyte, **D** after DLyte

of the CoCrMo alloy after application of the DLyte method could not be evaluated [73, 74]. In contrast, the Ti6Al4V material showed a significant reduction in the rim without a significant damage to the rest of the surface. The method was applied for textures with more pronounced rims where the rim reduction from 53 to 80% occurred without a damage to the surface geometry. The surface quality achieved may be influenced by the chloride ion content of the electrolyte, indicating a suitable reaction for anodic dissolution. At the same time, the electrolyte may alter the surface tension, which could lead to the formation of a stable TiO_2 film and thus increase corrosion resistance and alter the affinity of the proteins in the contact area [75].

3.2 Coefficient of Friction

Another parameter evaluated for all articulating surfaces was the friction coefficient in the pin-on-plate configuration. Results shows the average CoF value after the first cycle when the values stabilized (Fig. 5). Initially, the CoF values were observed to be the lowest, and then they increased with the accumulation of proteins in the contact region. This finding is partially corroborated by studies that have examined the shear stresses within the protein layers in the contact region [27, 34, 76, 77]. This phenomenon was also described in relation to the individual proteins in the contact area: albumin, γ-Globulin [78]. The polished CoCrMo alloy, commonly used for the articulating surfaces in implantology, showed the CoF value of 0.5 (SD 0.02). The use of textures resulted in an increase in the CoF value for the texture depths of 1–4 µm. The CoF increase was about 0.02 to 0.09. There was a slight decrease for the texture depths of 0.4 and 6 µm which may be due to a more pronounced deviation from the ε ratio which showed the lowest results in terms of the coefficient of friction [52]. The subsequent utilization of the DLyte method resulted in significant damage to the geometry of the contact area, thereby distorting the results due to local deformations that also altered the contact pressure distribution. In certain instances, the friction coefficient decreased, which can be attributed to differing protein aggregation processes on the surface due to the change in pressure. In this case, it is essential to consider the specific circumstances when interpreting the results. Further research is necessary to ascertain the viability of the DLyte method in CoCrMo alloy. In particular, future research should focus on optimizing the electrolyte exposure time, the type of electrolyte, and optimizing the technology to remove irregularities while avoiding any disturbance to the overall geometry.

Prior to the DLyte treatment, the Ti6Al4V alloy exhibited a markedly lower friction coefficient value of 0.32 (SD 0.01) compared to the CoCrMo alloy. Concurrently, the CoF values demonstrated a notable acceleration in stabilization with the advancement of continuous development. The

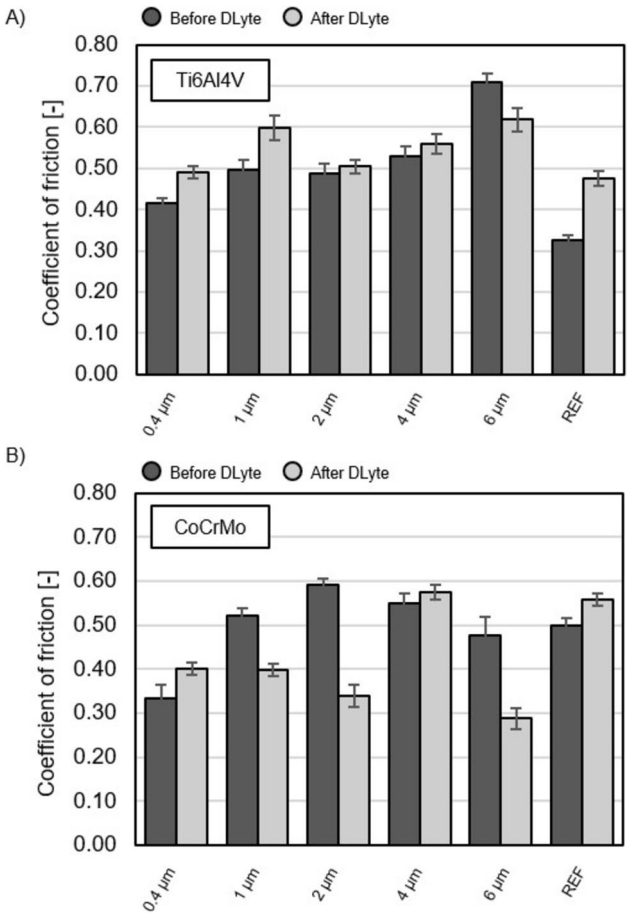

Fig. 5 Coefficient of friction: **A** Ti6Al4V alloy, and **B** CoCrMo alloy

incorporation of textures in the remaining samples resulted in an increase in friction compared to the reference, suggesting a heightened concentration of proteins in contact. The increase in coefficient of friction (CoF) was observed to be within the range of 28–118%. This increase can be attributed to protein friction, which is the response of proteins to shear friction. Previous studies have reported a decrease in friction with textured surfaces; however, it is often the case that phosphate-buffered saline (PBS) or Ringer's solution leads to a different lubrication mechanism [79]. The texture with a depth of 6 µm achieved the highest average coefficient of friction (0.71, SD 0.02). The significant deviation may be due not only to protein aggregation but also to a combination with adhesive wear in the contact region, as described by the study of Sonekar and Rathod [80]. In the case of the Ti6Al4V alloy, the DLyte method did not damage the overall geometry and the contact area remained in its original dimension, but there was a partial increase in the overall surface roughness compared to the original polished specimen. Nevertheless, the roughness of 30 nm was not exceeded for any of the textured samples. The DLyte method reduced the texture rims. The reduction was to the extent that there

was a full separation by the protein lubricating film, eliminating the risk of a significant abrasive and adhesive wear. With regard to the coefficient of friction, the DLyte-treated Ti6Al4V alloy surface exhibited a notable increase from 0.32 to 0.47 for the reference sample. Concurrently, there was a slight increase from 3 to 20% for all textures, with the exception of the 6 µm depth, where there was a decrease of 13%. These results are corroborated by the lubricating film itself, which effectively decouples the surfaces at a given geometry. This means that the frictional forces are solely generated by shear friction in the synovial fluid. In the case of the deeper 6 µm texture, it was also possible to observe a slight decrease in the thickness of the lubricating film. This, together with the deeper texture and the different contact pressure distribution, partly explains the change in the coefficient of friction behavior [81]. The results obtained for the textured surfaces show positive changes in terms of protein adhesion in contact, which is manifested by a change in the coefficient of friction. In the case of the Ti6Al4V alloy, there was a slight increase, which corresponds to the results obtained for the transition of the protein cluster in the contact [26]. At the same time, it is necessary to take into account the changes in the contact area in terms of the increase in the hydrodynamic pressure and the change in the geometry of the contact area due to the influence of the textures. In this case, the area is 15% smaller, which will lead to a tendency for the coefficient of friction to increase at the same contact pressure. In the case of CoCrMo, despite the reduction in contact area due to texture, there was a slight reduction in friction, indicating a better ability to form a lubricating film compared to the titanium alloy. A limitation of the study is the relevance of the evaluation in terms of the texture depth, as due to the random behavior of the contacting proteins, a larger number of samples need to be tested. Further research in this direction is planned, but the results partially suggest the advantage of the deeper textures due to their function as a lubricant reservoir and the possibility of trapping the wear particles directly in the texture, contributing to the overall wear reduction.

3.3 Film Thickness

The film thickness of both alloys was evaluated using colorimetric interferometry. In the case of Ti6Al4V, the results before and after treatment by electrochemical polishing were used. In the case of the CoCrMo alloy samples, only the results before electrochemical treatment were published, as there was significant surface damage, which would have led to misleading results. The surface evaluated was with a roughness commonly used in implantology, up to 12 nm (with the textures used being masked out). Conversely, the surface of the contact area exhibited deviations within 5% despite significant deviations from circularity. In the case of the CoCrMo alloy, measurements on the reference specimen demonstrated a film thickness of 39 nm (SD 11 nm), which only marginally separated the articulating surfaces. Conversely, the relatively high deviations were attributed to the passage of protein clusters across the contact surface, which locally increased the film thickness and thus affected the overall results. Subsequently, measurements were performed on textured samples. The data set could only be evaluated for textures with depths of 0.4 and 1 µm, where complete separation of the articulating surfaces was observed, thus minimizing abrasive wear. For deeper textures, significant abrasive damage to the glass significantly affected the results and prevented a proper evaluation. During the translational motion, the texture rims made contact with the glass surface, as the height of the rims exceeded the predicted thickness of the lubricant film. This resulted in the formation of scratches and damage to the chrome layer on the glass. The 0.4 µm deep texture exhibited a slight increase in film thickness compared to the reference sample (50 nm, SD 12 nm), with no significant change in the behavior of the lubrication layer. This indicates that the texture itself exerts an influence. In contrast, the 1 µm texture exhibited aggregation of protein clusters at the beginning of the experiment, leading to a local increase in film thickness up to 200 nm. Subsequently, the thickness of the protein layer increased, resulting in a further increase up to above 200 nm. All values of the film thickness are confronted with the heights of irregularities (including rims on the textures and overall roughness), which is demonstrated in the results by dashed lines (Fig. 6).

In comparison to the CoCrMo alloy, the Ti6Al4V samples exhibited a disparate behavior in the contact area. The surface roughness of the Ti6Al4V alloy was comparable to that of the CoCrMo alloy, with a range of 9–30 nm. Concurrently, however, minor scratches and localized damage were observed during surface polishing of the Ti6Al4V alloy. Following electrochemical treatment with DLyte, the protrusions were removed, yet the overall roughness remained unaltered, and the local damage was retained. Furthermore, irregularities can also affect the formation of the lubricating film, for example, by accelerating the aggregation of proteins in the contact area. This phenomenon can be observed in the reference sample (Fig. 7), where the formation of a cluster of proteins occurred from the outset of the experiment, which subsequently washed away from the contact area once it reached a critical size. This phenomenon can be observed by the rapid reduction of the film thickness below 100 nm. The reduction was such that only partial separation of the protein lubricating film occurred, thereby creating a risk of abrasive wear. In subsequent, another objective is to enhance the film thickness while simultaneously improving the overall surface roughness, thus ensuring the separation of the surfaces. The untextured surface of the Ti–6Al–4V alloy is hydrophilic in nature, and this hydrophilicity can be

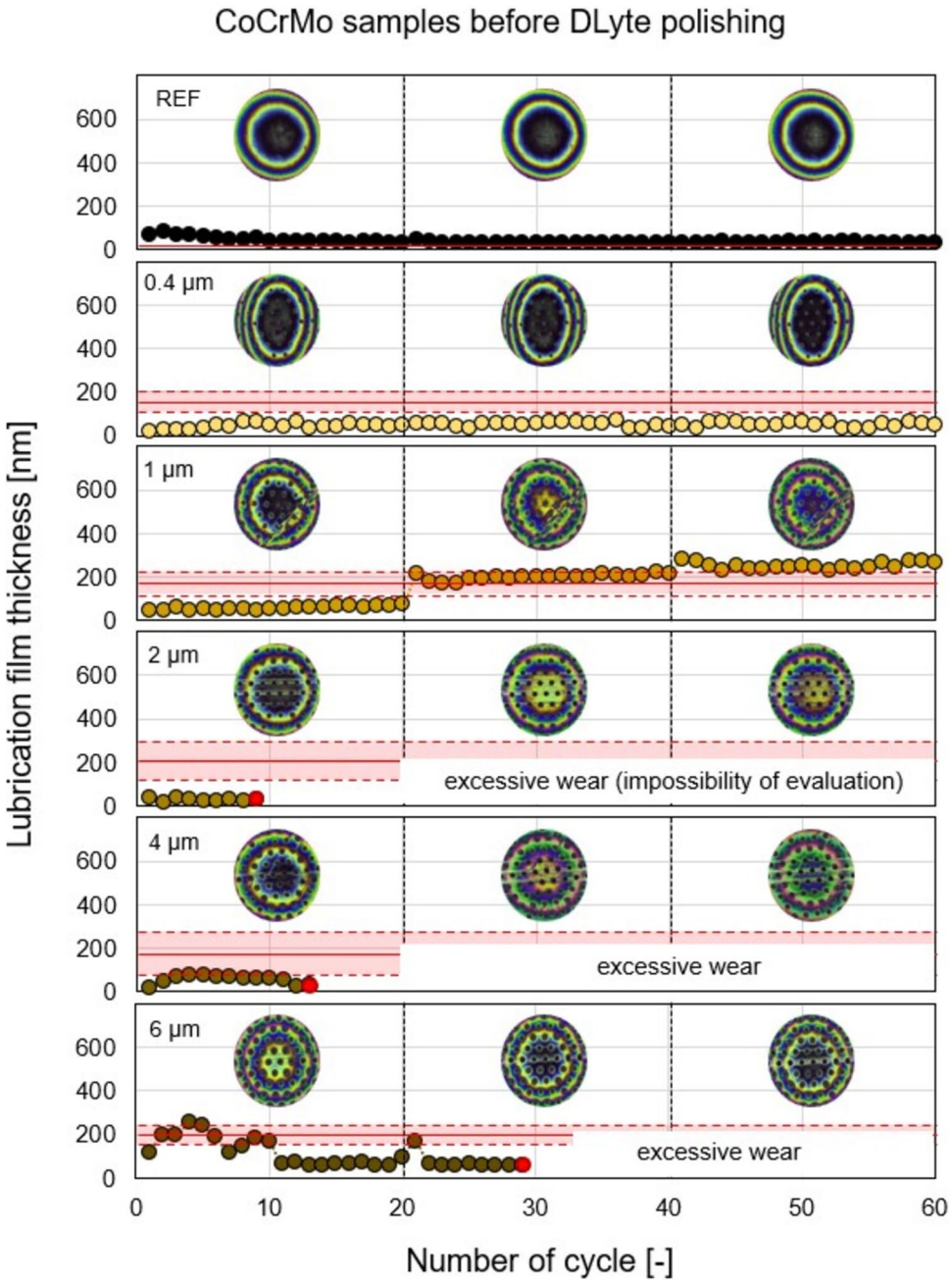

Fig. 6 Analysis of film thickness for the CoCrMo alloy before DLyte

supported by suitable texturing. Nevertheless, the improvement in wettability is a combined effect of the roughness factor resulting from surface texturing, texture geometry and, of course, the material itself [82].The subsequent results with a textured surface clearly demonstrate an increase in film thickness, which supports previous claims. Additionally, experimental studies on the effect of textures have demonstrated that, in addition to the change in wettability, the authors often describe the effect mainly as a change in hydrodynamic pressure. Also, the ability to capture proteins in contact using the geometry of textures acting as lubricant reservoirs has been observed [48, 55, 83]. In our work, for shallower textures of 0.4 and 1 µm, the separation is evident with a thickness of the lubricating film of 310–320 nm, which is significantly greater than surface irregularities. In the case of deeper textures, the separation of the surfaces is ductile, and the glass often collides with protrusions at the rim of the textures. Nevertheless, it is evident that film thicknesses above 230 nm can still be observed, which is many times the minimum roughness required for implants. Consequently, texturing is beneficial. However, this requires additional surface treatment to remove irregularities. In the case of the Ti6Al4V alloy, the DLyte method used showed more satisfactory results than in the case of the CoCrMo alloy.

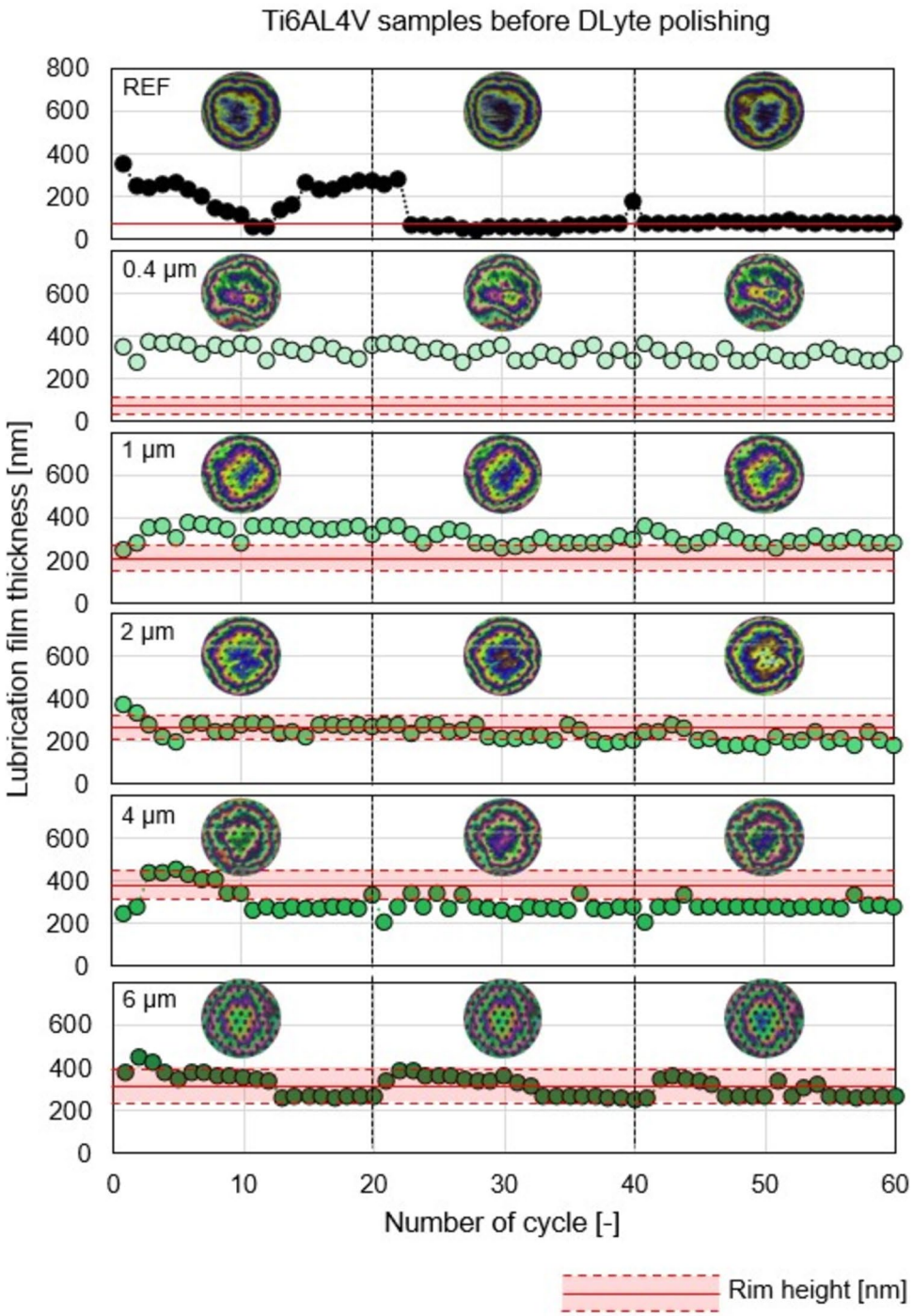

Fig. 7 Development of lubrication film thickness for different depths of textures for Ti6Al4V before DLyte

The objective is to eliminate significant irregularities while maintaining the original geometry of the surface, which implies that alterations in contact pressure are minimal.

The following results demonstrate the behavior of synovial fluid in the contact area following electrochemical treatment. The removal of the roughness has significantly shifted the range of potential roughness on the surface (area indicated by the dashed line), significantly reducing the risk of abrasive wear. In the case of the reference sample, without the influence of the texture, it is possible to observe the limit values of the film thickness at a thickness of approximately 60 nm. The nominal roughness of the given sample is up to 10 nm, with the possible presence of grooves caused by polishing, which increases the roughness. Under these conditions, there is a risk of contact and wear of the articulating surface. The following results demonstrate a clear effect of the presented texture. For each texture, there was an increase in the thickness of the lubricating film above 180 nm. The

highest values were achieved for shallower textures of 0.4–4 µm. These textures with parameter ε 0.013–0.133 created a lubricating film with a significant overlap of surface irregularities. The thicknesses ranged from 280 to 321 nm, with the highest local surface roughness being 107.5 nm. In the case of the 6 µm texture, the film thickness was reduced to an average value of 180 nm. However, these differences are already predictable. On the one hand, they may be associated with increasing depth and changes in hydrodynamic pressure, which is consistent with published studies [51, 52]. At the same time, the irregularity of the contact surface, which was evident on the observed interferogram, may also have an effect (Fig. 8). Such irregularities will affect both the contact pressure and may impede the accurate determination of the zero film thickness during calibration.

One of the limitations of the study is the pressure distribution in the contact region. In the future, it would be beneficial to consider a method that would allow for the production of a more accurate geometry, with the aim of more clearly separating the different processes in the contact

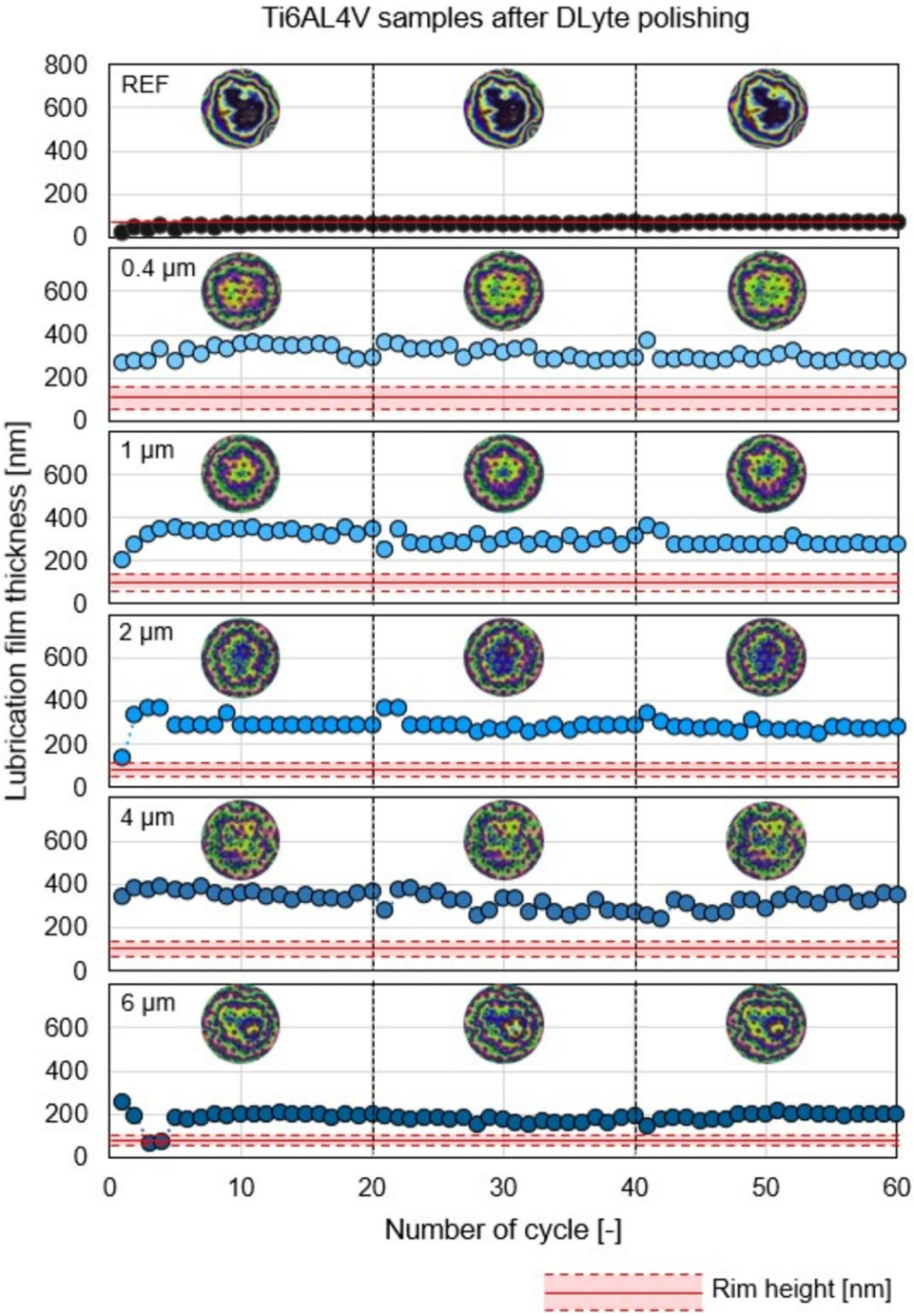

Fig. 8 Development of lubrication film thickness for different depths of textures for Ti6Al4V after DLyte

region. Additionally, it is important to note that the specimens were fabricated using the same method as conventional implants, which provides a more realistic representation of implant function. To ensure the reliability of the results, it is essential to increase the number of tested samples with a uniform texture and to account for potential random protein transitions across the contact region.

Another factor to consider for future research is the DLyte process. In the case of the Ti6Al4V, it has shown clear results in improving the surface and removing the unwanted irregularities that cause abrasive wear. In combination with laser machining, it is essential to incorporate the method into the machining process. At the same time, the suitability of the method needs to be considered not only in terms of roughness reduction, but also regarding its potential to improve the corrosion resistance and possibly to alter the wettability. Newer methods, such as electrolytic plasma polishing, might be considered [84]. It is also necessary to consider other options for texturing where the roughness would be significantly lower. The main motivation for further research is the focus on CoCrMo alloy, where we have not achieved satisfactory results. In this case, it is possible to use newer technologies such as laser shock peening, which uses high-energy laser pulses to induce compressive residual stresses in materials without causing melting of the material at the edges [85].

The variability of the synovial fluid composition should also be considered in the context of the results presented. In this study, we use clinical data based on the analysis of patient fluids after a joint replacement surgery [66]. Based on the results, a model synovial fluid that respects the given results and clinical data was prepared. However, there are variations due to the patient's age, sex, and general predisposition. An important factor is the concentration of hyaluronic acid and phospholipids, which may influence the overall lubrication mechanism. It would, therefore, be interesting to investigate these interactions further, but as the results suggest, these will be outliers without changing the overall positive trend [78].

4 Conclusions

The study provided a detailed description of the behavior of micro-textures in hard pairs used in implantology. These are the commonly used CoCrMo alloy and a promising biocompatible Ti6Al4V alloy. Both materials are suitable for 3D printing, thereby facilitating the customization of the implants, which would markedly enhance the implant survival rates. The aim of this work was to evaluate the behavior of the lubricant film at the joint site for the smooth surfaces and subsequently for the textured surfaces. The tests were carried out in a pin-on-plate configuration using a specially modified tribometer with the ability to use colorimetric interferometry. The coefficient of friction and the thickness of the lubricating film were evaluated, allowing us to assess the lubrication performance and to describe the behavior of proteins passing through the contact. Texturing the surface of the Ti6Al4V alloy gives us three main advantages:

- Micro-hydrodynamic bearings,
- The complete surface separation of the articulating materials,
- Potential lubricant reservoir during lubricant film formation.

In order to fully exploit the potential benefits of the textured surfaces, the laser-generated textures required further modification due to the appearance of significant irregularities at the rims of the textures. The DLyte electrochemical method was used to reduce the local irregularities and to create the conditions for the formation of a smooth lubricating film. At the same time, the aim was to prevent the adhesive wear of the articulating surfaces. The result was an increase in the protein lubricating layer that was many times greater than the unevenness of the joint surface. Overall, this result indicated that the DLyte process can be used as a finishing process for surface texturing. At the same time, the results demonstrated the beneficial effects of the micro-texturing. The following conclusions were made:

- Ti6Al4V alloys exhibit a higher surface affinity with aggregated proteins, which is manifested by a thicker lubricating film relative to the conventionally used CoCrMo alloy.
- Micro-textures are a suitable tool to increase the film thickness and to minimize the possible abrasive wear of surfaces.
- The use of a picosecond laser causes the material to melt at the rim of the texture, which increases the risk of the abrasive particles being released upon contact and subsequently leads to an increase in wear. However, the electrochemical machining DLyte method has proven to be a suitable solution for the Ti6Al4V alloy, effectively eliminating these issues.

Furthermore, the performance of the lubrication mechanisms varies depending on the wetting properties and surface energy of the material. The rate of the protein deposition, and therefore lubrication, is affected by the contact pressure, the relative velocity, and the contact temperature.

Author Contributions M. Ranuša and O. Kučera conceived the idea and designed the experiments. M. Ranuša and L. Odehnal performed

and analyzed the experiments and wrote the original draft of the manuscript. D. Nečas, M. Hartl and I. Křupka supervised the study. M. Vrbka supervised and financed the study.

Funding This research was carried out under the Project "Friction and lubrication of small joint implants produced by 3D metal printing additive technology" funded by the Czech Science Foundation, No. 22-02154S and by the Project "Mechanical Engineering of Biological and Bio-inspired Systems," funded as Project No. CZ.02.01.01/00/22_008/0004634 by Programme Johannes Amos Commenius, Call Excellent Research, administered by the Ministry of Education, Sports and Youth. Also, thanks to ProSpon, spol. s r. o. company for the preparation of the samples.

Data Availability The data that support the findings of this study are openly available in repository Zenodo at http://doi.org/https://doi.org/10.5281/zenodo.13235495.

Declarations

Conflict of interest The authors declare no conflict of interest.

References

1. Siddiqi, A., Levine, B.R., Springer, B.D.: Highlights of the 2021 American Joint Replacement Registry Annual Report. Arthroplasty Today **13**, 205–207 (2022)
2. Croes, M., Akhavan, B., Sharifahmadian, O., Fan, H., Mertens, R., Tan, R.P., et al.: A multifaceted biomimetic interface to improve the longevity of orthopedic implants. Acta Biomater. **110**, 266–279 (2020)
3. Fashanu, F.F., Marcellin-Little, D.J., Linke, B.S.: Review of surface finishing of additively manufactured metal implants. In: Proceedings of the ASME 2020 15th International Manufacturing Science and Engineering Conference MSEC2020, 2020 (2020)
4. Marian, M., Shah, R., Gashi, B., Zhang, S., Bhavnani, K., Wartzack, S., et al.: Exploring the lubrication mechanisms of synovial fluids for joint longevity—a perspective. Colloids Surf. B **206**, 111926 (2021)
5. Sing, S.L., Tey, C.F., Tan, J.H.K., Huang, S., Yeong, W.Y.: Chap 2: 3D printing of metals in rapid prototyping of biomaterials: techniques in additive manufacturing. In: Narayan, R. (ed.) Rapid Prototyping of Biomaterials, 2nd edn., pp. 17–40. Woodhead Publishing, Sawston (2020)
6. Khimich, M.A., Ibragimov, E.A., Chebodaeva, V.V., Prosolov, K.A., Tolmachev, A.I., Glukhov, I.A., et al.: From raw elements to 3D samples: an economical route for Co–Cr–Mo alloy fabrication. J. Alloys Compd. **978**, 173460 (2024)
7. Stamenković, D., Popović, M., Rudolf, R., Zrilić, M., Raić, K., Đuričić, K.O., et al.: Comparative study of the microstructure and properties of cast-fabricated and 3D-printed laser-sintered Co–Cr alloys for removable partial denture frameworks. Materials **16**(8), 3267 (2023)
8. Ocran, E.K., Guenther, L.E., Brandt, J.-M., Wyss, U., Ojo, O.A.: Corrosion and fretting corrosion studies of medical grade CoCrMo alloy in a clinically relevant simulated body fluid environment. Metall. Mater. Trans. A **46**, 2696–2709 (2015)
9. Metikoš-Huković, M., Babić, R.: Passivation and corrosion behaviours of cobalt and cobalt–chromium–molybdenum alloy. Corros. Sci. **49**, 3570–3579 (2007)
10. Chen, Y., Li, Y., Kurosu, S., Meng, Q., Tang, N., Koizumi, Y., et al.: Analysis of in vitro wear behavior and contact mechanisms of metal-on-metal hip joint bearings with different radial clearances. Mater. Trans. (2015). https://doi.org/10.2320/matertrans.M2014440
11. de Castro Girão, D., Béreš, M., Jardini, A.L., Filho, R.M., Silva, C.C., de Siervo, A., et al.: An assessment of biomedical CoCrMo alloy fabricated by direct metal laser sintering technique for implant applications. Mater. Sci. Eng. C **107**, 110305 (2020)
12. Dawei, L., Lihai, C., Yuqiang, M., Yandong, W., Xinghua, W., Pengcheng, R., et al.: The improved strength and fracture mechanism of additive manufactured Ti–6Al–4V alloys compared with corresponding as-rolled alloys. J. Mater. Res. **39**, 891–902 (2024)
13. Naghavi, S.A., Tamaddon, M., Garcia-Souto, P., Moazen, M., Taylor, S., Hua, J., et al.: A novel hybrid design and modelling of a customised graded Ti–6Al–4V porous hip implant to reduce stress-shielding: an experimental and numerical analysis. Front. Bioeng. Biotechnol. (2023). https://doi.org/10.3389/fbioe.2023.1092361
14. Grützmacher, P.G., Profito, F.J., Rosenkranz, A.: Multi-scale surface texturing in tribology—current knowledge and future perspectives. Lubricants **7**(11), 95 (2019)
15. Marian, M., Almqvist, A., Rosenkranz, A., Fillon, M.: Numerical micro-texture optimization for lubricated contacts—a critical discussion. Friction **10**, 1772–1809 (2022)
16. Sagbas, B., Durakbasa, N.: Surface texturing of vitamin E blended UHMWPE for reduction of wear. Acta Phys. Pol. A **125**, 481–483 (2014)
17. Ito, H., Kaneda, K., Yuhta, T., Nishimura, I., Yasuda, K., Matsuno, T.: Reduction of polyethylene wear by concave dimples on the frictional surface in artificial hip joints. J. Arthroplasty **15**, 332–338 (2000)
18. Gachot, C., Rosenkranz, A., Hsu, S.M., Costa, H.L.: A critical assessment of surface texturing for friction and wear improvement. Wear **372–373**, 21–41 (2017)
19. Lu, X., Khonsari, M.M.: An experimental investigation of dimple effect on the Stribeck curve of journal bearings. Tribol. Lett. **27**, 169–176 (2007)
20. Kovalchenko, A., Ajayi, O., Erdemir, A., Fenske, G., Etsion, I.: The effect of laser texturing of steel surfaces and speed-load parameters on the transition of lubrication regime from boundary to hydrodynamic. Tribol. Trans. **47**, 299–307 (2004)
21. Shen, G., Fang, F., Kang, C.: Tribological performance of bio-implants: a comprehensive review. Nanotechnol. Precis. Eng. **1**, 107–122 (2018)
22. Wei, X., Li, W., Liang, B., Li, B., Zhang, J., Zhang, L., et al.: Surface modification of Co–Cr–Mo implant alloy by laser interference lithography. Tribol. Int. **97**, 212–217 (2016)
23. Pettersson, U., Jacobson, S.: Friction and wear properties of micro textured DLC coated surfaces in boundary lubricated sliding. Tribol. Lett. **17**, 553–559 (2004)
24. Nakano, M., Korenaga, A., Korenaga, A., Miyake, K., Murakami, T., Ando, Y., et al.: Applying micro-texture to cast iron surfaces to reduce the friction coefficient under lubricated conditions. Tribol. Lett. **28**, 131–137 (2007)

25. Odehnal, L., Ranuša, M., Vrbka, M., Křupka, I., Hartl, M.: Tribological behaviour of Ti6Al4V alloy: an application in small joint implants. Tribol. Lett. **71**, 125 (2023)
26. Nečas, D., Vrbka, M., Křupka, I., Hartl, M.: The effect of kinematic conditions and synovial fluid composition on the frictional behaviour of materials for artificial joints. Materials **11**(5), 767 (2018)
27. Wang, F.C., Brockett, C., Williams, S., Udofia, I., Fisher, J., Jin, Z.M.: Lubrication and friction prediction in metal-on-metal hip implants. Phys. Med. Biol. **53**, 1277 (2008)
28. Whitby, R.D.: Coefficient of friction in artificial joints. Tribol. Lubr. Technol. **74**, 84–84 (2018)
29. Milstrey, A., Domnick, C., Garcia, P., Raschke, M., Evers, J., Ochman, S.: Trends in arthrodeses and total joint replacements in foot and ankle surgery in Germany during the past decade—back to the fusion? Foot Ankle Surg. **27**(3), 301–304 (2020)
30. Brewster, M.: Does total joint replacement or arthrodesis of the first metatarsophalangeal joint yield better functional results? A systematic review of the literature. J. Foot Ankle Surg. **49**, 546–552 (2010)
31. Shereff, M.J., Bejjani, F.J., Kummer, F.J.: Kinematics of the first metatarsophalangeal joint. J. Bone Jt Surg. **68**(3), 392–398 (1986)
32. Zhang, Y., Awrejcewicz, J., Szymanowska, O., Shen, S., Zhao, X., Baker, J.S., et al.: Effects of severe hallux valgus on metatarsal stress and the metatarsophalangeal loading during balanced standing: a finite element analysis. Comput. Biol. Med. **97**, 1–7 (2018)
33. Morgan, O.J., Hillstrom, H.J., Bitar, R., Sturnick, D., Koff, M.F., Ellis, S.J., et al.: Finite element modeling of planus and rectus foot types for the study of first metatarsophalangeal and first metatarsocuneiform joint contact mechanics. J. Biomech. Eng. **144**(8), 081005 (2022)
34. Ranuša, M., Čípek, P., Vrbka, M., Paloušek, D., Křupka, I., Hartl, M.: Tribological behaviour of 3D printed materials for small joint implants: a pilot study. J. Mech. Behav. Biomed. Mater. **132**, 105274 (2022)
35. Wang, H., Zheng, J., Sun, X., Luo, Y.: Tribo-corrosion mechanisms and electromechanical behaviours for metal implants materials of CoCrMo, Ti6Al4V and Ti15Mo alloys. Biosurf. Biotribol. **8**, 44–51 (2022)
36. Pratap, T., Patra, K.: Tribological performances of symmetrically micro-textured Ti–6Al–4V alloy for hip joint. Int. J. Mech. Sci. **182**, 105736 (2020)
37. Cremer, L., Nortje, B.D., van der Merwe, J., Becker, T.H.: Wear of conventional UHMWPE articulating against additively manufactured Ti–6Al–4V and Co–Cr–Mo. Biotribology **33–34**, 100231 (2023)
38. Sullivan, S.J.L., Topoleski, L.D.T.: Surface modifications for improved wear performance in artificial joints: a review. JOM **67**, 2502–2517 (2015)
39. Niemczewska-Wójcik, M., Piekoszewski, W.: The surface texture and its influence on the tribological characteristics of a friction pair: metal–polymer. Arch. Civ. Mech. Eng. **17**, 344–353 (2017)
40. Allen, Q., Raeymaekers, B.: Surface texturing of prosthetic hip implant bearing surfaces: a review. J. Tribol. **143**, 040801 (2021)
41. Soltani-Kordshuli, F., Choudhury, D., Goss, J.A., Campbell, M., Smith, E., Sonntag, S., et al.: Cartilage-inspired surface textures for improved tribological performance of orthopedic implants. J. Mech. Behav. Biomed. Mater. **138**, 105572 (2023)
42. Long, R., Li, M., Jin, Z., Zhang, Y., Han, H.: Tribological behavior of pits textured multi-rollers sliding–rolling tribo-pair under periodic varied load and dry wear. Adv. Mech. Eng. **14**, 16878132221092520 (2022)
43. Arulkumar, M., Prashanna Rangan, R., Prem Ananth, M., Srividhyasakthi, V., Aaditya, R.: Experimental verification on the influence of surface texturing on biomaterials and study of its tribological characteristics. Mater. Today Proc. (2023). https://doi.org/10.1016/j.matpr.2023.01.172
44. Alvarez-Vera, M., Ortega-Saenz, J.A., Hernandez-Rodríguez, M.A.L.: A study of the wear performance in a hip simulator of a metal–metal Co–Cr alloy with different boron additions. Wear **301**, 175–181 (2013)
45. Vishnoi, M., Kumar, P., Murtaza, Q.: Surface texturing techniques to enhance tribological performance: a review. Surf. Interfaces **27**, 101463 (2021)
46. Yu, H., Deng, H., Huang, W., Wang, X.: The effect of dimple shapes on friction of parallel surfaces. Proc. Inst. Mech. Eng. J **225**, 693–703 (2011)
47. Allen, Q., Raeymaekers, B.: Surface texturing of prosthetic hip implant bearing surfaces: a review. J. Tribol. **143**(4), 040801 (2020)
48. Schneider, J., Braun, D., Greiner, C.: Laser textured surfaces for mixed lubrication: influence of aspect ratio, textured area and dimple arrangement. Lubricants **5**(3), 32 (2017)
49. Wang, X., Kato, K., Adachi, K., Aizawa, K.: The effect of laser texturing of SiC surface on the critical load for the transition of water lubrication mode from hydrodynamic to mixed. Tribol. Int. **34**, 703–711 (2001)
50. Qiu, M., Delic, A., Raeymaekers, B.: The effect of texture shape on the load-carrying capacity of gas-lubricated parallel slider bearings. Tribol. Lett. **48**, 315–327 (2012)
51. Li, K., Yao, Z., Hu, Y., Gu, W.: Friction and wear performance of laser peen textured surface under starved lubrication. Tribol. Int. **77**, 97–105 (2014)
52. Raeymaekers, B., Etsion, I., Talke, F.E.: A model for magnetic tape/guide friction reduction by laser surface texturing. Tribol. Lett. **28**, 9–17 (2007)
53. Zhang, H., Qin, L., Hua, M., Dong, G., Chin, K.-S.: A tribological study of the petaloid surface texturing for Co–Cr–Mo alloy artificial joints. Appl. Surf. Sci. **332**, 557–564 (2015)
54. Choudhury, D., Vrbka, M., Mamat, A.B., Stavness, I., Roy, C.K., Mootanah, R., et al.: The impact of surface and geometry on coefficient of friction of artificial hip joints. J. Mech. Behav. Biomed. Mater. **72**, 192–199 (2017)
55. Braun, D., Greiner, C., Schneider, J., Gumbsch, P.: Efficiency of laser surface texturing in the reduction of friction under mixed lubrication. Tribol. Int. **77**, 142–147 (2014)
56. Nečas, D., Usami, H., Niimi, T., Sawae, Y., Křupka, I., Hartl, M.: Running-in friction of hip joint replacements can be significantly reduced: the effect of surface-textured acetabular cup. Friction **8**, 1137–1152 (2020)
57. Alla, R.K., Ginjupalli, K., Upadhya, N., Shammas, M., Ravi, R.K., Sekhar, R.: Surface roughness of implants: a review. Trends Biomater. Artif. Organs **25**, 112–118 (2011)
58. Hashmi, A.W., Mali, H.S., Meena, A., Saxena, K.K., Ahmad, S., Agrawal, M.K., et al.: A comprehensive review on surface post-treatments for freeform surfaces of bio-implants. J. Mater. Res. Technol. **23**, 4866–4908 (2023)
59. Kalman, L., Kalman, B.: Preliminary assessment of dry electropolishing technology on a novel additive manufactured Ti–6Al–4V implant abutment. Jpn J. Res. **2**, 1–4 (2021)
60. Guiomar Riu, P., Joan Josep Roa, R.: Chapter 7: can the Dry-Lyte® technology polish 3D printed ceramic/metal samples and in particular WC-Co? In: Ashutosh, S. (ed.) Advances in 3D Printing. IntechOpen, London (2023)
61. Järvenpää, A., Kim, D.B., Mäntyjärvi, K.: Chapter 14: metal additive manufacturing. In: Khoshnaw, F. (ed.) Welding of Metallic Materials, pp. 493–536. Elsevier, Amsterdam (2023)
62. Nečas, D., Vrbka, M., Gallo, J., Křupka, I., Hartl, M.: On the observation of lubrication mechanisms within hip joint replacements. Part II: hard-on-hard bearing pairs. J. Mech. Behav. Biomed. Mater. **89**, 249–259 (2019)

63. Čípek, P., Rebenda, D., Nečas, D., Vrbka, M., Krupka, I., Hartl, M.: Visualization of lubrication film in model of synovial joint. Tribol. Ind. **41**, 387–393 (2019)
64. Čípek, P., Vrbka, M., Rebenda, D., Nečas, D., Křupka, I.: Biotribology of synovial cartilage: a new method for visualization of lubricating film and simultaneous measurement of the friction coefficient. Materials **13**, 2075 (2020)
65. Hartl, M., Krupka, I., Poliscuk, R., Liska, M., Molimard, J., Querry, M., et al.: Thin film colorimetric interferometry. Tribol. Trans. **44**, 270–276 (2001)
66. Galandakova, A., Ulrichova, J., Langova, K., Hanakova, A., Vrbka, M., Hartl, M., et al.: Characteristics of synovial fluid required for optimization of lubrication fluid for biotribological experiments. J. Biomed. Mater. Res. B **105**, 1422–1431 (2017)
67. Durrant, M., Durrant, L., McElroy, T.: Establishing a common instantaneous center of rotation for the metatarso-phalangeal and metatarso-sesamoid joints: a theoretical geometric model based on specific morphometrics. J. Orthop. Surg. Res. **14**, 107 (2019)
68. Myant, C., Underwood, R., Fan, J., Cann, P.M.: Lubrication of metal-on-metal hip joints: the effect of protein content and load on film formation and wear. J. Mech. Behav. Biomed. Mater. **6**, 30–40 (2012)
69. Myant, C.W., Cann, P.: The effect of transient conditions on synovial fluid protein aggregation lubrication. J. Mech. Behav. Biomed. Mater. **34**, 349–357 (2014)
70. ISO: ISO 7206–2 I: Implants for Surgery—Partial and Total Hip Joint Prostheses Part 2: Articulating Surfaces Made of Metallic, Ceramic and Plastics Materials, p. 5. ISO, Geneva (2011)
71. Cubillos, P.O., Dos Santos, V.O., Pizzolatti, A.L.A., Moré, A.D.O., Roesler, C.R.M.: Surface finish of total hip arthroplasty implants: are we evaluating and manufacturing them appropriately? J. Test. Eval. **49**, 4550–4559 (2021)
72. Prasad, N., Syed, I., Subbu, S.: Laser dimple texturing—applications, process, challenges, and recent developments: a review. Aust. J. Mech. Eng. **20**, 1–16 (2019)
73. Ţălu, Ş, Stach, S., Klaić, B., Čelebić, A.: evaluation of topographical Co–Cr–Mo alloy surface changes after various finishing treatments. Acta Stomatol. Croat. **53**, 264–273 (2019)
74. Celebic, A., Svetlicic, V., Malina, J., Klaic, B.: Co–Cr–Mo alloy surface features and composition prior and after mechanical polishing and corrosion in fluids simulating oral conditions. In: Biomaterials Developments and Applications, pp. 415–433. Nova Science Publishers, Hauppauge (2009).
75. Zhang, Y., Li, J., Che, S., Tian, Y.: Electrochemical polishing of additively manufactured Ti–6Al–4V Alloy. Met. Mater. Int. **26**, 783–792 (2020)
76. Odehnal, L., Ranuša, M., Wimmer, M.A., Vrbka, M., Křupka, I.: Development of lubrication film and influence on friction in a total knee replacement during a gait cycle. Tribol. Int. **178**, 108073 (2023)
77. Talha, M., Ma, Y., Kumar, P., Lin, Y., Singh, A.: Role of protein adsorption in the bio corrosion of metallic implants—a review. Colloids Surf. B **176**, 494–506 (2019)
78. Ghosh, S., Choudhury, D., Das, N.S., Pingguan-Murphy, B.: Tribological role of synovial fluid compositions on artificial joints—a systematic review of the last 10 years. Lubr. Sci. **26**, 387–410 (2014)
79. Woźniak, A., Bialas, O., Adamiak, M., Hadzima, B., Szewczenko, J.: The influence of laser texturing on the tribological behavior of titanium alloy Ti6Al4V in medical applications. Arch. Civ. Mech. Eng. **24**, 146 (2024)
80. Sonekar, M.M., Rathod, W.S.: An experimental investigation on tribological behavior of bio-implant material (SS-316 l and Ti6Al4V) for orthopaedic applications. Mater. Today Proc. **19**, 444–447 (2019)
81. Lin, N., Li, D., Zou, J., Xie, R., Wang, Z., Tang, B.: Surface texture-based surface treatments on Ti6Al4V titanium alloys for tribological and biological applications: a mini review. Materials **11**(4), 487 (2018)
82. Pratap, T., Patra, K.: Mechanical micro-texturing of Ti–6Al–4V surfaces for improved wettability and bio-tribological performances. Surf. Coat. Technol. **349**, 71–81 (2018)
83. Choudhury, D., Ghosh, S., Ali, F., Vrbka, M., Hartl, M., Krupka, I.: The influence of surface modification on friction and lubrication mechanism under a bovine serum lubricated condition. Tribol. Trans. (2015). https://doi.org/10.1080/10402004.2015.1077409
84. Yang, D., Sun, H., Ji, G., Xiang, Y., Wang, J.: Effect of electrolytic plasma polishing on surface properties of titanium alloy. Coatings **14**(5), 615 (2024)
85. Inogamov, N.A., Zhakhovsky, V.V., Ilnitsky, D.K., Khokhlov, V.A.: Laser shock peening. J. Phys. Conf. Ser. **1787**, 012024 (2021)

Tribology International 211 (2025) 110832

Contents lists available at ScienceDirect

Tribology International

journal homepage: www.elsevier.com/locate/triboint

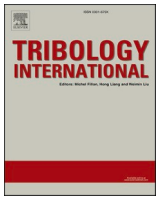

Tribological behaviour of additively manufactured Ti6Al4V with controlled surface structure: An application in small joint implants

Lukáš Odehnal [a,*], Matúš Ranuša [a], Martin Malý [b], Ivan Křupka [a], Daniel Koutný [b], Martin Hartl [a], Martin Vrbka [a]

[a] Department of Tribology, Faculty of Mechanical Engineering, Brno University of Technology, Technická 2896/2, Brno 616 69, Czech Republic
[b] Department of Reverse Engineering and Additive Technologies, Faculty of Mechanical Engineering, Brno University of Technology, Technická 2896/2, Brno 616 69, Czech Republic

ARTICLE INFO

Keywords:
3D printing of Ti6Al4V for joint implants
Lubrication mechanism
Albumin
Friction

ABSTRACT

This study conducts a tribological analysis of Ti6Al4V samples with and without surface structures, manufactured by 3D printing, to assess their suitability as friction pairs in joint replacements. The behaviour was analysed using a pin-on-plate tribometer under conditions simulating those typically observed in vivo, with a glass counterpart enabling optical observation. The grid structure outperformed other samples: while exhibiting comparable friction to a homogeneous surface, it was the only one capable of retaining albumin in the contact area and restoring the lubrication film after unloading. However, findings suggest further refinements are needed before the structure can be considered for application. Preliminary results indicate a need for greater proximity and regularity in structures to enhance performance.

1. Introduction

In the contemporary world, where individuals are striving to maintain an active lifestyle even at an advanced age, and where there are numerous cases of injury, the research and development of joint replacements represents an indispensable component of healthcare. Further advances may be made in the design of new types of joint replacement or the search for more suitable friction surfaces. The number of joint replacements performed is increasing annually. The observed trend between 2012 and 2023 reveals a sharp rise in the early years, followed by a stabilization of growth at approximately 15 % per year in recent years for hip and knee joints, according to the Annual Report 2024 from the American Joint Replacement Registry [1]. Nevertheless, the current generation of implants is not yet optimally developed for certain joints, necessitating early revision, which is highly undesirable. One joint where the utilisation of joint implants is less prevalent than that of the second possible intervention (arthrodesis) is the first metatarsophalangeal (1. MTP) joint of the big toe [2] with a decrease of 48 % for replacements and an increase of 76.9 % for arthrodesis between 2008 and 2017. This is primarily due to the limited lifespan of these implants, which is attributed to high rates of osteolysis, subsidence, and implant failure, necessitating revision surgery. It is important to highlight that the revision rate for this particular joint is relatively high. Titchener et al. [3] observed a revision rate of 24 %, with revisions occurring at a mean of 33 months following the initial surgery. Similarly, Barták et al. [4] reported complications in 37 % of cases, which necessitated revision surgery. The average time between the primary procedure and revision was 5.5 years, with a range of 4–7 years.

Currently, three predominant metallic biomaterials are utilized [5,6] in orthopaedic applications: stainless steel (most commonly SS 316 L), cobalt-based alloys (most commonly CoCr30Mo6), and titanium alloys (most commonly Ti6Al4V). When selecting a material for joint replacement, it is essential to consider its similarity to cortical bone in terms of mechanical properties. One key parameter in this regard is Young's modulus, which typically ranges between 10–30 GPa for cortical bone. Comparing the values of common implant materials, SS 316 L exhibits a modulus of approximately 200 GPa, CoCr30Mo6 reaches 240 GPa, and Ti6Al4V has a modulus of around 110 GPa. Although none of these materials perfectly match the mechanical properties of bone, titanium alloys exhibit the closest alignment. Nevertheless, the considerable disparity in elastic modulus may result in stress shielding [5], leading to bone resorption (osteolysis) and potentially result in implant loosening due to poor adhesion to the bone. Additionally, it includes vanadium (V) and aluminum (Al), which are known for their potential toxicity [5] and may

* Corresponding author.
E-mail address: Lukas.Odehnal@vut.cz (L. Odehnal).

https://doi.org/10.1016/j.triboint.2025.110832
Received 7 November 2024; Received in revised form 30 April 2025; Accepted 26 May 2025
Available online 27 May 2025

pose risks during long-term implantation. To mitigate these effects, alternative titanium alloys [7–11], such as Ti–Nb–Zr–Ta–Si, Ti-15Zr-4Nb–4Ta, Ti–Nb–Zr–Ta–Si–Fe, Ti-24Nb-4Zr-8Sn, Ti-Nb-Ga are being explored to optimize osseointegration while reducing stress shielding and adverse biological responses.

In terms of design, various solutions have historically been used for 1. MTP joint [12], including silastic double-stemmed flexible hinges, metallic hemiarthroplasties, and metal-on-polyethylene (MoP) total toe implants. Recently, experiments have also begun with alternative materials [13], such as gelfoam, synthetic artificial cartilage, and pyrocarbon. For example, pyrocarbon exhibits significantly lower wear compared to CoCr discs when tested with UHMWPE pins [14], which is attributed to higher adherence of phospholipids on the pyrocarbon surface and less UHMWPE attachment. This property suggests that pyrocarbon reduces adhesive wear. These days, typically the MoP configuration is used, while the metallic material most commonly utilised for the friction pair is CoCr30Mo6 alloy. However, in other components of the implant, Ti6Al4V alloy is often used to secure it to the bone [15,16] due to its material properties, which are more similar to those of human bone, thus facilitating the desired osteointegration [17]. In recent years, 3D printing has emerged as a prominent technology across all fields of manufacturing. This trend is also evident in the field of joint replacements [18,19], where the most commonly utilised material is the aforementioned Ti6Al4V alloy [20]. In the context of 3D metal printing, a number of possible methods have been identified [20], including laser powder bed fusion (L-PBF) and electron beam melting (EBM). L-PBF technologies, such as DMLS and SLM [5], enable the production of intricate and precise structures that are challenging to achieve with traditional manufacturing methods. These techniques facilitate the creation of implants with optimized shapes, including lightweight, porous, or lattice designs, which better align with the mechanical characteristics of bone and promote better integration with the surrounding tissue. Additionally, implants manufactured through L-PBF can reach material densities as high as 99 %, ensuring strong and durable components with excellent quality. Among benefits, such as individualisation and simplification of implants, other benefit of additive manufacturing is demonstrated in several studies [21,22] which indicate that the wear can be notably reduced through the use of additive manufacturing in comparison to conventional casting methods. In terms of research on Ti6Al4V alloy as a friction pair for implants, the current literature remains limited. Some studies have addressed the corrosion behaviour of this alloy—for instance, Fischer et al. [23] reported that, compared to conventionally manufactured Ti6Al4V, SLM-Ti6Al4V exhibits distinct electrochemical behaviour due to its unique surface oxide layer and microstructure, influencing corrosion resistance and protein adsorption. Similarly, Patel et al. [24] concluded that CoCr30Mo6 is more susceptible to degradation under combined mechanical and corrosive conditions, whereas Ti6Al4V offers greater durability for load-bearing orthopaedic implants.

The lubrication mechanism of joint replacements is a highly complex problem, as the joints are lubricated by synovial fluid (bovine calf serum in certain laboratory experiments), which is a highly complex non-Newtonian fluid [25] and also contains proteins that may behave differently under certain conditions [26]. Several studies have explored the behaviour of synovial fluid and the role of its components in joint lubrication. Myant et al. [27] demonstrated that the contact collects proteins to form a protein-gel phase with higher viscosity, resulting in a thicker film than predicted by classical elasto-hydrodynamic (EHD) lubrication theory, with behaviour influenced by contact conditions and lubricant properties, and later proposed a novel lubrication mechanism [28], named Protein Aggregation Lubrication (PAL), which is applicable to contact pairs lubricated by synovial fluid or any kind of lubricant containing proteins. This mechanism is based on the formation of a high-viscosity reservoir in the inlet zone. The reservoir is principally the consequence of shear aggregation of protein molecules within the inlet flow field. Subsequently, Lu et al. [29] validated computational lubrication models for hip replacements by comparing numerical predictions and experimental measurements of film thickness in a CoCr-on-glass hip bearing. While the model accurately predicted film thickness for low-viscosity mineral oil, it failed for bovine serum due to limitations in the viscosity model. Authors then proposed a new effective viscosity equation to improve predictions for protein-containing lubricants under transient conditions. Later, the lubrication mechanism was also described using an analytical model by Nissim et al. [30], which demonstrated that the mechanism can be modelled using classical EHD lubrication theory, supplemented by a protein concentration-dependent constitutive equation for fluid viscosity. It has been demonstrated that certain dependencies exist with regard to the behaviour of synovial fluid. It is evident that proteins form specific layers that facilitate an overall lubrication mechanism [31,32]. Nečas et al. [31] proposed a model in which γ-globulin strongly adsorbs onto surfaces, creating a boundary lubricating layer. This layer is further stabilized by hyaluronic acid (HA) and phospholipids, which enhance its strength and stability. Additionally, albumin contributes to improved lubrication by forming additional layers. In a similar vein, Tan et al. [33] introduced a dual-layered lubrication mechanism for artificial joints, comprising an adsorbed boundary layer and a liquid film. Their model shows that bovine serum γ-globulin BSG forms stronger adsorption layers than bovine serum albumin (BSA), highlighting its greater importance in joint lubrication and also showed the importance of HA in terms of protein aggregation as the formation of HA-protein chains helps preserve protein conformation, leading to a significant reduction in friction and wear. In protein-based lubricants [34], the friction coefficient increases due to protein adsorption and denaturation, with friction rising as sliding speed increases. Phospholipids contribute to higher friction between CoCr30Mo6 alloy and UHMWPE by diffusing into polyethylene, causing plasticization and a time-dependent increase in friction. On the other hand, the presence of HA reduces friction by increasing lubricant viscosity and forming a fluid film. Moreover, Murali et al. [35] showed that phospholipid liposomes can significantly enhance friction and wear performance by forming a protective multi-layered film on contact surfaces, stabilized through electrostatic interactions, thereby creating an effective lubricating layer.

The application of surface texturing has been demonstrated across a wide range of machine components. This includes the field of human joint replacements, where it has been proved that textures can perform four potential functions. These functions are as follows: acting as reservoirs for lubricant, providing space for the accumulation of debris generated by wear, functioning as micro-hydrodynamic bearings, and reducing the nominal contact area [36]. These effects collectively contribute to a reduction in the overall wear rate, which represents a primary objective in the field of joint replacements, as the ability of the prosthesis to last as long as possible in the patient's body is the main goal. A variety of shapes, depths and layouts [36,37] were evaluated in terms of their suitability for use. It has been demonstrated that the utilisation of textures in the contact area may serve to increase the coefficient of friction (CoF). Nevertheless, Shen et al. [38] showed that surface texturing improves tribological performance by reducing friction and preventing surface wear. The even distribution of texturing patterns proves to be most effective for artificial joints, and demonstrating that optimal surface roughness combined with surface texturing can improve tribological performance, and the results of the long-term testing indicate that there is a positive effect on durability, as it was demonstrated that the microstructures are capable of trapping hard wear particles [39], which do not further contribute to secondary wear. Surface texturing of joint implants showed positive behaviour in the context of reversal sliding motion [40], which is characteristic of human movement during typical walking activities, by quick decrease in coefficient of friction. Shen et al. [39] showed that textures with sharp corners are not the optimal choice for human joint implants, as it leads to interlocking phenomenon. The authors subsequently assigned a ranking to the texture parameters, identifying the following as the most

influential: area density, size, geometry, depth and distribution mode. The existing literature on the subject of dimple-shaped textures is replete with discussion of their behaviour, which can be characterised as affecting the pressure distribution in the contact area and changing the thickness of the lubricating film at the dimple interface [41]. An increase in thickness was observed at the rear end, while conversely a decrease in thickness was noted at the sides and front in direction of passing through the contact area. Liu et al. [42] studied the effect of textures with different cross-sections on Ti6Al4V alloy and demonstrated their suitability for interaction with gelatin microgel particles. All types of textures showed a reduction in the coefficient of friction compared to the non-textured surface. From the perspective of short-term tests, the study by Ranuša et al. [43] showed a positive influence on the lubricant film thickness through texturing, while also minimizing the possible abrasive wear of surfaces. Wang et al. [44] demonstrated the potential of using an additively manufactured Ti6Al4V alloy, which was textured using a laser, and then applied a self-lubricating coating based on Ti-TiN/PTFE to the resulting dents. The tested pair exhibited a consistently low friction coefficient of 0.12 and showed almost no weight loss. The tribological performance is attributed to the formation of a durable lubricant film, which is continuously replenished by the release of PTFE, aided by the capture of abrasive particles.

This paper builds upon our previous research [45], which demonstrated that the behaviour of the Ti6Al4V alloy is not entirely optimal. Nevertheless, the material can be used in the manufacture of small joint replacements, provided that the surface of the specimen undergoes some form of modification. The decision was taken to employ 3D printing technology to create structures on the sample surface for the purposes of this research, with the objective of answering the following question: *"What is the effect of a controlled surface structure on the tribological behaviour of the friction surface of an additively manufactured Ti6Al4V alloy?"* To address this question, the research focused on the description of outcome variables, such as lubrication film thickness, fluorescence intensity (the local concentration and distribution of protein albumin in the contact area), coefficient of friction, and wear scars after the experiments. the development of protein albumin contained in the model synovial fluid during the experiment in the contact area, as well as the analysis of friction and the analysis of the wear scar after the experiments. These variables were analysed for both the textured and non-textured surfaces to evaluate differences in their tribological performance.

2. Materials and methods

The study involved experiments on a tribometer (schematically depicted in Fig. 1) with a pin-on-plate configuration that allowed reciprocal motion [32,45,46]. Moreover, the simulator employed permits the simultaneous measurement of the coefficient of friction and observation of the contact area due to its construction.

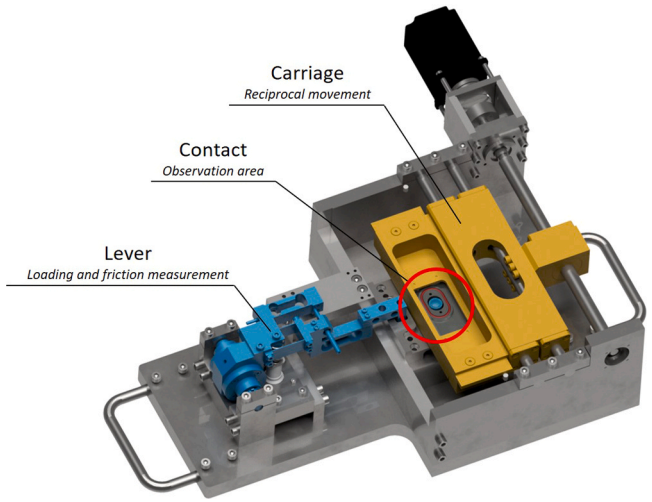

Fig. 1. Tribometer with pin-on-plate configuration.

The experiments were primarily designed to describe the thickness of the lubrication film and its development. Two optical observation methods were employed, as illustrated in Fig. 2. The primary methodology employed was colorimetric interferometry [47], which was augmented by fluorescent microscopy [48] in order to gain insight into the behaviour of protein albumin within the contact area.

2.1. Contact pair and lubricant

The experimental contact pair consisted of pins manufactured from the Ti6Al4V alloy and the B270 glass from the supplier L.E.T. optomechanika Praha, spol. s r.o. with the surface roughness of ~6 nm, a Young's modulus of 71 MPa, and a Poisson's ration of 0.22. The glass component was a necessary for enabling observation of the contact area using optical methods. Furthermore, the glass employed in experiments conducted with the use of colorimetric interferometry was coated with chromium (reflectivity of 25 %) and an anti-reflective layer on the other side produced by CRYTUR, spol. s r.o., thereby enhancing its functionality and resulting in higher surface roughness of ~13 nm. The pins were manufactured using Laser Powder Bed Fusion (L-PBF) technology from Ti6Al4V Grade 23 powder, which meets the ASTM F3001 specification. The SLM 280 HL 3D printer from Nikon SLM Solutions AG was used, which is equipped with a near-infrared ytterbium fibre laser with a maximum power of 700 W and a beam diameter of 82 μm, exhibiting a Gaussian power distribution. The L-PBF samples were fabricated with a layer thickness of 30 μm and under an inert gas (argon) with a maximum oxygen concentration of 0.05 %. In total, three variants of the pin were produced, each with a diameter of 9.8 mm and height of 12 mm. The first variant was produced with a homogeneous surface, whereas the second and third variants were manufactured with a surface structure designed to simulate texturing, created directly during the 3D printing process. The second and third types of pins had a structure based on the meander printing strategy with a rotation of either 0° or 90° in each layer, respectively (see Fig. 3). The process parameters for the creation of the structures were set as follows: hatch distance 0.179 mm, laser power 100 W, and laser speed 450 mm/s. The surface structure was created at a height of 2 mm. In order to conduct the comparable experiments, the surface of each pin (homogenous, grid-structured, line-structured) was ground and polished to a curvature radius of 100 mm and surface roughness (with masked structures) of $Ra = 60 \pm 10$ nm. The samples were not subjected to a heat treatment process as Khun [49] showed that such a process does not significantly impact the wear rate of the 3D printed Ti6Al4V, on the contrary, deterioration may occur at elevated temperatures.

The contact pair was flooded with a model synovial fluid that had been prepared synthetically and which corresponded in composition to the synovial fluid extracted from patients who had undergone arthroplasty [50]. The composition of the model synovial fluid is as follows: albumin (26.3 mg/ml), γ-globulin (8.2 mg/ml), hyaluronic acid (0.82 mg/ml), and phospholipids (0.35 mg/ml), which were diluted in phosphate-buffered saline (PBS). Given the potential for fluorescence microscopy, it was essential to stain the protein albumin with fluorescent markers. The staining of albumin was achieved through the use of fluorescein-5-isothiocyanate (FITC). The exclusive observation of albumin was chosen based on a previous study by Nečas et al. [31], which demonstrated that albumin plays a key role in the formation of the lubrication film. This finding was further supported by the fact that the behaviour of the complex solution (containing albumin, γ-globulin, and HA) closely resembled that of the solution with albumin alone.

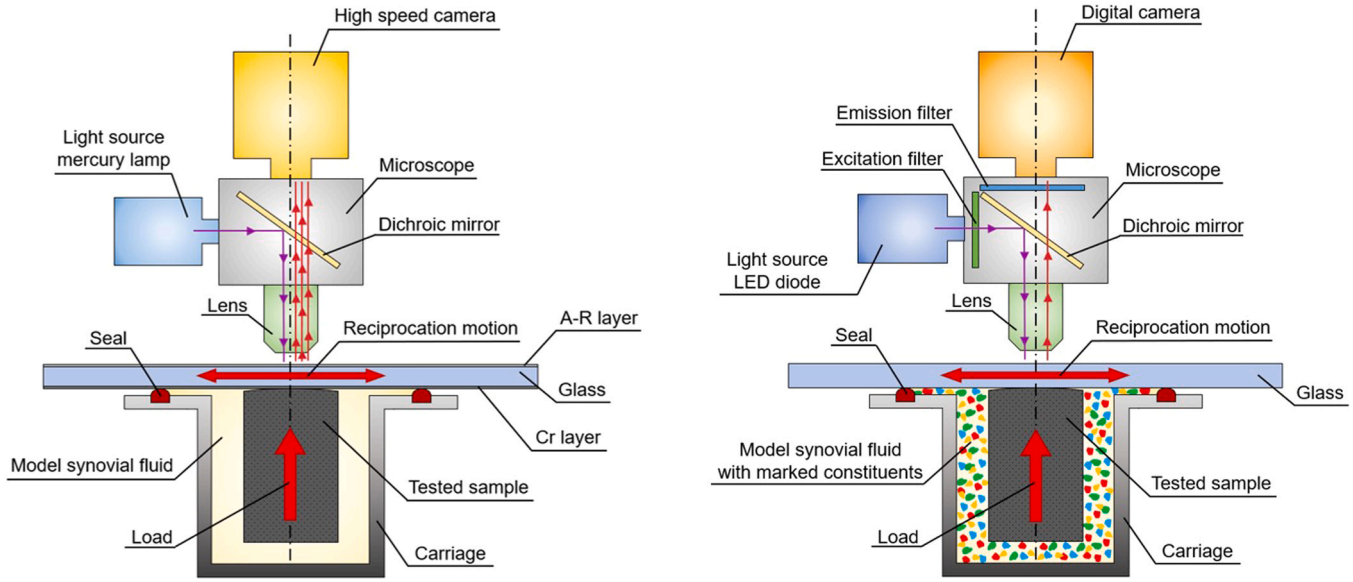

Fig. 2. Schemes of optical methods: Colorimetric interferometry (left) and Fluorescent microscopy (right).

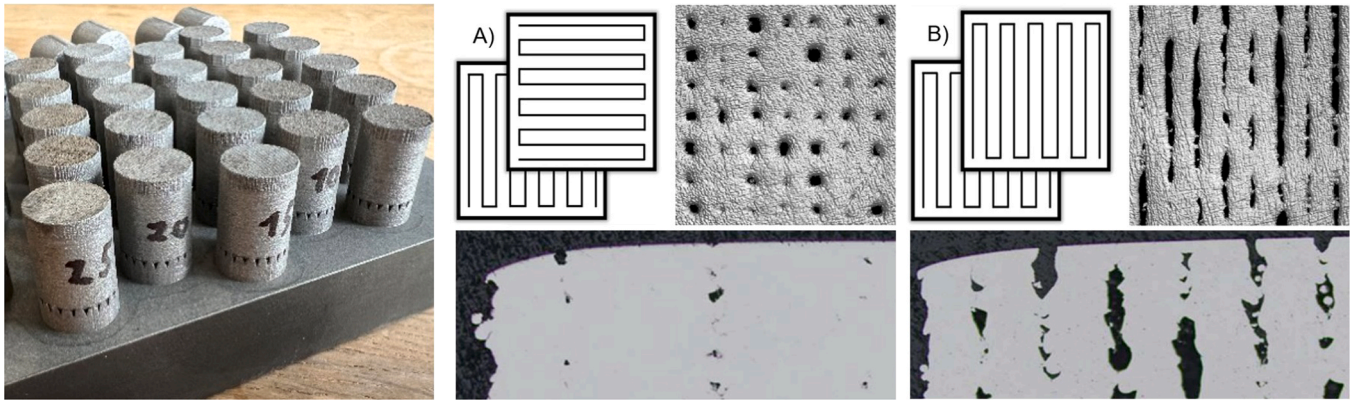

Fig. 3. The surface structure of tested pins and schematic representation of the printing strategy.

2.2. Experimental design and evaluation of the results

The experiments were designed to simulate, to some extent, the behaviour of a small human joint, namely the metatarsophalangeal joint of the big toe (1. MTP). In the absence of ISO standards defining the loading and kinematic conditions in this joint, information from available studies were used. The movement of this joint in a healthy condition was described by Durrant et al. [51], while Allan et al. [52] provided additional information on the kinematics of the joint in the sagittal plane. In addition, Al-Munajjed et al. [53] described another important parameter, namely the contact pressure generated in the 1. MTP joint. Based on these findings, the experimental conditions for reciprocal movement were selected as shown in Table 1, corresponding to the analysis we conducted in the preliminary study [45]. Due to a certain randomness in the dents on the tested samples, a uniform loading force was applied across all tests. However, this results in variations in the actual contact pressure among individual samples, as the size of the contact area is influenced by the dents. The reference contact pressure was calculated based on contact Hertz theory for the sample with a homogeneous surface in contact with glass, which is 35.1 MPa. The entire experiment consisted of a total of 60 cycles. Subsequently, following every 20 cycles, the contact pair was relieved (simulating joint unloading), which lasted for five minutes. The aforementioned interval was also used for the storage of the acquired image records during the measurements.

Table 1
Experimental conditions.

Normal load	Stroke	Speed	Frequency	Number of cycles
1 N	20 mm	20 mm/s	0.5 Hz	60*

* Each experiment included an interruption after each 20 cycles to simulate joint unloading.

A subsequent challenge that had to be addressed in the experimental design was the orientation of the structures during measurement. Based on the potential for comparison of the resulting data, the orientations were selected as follows: samples with line structures were tested so that the resulting dents (lines) were parallel to the direction of motion. This approach was selected in preference to testing lines perpendicular to the motion, as previous studies had not identified any benefit in doing so, due to the disruption of the lubricating film or even a complete collapse [54] that can be caused by outflow of the lubricant on sides of the groove. In accordance with the aforementioned selection of the line structure, the grid structure was also subjected to a corresponding rule, whereby the axis of the dents was consistently determined and aligned with the orientation of the movement (see Fig. 4).

The evaluation of the experiments was based on the methodology presented in the preliminary study [45]. The experiments were

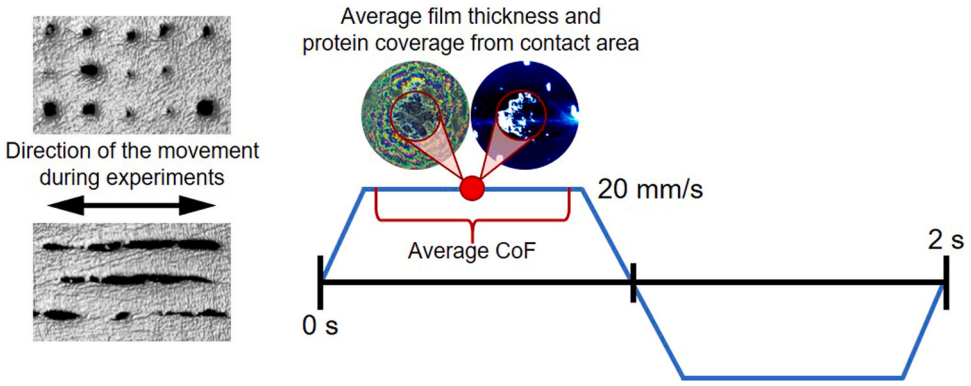

Fig. 4. Experimental design – orientation of samples during experiments (left); Scheme of the experimental evaluation principle (right).

evaluated in a single direction of motion, with the friction coefficient obtained from the mean of the filtered values from the entire area (the dead ends of the cycle were not considered in the evaluation). With regard to the evaluation of the lubrication film thickness and subsequent experiments conducted using fluorescence microscopy, the midpoint of the aforementioned one-way motion was identified as the optimal point for analysis as it is not affected by dead ends and the lubrication film is stable. The resulting values were subsequently plotted in the graphs presented in the Results and Discussion sections. The evaluation principle is illustrated in Fig. 4. In order to evaluate the results of the optical observations, custom software [47,55] were employed to obtain precise data regarding the thickness of the lubricating film and the concentration of albumin protein in the contact area.

3. Results

To ensure sufficient repeatability for each tested sample, all experiments from which the final graphs for friction and lubrication film thickness are shown were repeated three times. In all graphs, individual samples are distinguished by colour. The colour grey is used to indicate a pin with a homogeneous surface, blue for a pin with a grid structure and red for a pin with a line structure. Furthermore, the vertical dashed line represents the load relief phase, as described in the Materials and Methods section.

With regard to the friction coefficient, it can be observed that the value increased from the beginning of the experiment, but subsequently reached a similar value of approximately 0.43 for the homogeneous surface and grid structure. In contrast, the stabilisation for the line structure occurred at a value of approximately 0.48. The frictional behaviour of all samples is illustrated in Fig. 5. The most notable distinction was observed in the second phase of the experiment for the grid structure (20–40 cycles), where a considerable decline in the friction coefficient was evident after the unloading phase. Following a few cycles, the coefficient of friction approached the values of the sample with a homogeneous surface and followed a similar development and stabilisation trajectory. The experiments with the line structure exhibited the least visible discrepancies across the repeatability tests, indicating that this structure may offer the most stable contact pair behaviour. However, the coefficient of friction was the highest among the other samples.

The results obtained from the observation of the lubrication film thickness using colorimetric interferometry demonstrated that the lubrication film was disrupted for all samples at a specific stage of the experiment, typically prior to the end of the initial phase. This finding indicates that the incorporation of this phase did not negatively impact the formation of the lubrication film at the first sight as the disruption

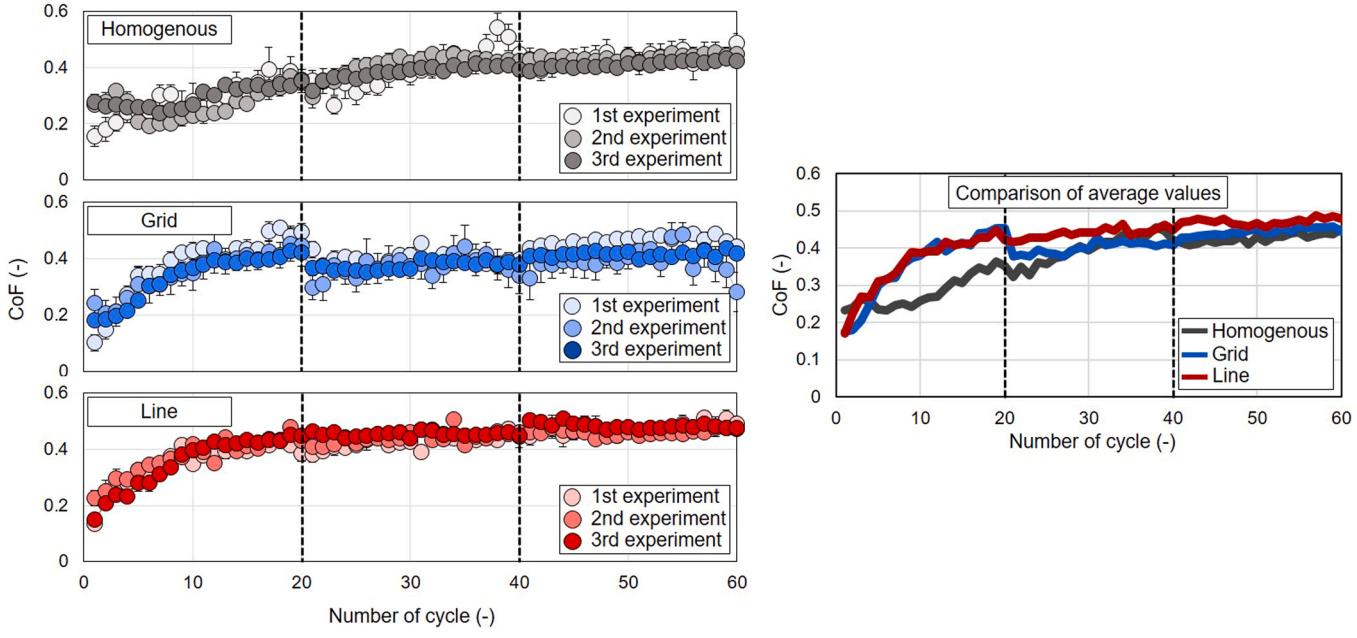

Fig. 5. CoF for individual samples with shown repeatability (left); comparison of the average values (right).

occurred even before this phase. This resulted in the friction pairs coming into contact with one another, thereby eliminating the possibility of separating them with the lubrication layer and, consequently, reducing the wear of contact pairs. The observation indicated that the implemented unloading phase affected the behaviour of the samples comprising the grid structure, but not those of the other samples. The samples with a grid structure exhibited an increase in the lubrication film between the initial and second phases of the experiment, resulting in the restoration of the lubrication film and the desired separation of the friction pairs. However, the lubrication film once again failed after a few cycles. The second unloading phase had no further effect on the behaviour of the lubrication film thickness. A comparison of the average values of the film thicknesses revealed comparable trends for samples with a grid structure and a homogeneous surface, which aligned with the results of friction. In contrast, samples with a line structure exhibited a notable reduction in film thickness. However, the observed differences in the average lubrication film thicknesses should be interpreted with caution, as they varied to some extent across repeatability.

To reinforce the insights gained from the friction and lubrication film thickness analyses, fluorescence microscopy was employed to examine the stained protein albumin and its behaviour within the contact region of the tested samples (see Fig. 7). Highly overexposed spots (structure dents), where the protein concentration is clearly higher due to trapping, were excluded from the evaluation using a threshold to avoid potential bias in the results. In terms of protein concentration in the contact area, the grid-structured samples exhibited the most favourable results, followed by the homogeneous samples, and the lowest concentration was observed in the line-structured samples. With regard to the grid structure, the most notable impact was observed after the unloading phase, where the protein concentration took several cycles to return to the anticipated level, therefore contributing to the load-carrying capacity of the lubrication film, and delaying direct contact between the friction bodies. In the case of the homogeneous surface, this occurred within two to three cycles. In contrast, no protein increase was observed in the contact area after unloading phase for the line structure.

Moreover, the static loaded images of the contact area before and after each phase of the experiment were compared within the fluorescence microscopy to evaluate the behaviour of the protein albumin and its capability to maintain within the contact area. It can be observed that the initial phase represents an outlier, as during this stage of the experiment, there was an increase in albumin concentration within the contact region for the homogeneous surface and grid structure, thereby forming some kind of layer. Whereas there was a decrease for the line structure. A comparison of the subsequent phases reveals a similarity in the pattern of the waveforms, with a consistent decline in concentration throughout the experimental period, when the albumin concentration stabilizes at the end of the experiment at a similar value to that established at the end of the first phase.

The images produced by the profilometer following the experiments indicate that the wear of contact bodies was not extensive. As the experiments were conducted only over a limited period (60 cycles), only the wear scars were analysed, as the wear rate would not have provided sufficient insight. It is notable that the samples exhibited certain differences. The sample with a homogenous surface exhibited the visually most pronounced change from the stage before the experiment. This sample also exhibited the occurrence of grooves, which were accompanied by areas where the material was observed to be pushed upwards during the course of the experiment. Only slight deformation at the middle of the contact area was observed for the line structure, while virtually no wear was observed for the grid structure. Furthermore, the images demonstrate that the created structures exhibit sunken edges, which eliminates the possibility of any negative influence on the behaviour observed during the experiments.

4. Discussion

4.1. General discussion

The objective of the presented study was to provide a detailed description of the tribological behaviour observed in three distinct specimens, all of which were manufactured using 3D printing technology from a Ti6Al4V alloy. Measurements and observations included: the friction coefficient, lubrication film thickness (colorimetric interferometry), development of protein ablumin in synovial fluid (fluorescence microscopy), and wear scars. The first sample was produced with a homogeneous surface. The second and third samples were created with a surface structure produced directly by 3D printing, with the resulting structures being of a grid and line-based configuration in accordance with the method of production. The experiments were conducted on the tribometer with a pin-on-plate configuration utilising a reciprocal movement using a synthetically prepared model synovial fluid as a lubricant. The kinematic and loading conditions were set in accordance with those employed in our preliminary study [45], which were as follows: a normal load of 1 N, a stroke of 20 mm, a speed of 20 mm/s, and 60 cycles with an interruption after each 20 cycles to simulate the joint unloading.

The results for the friction coefficient exhibited a comparable trend across all tested samples, which could be characterized by a gradual initial increase and subsequent stabilization at a value around which it fluctuated. However, a notable difference was observed in the case of the grid structure, where a partial decline in the coefficient of friction was evident following the initial phase of the experiment, with a reduction from approximately 0.43 to approximately 0.38. The reduction in the coefficient of friction at the beginning of the second experimental phase was presumably associated with an increase in the thickness of the lubrication film and a momentary separation of the friction pairs (see Fig. 6), which occurred following the unloading and reloading between the first and second experimental phases. This phenomenon was not observed in the other samples and could not be attributed to measurement error, as the similar trend was consistent across different samples with the grid structure during the repeatability testing. A number of studies have demonstrated a certain reduction in the coefficient of friction [56,57] following surface texturing. However, this dependence was not observed in the results of the present study, which may be attributed to a number of factors, including the application of different loads, relative velocities and contact materials. This was also demonstrated by Lee [58], who investigated the metal-on-metal contact pair. Following the application of textures, an increase in the friction coefficient was observed.

The results obtained from the colorimetric interferometry (see . 6) demonstrate that the lubrication film was disrupted, resulting in direct contact between the friction pairs. The images obtained did not reveal the formation of the PAL (a typical cluster of proteins in the inlet zone of the contact), as described by Myant et al. [28], even though a sufficiently thick lubricating film was present during the first few cycles. This can be mainly attributed to the different experimental conditions applied, primarily the lower sliding speeds used in our experiments. The most developed model of contact behaviour with synovial fluid, or more specifically with a lubricant containing proteins, was presented by Nissim et al. [30]. However, the conclusions of this study cannot be directly applied to the model used here, which operates under specific kinematic and loading conditions, including protein concentrations that differ from those used in our study. Nevertheless, the results of this study clearly show that the behaviour of the lubrication film does not align with classical EHD theory, and it is thus evident that lubrication with this type of SF depends on additional variables that the basic model does not reflect. In terms of lubrication film formation, differences can be observed compared to the homogeneous pin, such as the ability to restore the film after the completion of one experimental stage. Ranuša et al. [43] also presented a positive effect of dents, which were created

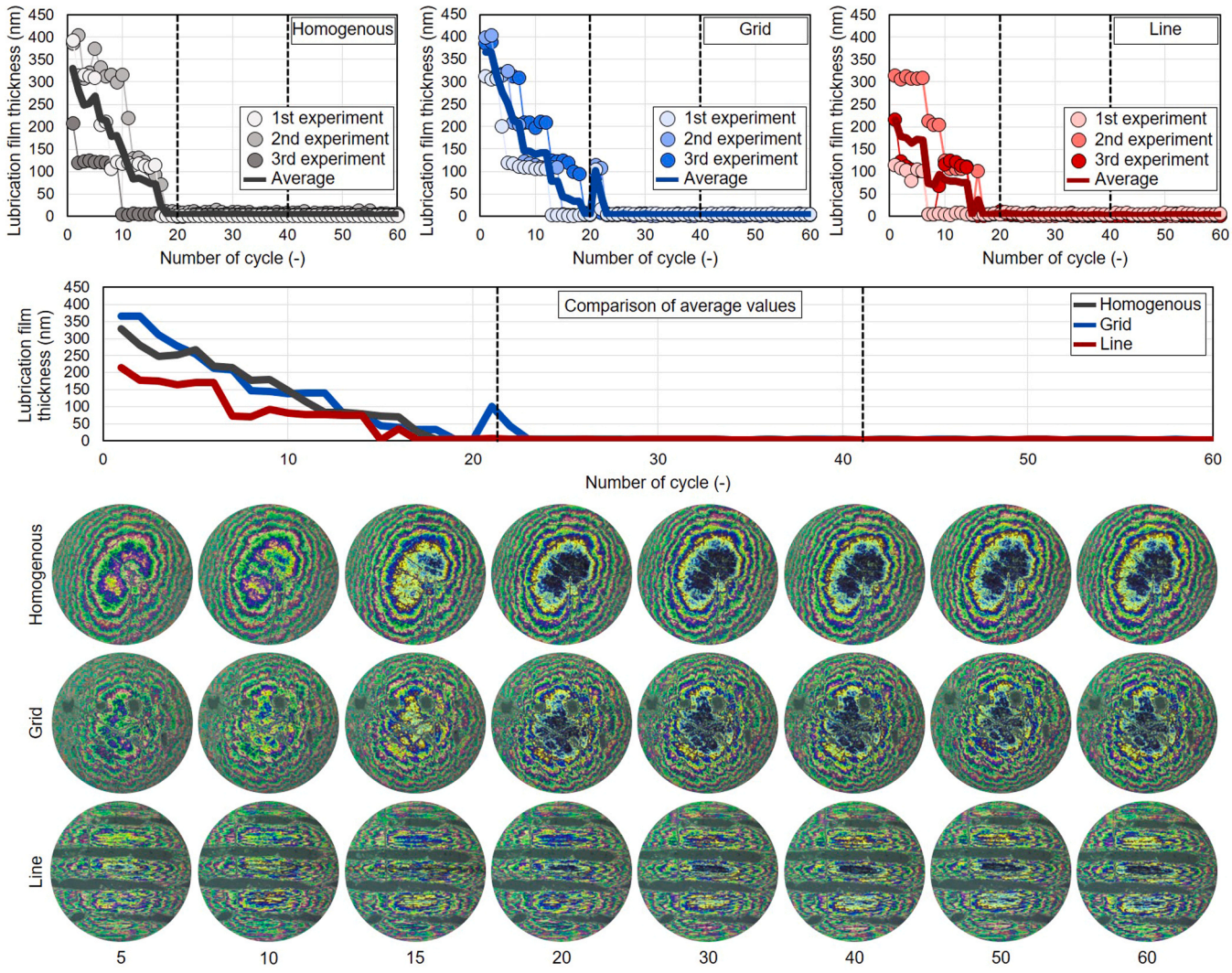

Fig. 6. Evolution of lubrication film thickness for all tested samples with shown repeatability (top); comparison of the average values (middle); images from colorimetric interferometry (bottom).

by targeted texturing and led to global increases in lubrication film thickness. Fluorescence microscopy revealed that the proteins are capable of forming a layer between the friction pairs. As illustrated in Figs. 7 and 8, protein albumin initially exhibits a tendency to be pushed into the irregularities on the surface of the samples during the initial phase of the experiment. This is followed by the formation of a thin boundary layer between the contact pairs, whereby the proteins adhere and become distributed across the surface. Liu et al. [42] demonstrated that surface textures are suitable for trapping and increasing the local concentration of gelatin particles. Although this specific aspect was not investigated in our study, it can be clearly stated that the textures act as reservoirs for the protein albumin, as evidenced by the fluorescence microscopy images showing significantly higher fluorescence intensity in the dent areas. This indicates the potential of the dents to positively influence the behaviour of the contact pair. The fluorescence intensity (quantity of proteins in the contact area) at the culmination of each stage is comparable between the homogeneous surface and grid structure, indicating the presence of a stable layer of adhered proteins. Based on the observations made, it was noted that following the unloading and reloading between phases, other proteins entered the contact area. However, they lacked the necessary strength of bonds to maintain their presence in the contact area, and after a few cycles, they were washed out. Moreover, a correlation can be observed between the development of the coefficient of friction and the accumulation of adhered proteins in the contact area. Initially, as the number of proteins increases, the coefficient of friction rises gradually. Subsequently, as the protein concentration in the contact area stabilises, forming a stable thin layer, the coefficient of friction also reaches a steady state. This correlation has been previously demonstrated [34,59], whereby an increase in the quantity of proteins present in the contact area is accompanied by an increase in the coefficient of friction.

Based on the results (see Fig. 8), we can observe that the grid structure samples contain the highest amount of albumin in the contact area compared to the other samples. This suggests that a thicker protein layer formed on these samples, which was not washed away during the experiment and provided better protection against wear-induced damage of the contact pairs [33]. The graph (see Fig. 10) illustrates the evolution of protein albumin over the course of one half cycle. In order to facilitate analysis, a representative evolution was selected (represented by the 10th cycle of the experiment), as by this stage, the lubrication film and protein presence in the contact area had stabilized. In the initial cycles, an excessive amount of proteins was present in the contact area but was gradually displaced during movement. Selecting the 10th cycle helped eliminate potential random variations observed during the first few cycles. The y-axis displays the normalised fluorescence intensity, enabling comparison of the trends across experiments conducted with fluorescence microscopy. Ambient light can significantly impact these experiments, making direct comparison challenging without

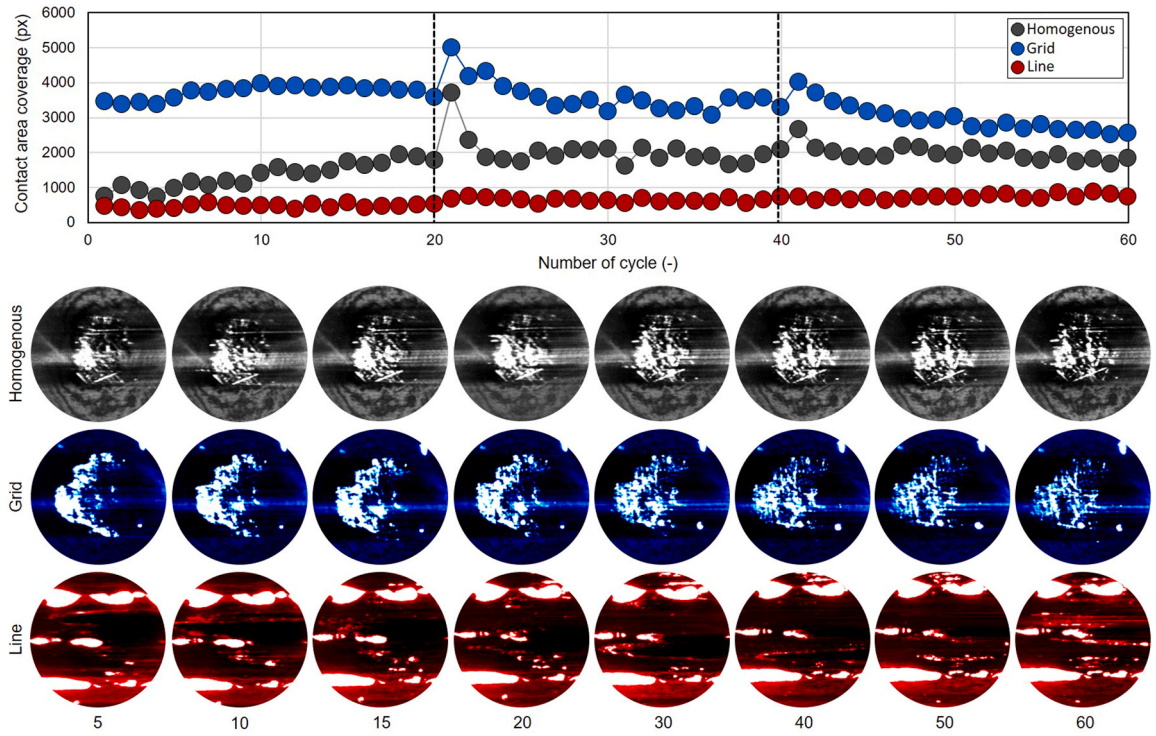

Fig. 7. Evolution of contact area coverage by protein albumin during the whole experiment (top) and fluorescence microscopy images for each sample (bottom).

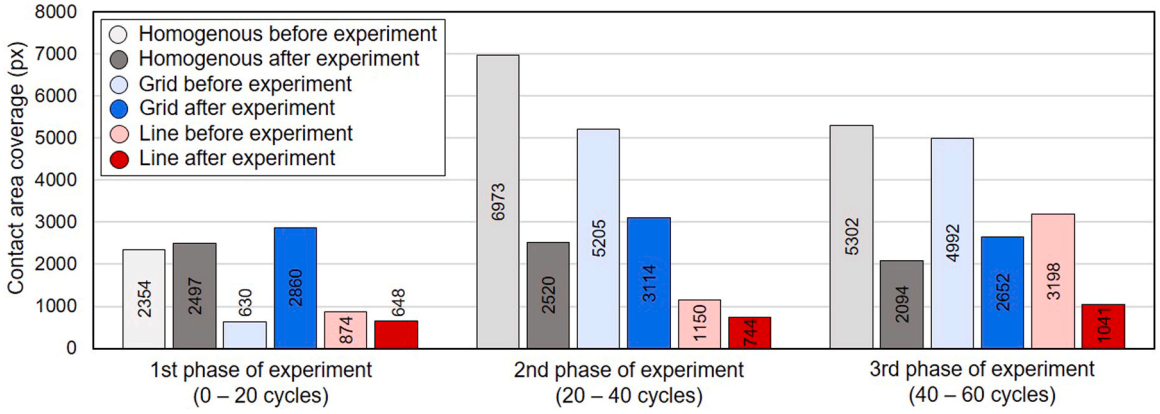

Fig. 8. Coverage of the sensed area (3 times larger in diameter than contact area) by protein albumin in static images before and after the phases of experiment.

normalisation. To this end, the initial value was shifted to 0, facilitating the presentation of dimensionless trends within the evaluated experimental area. The analysis is based on the evaluation of fluorescence intensity in the close area around the contact, which serves as an indicator of the presence of protein albumin. The homogeneous surface exhibited a typical non-stable evolution, whereby the clusters of proteins traversed the contact area and were unable to remain present within it. This was due to their inherent ability to adhere to the surface, which enabled them to pass freely through the contact area. In contrast, the structured samples exhibited a distinct behaviour. An improvement was observed for the sample with a grid structure, whereby the quantity of proteins present in the contact area increased from the original value and remained relatively stable throughout the course of a single cycle. However, the amount of protein in the contact area for the sample with a line structure remained below the original value for the entirety of the cycle, indicating that this structure was not optimal in terms of protein retention. Furthermore, it is evident that the quantity of protein albumin present within the contact area is considerably diminished in the case of the line structure. This is evidenced by the markedly reduced intensity of the stream observed in the outlet zone, in comparison to the other samples, where the stream of proteins exiting the contact area is distinctly visible on the right-hand side of the images (see Fig. 10).

It was evident that the wear of all samples produced via 3D printing technology (see Fig. 9) had improved from the samples prepared from Ti6Al4V using conventional methods in our preliminary study [24]. Furthermore, the absence of deep grooves that were observed for these samples indicated a notable enhancement in the quality of the printed samples. The most relevant improvement was observed in the sample with a grid structure, where it was not even possible to find a wear area on the samples after the experiments. It was even possible to record released wear particles moving within a created dimple using colorimetric interferometry during the experiment. This confirmed their ability to trap these wear particles [60] and prevent them from contributing to secondary wear.

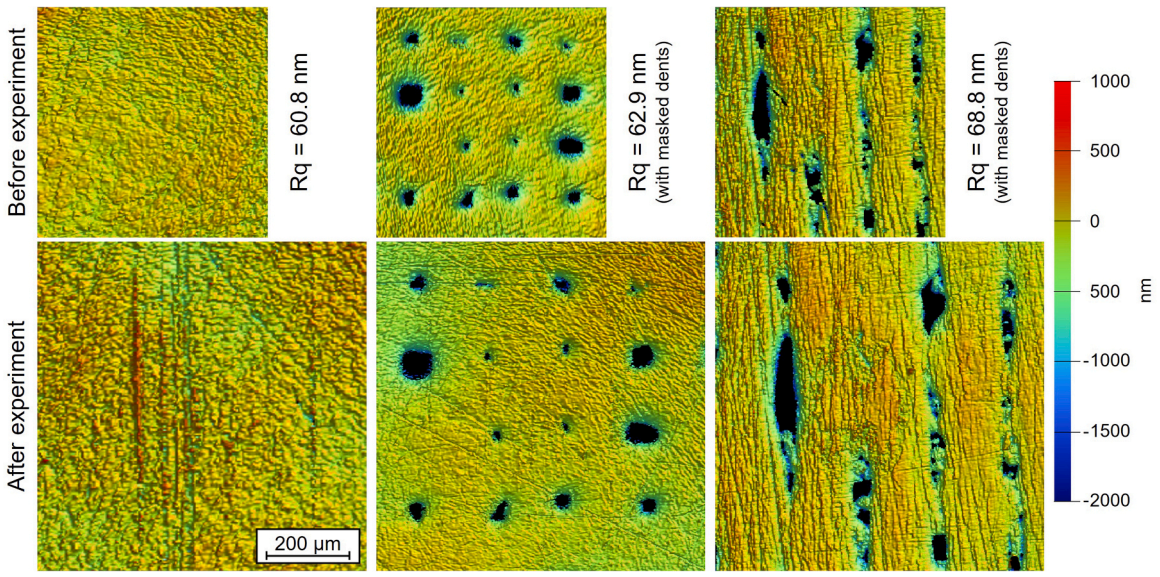

Fig. 9. Comparison of contact area before and after the experiment: homogenous (left), grid structure (middle), line structure (right).

4.2. Data repeatability

Based on the findings, it can be clearly observed that repeatability of the results is achievable, but the results are not perfectly identical, which is phenomenon typical for the biotribological experiments. This fact may be mainly attributed to the behaviour of the synovial fluid, which is a highly complex fluid [50] with non-Newtonian behaviour and it comprises components that can potentially influence its overall behaviour [61] based on the experimental setup and conditions. Another aspect is the fact that the samples were created using 3D printing, where the perfect match of the created structure on the surface (grid or line) was not guaranteed, as some of the expected dents may have been blinded during the production (see Fig. 3). As a result, these differences can lead to slightly different contact areas and contact pressures, which can negatively affect the repeatability. However, if we look at the plots obtained in the Results section, we can see that the values vary slightly across measurements, but the trends are identical. For this reason, repeating each experiment three times was chosen as sufficient to illustrate the repeatability properly.

4.3. Limitations of the study

One of the fundamental limitations of the study is the use of glass as a counterpart in the experiments. However, this choice was necessary in order to make observations of the contact area using optical methods, which would not have been possible with a non-transparent material. This approach increased the contact pressure and reduced the contact area in comparison to the real joint replacement, in which the metal material is in contact with the ultra-high molecular weight polyethylene (UHMWPE). In numerical terms, this represents an increase from 2.4 MPa to 35.1 MPa based on contact Hertz theory, accompanied by a change in the circular contact area from a diameter of 0.887 mm to 0.233 mm. It is acknowledged that these values may appear disparate; however, in the context of understanding the phenomena occurring within the contact area and conducting fundamental research, they are deemed to be acceptable.

A further potential discrepancy may emerge with regard to the dimensions of the contact area and the level of contact pressure, as a consequence of the specific structures present on the surface of the samples. It would be challenging to calculate the same contact pressure and, consequently, contact area size due to the random arrangement of the structures, which would make any such calculation highly unreliable. Accordingly, a methodology was established whereby all samples were evaluated under identical normal force conditions, resulting in minor fluctuations in contact pressure and contact area size due to the distribution of structures. It is also noteworthy that the results of the experiments indicated the development of only protein albumin. This decision was made on the basis of the time-consuming nature of the experiments, given that albumin is the most concentrated protein in the synovial fluid. Moreover, it has been demonstrated [31] that albumin plays a fundamental role in the formation of the lubricating film. Nevertheless, future research could benefit from exploring the effects of other components found in our model synovial fluid, such as γ-globulin, HA, and phospholipids. Alternatively, it may be valuable to investigate the possibility of developing a model synovial fluid that more closely mimics the composition and characteristics of the natural synovial fluid present in human joints.

5. Conclusions

This study demonstrated that 3D printing technology enables the production of structured surfaces that could potentially be implemented in artificial joint replacements. Specifically, Ti6Al4V alloy was additively manufactured in three surface variants: homogeneous, grid-structured, and line-structured. The selected manufacturing method proved effective, requiring only a finishing operation (polishing) to achieve a surface with promising properties. The tribological performance was assessed using a pin-on-plate configuration, where the plate was made of glass to enable optical observation of the contact area during the experiment. The study focused on measuring friction, lubrication film thickness, and the evolution of albumin proteins, as well as analysing the surface of the samples after testing.

The main conclusions of the article are summarised in the following bullet points:

- The 3D printed samples with a grid structure exhibited the most promising results in terms of their potential applicability as a friction surface for human artificial joints.
  - o Friction values were comparable to homogeneous surfaces.
  - o Lubrication film restoration was observed after unloading, unlike in other samples.
  - o Higher and stable presence of protein albumin in the contact area, indicating potential for lubrication film stability.

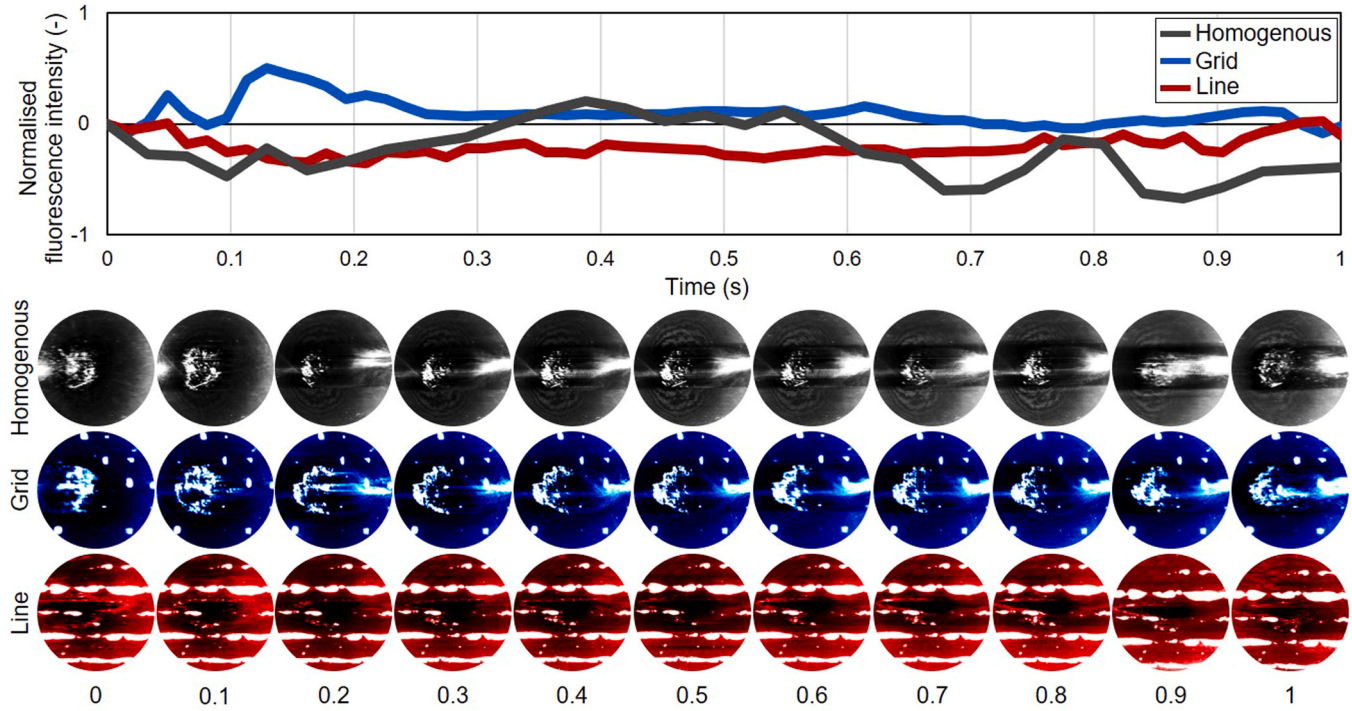

Fig. 10. Evolution of normalised fluorescence intensity (protein albumin) in the contact area (top) and images from fluorescence microscopy (bottom) for the 10th cycle of the experiment.

Further research should focus on optimizing printing parameters or exploring alternative 3D printing methods to achieve finer and more regular structures that better match the intended application. In addition, the application of coatings could enhance the tribological performance of these surfaces, as suggested by other studies. These modifications may help reduce wear and improve the stability of the lubrication film, which is crucial for long-term functionality. To further validate the potential of this approach, long-term wear tests will be conducted to assess the durability and performance of the produced surfaces under realistic operating conditions.

CRediT authorship contribution statement

Lukáš Odehnal: Writing – review & editing, Writing – original draft, Visualization, Validation, Methodology, Investigation, Data curation, Conceptualization. **Martin Vrbka:** Writing – review & editing, Project administration, Funding acquisition, Conceptualization. **Martin Hartl:** Project administration, Funding acquisition. **Daniel Koutný:** Supervision. **Ivan Křupka:** Supervision. **Martin Malý:** Writing – review & editing, Methodology. **Matúš Ranuša:** Writing – review & editing, Validation, Methodology, Investigation, Conceptualization.

Author contribution

L. Odehnal, M. Ranuša, and M. Vrbka conceived the idea. L. Odehnal and M. Ranuša designed the experiments. M. Malý designed the 3D printing parameters and produced the test samples. L. Odehnal performed the experiments and analysed the data. L. Odehnal wrote the original draft of the manuscript. M. Ranuša, M. Malý, M. Vrbka revised the manuscript. M. Vrbka and M. Hartl administrated the projects and secured the funding. D. Koutný and I. Křupka supervised the study.

Declaration of Generative AI and AI-assisted technologies in the writing process

During the preparation of this work the authors used Grammarly and DeepL in order to improve the language quality and increase readability. After using these tools, the authors reviewed and edited the content as needed and take full responsibility for the content of the publication.

Declaration of Competing Interest

The authors declare that they have no known competing financial interests or personal relationships that could have appeared to influence the work reported in this paper.

Acknowledgments

This research was supported by the project “Friction and lubrication of small joint implants produced by 3D metal printing additive technology” funded by Czech Science Foundation, grant number 22-02154S and the project “Mechanical Engineering of Biological and Bio-inspired Systems”, funded as project No. CZ.02.01.01/00/22_008/0004634 by Programme Johannes Amos Comenius, call Excellent Research, administered by the Ministry of Education, Sports and Youth.

Data Availability

The data that support the findings of this study are openly available in repository Zenodo at http://doi.org/10.5281/zenodo.14018227. A preprint version of this article is also available at http://doi.org/10.5281/zenodo.15430333.

References

[1] American Joint Replacement Registry. Elev Annu Rep AJRR Hip Knee Arthroplast 2024.
[2] Milstrey A, Domnick C, Garcia P, Raschke MJ, Evers J, Ochman S. Trends in arthrodeses and total joint replacements in foot and ankle surgery in Germany during the past decade—back to the fusion? Foot Ankle Surg 2021;27:301–4. https://doi.org/10.1016/j.fas.2020.05.008.
[3] Titchener AG, Duncan NS, Rajan RA. Outcome following first metatarsophalangeal joint replacement using TOEFIT-PLUS™: a mid term alert. Foot Ankle Surg 2015; 21:119–24. https://doi.org/10.1016/j.fas.2014.10.005.

[4] Barták V, Heřt J, Štědrý J, Popelka S, Hromádka R. Long-term results of total joint arthroplasty and phalangeal hemiarthroplasty of the first metatarsophalangeal joint using the ToeFit Plus™ system. Foot Ankle Surg 2022;28:56–61. https://doi.org/10.1016/j.fas.2021.01.014.

[5] Abd-Elaziem W, Darwish MA, Hamada A, Daoush WM. Titanium-based alloys and composites for orthopedic implants applications: a comprehensive review. Mater Des 2024;241:112850. https://doi.org/10.1016/j.matdes.2024.112850.

[6] Bandyopadhyay A, Mitra I, Goodman SB, Kumar M, Bose S. Improving biocompatibility for next generation of metallic implants. Prog Mater Sci 2023;133:101053. https://doi.org/10.1016/j.pmatsci.2022.101053.

[7] Sun Y, Liu Q, Yu Z, Ren L, Zhao X, Wang J. Study on osseointegration capability of β-type Ti–Nb–Zr–Ta–Si alloy for orthopedic implants. Materials 2024;17:472. https://doi.org/10.3390/ma17020472.

[8] Okazaki Y. A New Ti–15Zr–4Nb–4Ta alloy for medical applications. Curr Opin Solid State Mater Sci 2001;5:45–53. https://doi.org/10.1016/S1359-0286(00)00025-5.

[9] Kopova I, Stráský J, Harcuba P, Landa M, Janeček M, Bačákova L. Newly developed Ti–Nb–Zr–Ta–Si–Fe biomedical beta titanium alloys with increased strength and enhanced biocompatibility. Mater Sci Eng: C 2016;60:230–8. https://doi.org/10.1016/j.msec.2015.11.043.

[10] Injeti VSY, Nune KC, Reyes E, Yue G, Li SJ, Misra RDK. A comparative study on the tribological behavior of Ti-6Al-4V and Ti-24Nb-4Zr-8Sn alloys in simulated body fluid. Mater Technol 2019;34:270–84. https://doi.org/10.1080/10667857.2018.1550138.

[11] Alberta LA, Vishnu J, Douest Y, Perrin K, Trunfio-Sfarghiu A-M, Courtois N, et al. Tribocorrosion behavior of β-type Ti-Nb-Ga alloys in a physiological solution. Tribol Int 2023;181:108325. https://doi.org/10.1016/j.triboint.2023.108325.

[12] Esway J-E, Conti SF. Joint replacement in the Hallux metatarsophalangeal joint. Foot Ankle Clin 2005;10:97–115. https://doi.org/10.1016/j.fcl.2004.09.002.

[13] Maestro M, Frey-Ollivier S, Schramm M. Quoi de neuf sur les prothèses métatarsophalangiennes du 1er rayon (MtP1). Rev De Chir Orthopédique Et Traumatol 2024;110:1026–39. https://doi.org/10.1016/j.rcot.2024.07.027.

[14] Joyce TJ, Ouenzerfi G, Kandemir G, Trail I, Massardier V, Othmani R, et al. Significantly less wear of UHMWPE rubbing against pyrocarbon than against CoCr. J Mech Behav Biomed Mater 2024;160:106768. https://doi.org/10.1016/j.jmbbm.2024.106768.

[15] Strauss J, Salojee M, Du Plessis A, Zhirnov Ivan, Krakmale P, Khodja M. An investigation into the properties of 3D printed Ti6Al4V FCC lattice structures with different strut thicknesses. MATEC Web Conf 2022;370:08002. https://doi.org/10.1051/matecconf/202237008002.

[16] Deng F, Liu L, Li Z, Liu J. 3D printed Ti6Al4V bone scaffolds with different pore structure effects on bone ingrowth. J Biol Eng 2021;15:4. https://doi.org/10.1186/s13036-021-00255-8.

[17] Ran Q, Yang W, Hu Y, Shen X, Yu Y, Xiang Y, et al. Osteogenesis of 3D printed porous Ti6Al4V implants with different pore sizes. J Mech Behav Biomed Mater 2018;84:1–11. https://doi.org/10.1016/j.jmbbm.2018.04.010.

[18] Patel K, Dunn KW. Salvage of failed first metatarsophalangeal joint fusion utilizing custom 3D implant. Foot Ankle Surg: Tech, Rep Cases 2023;3:100309. https://doi.org/10.1016/j.fastrc.2023.100309.

[19] Hu Y, Yang K, Liu H, Wang L, Wang S, Zhang X, et al. 3D-printed custom implant for the management of "locked" posterior dislocation of the shoulder joint with reverse Hill-Sachs lesion: a case report. Front Bioeng Biotechnol 2023;11. https://doi.org/10.3389/fbioe.2023.1259255.

[20] Narra SP, Mittwede PN, Devincent Wolf S, Urish KL. Additive manufacturing in total joint arthroplasty. Orthop Clin North Am 2019;50:13–20. https://doi.org/10.1016/j.ocl.2018.08.009.

[21] Bartolomeu F, Buciumeanu M, Pinto E, Alves N, Silva FS, Carvalho O, et al. Wear behavior of Ti6Al4V biomedical alloys processed by selective laser melting, hot pressing and conventional casting. Trans Nonferrous Met Soc China 2017;27:829–38. https://doi.org/10.1016/S1003-6326(17)60060-8.

[22] Goyal V, Verma G. Tribological behavior of direct metal laser sintering–manufactured Ti6Al4V alloy in different biofluids for orthopedic implants. J Tribol 2024;146. https://doi.org/10.1115/1.4064506.

[23] Fischer D, Cheng K yuan, Neto MQ, Hall D, Bijukumar D, Espinoza Orías AA, et al. CorrosioN BEHAVIOR OF SELECTIVE LASER MELting (SLM) manufactured Ti6Al4V alloy in saline and BCS solution. J Bio Tribocorros 2022;8. https://doi.org/10.1007/s40735-022-00657-1.

[24] Patel MV, Cudjoe E, Ryu JJ. Sliding contact fatigue damage of metallic implants in a simulated body fluid environment. Lubricants 2024;12. https://doi.org/10.3390/lubricants12120437.

[25] Mavraki A, Cann PM. Lubricating film thickness measurements with bovine serum. Tribol Int 2011;44:550–6. https://doi.org/10.1016/j.triboint.2010.07.008.

[26] Odehnal L, Ranuša M, Wimmer MA, Vrbka M, Křupka I. Development of lubrication film and influence on friction in a total knee replacement during a gait cycle. Tribol Int 2023;178:108073. https://doi.org/10.1016/j.triboint.2022.108073.

[27] Myant C, Cann P. In contact observation of model synovial fluid lubricating mechanisms. Tribol Int, 63. Elsevier Ltd; 2013. p. 97–104. https://doi.org/10.1016/j.triboint.2012.04.029.

[28] Myant C, Underwood R, Fan J, Cann PM. Lubrication of metal-on-metal hip joints: The effect of protein content and load on film formation and wear. J Mech Behav Biomed Mater 2012;6:30–40. https://doi.org/10.1016/j.jmbbm.2011.09.008.

[29] Lu X, Nečas D, Meng Q, Rebenda D, Vrbka M, Hartl M, et al. Towards the direct validation of computational lubrication modelling of hip replacements. Tribol Int 2020;146:106240. https://doi.org/10.1016/j.triboint.2020.106240.

[30] Nissim L, Butt H, Gao L, Myant C, Hewson R. Role of protein concentration on transient film thickness in synovial fluid lubricated joints. Biotribology 2021;28:100191. https://doi.org/10.1016/j.biotri.2021.100191.

[31] Nečas D, Vrbka M, Marian M, Rothammer B, Tremmel S, Wartzack S, et al. Towards the understanding of lubrication mechanisms in total knee replacements – part I: experimental investigations. Tribol Int 2021;156:106874. https://doi.org/10.1016/j.triboint.2021.106874.

[32] Čípek P, Rebenda D, Nečas D, Vrbka M, Křupka I, Hartl M. Visualization of lubrication film in model of synovial joint. Tribology Ind 2019;41:387–93. https://doi.org/10.24874/ti.2019.41.03.08.

[33] Tan Q, Zhang Y, Li X, Pu J, Yang S, Jin Z. Effect of synovial fluid constituent on the tribological behaviors of UHMWPE-CoCrMo alloy contact pair. Ind Lubr Tribol. 2023;75:282–91. https://doi.org/10.1108/ILT-10-2022-0314.

[34] Shinmori H, Kubota M, Morita T, Yamaguchi T, Sawae Y. Effects of synovial fluid constituents on friction between UHMWPE and CoCrMo. Tribol. Online 2020;15:283–92. https://doi.org/10.2474/TROL.15.283.

[35] Murali M, Cann P, Masen M. Development of a biomimetic water-based lubricant: Nanoencapsulation of stearic acid using liposomes. Tribol Int 2025;201:110238. https://doi.org/10.1016/j.triboint.2024.110238.

[36] Allen Q, Raeymaekers B. Surface texturing of prosthetic hip implant bearing surfaces: a review. J Tribol 2021;143. https://doi.org/10.1115/1.4048409.

[37] Choudhury D, Rebenda D, Sasaki S, Hekrle P, Vrbka M, Zou M. Enhanced lubricant film formation through micro-dimpled hard-on-hard artificial hip joint: an in-situ observation of dimple shape effects. J Mech Behav Biomed Mater 2018;81:120–9. https://doi.org/10.1016/j.jmbbm.2018.02.014.

[38] Shen G, Zhang J, Culliton D, Melentiev R, Fang F. Tribological study on the surface modification of metal-on-polymer bioimplants. Front Mech Eng 2022;17:26. https://doi.org/10.1007/s11465-022-0682-6.

[39] Shen G, Zhang J, Kang C, Fang F. Study on surface texture patterns for improving tribological performance of bioimplants. Surf Coat Technol 2021;422:127567. https://doi.org/10.1016/j.surfcoat.2021.127567.

[40] Chyr A, Qiu M, Speltz JW, Jacobsen RL, Sanders AP, Raeymaekers B. A patterned microtexture to reduce friction and increase longevity of prosthetic hip joints. Wear 2014;315:51–7. https://doi.org/10.1016/j.wear.2014.04.001.

[41] Sun J, Bai L, Guo F, Khan ZA. Experimental study on the effect of micro-texture on EHL point-contact film thickness subject to sliding conditions. Materials 2022;15:7926. https://doi.org/10.3390/ma15227926.

[42] Liu Q, Shentu J, Yang D, Ni Y, Yuan H, Guo J, et al. Study on the surface texture-microparticles synergistic lubrication mechanism of artificial joint. J Tribol 2025;147. https://doi.org/10.1115/1.4066949.

[43] Ranuša M, Odehnal L, Kučera O, Nečas D, Hartl M, Křupka I, et al. Effect of surface texturing on friction and lubrication of Ti6Al4V biomaterials for joint implants. Tribol Lett 2025;73. https://doi.org/10.1007/s11249-024-01950-5.

[44] Wang B, Zhao X, Li S, Huang S, Lai W, You D, et al. Self-lubricating coating with zero weight loss performance on additively manufactured Ti-6Al-4V. Surf Coat Technol 2022;447:128847. https://doi.org/10.1016/j.surfcoat.2022.128847.

[45] Odehnal L, Ranuša M, Vrbka M, Křupka I, Hartl M. Tribological behaviour of Ti6Al4V alloy: an application in small joint implants. Tribol Lett 2023;71:125. https://doi.org/10.1007/s11249-023-01795-4.

[46] Ranuša M, Čípek P, Vrbka M, Paloušek D, Křupka I, Hartl M. Tribological behaviour of 3D printed materials for small joint implants: a pilot study. J Mech Behav Biomed Mater 2022;132:105274. https://doi.org/10.1016/j.jmbbm.2022.105274.

[47] Hartl M, Krupka I, Poliscuk R, Liska M, Molimard J, Querry M, et al. Thin film colorimetric interferometry. Tribology Trans 2001;44:270–6. https://doi.org/10.1080/10402000108982458.

[48] Smart AE, Ford RAJ. Measurement of thin liquid films by a fluorescence technique. Wear 1974;29:41–7.

[49] Win Khun N, Quan Toh W, Liu E. Study on changes in hardness and wear resistance of 3D printed Ti6Al4V with heat treatment temperature. Tribology Ind 2023;45:129–35. https://doi.org/10.24874/ti.1421.12.22.02.

[50] Galandáková A, Ulrichová J, Langová K, Hanáková A, Vrbka M, Hartl M, et al. Characteristics of synovial fluid required for optimization of lubrication fluid for biotribological experiments. J Biomed Mater Res B Appl Biomater 2017;105:1422–31. https://doi.org/10.1002/jbm.b.33663.

[51] Durrant M, Durrant L, Mcelroy T. Establishing a common instantaneous center of rotation for the metatarso-phalangeal and metatarso-sesamoid joints: a theoretical geometric model based on specific morphometrics. J Orthop Surg Res 2019;14. https://doi.org/10.1186/s13018-019-1110-4.

[52] Allan JJ, Mcclelland JA, Munteanu SE, Buldt AK, Landorf KB, Roddy E, et al. First metatarsophalangeal joint range of motion is associated with lower limb kinematics in individuals with first metatarsophalangeal joint osteoarthritis. J Foot Ankle Res 2020;13. https://doi.org/10.1186/s13047-020-00404-0.

[53] Al-Munajjed AA, Bischoff JE, Dharia MA, Telfer S, Woodburn J, Carbes S. Metatarsal loading during gait—a musculoskeletal analysis. J Biomech Eng 2016;138. https://doi.org/10.1115/1.4032413.

[54] Kaneta M. Effects of surface roughness in elastohydrodynamic lubrication. JSME Int J Ser 3, Vib, Control Eng Eng Ind 1992;35:535–46. https://doi.org/10.1299/jsmec1988.35.535.

[55] Čípek P, Vrbka M, Rebenda D, Nečas D, Křupka I. Biotribology of synovial cartilage: a new method for visualization of lubricating film and simultaneous measurement of the friction coefficient. Materials 2020;13:2075. https://doi.org/10.3390/ma13092075.

[56] Pratap T, Patra K. Tribological performances of symmetrically micro-textured Ti-6Al-4V alloy for hip joint. Int J Mech Sci 2020;182:105736. https://doi.org/10.1016/j.ijmecsci.2020.105736.

[57] López-Cervantes A, Domínguez-López I, Barceinas-Sánchez JDO, García-García AL. Effects of surface texturing on the performance of biocompatible UHMWPE as a bearing material during in vitro lubricated sliding/rolling motion. J Mech Behav Biomed Mater 2013;20:45–53. https://doi.org/10.1016/j.jmbbm.2012.12.010.
[58] Lee H, Lee S, Park J-K, Yang M. Friction and wear characteristics of surface-modified titanium alloy for metal-on-metal hip joint bearing. Int J Precis Eng Manuf 2018;19:917–24. https://doi.org/10.1007/s12541-018-0108-x.
[59] Flannery M, Jones E, Birkinshaw C. Analysis of wear and friction of total knee replacements part II: friction and lubrication as a function of wear. Wear 2008;265:1009–16. https://doi.org/10.1016/j.wear.2008.02.023.
[60] Sawano H, Warisawa S, Ishihara S. Study on long life of artificial joints by investigating optimal sliding surface geometry for improvement in wear resistance. Precis Eng 2009;33:492–8. https://doi.org/10.1016/j.precisioneng.2009.01.005.
[61] More S, Kotiya A, Kotia A, Ghosh SK, Spyrou LA, Sarris IE. Rheological properties of synovial fluid due to viscosupplements: a review for osteoarthritis remedy. Comput Methods Prog Biomed 2020;196:105644. https://doi.org/10.1016/j.cmpb.2020.105644.

Tribology International 216 (2026) 111599

Contents lists available at ScienceDirect

Tribology International

journal homepage: www.elsevier.com/locate/triboint

Additively manufactured Ti6Al4V with controlled surface structure as a potential material for joint implants: Long-term wear performance and durability

Lukáš Odehnal [a,*], Matúš Ranuša [a], Pavel Čípek [a], Martin Malý [b], Veronika Mazánová [c], Antonín Dlouhý [c], Daniel Koutný [b], Martin Hartl [a], Martin Vrbka [a]

[a] Department of Tribology, Faculty of Mechanical Engineering, Brno University of Technology, Technická 2896/2, Brno 616 69, Czech Republic
[b] Department of Reverse Engineering and Additive Technologies, Faculty of Mechanical Engineering, Brno University of Technology, Technická 2896/2, Brno 616 69, Czech Republic
[c] Institute of Physics of Materials, Czech Academy of Sciences, Žižkova 22, Brno 616 62, Czech Republic

ARTICLE INFO

Keywords:
3D printed Ti6Al4V
Surface structures
Long-term wear
Fluorescence microscopy

ABSTRACT

In this study, a comprehensive investigation of long-term wear and extended fluorescent experiments was supported by microstructural and chemical analysis. The aim was to compare the differences between a 3D printed Ti6Al4V alloy with a controlled surface structure created directly during the 3D printing process with a conventionally manufactured CoCr30Mo6 alloy. The primary equipment consisted of two tribometers with a pin-on-plate configuration. This enabled conducting these two types of experiments under kinematic and load conditions closely resembling in vivo environments. The Ti6Al4V alloy consistently outperformed the conventional alloy, showing lower wear of the UHMWPE plate and the tested pins. Additionally, fluorescence microscopy revealed that lubrication film formation was more stable for Ti6Al4V, with longer retention of all model synovial fluid constituents in the contact area. The results demonstrate the potential of 3D printed Ti6Al4V alloy as a material for frictional surfaces in joint implants. However, there are still opportunities for improvement, such as applying coatings to enhance performance.

1. Introduction

The 21st Annual Report by the National Joint Registry [1] reveals that a total of 1,682,998 primary hip replacements have been performed since the registry's establishment in 2003 in all participating hospitals across England, Wales, Northern Ireland, the Isle of Man, and Guernsey. The metal-on-polyethylene (MoP) combination was the most prevalent, accounting for 868,700 cases, which represented approximately 52 % of all cases. These data indicate that MoP implants remain the most widely used in clinical practice despite ongoing advances in joint replacement research and technologies. The long-term performance of these types of joint implants is often limited by wear and degradation of the articulating materials. Typically, it is composed of ultra-high molecular weight polyethylene (UHMWPE) due to its favourable biocompatibility and low coefficient of friction (CoF). However, this contact pair also presents certain disadvantages, such as severe wear and the generation of wear debris during sliding against a harder metallic counterpart [2], which can result in osteolysis and aseptic loosening [3,4], which are the leading causes of revision surgeries.

The most prevalent metallic components of joint implants are still made from either cobalt-chromium, titanium, or stainless steel alloys [5,6]. The most widely employed titanium alloy (Ti6Al4V) is extensively utilised in components that facilitate the secure integration of implants into bone tissue. This phenomenon can be attributed to its low modulus of elasticity, a property that enhances the process of osteointegration while concurrently preserving optimal biocompatibility and corrosion resistance [7,8]. Nevertheless, although Ti6Al4V is among the materials closest to the elastic modulus of bone, a significant difference remains, which can lead to stress shielding [9] and subsequent osteolysis. Despite the mentioned advantages, however, numerous studies have emphasised that Ti6Al4V suffers from unsatisfactory tribological performance, which limits its long-term reliability in mechanical and biomedical applications. In the field of joint replacement research, Ti6Al4V has been demonstrated to result in increased counterface wear and polyethylene

* Corresponding author.
E-mail address: Lukas.Odehnal@vut.cz (L. Odehnal).

https://doi.org/10.1016/j.triboint.2025.111599
Received 20 October 2025; Received in revised form 1 December 2025; Accepted 18 December 2025
Available online 19 December 2025

damage in comparison to CoCr30Mo6 or ceramics, thereby underlining its inherent tribological disadvantage [10,11].

To overcome these challenges and find applications for frictional surfaces of joint implants, researchers have increasingly turned to additive manufacturing (AM) in recent years. This approach has opened up new possibilities in the design and production of products across all areas of manufacturing. A comparable tendency has been identified in the domain of orthopaedic implants [12], particularly concerning the utilisation of titanium alloys, including Ti6Al4V. One of the advantages of using AM, especially techniques such as Selective Laser Melting (SLM) or Electron Beam Melting (EBM), is the capability to produce both macrostructure and microstructure. SLM-produced titanium alloys exhibit superior mechanical strength and enhanced wear resistance compared to conventionally manufactured titanium alloys, primarily due to their fine-grained microstructures formed by rapid solidification [13]. In addition to improved strength, these additively manufactured Ti6Al4V parts can achieve excellent ductility and fatigue performance when appropriate heat treatments, densification strategies, and surface finishing procedures are applied [14]. The porosity, lattice structure, surface roughness, and post-processing treatments can be adjusted to optimise mechanical properties and biological response, such as osseointegration and bone ingrowth [15,16]. As demonstrated in the study by Ren et al. [17], the incorporation of micro- and nano-structured surfaces within the 3D printing process of Ti6Al4V has been shown to enhance osteogenic behaviour. This improvement is attributed to the following mechanisms: enhanced protein adsorption, promotion of mesenchymal stem cell differentiation into osteoblasts, increased contact area with bone, reduced implant micromotion, and the potential enhancement of implant integration at the bone interface. These findings underscore the significance of surface morphology and controlled porosity in facilitating the biological fixation of implants. Moreover, SLM enables the fabrication of highly complex and patient-specific implant [18] geometries that cannot be produced using traditional manufacturing techniques, making this technology highly attractive for next-generation biomedical implants. In addition, if it turns out that the 3D printed Ti6Al4V alloy can also be used for friction surfaces, it could simplify implant design, reduce the number of individual parts, and concurrently reduce the number of material interfaces.

Several studies consistently demonstrate that additively manufactured Ti6Al4V exhibits superior tribological performance compared to conventionally produced materials. Bartolomeu et al. [19] and Goyal et al. [20] reported improvements in the wear resistance of additively manufactured Ti6Al4V compared to conventionally manufactured, which they attributed to the presence of harder microstructural constituents. Jeyaprakash et al. [21] observed similar trends, showing that the wear rate was reduced by 62.1 % when using the SLM-fabricated alloy, accompanied by a 62.7 % decrease in the coefficient of friction and an increase in hardness. Tribocorrosion studies further underscore the robustness of Ti6Al4V, with Patel et al. [22] demonstrating that, under combined mechanical and corrosive loading, Ti6Al4V maintained its integrity better than CoCr30Mo6, indicating more reliable behaviour for load-bearing implants. Beyond bulk material properties, structured surfaces produced by 3D printing can also enhance lubrication performance, as shown by Odehnal et al. [23], who reported that such surfaces improved synovial fluid film stability. Despite these advantages, additive manufacturing also presents challenges. As-built parts frequently demonstrate elevated surface roughness, residual porosity, unmelted particles, or microcracks. These factors have the capacity to exert a detrimental effect on fatigue strength, corrosion resistance, and wear behaviour [16]. The superior wear performance of AM alloys is closely linked to their unique microstructures. While conventionally manufactured Ti6Al4V solidifies into $\alpha+\beta$ lamellae, laser powder bed fusion (LPBF) processing produces a much finer α' martensite due to rapid cooling [24]. Bartolomeu et al. [19] quantified these differences, showing an α/β ratio of 25/75 in cast alloys versus 75/25 in SLM samples. Process optimisation can further enhance properties, as shown by Shi et al. [25], who reported that a laser line energy density of 0.24 J/mm maximised microhardness and produced excellent wear resistance with a friction coefficient of 0.15. Additional tribocorrosion and tribological studies confirmed that LPBF alloys outperformed conventional materials, exhibiting 30–40 % lower wear volumes [26], up to 14 % lower wear under identical test conditions [27], and better wear resistance and frictional stability even in dry sliding [28]. The role of processing parameters has also been highlighted. Predictive models for SLM Ti6Al4V showed that density, hardness, and shear strength are sensitive to energy input and scan strategy, indicating that tribological properties are tunable via process optimisation [29]. Reviews of LPBF Ti6Al4V summarised that higher laser power, rescanning strategies, and optimised hatch spacing reduce porosity, stabilise α' morphology, and improve wear consistency [30,31].

Several surface engineering approaches have been proposed to mitigate the identified weaknesses and enhance the tribological performance of Ti6Al4V. Thermal oxidation treatments produce hardened subsurface layers with a surface hardness of approximately 970 HK, reducing wear by a factor of 4–6 compared to ureated alloys [32]. In-situ laser polishing reduces surface roughness by more than 80 %, decreases porosity in the remelted layer, and improves both wear and corrosion resistance due to defect reduction and grain refinement [33]. Exploration has extended to composite and coated variants, including Ti6Al4V reinforced with ZrO_2, which has been shown to exhibit superior wear resistance compared to unmodified alloys [34]. One of the most common approaches adopted is the utilisation of surface texturing, with the textures functioning as reservoirs for lubricant, storing released wear particles, acting as micro-hydrodynamic bearings, and reducing nominal contact area [35]. In the study by Shen et al. [36], the authors focused on the influence of surface roughness and surface texturing, demonstrating that the optimal combination of these two parameters may be crucial for improving tribological performance. Besides, they verified that in the CoCr30Mo6/UHMWPE contact pair, the textures reduced the frictional force. Another important conclusion for the CoCr30Mo6/UHMWPE contact pair was presented by Shen et al. [37], who verified that in this particular material combination, the textures can capture released wear particles, thereby removing them from the contact area for subsequent sliding.

The lubricating environment further influences the tribological response of Ti6Al4V. The process of joint lubrication is a complex one, governed by various mechanisms that depend on the load and the motion regime. In the context of rapid articulation, the presence of synovial fluid (SF) facilitates hydrodynamic (HD) or elastohydrodynamic lubrication (EHL). Conversely, under high loads or in slow motion, the predominant form of lubrication is boundary lubrication, achieved through adsorbed molecular films [38]. Based on the lubrication behaviour, Myant et al. [31] proposed protein aggregation lubrication (PAL). They described the main differences between the EHL and the real behaviour of fluids containing proteins, which creates the protein-rich, high-viscosity phase of aggregated molecules at the inlet of the contact area. The major constituents of SF (hyaluronan, lubricin, phospholipids, and proteins such as albumin or γ-globulin) play complementary roles in this process. Research consistently shows that dry conditions lead to severe wear. In contrast, the presence of simulated synovial fluid (SSF) or bovine serum significantly reduces debris formation, as protein adsorption films stabilise the contact [39,40]. A study by Goyal et al. [20] found that both cast and AM Ti6Al4V followed the same wear severity ranking when compared with physiologic saline (PSS), simulated body fluid (SBF), and phosphate-buffered saline (PBS). The ranking was as follows: PBS > SBF > PSS. As demonstrated by Nečas et al. [41], the significance of the individual constituents of SF and their role in lubrication formation is paramount. In the following study by Nečas et al. [42], the direct behaviour was incorporated into individual constituents. In this regard, it was observed that the γ-globulin and hyaluronic acid (HA) form a thin yet highly stable and uniform boundary layer. In contrast, the subsequent film thickness is exclusively

attributable to albumin, due to its alternating layers.

This study builds upon our previous research [23], which investigated lubrication formation in short-term experiments of additively manufactured Ti6Al4V samples. While short-term behaviour is relatively well documented, the long-term tribological performance of AM Ti6Al4V, especially when combined with targeted surface structures, remains largely unexplored. In particular, no study has yet clarified how such AM-generated structures influence the evolution of synovial fluid constituents, frictional behaviour, and wear mechanisms over extended periods when compared with clinically established CoCr30Mo6 alloys. This knowledge gap is critical for assessing the realistic potential of AM Ti6Al4V for future implant applications. To address this gap, the present work aims to answer the following research question: *"How does 3D printed Ti6Al4V with a targeted grid-type surface structure perform under long-term wear conditions in comparison with conventional CoCr30Mo6?"* The investigation employs long-term wear experiments conducted using a newly developed wear simulator, supplemented by extended fluorescence-based experiments to characterise the advanced stages of lubricating film behaviour. The study evaluates wear, friction, and lubricant behaviour in the contact zone and is further supported by detailed material and chemical analysis of the samples.

2. Materials and methods

The primary objective of this study was to investigate the long-term behaviour of friction pairs by specifically comparing an additively manufactured Ti6Al4V alloy, which has a surface structure formed directly during the 3D printing process, to a conventional CoCr30Mo6 alloy. For this purpose, a new long-term wear simulator was developed (see Figs. 1A and 1B).

The simulator consists of two test stations that operate in tandem, facilitating a direct comparison of the tests and enabling the identification of potential discrepancies. The simulator is powered by a servo motor coupled with a gearbox, ensuring the output speed required for the desired test parameters. Through the design of the mechanical system, the rotational motion of the drive is transformed into linear reciprocating motion with a sinusoidal velocity profile, replicating realistic joint movement conditions. The guide rods control the movement of the counterpart (UHMWPE plate) relative to the alloy specimen under investigation. The dead weight of the load bar is compensated by a spring, while additional loading is applied using calibrated weights. A force sensor mounted on the load bar provides real-time feedback on the applied load. Each test station is equipped with a peristaltic pump system to ensure proper chamber filling before the experiment, continuous lubricant replenishment during the test, and removal of lubricant containing wear particles at the end of the experiment for further analysis. The other device used in this study was a tribometer with a pin-on-plate configuration (see Fig. 1C) and an attached fluorescence microscopy setup (see Fig. 1D), which has been previously introduced [23,43,44].

2.1. Contact pair and lubricant

The experiments were designed to replicate real in vivo conditions as closely as possible in a laboratory setting. Four distinct material

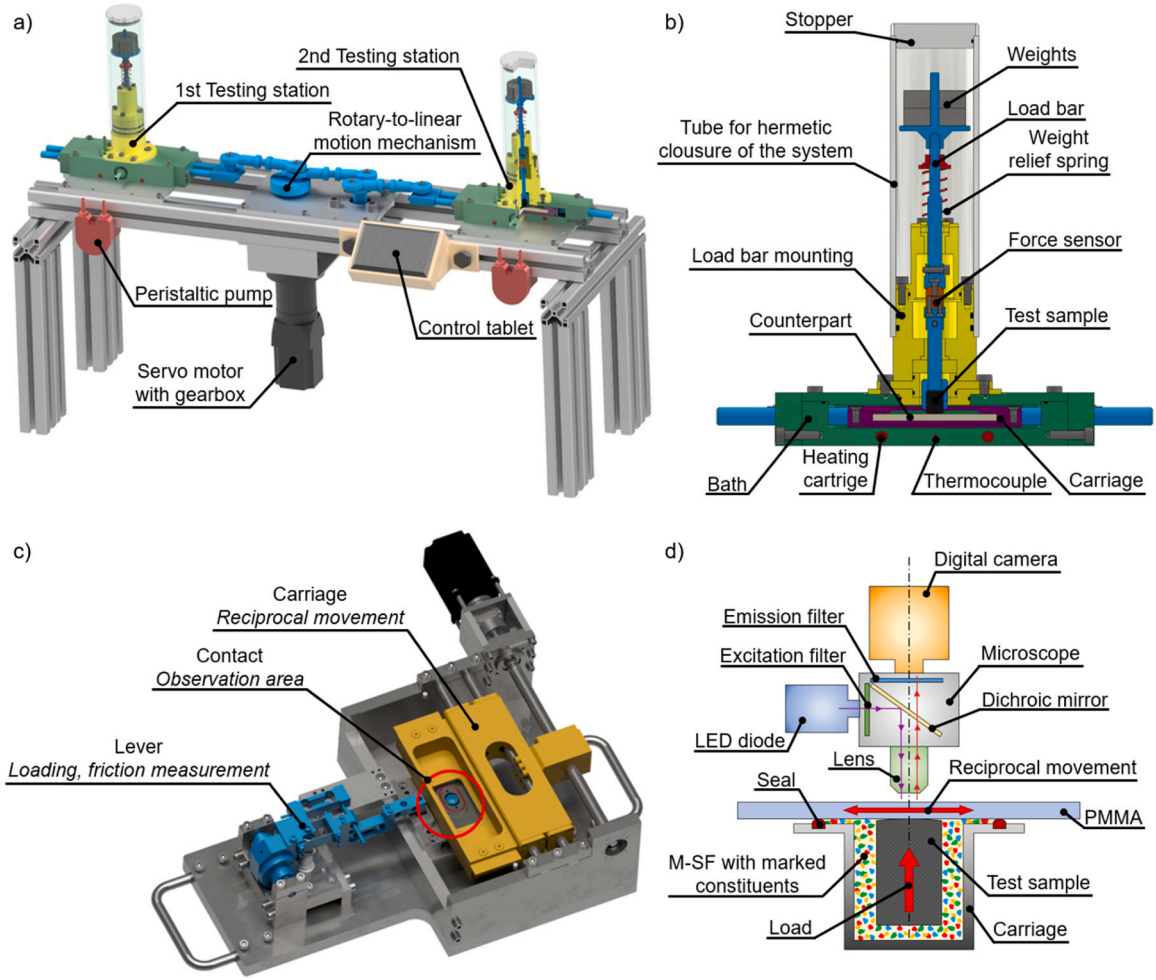

Fig. 1. a) Long-term wear simulator, b) Detail of long-term wear simulator testing station, c) Tribometer with Pin-on-plate configuration [23], d) Scheme of fluorescent microscopy setup [23].

combinations were subjected to testing: Ti6Al4V/UHMWPE and CoCr30Mo6/UHMWPE were utilised for the long-term wear experiments, while Ti6Al4V/PMMA and CoCr30Mo6/PMMA were employed for investigating the lubrication film behaviour within the contact area using fluorescence microscopy. For these observations, it was necessary for one of the contacting components to be transparent; therefore, polymethyl methacrylate (PMMA) was chosen over UHMWPE. The Ti6Al4V specimens were manufactured using the Laser Powder Bed Fusion process from ASTM F3001-compliant Ti6Al4V ELI powder (Carpenter Additive), as previously described in our study [23]. Fabrication was performed with an SLM 280^{HL} 3D printer (Nikon SLM Solutions AG). Based on the findings of our previous study [23], we decided to include only the grid structure in these experiments, as it had the best outcomes from the short-term experiments. To generate the intended surface and subsurface structures, a meander printing strategy was employed, characterised by a 90° rotation between successive layers. The processing parameters were set to a layer thickness of 30 μm, a hatch distance of 179 μm, a laser power of 100 W, and a scan speed of 450 mm/s. The meander printing strategy, using a 179 μm hatch distance, ensures the formation of grid-like structures on the final surface. This printing strategy was applied only to the top 2 mm of the sample, while the remaining volume was homogeneous. The CoCr30Mo6 specimens (ASTM F75) were produced by conventional methods (cold drawing), cut from bars, and subsequently machined. Before testing, both Ti6Al4V and CoCr30Mo6 samples were subjected to a polishing procedure to achieve a curvature radius of 100 mm and an average surface roughness of approximately 50 nm.

The lubricant employed in the experimental procedure was a synthetically prepared model synovial fluid (M-SF), formulated to resemble the composition of synovial fluid obtained from patients following total arthroplasty [45]. The composition of the solution was as follows: albumin (26.3 mg/ml), γ-globulin (8.2 mg/ml), hyaluronic acid (0.82 mg/ml), and phospholipids (0.35 mg/ml), all diluted in phosphate-buffered saline (PBS). It was observed that bacterial growth occurred in the absence of complete sterility within the test chambers. This was due to the presence of air and a constant temperature of 37 °C. The bacterial growth resulted in the degradation of the lubricant, which manifested as blackening and the formation of odour. To suppress bacterial development, a 1 % solution of L-Glutamine-Penicillin-Streptomycin was added to the M-SF. For fluorescence microscopy observations, the main components of M-SF (albumin, γ-globulin, and hyaluronic acid) were fluorescently labelled. The following dyes were utilised: rhodamine-B-isothiocyanate (RBITC) for albumin, and fluorescein-5-isothiocyanate (FITC) for γ-globulin and hyaluronic acid.

2.2. Experimental design

To ensure a comprehensive analysis of the observed samples, three primary analyses, each consisting of several steps or evaluations, were conducted.

1. Long-term wear tests
   - Volume loss
   - Wear rate
   - Surface topography
2. Microstructure and chemistry of pins after wear
   - Scanning electron microscopy (SEM) combined with chemical analysis using Energy Dispersive X-Ray Spectroscopy (EDS)
   - Nanofabrication of surface thin lamellae by the applied focused ion beam technique (FIB)
   - Scanning transmission electron microscopy (STEM) of FIBed lamellae, accompanied by EDS
3. Mid-term experiments using fluorescence microscopy
   - Contact area coverage by M-SF constituents
   - Fluorescence intensity of the contact area
   - Coefficient of friction

In the experiments, although they were conducted on different devices (long-term and mid-term), we aimed to unify the conditions as much as possible. Based on the analysis presented in our previous studies [23,44], we maintained identical kinematic and loading conditions, which also comply with ASTM F732, the standard for long-term wear evaluation of polyethylene used in joint implants. The conditions were as follows: a stroke of 20 mm, a relative speed of 40 mm/s, and a load of 2 N, resulting in a contact pressure of ~3.5 MPa (due to the structured surface of Ti6Al4V samples, the final value can vary, and it is not easy to calculate the exact value due to the randomness of structures). The long-term experiments were performed at three different sliding distances: 100,000, 200,000, and 300,000 cycles. For the mid-term experiments using fluorescence microscopy, we selected 1000 cycles, which was the limit before critical wear of the PMMA plate occurred, making it impossible to evaluate the results further; however, this still provided a solid portion of cycles to describe the behaviour of M-SF constituents.

2.3. Evaluation of the results

The primary assessment of wear scars and subsequent analysis for long-term wear tests were conducted using an optical profilometer, Bruker Countour GTX8. The images obtained during the fluorescence microscopy assessment were processed with Andor Solis software, which also supplied the average intensity of the contact area. Further evaluation of the contact area coverage by M-SF constituents was performed using MATLAB. The procedure involved drawing a calibration image, masking the evaluated contact area, setting a threshold when a certain intensity is exceeded, converting the background to black and passing areas to white, calculating the white area relative to black, and, for structured samples, subtracting the area covered by structures based on the calibration image.

A combination of multiple SEM characterisation techniques was applied to investigate the sample surface after testing. To analyse the surface features and their chemical composition, a Tescan LYRA 3 XMH FEG/SEMxFIB equipped with Energy Dispersive X-ray Spectroscopy (EDS) detectors from Oxford Instruments was used. The EDS spectrum was collected using an accelerating voltage of 20 kV. This microscope operated in both standard secondary electron (SE) and backscattered electron (BSE) regimes. Dualbeam scanning electron microscope FEI Helios nanoLab660 enabled the preparation of thin lamellae for STEM observation by means of FIB machining. Site-specific FIB foils were extracted from the tip of the pins, oriented perpendicular to the test direction. Before the trenching and polishing, the region was covered by either the W of the Pt protective layer in two steps. The first protective layer was deposited with the assistance of electrons, and the second one using an ion beam. The high quality of final FIB foils was reached by applying specific polishing conditions. A 30 kV accelerating voltage and a gradually decreasing current, from 0.79 nA to 80 pA, were applied to achieve the desired thickness of the lamella. Afterwards, the final polishing was performed using 5 kV and 2 kV to reduce the layer thickness to the desired final value and to minimise the damage caused by Ga-ions. The JEOL JEM-2100F transmission electron microscope, operated at 200 kV and equipped with Gatan image-acquisition systems and an Oxford Instruments EDS detector, was used throughout the study. The TEM micrographs were predominantly acquired in the scanning transmission electron microscopy (STEM) mode with a camera length of 800 mm. Bright Field (BF) and High Angular Annual Dark Field (HAADF) detectors were employed to collect the transmitted and diffracted electron intensities, respectively.

3. Results

The results presented herein include both long-term wear tests and

mid-term experiments performed using fluorescence microscopy. The long-term wear behaviour of the two alloys under investigation (3D printed Ti6Al4V with surface structure and conventional CoCr30Mo6) against UHMWPE plates was evaluated through two parallel measurements, carried out simultaneously on the independent test stations of the wear simulator. In the results graphs, these two results are represented as an average, with error bars showing the standard deviation. To ensure adequate repeatability, the fluorescence microscopy experiments were conducted three times for each configuration. In the corresponding images and graphs, different colours were assigned to the constituents of the M-SF: red for albumin, green for γ-globulin, and blue for hyaluronic acid.

3.1. Long-term wear tests

The long-term wear tests were conducted at three distinct sliding distances: 100,000, 200,000, and 300,000 cycles, corresponding to 4, 8, and 12 kilometres, respectively. The resulting volume loss of the UHMWPE plates from two experiments is presented in Fig. 2 as an average supplemented by standard deviation. The overall volume loss of UHMWPE was lower when paired with Ti6Al4V compared to CoCr30Mo6. Based on the values of wear rate (see values within individual bars in Fig. 2), it is clearly visible that while paired with Ti6Al4V alloy, the development of wear remains nearly constant across different sliding distances, while for CoCr30Mo6 alloy, we observed an initial high wear, which was followed by a gradual decrease for longer sliding distances.

It can be observed that the wear differs between the two observed configurations. For Ti6Al4V, the wear track showed generally milder overall wear, but deeper, localised grooves were present. These grooves roughly correspond to the spacing of the surface structures present on the surface of the pins. In contrast, the CoCr30Mo6 exhibited a more uniform wear track, which was wider and, depending on the degree of pin wear (see Fig. 3), featured either larger or smaller protrusions along its path. In the case of the cobalt alloy, all tests consistently revealed visibly deeper and larger wear areas on the pins. In contrast, the titanium pins exhibited only shallow grooves, and these were limited to localised regions. For both materials, however, it is evident that even the considerably harder counterpart undergoes wear, indicating the presence of three-body abrasion. Moreover, profilometry revealed distinct spots on the UHMWPE plate with markedly higher intensity after the tests. We therefore hypothesise that once a particle is released from the pin, it tends to adhere to the UHMWPE surface, which subsequently promotes further scratching of the pins.

3.2. Microstructure and chemistry of pins after wear

The top of the Ti6Al4V pin subjected to 300,000 wear cycles was investigated by SEM operating in the secondary electron (SE) regime, and the resulting structure is documented in Fig. 4. The overview micrograph in Fig. 4a reveals a quasiregular structure of the pores that originate from the 3D printing process described in the section Contact pair and lubricant.

The pores often contain UHMWPE debris, the chemical composition of which was characterised by point EDS analysis. We note that a pin region studied by the EDS technique is delimited by a rectangle in Fig. 4a. Individual EDS positions are highlighted in the micrograph in Fig. 4b. Here, the analyses in positions 1–3 probe the chemical composition of the matrix alloy. In contrast, the chemistry in positions 4 and 5 suggests the presence of the UHMWPE debris. These chemical data are summarised in Table 1.

Similarly, the structure generated by 300,000 wear cycles at the top of the CoCr30Mo6 pin is shown in the SEM SE micrograph presented in Fig. 4c. In contrast to the relatively flat Ti6Al4V surface with shallow scratches (Fig. 4a), more pronounced scratches are observed on the CoCr30Mo6 pin; their detailed configuration is documented in Fig. 4d.

STEM experiments were conducted to characterise the microstructure at and immediately beneath the wear surface of Ti6Al4V and CoCr30Mo6 pins. Thin FIB lamellae cut normal to the central top regions, and perpendicular to the wear marks, were investigated after 300,000 wear cycles. Results obtained for the Ti6Al4V pin are presented in Fig. 5. The overview micrograph in Fig. 5a covers almost the whole region of the lamella where the original pin surface, subjected to wear, delimits the lamella on the right side. Deeper under the surface, the alloy microstructure exhibits a martensitic morphology [46], which is often attributed to the rapid heating and subsequent cooling from β-transus during the 3D printing process [47]. Points A and B shown in Fig. 5a mark sample locations that were investigated in detail in Fig. 5b (points A and B) and Fig. 5c (point B). A closer look at the subsurface microstructure reveals a layer of nanograins separating the surface from the

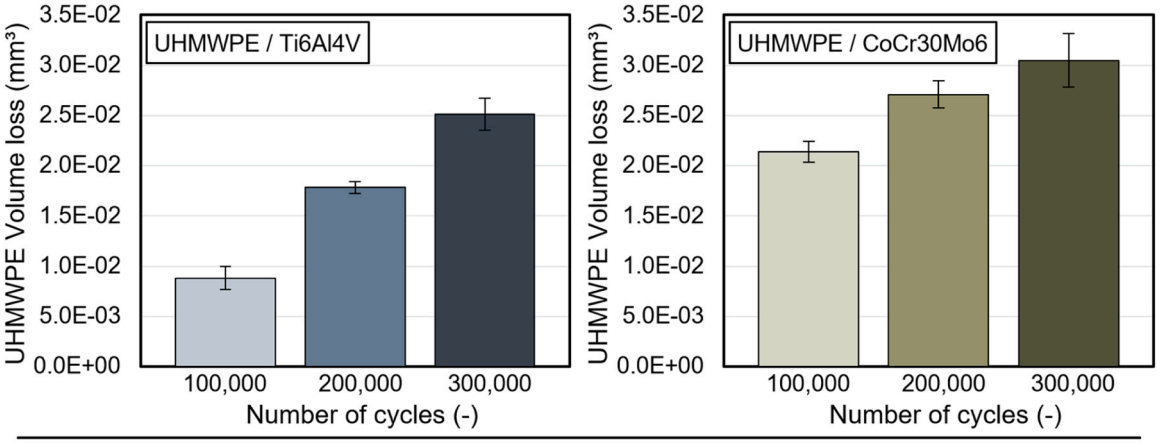

	UHMWPE / Ti6Al4V			UHMWPE / CoCr30Mo6		
Number of cycles (-)	100 000	200 000	300 000	100 000	200 000	300 000
Wear rate (x10^{-6} mm^3/Nm)	1.1033	1.1148	1.0475	2.6374	1.6769	1.2562

Fig. 2. Comparison of UHMWPE volume loss against 3D printed Ti6Al4V with surface structures and CoCr30Mo6 in long-term wear tests based on the number of cycles, supplemented by an actual wear rate.

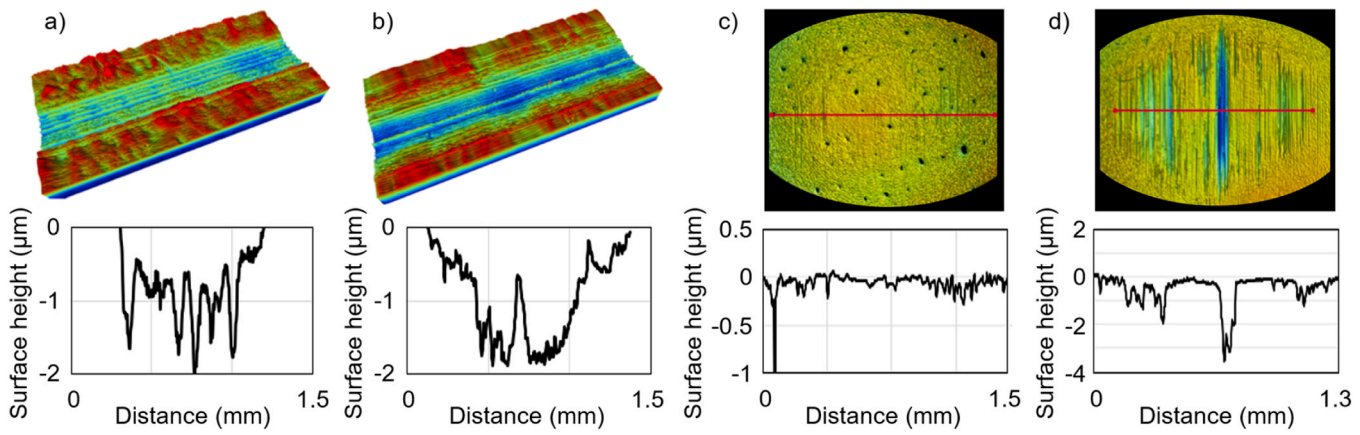

Fig. 3. Comparison of UHMWPE topography after 300,000 cycles experiment against: a) 3D printed Ti6Al4V with surface structures; b) CoCr30Mo6, and comparison of c) Ti6Al4V and d) CoCr30Mo6 pins wear.

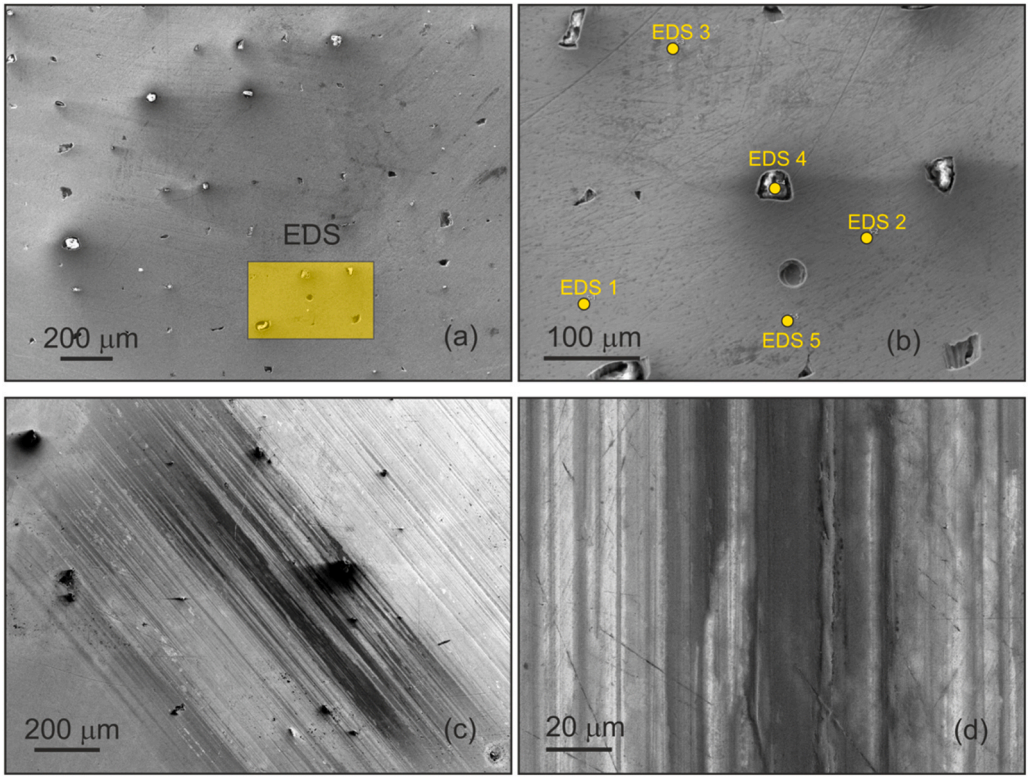

Fig. 4. (a) Quasiregular distribution of pores on the Ti6Al4V surface after wear (the yellow rectangle highlights the area of point EDS analyses); (b) Positions of individual points EDS experiments; (c) Deep scratches on the surface of the CoCr30Mo6 pin after wear; (d) Detailed morphology of the scratches.

Table 1
Local chemical composition acquired at the Ti6Al4V pin surface after wear.

EDS no.	C	O	Na	Mg	Al	Si	P	S	Cl	Ca	Ti	V	Zn
1	13.8	23.5	–	–	5.6	0.3	–	–	–	–	54.5	2.3	–
2	14.1	13.4	–	–	6.4	–	–	–	–	–	63.5	2.6	–
3	19.4	16.9	3.6	–	5.3	0.2	0.1	–	0.8	–	51.8	2.1	–
4	87.6	11.7	0.2	–	0.1	–	–	0.2	0.1	0.0	0.2	–	–
5	67.5	20.8	1.3	0.1	1.0	0.1	–	0.1	–	0.4	6.5	0.3	1.9

martensite. The unsharp border between the layer and martensite is tentatively marked by a red dashed line in the HAADF micrograph in Fig. 5b. An average width of the nanograin layer can be estimated as 200 nm. A more detailed view of the surface region is presented in the BF STEM image in Fig. 5c. The original surface, located on the right, is protected by a tungsten layer deposited before the FIB cutting. Under the protective layer, an oxide scale (bright STEM contrast with a thickness of approximately 35 nm) is directly connected to the Ti6Al4V nanograins

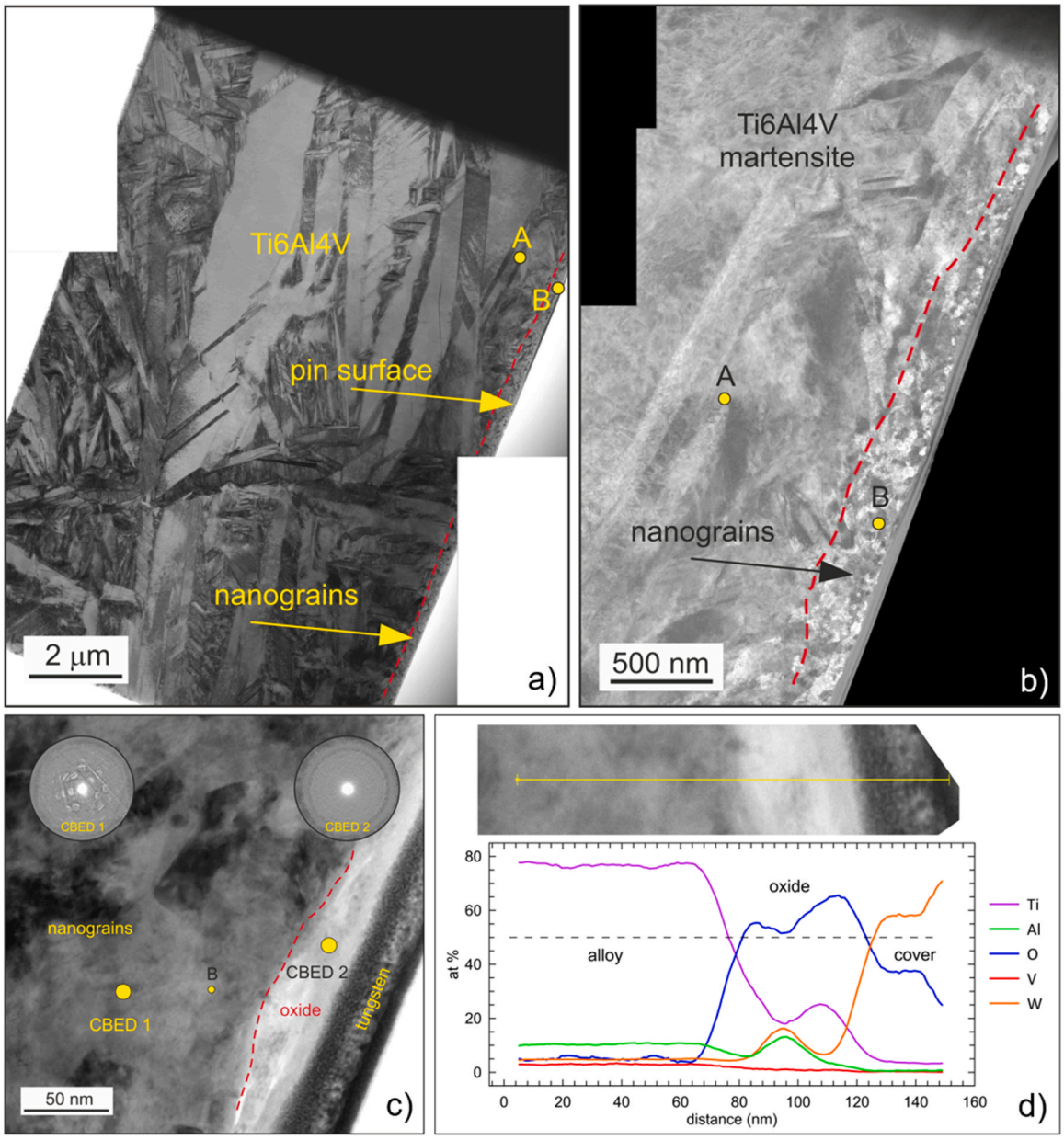

Fig. 5. STEM and EDS characterisation of the Ti6Al4V lamella cut normal to the pin surface and perpendicular to the wear direction: (a) Microstructural overview; (b) Layer of nanograins next to the pin surface; (c) CBED patterns taken from the crystalline alloy and the amorphous oxide scale; (d) EDS linescan across the oxide scale.

on the left. Insets in Fig. 5c present the results of convergent beam electron diffraction (CBED) experiments performed in the position of the nanograin region (CBED position 1) and in the oxide layer (CBED position 2). The CBED patterns clearly show that, in contrast to the crystalline Ti6Al4V alloy, the surface oxide scale is amorphous. The EDS linescan experiment, whose results are summarised in Fig. 5d, reveals the chemical compositions of the oxide and subsurface regions. The elemental EDS profiles acquired along the line extending from the nanograin region and crossing the oxide layer confirmed the nominal composition of the alloy and suggest that the TiO_2 phase predominantly forms the oxide layer.

In a close analogy to the results presented in Fig. 5 for the Ti6Al4V, Fig. 6 shows similar data obtained for the pin made of the CoCr30Mo6 alloy. The general state of the microstructure is presented in Fig. 6a, where a dark region on the right corresponds to the protective tungsten layer deposited on a thin surface oxide that forms on the heavily deformed CoCr30Mo6 grains. Points A and B shown in Fig. 6a mark sample locations that were investigated in detail in Fig. 6b (point A) and Fig. 6c (point B). The high-magnification micrograph in Fig. 6b helps characterise the varying thickness of the surface oxide scale, the average depth of which is estimated to be 150 nm. Moreover, the CBED experiments summarised in Fig. 6c again confirmed that the oxide scale is amorphous. Finally, the linescan EDS analysis yielded results shown in Fig. 6d. The elemental scans cross the oxide layer indicate that the oxide composition is not far from a complex phase $Fe_3P_2O_8$. Further work is required to characterise the internal structure of the oxide scale and its detailed chemical composition.

3.3. *The evolution of M-SF constituents during the mid-term experiments*

During the course of the experiments, the three constituent elements of M-SF were monitored and evaluated. Two complementary

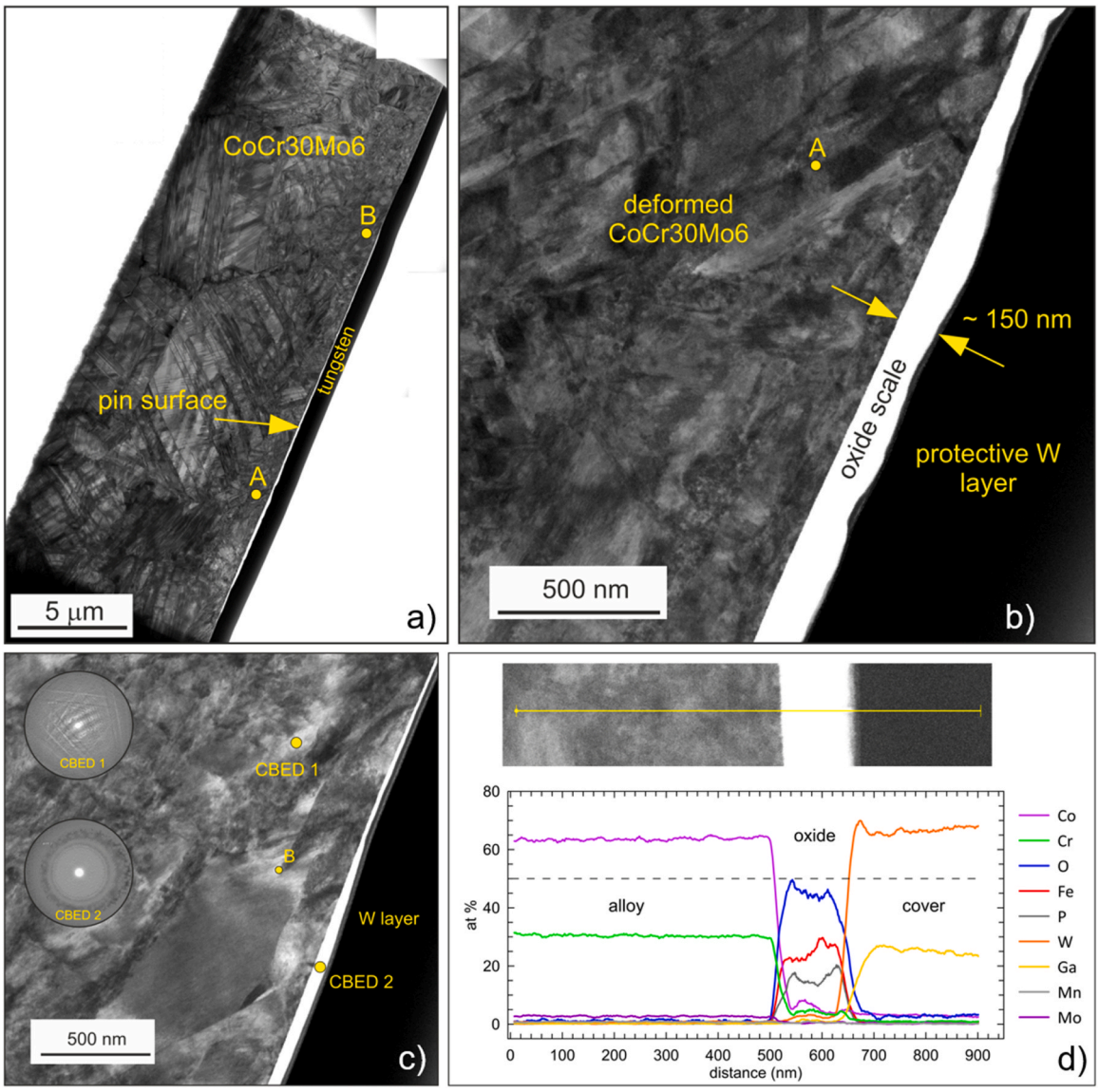

Fig. 6. STEM and EDS characterisation of the CoCr30Mo6 lamella cut normal to the pin surface and perpendicular to the wear direction: (a) Microstructural overview; (b) Thickness of the oxide scale; (c) CBED patterns taken from the crystalline alloy and the amorphous oxide scale; (d) EDS linescan across the oxide scale.

approaches were applied: (i) quantifying the presence of constituents within the contact area (contact area coverage), and (ii) analysing the standardised fluorescence intensity in the contact area. To ensure sufficient repeatability, each material configuration with a different labelled M-SF constituent was repeated three times. The results clearly show that each constituent exhibits a distinct temporal evolution as well as different behaviour depending on the alloy.

To evaluate textured samples in terms of their contact area coverage, an approach was adopted in which the total coverage was initially calculated, and the area corresponding to the textures, as determined from a calibration image, was subsequently subtracted. Although this procedure introduces a certain degree of uncertainty, we consider it more appropriate than including the textures in the analysis. Without this correction, the alloys would not be comparable, as the textures tend to accumulate large amounts of M-SF constituents and exhibit substantially higher fluorescence intensity than the surrounding regions. Due to the duration of the experiments and the large amount of data to be collected, we used fluorescence microscopy to observe 10 cycles at a time, every 100 cycles. This is represented in the graph, which shows the average fluorescence intensity of those 10 cycles. It is evident that, in the case of the cobalt alloy, a substantial proportion of the synovial fluid components was rapidly flushed out. In contrast, the titanium alloy demonstrated a relatively stable region of approximately 400–500 cycles in all experiments, after which a decrease was observed (see Fig. 7).

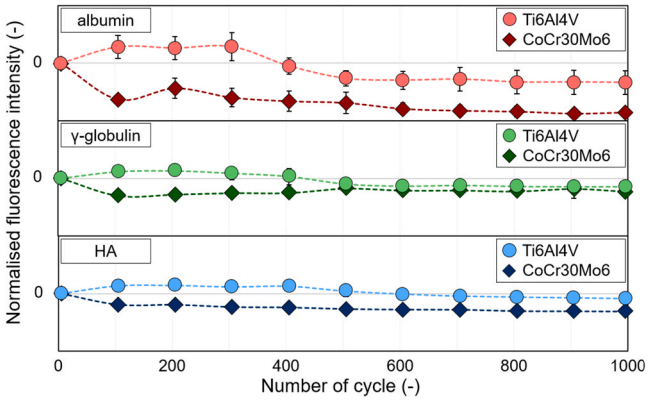

Fig. 7. Comparison of Ti6Al4V and CoCr30Mo6 alloy based on normalised fluorescence intensity.

This finding indicates that the structured titanium surface exhibits a greater capacity to retain fluid components within the contact area over time.

A detailed breakdown of the behaviour of individual synovial components is shown in Fig. 8. We focused on analysing two reversal points and the central part of the stroke. The graphs illustrate the percentage of contact area covered by each component, and we observed a consistent trend: at the stroke reversals, a high accumulation of components was present; nevertheless, after an initial increase, the amount started to decrease until a breakdown occurred. This pattern was also similar for

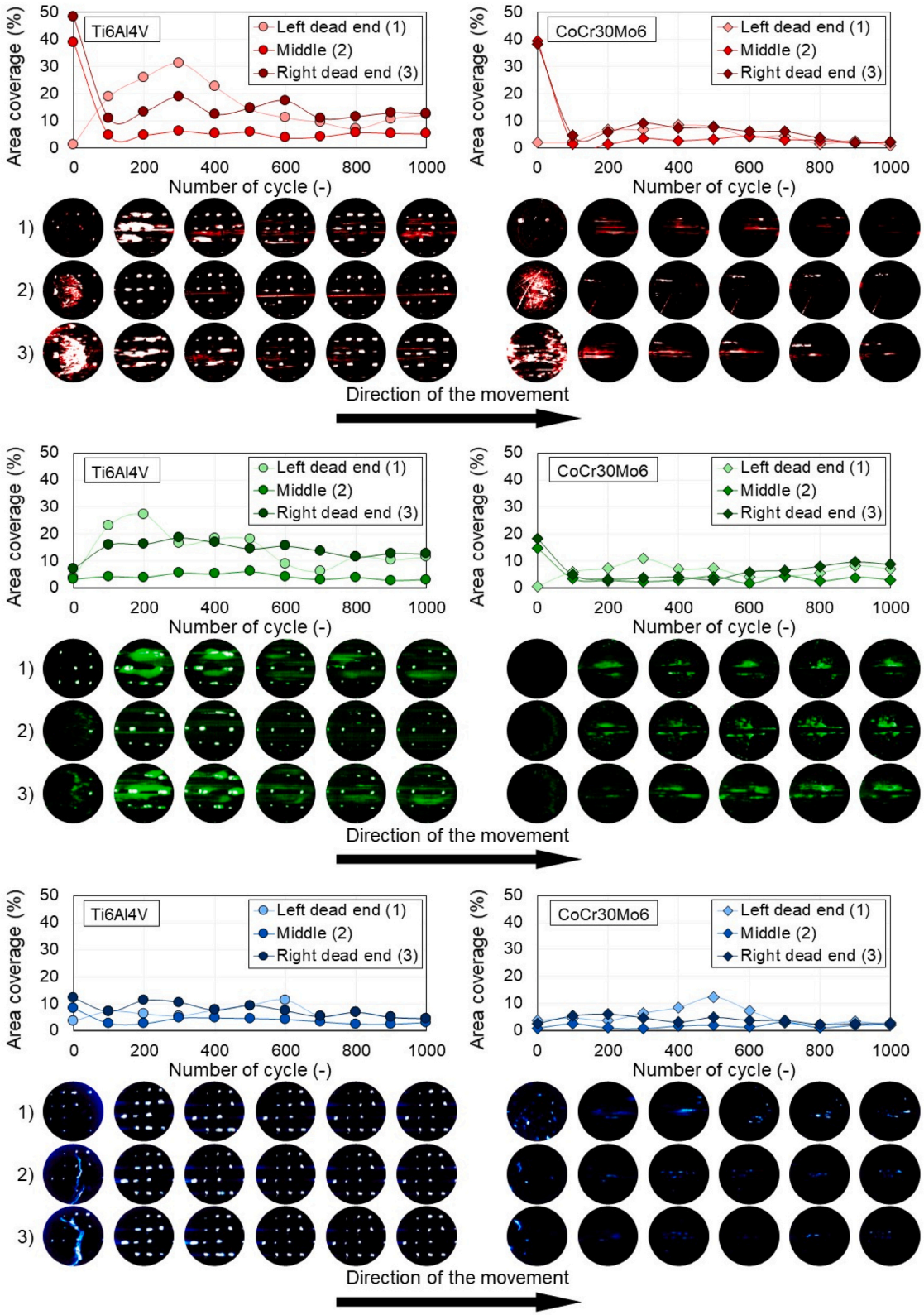

Fig. 8. Contact area coverage evolution of albumin (top), γ-globulin (middle), and HA (bottom) during the experiment for both tested alloys (each point in the graph represents a mean value from three measurements).

globulin and hyaluronic acid. The main difference was in the overall decrease in coverage of the contact area, which corresponds well with the respective concentrations of each component in our model synovial fluid.

Based on the observations using fluorescent microscopy, it is evident that the structures affect the behaviour of M-SF constituents. Upon examining the evolution of the Ti6Al4V alloy, it is evident that an inevitable increase in intensity was observed during the first few cycles. However, between 400 and 500 cycles, the intensity dropped below its starting value. The behaviour depicted in Figs. 7–10 has a clear explanation. By observing the entire fluorescence microscopy videos from the experiments, it is clearly visible that the created structures can collect the constituents of M-SF. This behaviour was observed for all the examined constituents (albumin, γ-globulin, and HA). Three fundamental phases were identified during the observation, which may vary or be complemented by additional ones. The detailed description of these phases is as follows, supplemented with fluorescence microscopy images captured in Fig. 9:

1. The first phase, which usually occurs at the beginning of the experiment, can be described as follows: the constituents tend to accumulate in the vicinity of the structures located within the contact area, gradually forming an increasingly larger agglomeration at the lateral edges in the direction of movement. After a specific period, once saturation is reached and a large amount of proteins accumulates around the structures, the entire cluster detaches and begins to move freely across the contact area.
2. The second phase typically appears at later stages of the experiment, when structures located near the edge of the contact area act as obstacles to the flow of proteins from the contact zone. The proteins gradually flow around these structures, eventually forming a droplet-shaped pattern around each of them.
3. In the final phase, these phenomena gradually disappear, and only the random release of constituent clusters from the structures occurs.

The course and alternation of the phases were not the same for all the observed constituents. For albumin, the first stage remained stable until cycle 300, at which point both phases appeared simultaneously; however, the first one gradually disappeared. Between cycles 500 and 800, only the second phase was observable, and from cycle 900, the third phase occurred. For HA, only the first and third phases occurred, while the first phase was present throughout the entire course of the experiment, except for cycles 500–800, which corresponded to the decrease in intensity after 400 cycles. Nevertheless, the return at around 800 cycles did not affect the intensity. The γ-globulin behaved similarly to HA, except that the first phase did not come back at the end of the experiment, while the first phase again disappeared after 400 cycles.

As part of these experiments, the progression and development of the coefficient of friction in specific configurations were also measured. The representation of these results is shown in Fig. 10. We can observe that repeatability was achieved to some extent, along with different behavioural trends. In the experiments using the Ti6Al4V alloy, a gradual increase in the coefficient of friction was observed during the initial ~400 cycles, after which it stabilised and maintained this value for the remainder of the experiment. However, when examining the development of the CoCr30Mo6 alloy, we can observe that the coefficient of friction increases continuously throughout almost the entire experiment.

4. Discussion

The present study describes the differences in long-term wear performance between 3D printed Ti6Al4V alloy with a surface structure created directly during the 3D printing process and conventionally manufactured samples from CoCr30Mo6. Additionally, the acquisition of supplementary data was achieved by implementing fluorescence microscopy, which facilitated the observation of the initial 1000 cycles. To gain further insight into the behaviour exhibited by each alloy, they underwent microstructure and chemical analysis after the experiments. The ensuing results then summarise information regarding: volume loss and wear rate of UHMWPE, scratches formed on pins, microstructure and chemical analysis, behaviour and development of the M-SF constituents during the course of the experiment, and coefficient of friction.

The primary consideration in the context of joint implant failure is the minimisation of wear on the frictional surfaces of the implant components. For this purpose, a new long-term wear simulator was

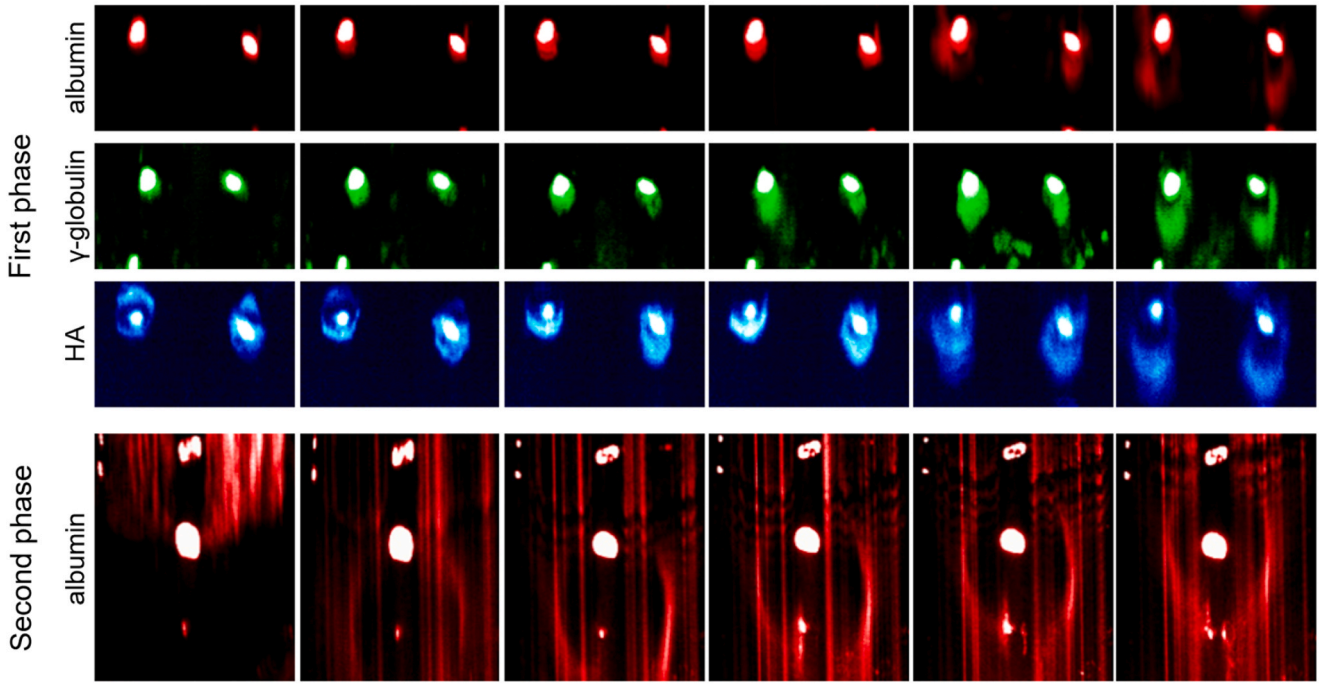

Fig. 9. The influence of surface structures on M-SF constituents during the experiments.

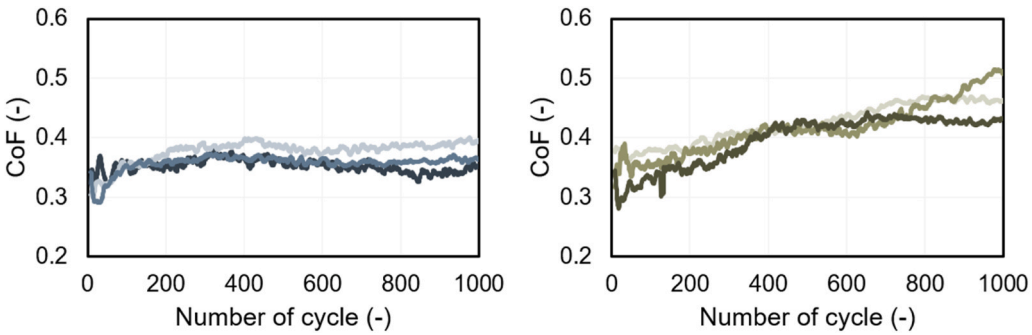

Fig. 10. The evolution of CoF for three measurements: Ti6Al4V/PMMA (left), and CoCr30Mo6/PMMA (right).

constructed. This simulator is suitable for the purposes outlined above, as it is capable of applying loading and kinematic conditions relevant to several joint implants in a simplified configuration. Furthermore, it meets the conditions defined by the appropriate standards. The findings of the long-term wear experiments demonstrated that the 3D printed Ti6Al4V alloy with a controlled surface structure exhibited superior performance in comparison to the conventionally prepared CoCr30Mo6 alloy in two distinct aspects: firstly, the overall volume loss of UHMWPE was reduced, and secondly, the wear of the tested pins was minimised. This finding aligns with the conclusions drawn from the existing literature on the subject [19–21], which suggests that the AM Ti6Al4V achieves a lower rate of wear due to its specific design parameters. In addition, the Ti6Al4V alloy demonstrated a relatively consistent wear rate in comparison to CoCr30Mo6 (see Fig. 2). For the CoCr30Mo6 alloy, significant and rapid wear was observed during the initial 100,000 cycles, after which a tendency towards stability was evident. This behaviour of Ti6Al4V may be associated with the oxidic layer that has been observed to form naturally at the surface of the alloy. The oxidic layer exhibits a higher hardness than the substrate, consequently requiring more time to remove. As demonstrated in Figs. 3c and 3d, the images of the tested pins following experiments with 300,000 cycles illustrate substantial surface damage on the CoCr30Mo6 specimen. In contrast, only a few separated surface grooves were observed on the Ti6Al4V specimen.

Based on the microstructural observations of the Ti6Al4V alloy just beneath the surface, it is evident that a layer with nanograins formed in the near-surface region of the sample (see Fig. 5). This phenomenon, referred to as the Tribologically Transformed Structure (TTS), is typical for Ti6Al4V alloys subjected to fretting wear [48]. However, the samples were polished against a counterbody to ensure the formation of a dome with a predefined curvature radius. Therefore, the layer of nanograins could have formed already during the sample preparation process. To clarify this possibility, additional STEM and EDS characterisation of Ti6Al4V lamellae was conducted outside the contact area. The result of this experiment is presented in Fig. 11, where the STEM BF micrograph clearly documents the presence of the nanograin layer sandwiched between the surface oxide and the Ti6Al4V martensite. The dashed line marks a nanograin-martensite border.

The results showed that a nanograin structure was also formed outside the contact area, indicating that the polishing procedure affected its formation. Therefore, it is not possible to quantify the exact depth of the nanograin structure created directly during the sliding tests. From the STEM analysis (see Fig. 5c), it is evident that an oxide layer forms on the surface of the Ti6Al4V alloy, resulting in a layer approximately 35 nm thick for the specimen after 300,000 experiments. Under sliding contact, Ti6Al4V surfaces tend to form a dynamic oxide layer, which undergoes cyclic wear and reformation—a process referred to as tribo-oxidation. Li et al. [49] observed that varying the sliding velocity alters the dominant tribo-oxide phases and wear mechanisms in Ti6Al4V, highlighting a transition between oxidative wear and delamination depending on speed. Moreover, the passive films can self-heal when

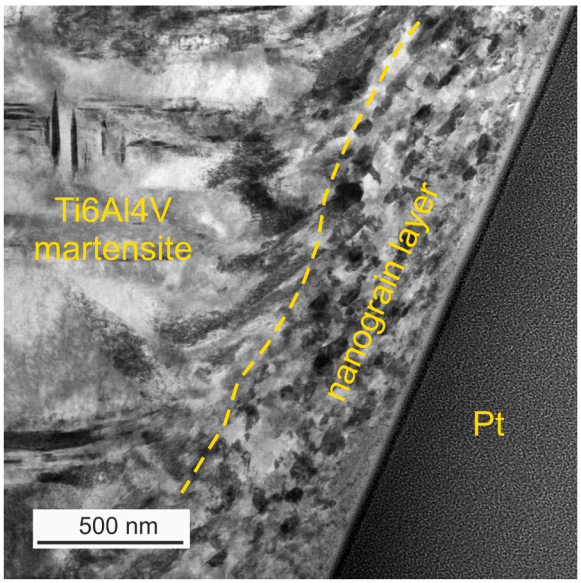

Fig. 11. STEM BF micrograph showing microstructure beneath the surface of the FIB lamella taken from the Ti6Al4V pin location outside the contact area. The dashed line marks a border between the nanograin layer and the Ti6Al4V martensite.

damaged. The results in Fig. 5 suggest that a relatively stable and thick oxide layer was formed, which may have contributed to the more stable wear behaviour of the Ti6Al4V alloy (see the wear rate development in Fig. 2) compared to the CoCr30Mo6 alloy and its rapid increase of wear at the beginning of the experiment.

Observations made using fluorescent microscopy reveal that surface structures play a significant role in the formation and development of the lubrication film. As our primary interest lay in describing the direct effect of the structures present in the contact area, we did not focus on the phenomenon, which had already been described by Myant et al. [50] at the inlet zone to the contact area. Drawing from the observations made, it can be concluded that the structures on the Ti6Al4V surface influenced the stability of the lubrication film. A higher quantity of M-SF constituents was noted in the contact area throughout the entire 1000-cycle experiment, compared to conventionally manufactured CoCr30Mo6. In the case of fluorescent microscopy, it was not possible to obtain longer experiments due to the degradation (wear) of the PMMA plate. This finding is in agreement with that of Rebenda et al. [48], who demonstrated that protein adsorption was more effective for additively manufactured Ti6Al4V compared to CoCr30Mo6 or FeNiCr. It was determined that more cycles would result in unevaluable images. Furthermore, it was observed that, at specific points during the experiment, the structures were capable of releasing M-SF constituents that had accumulated within them (see Fig. 9). This process served to

enhance film stability by effectively functioning as a lubricant reservoir [35]. It is noteworthy that this behaviour was not observed throughout the entire duration of the experiment; instead, it terminated at approximately 400–500 cycles. It is hypothesised that this is primarily attributable to the aggregate quantity of M-SF constituents present within the contact area or its immediate vicinity. As demonstrated in Fig. 8, the number of M-SF constituents is observed to be at its maximum at the dead ends of the cycle. It is evident that during the movement, M-SF constituents are observed to be dragged into the contact area at the dead ends. A number of these constituents are found to accumulate within the structures. After a period of time, when the structures reach capacity, drop-shaped formations appear at the outlet zone of each structure. These formations subsequently undergo a release into the contact area once internal forces are dissipated. The same behaviour was observed for all three observed M-SF constituents (see Fig. 9). This observation therefore shows that the effect of structures is limited by the amount of available synovial fluid components, and for their continued operability, it would be necessary to arrange for the delivery of new components into the contact area. Furthermore, an additional phase of behaviour was observed in the protein albumin (a phenomenon not observed in other M-SF constituents). Following the initial phase, a second phase was identified, during which structures near the edge of the contact area acted as points of alteration for the local contact pressure. The protein albumin exhibited flow behaviour, circumnavigating these structures and subsequently exiting the contact area.

Based on the previously discussed stable oxide layer formed on Ti6Al4V and the minimal wear observed on these pins after the experiments, we can also address the stable evolution of the coefficient of friction (see Fig. 10). It can be observed that, for the Ti6Al4V alloy, the coefficient of friction stabilised shortly after the beginning of the experiment, whereas for CoCr30Mo6, a continuous gradual increase in CoF was recorded, indicating greater stability of the Ti6Al4V alloy throughout the experiment. These findings suggest that the surface structures of additively manufactured Ti6Al4V positively affect the coefficient of friction. As Rebenda et al. [48] reported, CoCr30Mo6 outperformed the 3D printed Ti6Al4V without structures in a test against the PMMA cup of a hip implant.

4.1. Limitations of the study

In this research, a simplified configuration of pin-on-plate was used instead of the most typical configuration for joint implants – ball-in-socket – due to its simplicity. The contact pressure and contact area will deviate from the expected values due to the transition from conformal to nonconformal contact. Nevertheless, this simplification was necessary to precisely observe and describe emerging phenomena and behaviour in the contact area. However, this transition to a simplified configuration is justified by the fact that this research is part of the fundamental research project, the aim of which is to identify new possibilities in the materials for joint implants. Following the preliminary verification of functionality, the next stage will be the initiation of real configurations.

A particular limitation arises from substituting the counterpart material from UHMWPE to PMMA for the purpose of conducting experiments using fluorescence microscopy. Nevertheless, this substitution was imperative to facilitate the utilisation of this optical observation method, as one of the components must be transparent. For these experiments, the loading conditions were maintained at the same value, resulting in a variation in contact pressure. The contact pressure was recalculated for both the CoCr30Mo6 and Ti6Al4V. This resulted in a change from 3.3 MPa to 7.2 MPa. It should be noted that the contact pressure was calculated for a plane material without structures, due to the randomness caused by the manufacturing method. In reality, the contact area and contact pressure would differ slightly for the Ti6Al4V alloy. Notwithstanding, both of these contact pressure values remain within the pertinent range for the application of joint implants. A further discrepancy arises from the alteration of the contact pair in the context of average surface roughness, which exhibits a marked increase in the case of UHMWPE compared to PMMA.

A further limitation of the present study is the absence of fatigue testing. Although the tribological behaviour and lubrication mechanisms were thoroughly examined, the long-term structural integrity of additively manufactured Ti6Al4V under cyclic loading was not assessed. Fatigue performance is a critical requirement for joint implant applications, as repeated loading may initiate or propagate subsurface defects associated with the AM process or the as-built surface features. Therefore, while the results presented here provide valuable insight into the wear behaviour and lubrication support mechanisms, a comprehensive fatigue evaluation will be necessary to fully validate the suitability of this material and surface condition for long-term orthopaedic use.

5. Conclusions

The main conclusions are summarised in the following bullet-point list:

- In the long-term wear experiments, the UHMWPE plates showed slightly lower total volumetric loss when paired with Ti6Al4V compared to the conventionally manufactured CoCr30Mo6.
- Ti6Al4V pins showed significantly less wear than the CoCr30Mo6 ones, thereby reducing the potential release of harmful particles into the body.
- Surface structures formed directly during the 3D printing process on Ti6Al4V surfaces served as effective lubricant reservoirs, thereby improving film stability and providing a longer-lasting supply of M-SF constituents to the contact area.

These findings demonstrate the potential of 3D printed Ti6Al4V alloy with a controlled surface structure for advanced joint replacement components, where the surface functionality can be tailored to optimise lubricant retention in the contact area and improve wear performance. Based on the findings in this article, the authors suggest further investigating the potential of this approach, with a focus on enhancing the reinforcement of 3D printed structures, as the results demonstrated that achieving optimal feature dimensions is currently limited by the capabilities of the selected AM process and printer. These limitations led to irregularities in both the size and depth of the generated structures. Furthermore, future work should also explore suitable surface coatings to minimise the likelihood of wear-particle release from regions where the laser did not etch the surface as precisely as intended.

Authors contribution

L. Odehnal, M. Ranuša, and M. Vrbka conceived the idea. P. Čípek, M. Ranuša, and L. Odehnal developed the long-term wear simulator. M. Malý produced test samples from Ti6Al4V. L. Odehnal designed the experiments. L. Odehnal and M. Ranuša performed the experiments. L. Odehnal evaluated and analysed the data. V. Mazánová and A. Dlouhý provided the microstructural and chemical analysis. L. Odehnal wrote the original draft of the manuscript. M. Ranuša, P. Čípek, V. Mazánová, A. Dlouhý, and M. Vrbka revised the manuscript. M. Vrbka, D. Koutný, and M. Hartl supervised the study, administered the projects, and secured the funding.

CRediT authorship contribution statement

Lukáš Odehnal: Writing – review & editing, Writing – original draft, Visualization, Validation, Methodology, Investigation, Formal analysis, Conceptualization. **Matúš Ranuša:** Writing – review & editing, Methodology, Investigation, Conceptualization. **Pavel Čípek:** Writing – review & editing, Software. **Martin Malý:** Resources. **Veronika Mazánová:** Writing – review & editing, Validation, Formal analysis.

Antonín Dlouhý: Writing – review & editing, Validation, Formal analysis. **Daniel Koutný:** Supervision, Project administration, Funding acquisition. **Martin Hartl:** Supervision, Project administration, Funding acquisition. **Martin Vrbka:** Writing – review & editing, Supervision, Project administration, Funding acquisition, Conceptualization.

Declaration of generative AI and AI-assisted technologies in the writing process

During the preparation of this work, the authors utilised Grammarly and DeepL to enhance language quality and improve readability. After using these tools, the authors reviewed and edited the content as needed, taking full responsibility for the content of the publication.

Declaration of Competing Interest

The authors declare that they have no known competing financial interests or personal relationships that could have appeared to influence the work reported in this paper.

Acknowledgment

This research was supported by the project *"3D printed individualised segmental joint implant: optimisation of fixation to bone and biotribology of articular surface"*, funded as project No. NW25–08–00044 by the Ministry of Health of the Czech Republic in cooperation with the Czech Health Research Council and by the project *"Mechanical Engineering of Biological and Bio-inspired Systems"*, funded as project No. CZ.02.01.01/00/22_008/0004634 by Programme Johannes Amos Comenius, call Excellent Research, administered by the Ministry of Education, Sports and Youth.

We acknowledge CzechNanoLab Research Infrastructure supported by MEYS CR (LM2023051).

Data availability

The data supporting the findings of this study are openly available in the Zenodo repository at http://doi.org/10.5281/zenodo.17340674.

References

[1] 1st Anual Report - National Joint Registry n.d. ⟨https://reports.njrcentre.org.uk/⟩ (accessed August 27, 2025).
[2] Shahemi N, Liza S, Abbas AA, Merican A. Long-term wear failure analysis of uhmwpe acetabular cup in total hip replacement. J Mech Behav Biomed Mater 2018;87:1–9. https://doi.org/10.1016/j.jmbbm.2018.07.017.
[3] Kandahari AM, Yang X, Laroche KA, Dighe AS, Pan D, Cui Q. A review of UHMWPE wear-induced osteolysis: the role for early detection of the immune response. Bone Res 2016;4:16014. https://doi.org/10.1038/boneres.2016.14.
[4] Deans CF, Buckner BC, Garvin KL. Wear, osteolysis, and aseptic loosening following total hip arthroplasty in young patients with highly cross-linked polyethylene: a review of studies with a follow-up of over 15 years. J Clin Med 2023;12:6615. https://doi.org/10.3390/jcm12206615.
[5] AD S, SPA P, Naveen J, Khan T, Khahro SH. Advancement in biomedical implant materials—a mini review. Front Bioeng Biotechnol 2024;12. https://doi.org/10.3389/fbioe.2024.1400918.
[6] Bandyopadhyay A, Mitra I, Goodman SB, Kumar M, Bose S. Improving biocompatibility for next generation of metallic implants. Prog Mater Sci 2023;133:101053. https://doi.org/10.1016/j.pmatsci.2022.101053.
[7] Sarraf M, Rezvani Ghomi E, Alipour S, Ramakrishna S, Liana Sukiman N. A state-of-the-art review of the fabrication and characteristics of titanium and its alloys for biomedical applications. Biodes Manuf 2022;5:371–95. https://doi.org/10.1007/s42242-021-00170-3.
[8] Marin E, Lanzutti A. Biomedical applications of titanium alloys: a comprehensive review. Materials 2023;17:114. https://doi.org/10.3390/ma17010114.
[9] Abd-Elaziem W, Darwish MA, Hamada A, Daoush WM. Titanium-based alloys and composites for orthopedic implants applications: a comprehensive review. Mater Des 2024;241:112850. https://doi.org/10.1016/j.matdes.2024.112850.
[10] Long M, Rack HJ. Titanium alloys in total joint replacement—a materials science perspective. Biomaterials 1998;19:1621–39. https://doi.org/10.1016/S0142-9612(97)00146-4.
[11] Doni Z, Alves AC, Toptan F, Gomes JR, Ramalho A, Buciumeanu M, et al. Dry sliding and tribocorrosion behaviour of hot pressed CoCrMo biomedical alloy as compared with the cast CoCrMo and Ti6Al4V alloys. Mater Des (1980-2015) 2013;52:47–57. https://doi.org/10.1016/j.matdes.2013.05.032.
[12] Das A, Rajkumar P. Metal 3D printing of biometals for prostheses and implants: a review. Explor BioMatX 2025;2. https://doi.org/10.37349/ebmx.2025.101338.
[13] Mohammed MT, V G S, A V S. SLM-built titanium materials: great potential of developing microstructure and properties for biomedical applications: a review. Mater Res Express 2020;6:122006. https://doi.org/10.1088/2053-1591/ab624c.
[14] Bartolomeu F, Gasik M, Silva FS, Miranda G. Mechanical properties of Ti6Al4V fabricated by laser powder bed fusion: A review focused on the processing and microstructural parameters influence on the final properties. Metals (Basel) 2022;12:986. https://doi.org/10.3390/met12060986.
[15] Kajzer W, Wielgus G, Kajzer A. Mechanical and physicochemical properties of Ti6Al4V alloy after plastic working and 3D printing intended for orthopedics implants. Appl Sci 2024;14:11181. https://doi.org/10.3390/app142311181.
[16] García-Hernández C, García-Cabezón C, González-Diez F, Ampudia M, Juanes-Gusano D, Rodriguez-Cabello JC, et al. Effect of processing on microstructure, mechanical properties, corrosion and biocompatibility of additive manufacturing Ti-6Al-4V orthopaedic implants. Sci Rep 2025;15:14087. https://doi.org/10.1038/s41598-025-98349-6.
[17] Ren B, Wan Y, Liu C, Wang H, Yu M, Zhang X, et al. Improved osseointegration of 3D printed Ti-6Al-4V implant with a hierarchical micro/nano surface topography: an in vitro and in vivo study. Mater Sci Eng C 2021;118:111505. https://doi.org/10.1016/j.msec.2020.111505.
[18] Di Laura A, Henckel J, Hart A. Custom 3D-printed implants for acetabular reconstruction. JBJS Open Access 2023;8. https://doi.org/10.2106/JBJS.OA.22.00120.
[19] BARTOLOMEU F, BUCIUMEANU M, PINTO E, ALVES N, SILVA FS, CARVALHO O, et al. Wear behavior of Ti6Al4V biomedical alloys processed by selective laser melting, hot pressing and conventional casting. Trans Nonferrous Met Soc China 2017;27:829–38. https://doi.org/10.1016/S1003-6326(17)60060-8.
[20] Goyal V, Verma G. Tribological behavior of direct metal laser sintering–manufactured Ti6Al4V alloy in different biofluids for orthopedic implants. J Tribol 2024;146. https://doi.org/10.1115/1.4064506.
[21] Jeyaprakash N, Yang C-H, Prabu G, Radhika N. Mechanism correlating microstructure and wear behaviour of Ti-6Al-4V plate produced using selective laser melting. Metals (Basel) 2023;13:575. https://doi.org/10.3390/met13030575.
[22] Patel MV, Cudjoe E, Ryu JJ. Sliding contact fatigue damage of metallic implants in a simulated body fluid environment. Lubricants 2024;12:437. https://doi.org/10.3390/lubricants12120437.
[23] Odehnal L, Ranuša M, Malý M, Křupka I, Koutný D, Hartl M, et al. Tribological behaviour of additively manufactured Ti6Al4V with controlled surface structure: An application in small joint implants. Tribol Int 2025;211:110832. https://doi.org/10.1016/j.triboint.2025.110832.
[24] Rafi HK, Karthik NV, Gong H, Starr TL, Stucker BE. Microstructures and mechanical properties of Ti6Al4V parts fabricated by selective laser melting and electron beam melting. J Mater Eng Perform 2013;22:3872–83. https://doi.org/10.1007/s11665-013-0658-0.
[25] Shi X, Lu P, Ye X, Ren S, Wang Y, Xie Z, et al. Study of mechanical and tribological properties of Ti–6Al–4V alloy fabricated by powder bed fusion laser beam. Powder Metall 2023;66:116–28. https://doi.org/10.1080/00325899.2022.2116405.
[26] Feyzi M, Baghi AD, Fallahnezhad K, Nafisi S, Ghomashchi R, Hashemi R. Bio-tribocorrosive performance of additively manufactured Ti-6Al-4 V alloy via laser powder bed fusion (L-PBF). Prog Addit Manuf 2025;10:5043–56. https://doi.org/10.1007/s40964-024-00886-5.
[27] LEKATOU AG, EFREMENKO BV, HAOUI V, EFREMENKO VG, EMMANOUILIDOU S, ZURNADZHY VI, et al. Microstructure, electrochemical, wear and corrosive wear performance of laser-based powder bed fusion and wrought biomedical Ti−6Al−4V alloys. Trans Nonferrous Met Soc China 2025;35:2612–31. https://doi.org/10.1016/S1003-6326(25)66836-1.
[28] Li H, Ramezani M, Chen ZW. Dry sliding wear performance and behaviour of powder bed fusion processed Ti–6Al–4V alloy. :203103 Wear 2019:440–1. https://doi.org/10.1016/j.wear.2019.203103.
[29] Bartolomeu F, Faria S, Carvalho O, Pinto E, Alves N, Silva FS, et al. Predictive models for physical and mechanical properties of Ti6Al4V produced by Selective Laser Melting. Mater Sci Eng A 2016;663:181–92. https://doi.org/10.1016/j.msea.2016.03.113.
[30] Ni C, Zhu J, Zhang B, An K, Wang Y, Liu D, et al. Recent advance in laser powder bed fusion of Ti–6Al–4V alloys: microstructure, mechanical properties and machinability. Virtual Phys Prototyp 2025;20. https://doi.org/10.1080/17452759.2024.2446952.
[31] Kuntoğlu M, Salur E, Gupta MK, Waqar S, Szczotkarz N, Vashishtha G, et al. A review on surface morphology and tribological behavior of titanium alloys via SLM processing. Rapid Prototyp J 2025;31:271–85. https://doi.org/10.1108/RPJ-08-2024-0328.
[32] Borgioli F, Galvanetto E, Iozzelli F, Pradelli G. Improvement of wear resistance of Ti–6Al–4V alloy by means of thermal oxidation. Mater Lett 2005;59:2159–62. https://doi.org/10.1016/j.matlet.2005.02.054.
[33] Li J, Wu H, Liu H, Zuo D. Surface and property characterization of selective laser-melted Ti-6Al-4V alloy after laser polishing. Int J Adv Manuf Technol 2023;128:703–14. https://doi.org/10.1007/s00170-023-11880-6.
[34] Madeira S, Buciumeanu M, Nobre D, Carvalho O, Silva FS. Development of a novel hybrid Ti6Al4V–ZrO2 surface with high wear resistance by laser and hot pressing techniques for dental implants. J Mech Behav Biomed Mater 2022;136:105508. https://doi.org/10.1016/j.jmbbm.2022.105508.

[35] Allen Q, Raeymaekers B. Surface Texturing of Prosthetic Hip Implant Bearing Surfaces: A Review. J Tribol 2021;143. https://doi.org/10.1115/1.4048409.
[36] Shen G, Zhang J, Culliton D, Melentiev R, Fang F. Tribological study on the surface modification of metal-on-polymer bioimplants. Front Mech Eng 2022;17:26. https://doi.org/10.1007/s11465-022-0682-6.
[37] Shen G, Zhang J, Kang C, Fang F. Study on surface texture patterns for improving tribological performance of bioimplants. Surf Coat Technol 2021;422:127567. https://doi.org/10.1016/j.surfcoat.2021.127567.
[38] Marian M, Shah R, Gashi B, Zhang S, Bhavnani K, Wartzack S, et al. Exploring the lubrication mechanisms of synovial fluids for joint longevity – a perspective. Colloids Surf B Biointerfaces 2021;206:111926. https://doi.org/10.1016/j.colsurfb.2021.111926.
[39] Zhang X, Chen K, Xu L, Qi J, Luo Y, Zhang D. Tribological behavior of Ti6Al4 V alloy swing against UHMWPE under different lubrication. J Thermoplast Compos Mater 2022;35:740–57. https://doi.org/10.1177/0892705719881180.
[40] Feldshtein EE, Vitjaz PA, Leksycki K. Tribotechnical characteristics of Ti6Al4V titanium alloy–ultra-high-molecular-weight polyethylene friction pairs. J Frict Wear 2020;41:399–404. https://doi.org/10.3103/S1068366620050098.
[41] Nečas D, Vrbka M, Rebenda D, Gallo J, Galandáková A, Wolfová L, et al. In situ observation of lubricant film formation in THR considering real conformity: The effect of model synovial fluid composition. Tribol Int 2018;117:206–16. https://doi.org/10.1016/j.triboint.2017.09.001.
[42] Nečas D, Vrbka M, Galandáková A, Křupka I, Hartl M. On the observation of lubrication mechanisms within hip joint replacements. Part I: Hard-on-soft bearing pairs. J Mech Behav Biomed Mater 2019;89:237–48. https://doi.org/10.1016/j.jmbbm.2018.09.022.
[43] Čípek P, Rebenda D, Nečas D, Vrbka M, Křupka I, Hartl M. Visualization of lubrication film in model of synovial joint. Tribol Ind 2019;41:387–93. https://doi.org/10.24874/ti.2019.41.03.08.
[44] Odehnal L, Ranuša M, Vrbka M, Křupka I, Hartl M. Tribological Behaviour of Ti6Al4V Alloy: An Application in Small Joint Implants. Tribol Lett 2023;71:125. https://doi.org/10.1007/s11249-023-01795-4.
[45] Galandáková A, Ulrichová J, Langová K, Hanáková A, Vrbka M, Hartl M, et al. Characteristics of synovial fluid required for optimization of lubrication fluid for biotribological experiments. J Biomed Mater Res B Appl Biomater 2017;105:1422–31. https://doi.org/10.1002/jbm.b.33663.
[46] Zhou X, Li Y, Han Z, Liu Z, Liu K, Tu Y, et al. Unusual stress-induced martensite transformation in Ti-6Al-4V alloy enabled by solution treatment in the lower α+β regime. J Alloy Compd 2023;956:170330. https://doi.org/10.1016/j.jallcom.2023.170330.
[47] Oh SA, Aroh JW, Lamprinakos NL, Chuang CA, Bucsek AN, Rollett AD. Martensite decomposition during rapid heating of Ti-6Al-4V studied via in situ synchrotron X-ray diffraction. Commun Mater 2024;5:58. https://doi.org/10.1038/s43246-024-00492-6.
[48] Lefranc V, Baydoun S, Gandiolle C, Héripré E, Vallet M, Fouvry S, et al. Heterogeneity in tribologically transformed structure (TTS) of Ti–6Al–4V under fretting. Wear 2023;522:204680. https://doi.org/10.1016/j.wear.2023.204680.
[49] Li XX, Zhou Y, Ji XL, Li YX, Wang SQ. Effects of sliding velocity on tribo-oxides and wear behavior of Ti–6Al–4V alloy. Tribol Int 2015;91:228–34. https://doi.org/10.1016/j.triboint.2015.02.009.
[50] Myant CW, Cann P. The effect of transient conditions on synovial fluid protein aggregation lubrication. J Mech Behav Biomed Mater 2014;34:349–57. https://doi.org/10.1016/j.jmbbm.2014.02.005.